Volume 67A
Number 5
Sept.–Oct. 1963

Physics and Chemistry

6

U.S. DEPARTMENT OF COMMERCE

SECTION A

JOURNAL OF RESEARCH

NATIONAL BUREAU OF STANDARDS

Journal of Research

of the

National Bureau of Standards

A. Physics and Chemistry

SEPT.–OCT. • 1963

VOLUME • 67A

NUMBER • 5

Editor: C. W. Beckett

Associate Editors: D. D. Wagman
J. M. Richardson

Publication dates:
Feb. 1, Apr. 1, June 1, Aug. 1, Oct. 1, Dec. 1, 1963

JOURNAL OF RESEARCH

The National Bureau of Standards Journal of Research reports research and development in the fields of activity shown at right. Also included from time to time are survey articles on topics closely related to the Bureau's scientific and technical program.

The Journal is published in four separate sections as follows:

A. Physics and Chemistry

Contains papers of interest primarily to scientists working in these fields. Issued six times a year. Annual subscription: domestic, $4.00; foreign, $4.75.

B. Mathematics and Mathematical Physics

Presents studies and compilations designed mainly for the mathematician and the theoretical physicist. Issued quarterly. Annual subscription: domestic, $2.25; foreign, $2.75.

C. Engineering and Instrumentation

Reports research and development results of interest chiefly to the engineer and the applied scientist. Issued quarterly. Annual subscription: domestic, $2.25; foreign, $2.75.

D. Radio Propagation

Reports work in radio propagation, upper atmospheric physics, and communications. Issued six times a year. Annual subscription: domestic, $4.00; foreign, $4.75.

U.S. DEPARTMENT OF COMMERCE
Luther H. Hodges, Secretary
NATIONAL BUREAU OF STANDARDS
A. V. Astin, Director

Functions and Activities

The functions of the National Bureau of Standards are set forth in the Act of Congress, March 3, 1901, as amended. These include the development and maintenance of the national standards of measurement and the provision of means and methods for making measurements consistent with these standards; the determination of physical constants and properties of materials; the development of methods and instruments for testing materials, devices, and structures; advisory services to government agencies on scientific and technical problems; invention and development of devices to serve special needs of the Government; and the development of standard practices, codes, and specifications. The work includes basic and applied research, development, engineering instrumentation, testing, evaluation, calibration services, and various consultation and information services. The Bureau also serves as the Federal technical research center in a number of specialized fields. The scope of activities of the National Bureau of Standards is suggested in the following listing of the divisions and sections engaged in technical work.

Washington, D.C.

Electricity. Resistance and Reactance. Electrochemistry. Electrical Instruments. Magnetic Measurements. Dielectrics. High Voltage. Absolute Electrical Measurements.

Metrology. Photometry and Colorimetry. Refractometry. Photographic Research. Length. Engineering Metrology. Mass and Volume.

Heat. Temperature Physics. Heat Measurements. Cryogenic Physics. Equation of State. Statistical Physics.

Radiation Physics. X-ray. Radioactivity. Radiation Theory. High Energy Radiation. Radiological Equipment. Nucleonic Instrumentation. Neutron Physics.

Analytical and Inorganic Chemistry. Pure Substances. Spectrochemistry. Solution Chemistry. Standard Reference Materials. Applied Analytical Research. Crystal Chemistry.

Mechanics. Sound. Pressure and Vacuum. Fluid Mechanics. Engineering Mechanics. Rheology. Combustion Controls.

Polymers. Macromolecules: Synthesis and Structure. Polymer Chemistry. Polymer Physics. Polymer Characterization. Polymer Evaluation and Testing. Applied Polymer Standards and Research. Dental Research.

Metallurgy. Engineering Metallurgy. Metal Reactions. Metal Physics. Electrolysis and Metal Deposition.

Inorganic Solids. Engineering Ceramics. Glass. Solid State Chemistry. Crystal Growth. Physical Properties. Crystallography.

Building Research. Structural Engineering. Fire Research. Mechanical Systems. Organic Building Materials. Codes and Safety Standards. Heat Transfer. Inorganic Building Materials. Metallic Building Materials.

Applied Mathematics. Numerical Analysis. Computation. Statistical Engineering. Mathematical Physics. Operations Research.

Data Processing Systems. Components and Techniques. Computer Technology. Measurements Automation. Engineering Applications. Systems Analysis.

Atomic Physics. Spectroscopy. Infrared Spectroscopy. Far Ultraviolet Physics. Solid State Physics. Electron Physics. Atomic Physics. Plasma Spectroscopy.

Instrumentation. Engineering Electronics. Electron Devices. Electronic Instrumentation. Mechanical Instruments. Basic Instrumentation.

Physical Chemistry. Thermochemistry. Surface Chemistry. Organic Chemistry. Molecular Spectroscopy. Elementary Processes. Mass Spectrometry. Photochemistry and Radiation Chemistry.

Office of Weights and Measures.

Boulder, Colo.

Cryogenic Engineering Laboratory

Cryogenic Processes. Cryogenic Properties of Solids. Cryogenic Technical Services. Properties of Cryogenic Fluids.

Central Radio Propagation Laboratory

Ionosphere Research and Propagation. Low Frequency and Very Low Frequency Research. Ionosphere Research. Prediction Services. Sun-Earth Relationships. Field Engineering. Radio Warning Services. Vertical Soundings Research.

Troposphere and Space Telecommunications. Data Reduction Instrumentation. Radio Noise. Tropospheric Measurements. Tropospheric Analysis. Spectrum Utilization Research. Radio-Meteorology. Lower Atmosphere Physics.

Radio Systems. Applied Electromagnetic Theory. High Frequency and Very High Frequency Research. Frequency Utilization. Modulation Research. Antenna Research. Radiodetermination.

Upper Atmosphere and Space Physics. Upper Atmosphere and Plasma Physics. High Latitude Ionosphere Physics. Ionosphere and Exosphere Scatter. Airglow and Aurora. Ionospheric Radio Astronomy.

Radio Standards Laboratory

Radio Standards Physics. Frequency and Time Disseminations. Radio and Microwave Materials. Atomic Frequency and Time-Interval Standards. Radio Plasma. Microwave Physics.

Radio Standards Engineering. High Frequency Electrical Standards. High Frequency Calibration Services. High Frequency Impedance Standards. Microwave Calibration Services. Microwave Circuit Standards. Low Frequency Calibration Services.

Joint Institute for Laboratory Astrophysics-NBS Group (Univ. of Colo.).

Order all publications from the Superintendent of Documents
U.S. Government Printing Office, Washington, D.C. 20402

Use of funds for printing this publication approved by the Director of the Bureau of the Budget (June 19, 1961).

JOURNAL OF RESEARCH of the National Bureau of Standards—A. Physics and Chemistry
Vol. 67A, No. 5, September–October 1963

Reduction of Space Groups to Subgroups by Homogeneous Strain

H. S. Peiser, J. B. Wachtman, Jr., and R. W. Dickson

(June 10, 1963)

It is assumed that the symmetry elements possessed by a strained crystal will be those common to the unstrained crystal and to the macroscopic state of strain. This principle has been applied to show all of the possible subgroups to which a given space group can be lowered by homogeneous strain for all of the 230 crystallographic space groups.

1. Introduction

The symmetry of strained crystals is important in the following considerations:

(1) The presence or absence of internal friction resulting from the motion of point defects in a crystal can depend upon whether or not the initially equivalent sites accessible to the defect are inequivalent in the strained crystal [*1*, *2*, *3*, *4*].[1] An isolated point defect, such as a vacancy, will occupy any one of a set of atomic sites extending throughout the crystal with equal probability in the absence of strain; if the set splits into inequivalent subsets under strain, internal friction will occur when the frequency of an alternating strain is approximately equal to the jump frequency for the point defect.

(2) Any tensor property of a crystal, such as piezoelectricity, depends primarily upon the symmetry of the unstrained crystal, but additional tensor components may be introduced by straining the crystal in such a way as to change its symmetry.

(3) A classification of the types of polymorphism of crystals has been proposed by M. J. Buerger [*5*]; in some categories no bonds are broken but only a symmetry change takes place. Some structural changes can be induced by homogeneous strain.

(4) Introduction into crystals of impurity atoms is accompanied by strain which may lower the symmetry. Such symmetry inversions are well known and properly regarded as phase transformations. At the same time it is tempting to broaden the use of the term solid solution to include inversions in which some crystallographic parameter measuring the departure from higher symmetry is a continuous and increasing function of impurity concentration (in a range including zero concentration). If this function is linear to first approximation the behavior would be a simple extension of Vegard's Law. In any event this phenomenon would be limited to symmetry inversions in conformity with strict postulates applying to continuous transformations by strain, that is second-order transformations in the strict sense used by Landau and Lifshitz as discussed by Dimmock [*6*].

(5) Large strain fields exist near dislocations and accompanying symmetry changes may be associated with large local variations in physical properties such as enhanced diffusion near a dislocation.

(6) Strain-induced alteration of symmetry may cause change in electron-spin resonance [*7*] or infrared absorption [*8*]; measurement of these changes may give information on the type of site occupied by a given point defect.

(7) The lowering of the symmetry of a crystal of doubtful point group may make a more definitive test available for determining the class of the unstrained crystal.

There are probably other effects associated with strain-induced lowering of symmetry, but the aim of the present paper is confined to the solution of the formal problem of the possible lowering of space-group symmetry by homogeneous strain.

The usual concept of homogeneous strain can be extended downward in scale to describe accurately the change of shape of the unit cell, but it will not in general describe the atomic movements within the cell. However, the present considerations involve only the symmetry of the crystal structure. The atoms within the unit cell need not move as if they were suspended in a continuous medium undergoing homogeneous strain. It is only required that their movements be consistent with the symmetry of the macroscopic strain.

2. Scope of Present Paper

In general, a crystal may be subjected to a stress that causes a strain which need not be homogeneous and which may have a special amplitude. This paper is, however, restricted to the consideration of homogeneous strain of arbitrary amplitude.

It may seem more natural to consider an applied stress as an imposed condition rather than a state of strain. It makes no difference to the present argument which is taken as the imposed condition because only the symmetry elements are significant. We defer discussion of this point until Curie's principle is taken up in the next section.

Strain gradients may be important in some processes, such as Nabarro-Herring creep [*9*, *10*] but the effect of a strain gradient must be superimposed

[1] Italicized figures in brackets indicate the literature references at the end of this paper.

on the effect of the average value of the strain in the region in which the physical process under consideration takes place. Creep involves transport of matter over macroscopic distances and may be associated with a strain gradient even though the average strain is zero. The properties listed in the introduction are, however, more likely to depend on average strain over an appropriate volume than on strain gradient because the smallest volume of crystal which can be used for discussion of these properties is comparable to the unit cell of the crystal. Accordingly, attention is restricted to homogeneous strain in this paper although it is recognized that symmetry changes caused by strain gradients may be significant for some physical properties.

One may specialize a strain with respect to orientation or with respect to magnitude, but the former is of more general interest. Thus one might apply a tensile stress to a tetragonal crystal in such a way as to lower it to orthorhombic symmetry and then look for effects on physical properties. Such an experiment would require only a knowledge of crystal orientation. Alternatively, one might apply a tensile stress along the unique axis of a tetragonal crystal and choose its amplitude such that this axis is made equal to the other two thus imposing a pseudocubic character on the crystal. Such an experiment requires a knowledge not only of crystal orientation but also of lattice parameters and elastic constants. This second type of experiment seems of limited interest and we restrict consideration in this paper to strain which may be specialized with respect to orientation, but not with respect to magnitude.

A strained crystal may undergo a phase change and the space group of the new polymorph need not necessarily be symmetry related to the starting crystal. We therefore specifically exempt phase changes from these considerations except those introduced by a continuous process such as those noted in the introduction.

3. Working Principle and Uniqueness of Symmetry Reduction

The components of homogeneous macroscopic strain form a tensor of second rank conveniently represented by a triaxial ellipsoid of symmetry point group mmm. When any two of its major axes are equal the ellipsoid acquires rotational symmetry about the third major axis. When all three major ellipsoid axes are equal it becomes a sphere. In our study of symmetry of strained crystals it is necessary to consider all kinds of possible orientations of the strain ellipsoid relative to the crystal symmetry elements.

We assume that homogeneously strained crystals will have all the symmetry elements common to the unstrained crystal and to the macroscopic strain, but will possess no other symmetry elements. It is an extension of Curie's principle [*11*] to include space-group as well as point-group operations. Curie's principle has been discussed by Shubnikov [*12*] and Koptsik [*13*].

Homogeneous strain possesses all possible translational symmetry elements and therefore preserves all lattice translations, all glide planes parallel to mirror planes of the strain, and screw axes parallel to rotation axes of equal or higher order.

In applying this principle to specific groups it is convenient to characterize strain by its point group. A situation sometimes arises in which the strain has a mirror plane parallel to a glide plane in the space group of the unstrained crystal. We assume the glide plane remains in the strained crystal. The same assumption is made regarding the retention of an n-fold screw axis in the crystal when it is parallel to an n-fold rotation axis in the strain. The process of taking symmetry operations common to the macroscopic strain and to the unstrained crystal must be understood to have this meaning. This situation is a consequence of the well known fact that a crystal may have glide planes and screw axes corresponding to the mirror planes and rotation axes of its point group.

The process of finding the space group of a homogeneously strained crystal can then be carried out in either of two ways. First, the elements strictly common to the point group of the unstrained crystal and to the point group of the strain can be found to give the point group of the strained crystal. There will in general be several space groups corresponding to this final point group. The correct space group will be the one which not only belongs to the final point group but which is also a subgroup of the initial space group. The subgroups of the space groups are listed in the Internationale Tabellen zur Bestimmung von Kristallstrukturen [*14*]. Second, one can bypass consideration of the point group of the crystal and work directly with its space group, taking its elements in common with the point group of the strain in the sense explained in the last paragraph. The writers have used both methods as a check and a few misprints in the Internationale Tabellen were found.

One can now see that it makes no difference to the present work whether stress or strain is used as the imposed condition because in either case only the point-group symmetry is involved.

The reduction of the symmetry of a given crystal by a given strain with specified orientation is unique. The second process, described above, for finding the final space group from the initial space group and the strain is clearly unique. A given symmetry operation in the point group of the strain either does or does not have a corresponding operation in the space group of the unstrained crystal; the number of operations in this point group is finite and small so that every one can be examined to give a definite, unique answer for the final space group. The association of crystal with space group might be questioned but this is also unique. In particular, it will be possible to find a general position (characterized by point symmetry 1 and by a specific arrangement of the atoms around the position) which is acted on by every element of the space group so that in every primitive cell there are a number N, equal to the order of the point group, of identical, distinct positions. Application of the strain cannot raise the

point symmetry, but can only remove some of the symmetry operations originally relating the N positions. Thus, the original set of N positions splits into an integral number, N/n, of subsets each containing n equivalent general positions in the strained crystal where n is the order of the point group of a strained crystal. A set of general positions defines a space group so the association of the strained crystal with a space group is unique.

An alternate approach to the lowering of crystal symmetry using matrix representation of the symmetry operations has been discussed by Ordway [*15*].

4. Results

The reduction scheme for crystallographic point groups is shown in figure 1. This result has been given before and the rules for its construction have been discussed [*1*, *3*]. It is shown here for completeness and to illustrate the important fact, not previously discussed, that some of the point-group reductions can be made in two or more crystallographically equivalent ways. Thus, the reduction from 4/mmm can be made either by retaining the (100), (010), and (001) mirror planes or by retaining the (110), ($1\bar{1}0$), and (001) mirror planes depending on the orientation of the strain. Thus, two or more space-group reductions, corresponding to two or more strain orientations, can be associated with a given point-group reduction.

A given strain orientation (relative to the crystal) that is not represented by a single tieline can be considered as an equivalent sum of strains successively lowering the symmetry along two or more tielines.

The Bravais-lattice reduction scheme for homogeneous strain is shown in figure 2. Here a given starting lattice must go to a lattice with a larger number of parameters so that only transitions downward along the tielines shown are possible under homogeneous strain.

The results in figure 2 can be combined with the results for centrosymmetric point groups in figure 1 to give the reduction scheme for the combined centrosymmetric point groups—Bravais lattices shown in figure 3. This chart shows that certain possibilities are ruled out by the Bravais-lattice re-

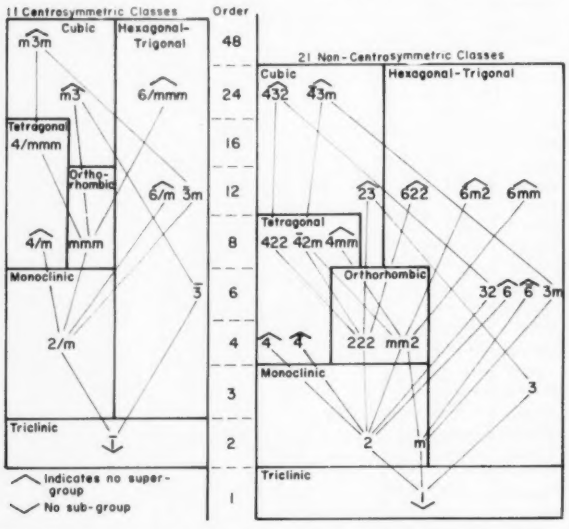

FIGURE 1. *Reduction of point groups to subgroups by homogeneous strain.*

It is a nec ssary condition that a subgroup belong to a different crystal system than the corresponding supergroup. The point group designations are those of the International Tables [*16*].

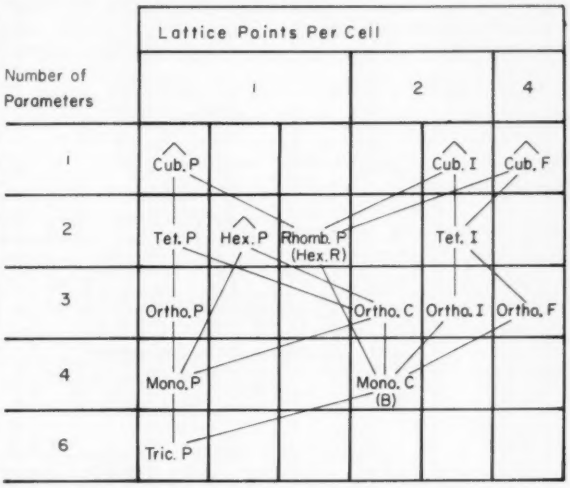

FIGURE 2. *Reduction of Bravais-lattice symmetry by homogeneous strain.*

It is a necessary condition that a lattice go to one with a larger number of parameters. P means primitive, R stands for the compound hexagonal lattice derivable from the primitive thombohedral, C means centered on the C face, I means body centered, and F means centered on all faces.

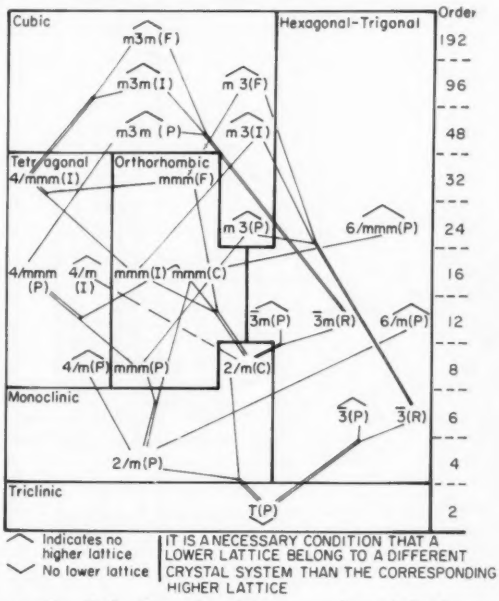

FIGURE 3. *Reduction of point-group—Bravais-lattice combination by homogeneous strain for centrosymmetric point groups.*

duction scheme. Thus, a space group associated with point group m3m and with a face-centered lattice can go to a space group associated with point group 4/mmm but only to one with a body-centered lattice, not to one with a primitive lattice. These restrictions are automatically obeyed when either of the two processes described earlier is used to obtain a reduced space group. The relations in figure 3 do provide a useful partial check on such results. The writers have constructed a chart similar to figure 3 for the noncentrosymmetric point groups combined with the Bravais lattices. The construction is easy, but slightly tedious, and the results do not warrant publication as a step in the process of checking the final product, the space-group charts.

The final results are shown in figure 4, for centrosymmetric space groups, and figure 5 for noncentrosymmetric space groups. This division into two charts is possible because homogeneous strain is centrosymmetric and cannot change the space-group property of being centrosymmetric or noncentrosymmetric.

As in the scheme shown in figure 1 a plane of symmetry on strain transformation is preserved only if it is perpendicular to one of the principal axes of the strain ellipsoid for any permissible choice of prin-

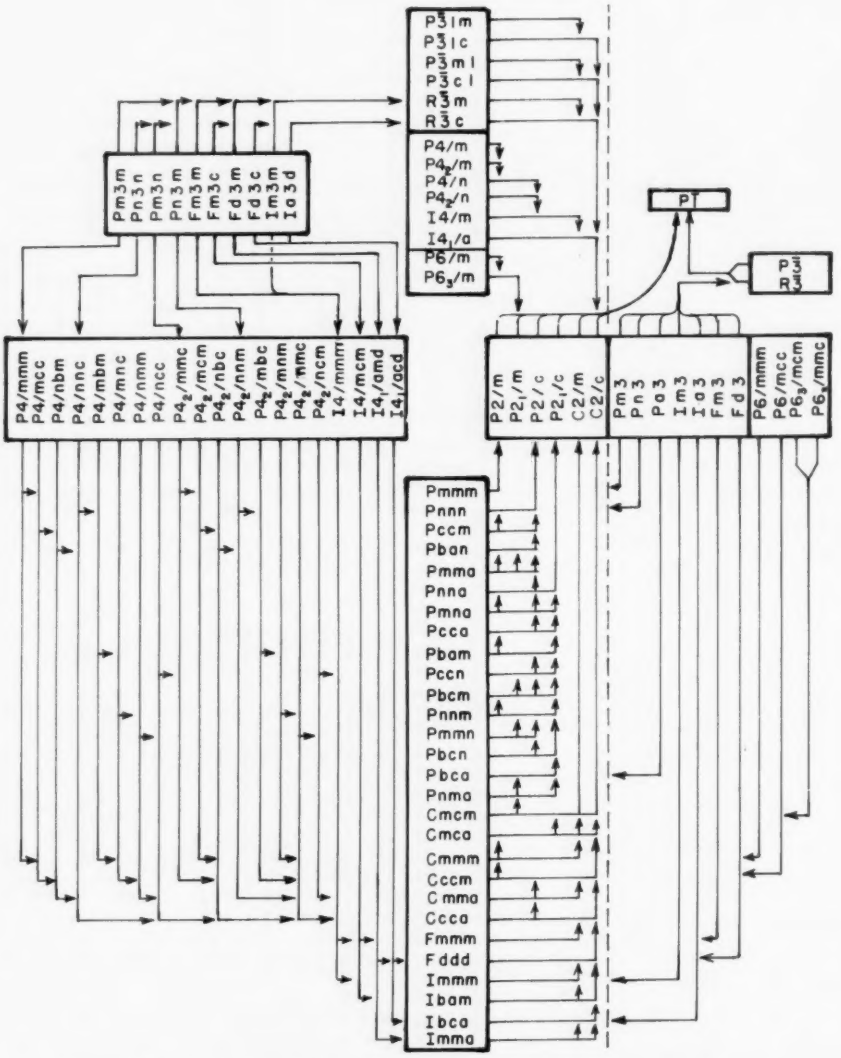

FIGURE 4. *Reduction of centrosymmetric space groups by homogeneous strain.*

The notation of the International Tables [16] is used. Space groups associated with a single point group are enclosed in boxes. Arrows are drawn from starting space group to subgroup reached by homogeneous strain. A space group having no entering arrow cannot be obtained by homogeneous strain from a higher symmetry space group.

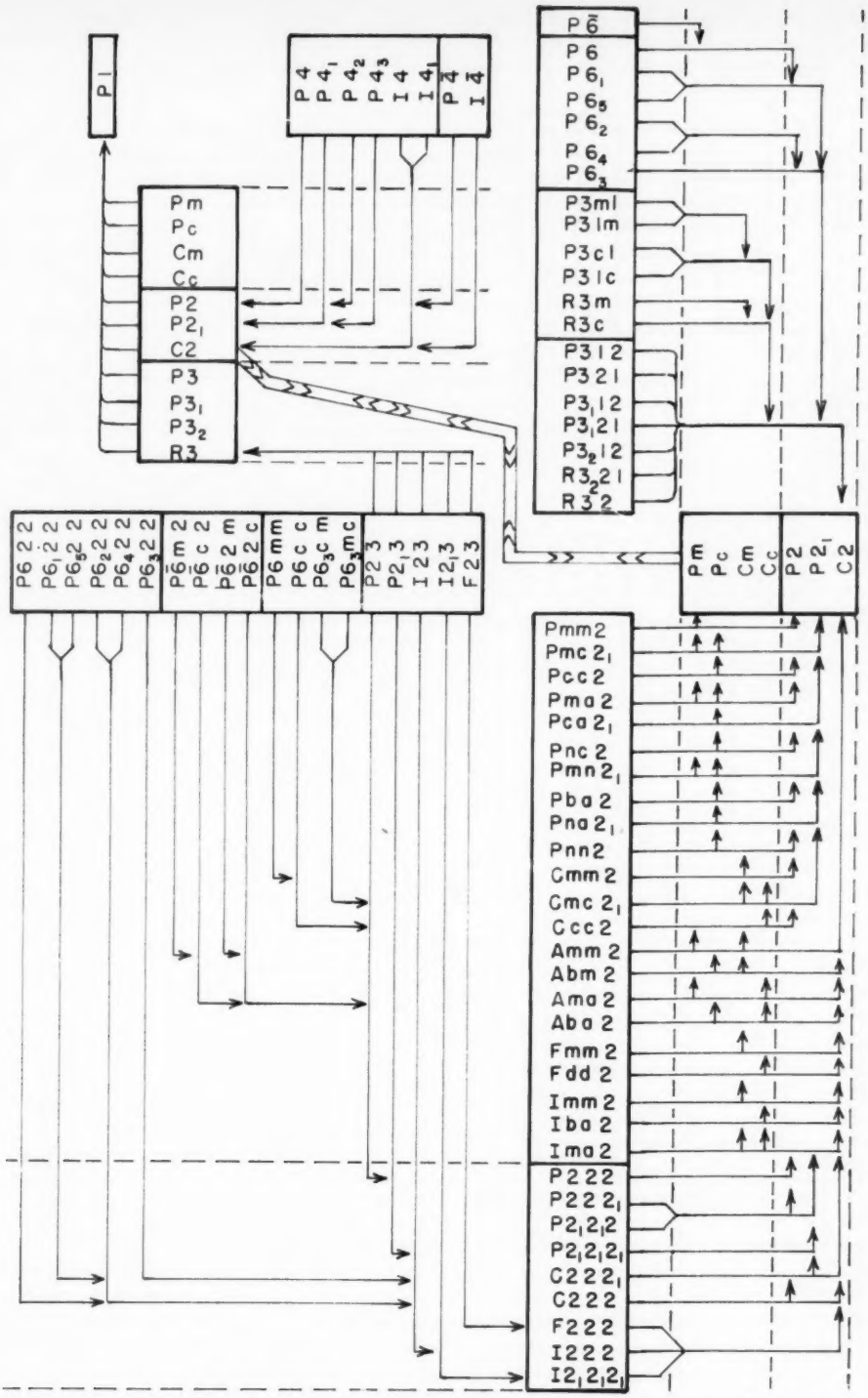

FIGURE 5. *Reduction of noncentrosymmetric space groups by homogeneous strain.*

The vertical column, consisting of space groups associated with point groups 6, $\bar{6}$, 3m, 32 mm2, and 222, has been repeated on page 400 to provide sufficient space for entry and exit of arrows. The space groups associated with point groups m and 2 have been shown twice on the left hand page for the same reason. The text gives an example of the use of this chart.

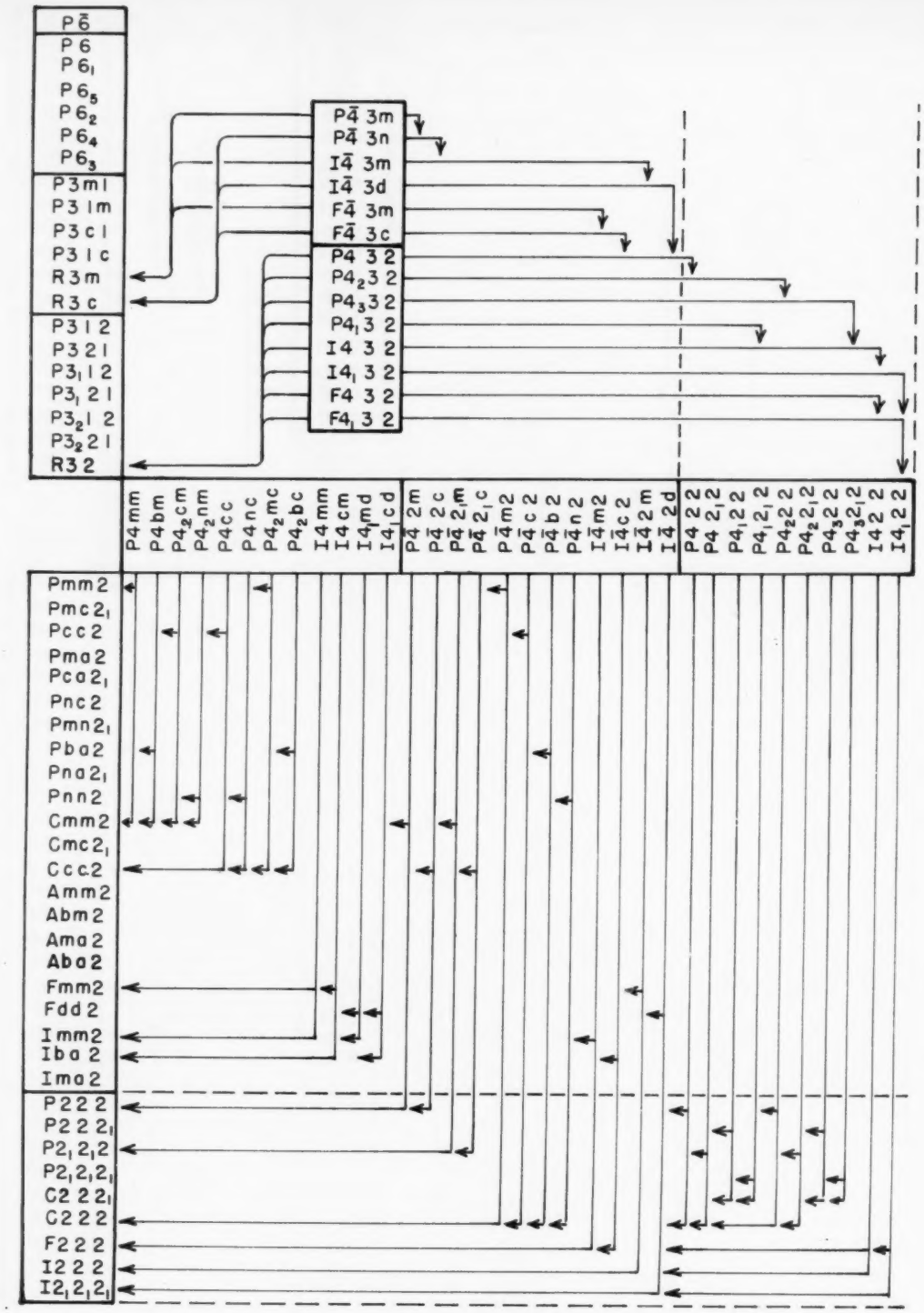

FIGURE 5. *Reduction of noncentrosymmetric space groups by homogeneous strain.*—Continued.

cipal axes. A symmetry axis can be retained only if it is parallel to one of these principal axes of the ellipsoid. An axis of order higher than two can be retained only if it is perpendicular to the circular section of an ellipsoid of revolution. A plane of symmetry parallel or a two-fold axis perpendicular to an axis of order higher than two cannot be removed without simultaneous loss of the higher-order axis.

To illustrate the use of these charts, we discuss the reduction of group P4mm associated with point group 4mm. Figure 1 shows that 4mm goes directly to mm2 but the latter can occur in two crystallographically different orientations depending on whether the mirror planes (100) and (010) are retained or alternatively the planes (110) and ($1\bar{1}0$). We thus expect to obtain two space groups associated with mm2 from P4mm and figure 5 shows that these are Pmm2 and Cmm2. The former corresponds to retention of (100) and (010) mirror planes and of the original coordinate axes. The latter corresponds to retention of (110) and ($1\bar{1}0$) mirror planes and to a change of cell to a C-face-centered cell of twice the volume with its [100] axis along [$1\bar{1}0$] of the original cell. Pmm2 can go to Pm with point group m in two ways and then to P1, the final space group with no symmetry to which all noncentrosymmetric space groups must ultimately reduce. Pmm2 can alternatively go to P2 and then to P1. Returning to the other branch coming from P4mm, we see that Cmm2 can go either to Cm and then to P1, or to P2 and then P1.

The behavior of a set of Wyckoff positions under homogeneous strain is important in determining whether internal friction can occur [3] and may be relevant to the subjects mentioned in the introduction. We have noted in the previous section that the set of N general positions of an initial space group always map onto N/n sets of general positions in the lower space group. The mapping of a set of special positions of the starting space group onto sets of special and/or general positions of the lower space group is more complicated. In particular it should be noted that splitting into unequal subsets is possible for some special orientations of the strain ellipsoid relative to symmetry elements of the point group [3]. For example the oxygen ions in corundum (α–Al_2O_3, R3c) occupy a set of positions designated "e" by Wyckoff and located on diad axes. The other symmetry operations generate a set of six equivalent e-type positions per primitive cell. Tensile strain parallel to an a-axis retains the centers of symmetry, the diad axes parallel to, and the glide planes perpendicular to the direction of the tensile strain. The set of six initially equivalent oxygen positions then splits into one subset of four and another of two equivalent positions. A table of the mapping of special positions onto positions of subgroups has not yet been completed.

The authors thank Dr. J. D. H. Donnay for helpful discussions. This work was partially supported by the Advanced Research Projects Agency.

5. References

[1] J. B. Wachtman, Jr., and H. S. Peiser, Symmetry conditions for internal friction caused by jumping of point defects in crystals, Appl. Phys. Letters **1,** 20 (1962).

[2] A. S. Nowick and W. R. Heller, Elastic dipole and its role in anelasticity, Bull. Am. Phys. Soc. **7,** 224 (1962).

[3] J. B. Wachtman, Jr., H. S. Peiser, and E. P. Levine, Symmetry splitting of equivalent sites in oxide crystals and related mechanical effects, J. Research NBS **67A** (Phys. and Chem.) No. 4, 281–289 (1963).

[4] A. S. Nowick and W. R. Heller, Criteria for occurrence of internal friction due to point defects in crystals, Bull. Am. Phys. Soc. **8,** 236 (1963).

[5] M. J. Buerger, Crystallographic aspects of phase transformations, pp. 183–211 in Phase Transformations in Solids, edited by R. Smoluchowski, J. E. Mayer, and W. A. Weyl (John Wiley & Sons, New York, N.Y., 1951).

[6] J. O. Dimmock, Use of symmetry in the determination of magnetic structures, Phys. Rev. **130,** 1337 (1963).

[7] G. D. Watkins and J. W. Corbett, Defects in irradiated silicon. I. Electron spin resonance of the Si–A center, Phys. Rev. **121,** 1001 (1961).

[8] J. W. Corbett, G. D. Watkins, R. M. Chrenko, and R. S. McDonald, Defects in irradiated silicon. II. Infrared absorption of the Si–A center, Phys. Rev. **121,** 1015 (1961).

[9] F. R. N. Nabarro, Deformation of crystals by the motion of single ions, Report of a Conference on Strength of Solids, The Physical Society, London, 75–90 (1948).

[10] C. Herring, Diffusional viscosity of a polycrystalline solid, J. Appl. Phys. **21,** 437–45 (1950).

[11] P. Curie, Sur la symétrie dans les phénomènes physique, symétrie d'un champs électrique et d'un champs magnétique, J. de Phys. (3) **3,** 393 (1894).

[12] A. V. Shubnikov, On symmetry of vectors and tensors, Izv. ANSSSR, Ser. fiz. **13,** 347 (1949).

[13] V. A. Koptsik, On the superposition of symmetry groups in crystal physics, Kristallografiya **2,** 99 (1957); Soviet Physics Crystallography **2,** 95 (1957).

[14] Internationale Tabellen zur Bestimmung von Kristallstrukturen, Erster Band, Gruppentheoretische Tafeln xii+452 pp. Gebrueder Borntraeger, Berlin (Reprinted with corrigenda by Edwards Brothers, Inc., Ann Arbor, Mich. 1944).

[15] F. Ordway, Effect of homogeneous strain on crystal symmetry and the equivalence of postions for localized defects (unpublished).

[16] International Tables for X-ray Crystallography Vol. I. Edited by N. F. M. Henry and K. Lonsdale, Kynoch Press (1952).

(Paper 67A5-229)

JOURNAL OF RESEARCH of the National Bureau of Standards—A. Physics and Chemistry
Vol. 67A, No. 5, September–October 1963

High-Temperature Thermodynamic Functions for Zirconium and Unsaturated Zirconium Hydrides

Thomas B. Douglas

(June 12, 1963)

Giving greatest weight to the experimentally measured highest decomposition pressures and the enthalpies in one-phase fields, thermodynamically interconsistent integral and differential enthalpies (heat contents), heat capacities, entropies, and Gibbs free energies are derived for the crystalline one- and two-phase fields of the zirconium-hydrogen system for all stoichiometric compositions from Zr to $ZrH_{1.25}$ and over the temperature range 298.15 to 1,200 °K. These properties are derived in analytical form, and in most cases are represented by numerical equations, with tabulation for zirconium and H/Zr atom ratios of 0.25, 0.50, 0.57, 0.75, 1.00, and 1.25. Most of the unique phase-field boundaries which are consistent with the derived properties are located and are compared with those previously reported. In the Zr-H system the enthalpies are shown to relate certain properties at different compositions as well as at different temperatures. Some of the various data show good interconsistency, while others reveal discrepancies which are discussed critically.

Contents

		Page
1.	Introduction	403
2.	Thermodynamic preliminaries	405
2.1.	Conventions	405
2.2.	General thermodynamic relations	405
3.	Basic data used	406
4.	Alpha-zirconium	408
5.	The α and $(\alpha+\delta)$ phase fields	409
5.1.	Choice of the α-phase eutectoid point	409
5.2.	Enthalpy and related properties	409
5.3.	Hydrogen activity and the $\alpha/(\alpha+\delta)$ boundary	410
5.4.	Entropy	411
5.5.	Some partial molal properties with respect to zirconium	412
6.	The β (hydrogen-rich), $(\beta+\delta)$, and δ phase fields	413
6.1.	The β enthalpy and other properties ($x \geqq 0.57$)	413
6.2.	Procedure giving thermodynamic consistency	414
6.3.	Other β properties ($x \geqq 0.57$)	415
6.4.	Other $(\beta+\delta)$ properties	416
6.5.	Other δ properties	416
6.6.	Discussion of the δ phase-field boundaries	417
7.	The β (hydrogen-poor) and $(\alpha+\beta)$ phase fields	418
7.1.	Discussion of thermodynamic consistency	418
7.2.	The β properties ($x \leqq 0.57$)	419
7.3.	Derived $(\alpha+\beta)$ boundaries	421
7.4.	The $(\alpha+\beta)$ properties	421
8.	Tables of thermodynamic functions	423
9.	References	424

1. Introduction

Among transition-metal hydrides, the zirconium-hydrogen system has been studied very extensively in recent years because of the practical importance of and theoretical interest in the system. Zirconium hydrides are potentially valuable thermal-neutron moderators which in some cases can reach elevated temperatures without attaining excessive pressures. The wide ranges of composition, interrupted by lattice changes and marked miscibility gaps, offer a fruitful system for studying the structure of interstitial solid hydrides.

Experimental data on the thermodynamic and other physical properties of the system have been published by a number of investigators. Some of these have measured equilibrium pressures of hydrogen in certain ranges of temperature and composition [1, 2, 3, 4, 5, 6, 7, 8].[1] The rates of diffusion of hydrogen in the metal have been studied [9, 7]. X-ray [10] and neutron-diffraction [11] studies have given information on the zirconium- and hydrogen-atom spacings, respectively. Measurements have been made of thermal conductivity [12] and thermal expansion [12, 13, 14]. The enthalpies or heat capacities have been measured for the "saturated" composition ZrH_2 at low temperatures [15], and for several "unsaturated" compositions at high temperatures [16, 12]. Many of these data have served to outline the phase diagram of the system by a variety of methods, as the author showed in a previous paper [17]. Attention may also be called to some of the publications which have been particularly directed toward reviewing these properties, correlating them thermodynamically, and discussing their bearing on an interpretation of the structures of these phases [4, 15, 17, 18, 19].

In this paper is presented a consistent set of the common integral and partial thermodynamic functions of the zirconium-hydrogen system based on some of the aforementioned data. These functions were derived from the data without recourse to extra-thermodynamic considerations except, incidentally, such general and well-established ones as the laws of dilute solutions. The composition range covered is from Zr to $ZrH_{1.25}$, and the temperature range from 298.15 to 1,200 °K. (Though thermodynamic data are available for higher temperatures [1] and higher hydrogen contents [2,3,5,8,10], these were omitted from consideration because of their generally inferior precision or lack of agreement.) The coexistence of phases in equilibrium is in a sense accidental, and the theoretical interest in the system

[1] Figures in brackets indicate the literature references at the end of this paper.

therefore centers mainly in the properties of individual phases. But from a practical standpoint the equilibrium reproportionation of phases with temperature change of a given overall composition occurs fairly rapidly in some cases and is of interest; for this reason properties have been evaluated for two-phase as well as for one-phase regions. As will be pointed out, the available data show excellent interconsistency in some ranges of composition and temperature. In other regions considerable discrepancies were found which introduce considerable uncertainty into the adopted thermodynamic functions, particularly in two-phase regions. It will be evident that the requirement of thermodynamic consistency for a multicomponent system imposes an often unsuspected multitude of restrictions on the relations of the properties for neighboring compositions and temperatures, particularly near the center of the region under consideration in the phase diagram. This is true even for a two-component system which, like the present one, has a phase diagram which is only moderately complex.

The opinion has been expressed [6] that the purity of the zirconium used in the various experimental studies on the zirconium-hydrogen system was not sufficiently high for the results of a full thermodynamic analysis to be of any great significance. The present paper will illustrate that such an analysis can be rather laborious, and that, in the present case, it reveals numerous inconsistencies in the data which lend some weight to that opinion. Nevertheless, the author feels that only by a thermodynamic correlation of this type can the interconsistencies of the various data be tested, a better idea of their reliability be gained, additional properties of the system be derived, and the need for additional experimental work in certain areas be suggested. However, to the extent that the data are inconsistent, an adopted correlation will necessarily be somewhat arbitrary, particularly since the theoretical number of different ways to weight the numerous interrelated data is found to be quite large. In another sense, one can be arbitrary in deciding which borderline theoretical relationships are sufficiently valid to impose on the correlation.

The phase diagram of the zirconium-hydrogen system in the region treated in this paper is shown in figure 1. The symbols α, β, and δ[2] refer to single-phase regions where the zirconium lattice is close-packed hexagonal, body-centered cubic, and face-centered tetragonal,[3] respectively. The points shown on the diagram are those on phase-field boundaries as found by various investigators, and the solid boundaries are those to which the thermo-

[2] Some authors have used "γ" in place of "δ" in this system. "γ," however, has come to be used [3, 12] to designate a type of metastable phase in the system not discussed in the present paper.

[3] Face-centered cubic may here be considered a special case of face-centered tetragonal. By a simple rotation of crystal axes, the δ face-centered tetragonal lattice may be transformed into body-centered tetragonal (with a different unit cell), for comparison with the β body-centered cubic lattice.

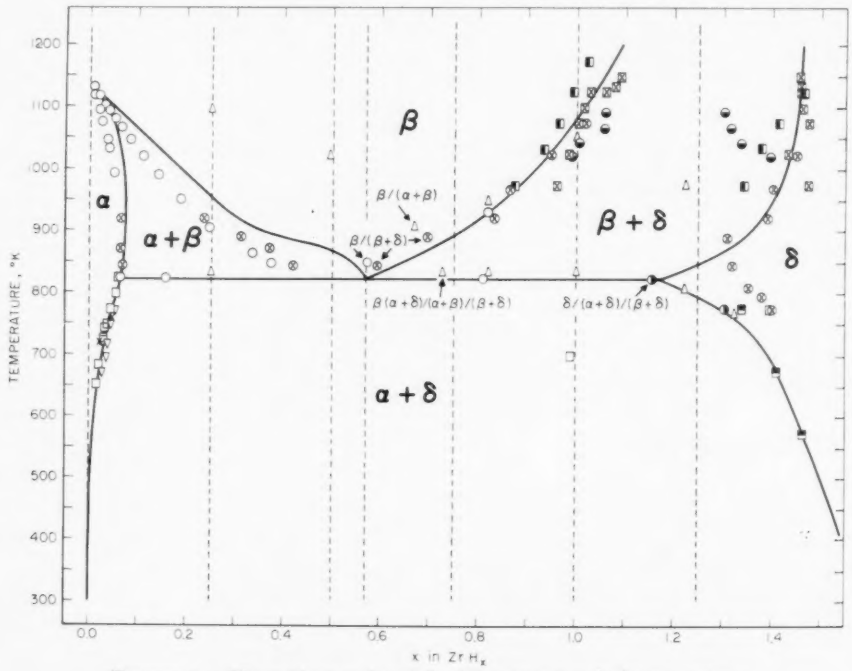

FIGURE 1. *Phase diagram (partial) of the zirconium-hydrogen system.*

(Observed points on phase boundaries are shown as follows. *From equilibrium hydrogen pressures:* ◒ Hall, Martin, and Rees [2]; □ Gulbransen and Andrew [4]; ⊠ Edwards, Levesque, and Cubicciotti [5]; ○ Ells and McQuillan [6]; X Mallett and Albrecht [7]; ⊗ LaGrange, Dykstra, Dixon, and Merten [8] *From hydrogen diffusion:* ▽ Schwartz and Mallett [9]. *From X-ray diffraction:* △ Vaughan and Bridge [10]. *From thermal expansion:* ◧ Beck [12]; ◓ Espagno, Azou, and Bastien [14]. *From enthalpy:* ◒ Douglas [17]. The interconsistent thermodynamic functions formulated in this paper correspond to the solid-curve boundaries, and are tabulated along the dotted lines.)

dynamic properties adopted in this paper correspond. The majority of these properties are presented in analytical form for the continuous ranges of temperature and composition, and are tabulated along the dotted vertical lines shown in the figure.

2. Thermodynamic Preliminaries

2.1. Conventions

The unit of energy used throughout is the defined thermochemical calorie (=4.1840 j), and all temperatures are in deg K. All extensive properties of a zirconium hydride are evaluated for "one mole," defined as containing a total of 1 g-atom of Zr and x g-atoms of H,[4] even when one mole so defined is composed of two or more phases in equilibrium. The components are taken to be alpha-zirconium (at *all* temperatures, to preserve continuity into the small 64° temperature interval covered where beta-zirconium is more stable) and "normal" molecular hydrogen in the usual standard state of the ideal gas at 1 atm.[5]

The symbols in common usage have been adopted so far as possible. Those not specifically defined are:

a_i: Thermodynamic activity of component i. (a_2 is taken equal to the equilibrium pressure of H_2(g) in atm.)

b, c, $b+c$: Generalized notation for particular one- or two-phase fields. (In the absence of specific designation, the phase field is implied as any one, or the particular one under discussion.)

C_p: Heat capacity at constant pressure and constant overall composition (cal mole^{-1} deg K^{-1}).

f: "Of formation" (usually from the components in their standard states).

G: Absolute Gibbs free energy (cal mole^{-1}).

H: Absolute enthalpy (heat content) (cal mole^{-1}).

H': "Intrinsic enthalpy" (ΔH of the reaction of eq (30)).

H_2(g): Hydrogen gas.

i (subscript): A particular component (either).

ln: Natural logarithm.

log: Logarithm to the base 10.

R: The molar gas constant (=1.98725 cal mole^{-1} deg K^{-1}).

S: Absolute entropy (cal mole^{-1} deg K^{-1}).

T: Absolute temperature (deg K, Int. Temp. Scale of 1948).

x: Atoms of H per atom of Zr (in the overall composition when two phases are present).

x_b and x_c: Define the compositions of the two coexistent phases ZrH_{x_b} and ZrH_{x_c} which lie on the phase-field boundaries of the $(b+c)$ field.

Y: Generalized notation for one of H, C_p, S, or G.

$\overline{Y}_i$: Partial molal Y with respect to component i.

α, β, δ: Types of single phases of ZrH_x. (See fig. 1.)

$(\alpha+\beta)$, etc.: Two-phase field, or an overall composition lying therein.

$\alpha/(\alpha+\beta)$, etc.: Boundary between the α and $(\alpha+\beta)$ fields, etc.

1 (subscript): The component zirconium, Zr.

2 (subscript): The component molecular hydrogen, H_2.

A numerical subscript or superscript other than 1 or 2: When $\leqq 2$, a particular value of x; when >2, a particular value of T. (The absence of such subscripts implies general values of x and T, or a particular set under discussion.)

° or °(superscript): In the standard state (see text); deg temperature.

2.2. General Thermodynamic Relations

Several well-known thermodynamic relations frequently used in subsequent derivations or calculations are assembled here. These have been adapted to the specialized definition of one mole of Zr, H_2, and ZrH_x stated above.

Total properties are often conveniently derived using

$$C_p^\circ=[\partial(H^\circ-H^\circ_{298.15})/\partial T]_x; \tag{1}$$

$$(\partial S^\circ/\partial T)_x=C_p^\circ/T; \tag{2}$$

$$-(G^\circ-H^\circ_{298.15})/T=S^\circ-(H^\circ-H^\circ_{298.15})/T. \tag{3}$$

(Equation (3) has been used throughout this paper to obtain the free-energy function.) A relation similar to eq (3) applies to the relative partial molal properties:

$$(\overline{G}_i-G_i^\circ)/T=(\overline{H}_i-H_i^\circ)/T-(\overline{S}_i-S_i^\circ). \tag{4}$$

The total and partial properties are related by

$$Y^\circ=\overline{Y}_1+\tfrac{1}{2}x\overline{Y}_2 \tag{5}$$

and

$$\overline{Y}_2=2(\partial Y^\circ/\partial x)_T, \tag{6}$$

integration of the latter between two compositions x' and x'' giving

$$Y^\circ_{x''}-Y^\circ_{x'}=\frac{1}{2}\int_{x'}^{x''}\overline{Y}_2 dx. \tag{7}$$

[4] This convention seemed more logical than one based on mole fractions, since it is probable that hydrogen (as atoms) enters the zirconium lattices interstitially (with vacancies) instead of substitutionally.

[5] By this convention one mole of ZrH_x thus contains one mole of Zr and $\frac{1}{2}x$ moles of the component H_2. The conversion to standard states involving β-Zr and atomic H could of course readily be made if desired.

From eqs (5) and (6)

$$\overline{Y}_1 = Y^\circ - x(\partial Y^\circ/\partial x)_T. \tag{8}$$

The Gibbs-Duhem equation takes the form

$$[\partial(\overline{Y}_1 - Y_1^\circ)/\partial x]_T + \tfrac{1}{2}x[\partial(\overline{Y}_2 - Y_2^\circ)/\partial x]_T = 0. \tag{9}$$

By the definition of activity

$$(\overline{G}_i - G_i^\circ)/T = R \ln a_i. \tag{10}$$

The variation of the partial molal free energy with temperature is given by

$$\left[\partial\left(\frac{\overline{G}_i - G_i^\circ}{T}\right)/\partial T\right]_x = -(\overline{H}_i - H_i^\circ)/T^2. \tag{11}$$

From eq (5) follows the standard heat, entropy, and free energy of formation at any temperature. Since

$$\Delta Yf^\circ = Y^\circ - (Y_1^\circ + \tfrac{1}{2}xY_2^\circ), \tag{12}$$

we have

$$\Delta Hf^\circ = (\overline{H}_1 - H_1^\circ) + \tfrac{1}{2}x(\overline{H}_2 - H_2^\circ); \tag{13}$$

$$\Delta Sf^\circ = (\overline{S}_1 - S_1^\circ) + \tfrac{1}{2}x(\overline{S}_2 - S_2^\circ); \tag{14}$$

$$\Delta Gf^\circ = (\overline{G}_1 - G_1^\circ) + \tfrac{1}{2}x(\overline{G}_2 - G_2^\circ). \tag{15}$$

The molal enthalpy, heat capacity, entropy, or free energy in a two-phase field is the sum of those of the component (or "terminal") phases:

$$Y_x^{b+c} = [(x_c - x)/(x_c - x_b)]Y^b + [(x - x_b)/(x_c - x_b)]Y^c. \tag{16}$$

In the present case it is particularly simple to relate two common alternative conditions determining this separation into the two terminal phases. One commonly stated obvious condition is that a straight line be tangent to the *continuous* free-energy isotherm at x_b and x_c and lie lower than the isotherm between x_b and x_c. Hence

$$(dG/dx)_{x_b} = (dG/dx)_{x_c}, \tag{17}$$

and hence from eq (6)

$$(\overline{G}_2)_{x_b} = (\overline{G}_2)_{x_c} \equiv \overline{G}_2. \tag{18}$$

From eqs (5) and (18)

$$G_{x_b} = (\overline{G}_1)_{x_b} + \tfrac{1}{2}x_b\overline{G}_2 \tag{19}$$

and

$$G_{x_c} = (\overline{G}_1)_{x_c} + \tfrac{1}{2}x_c\overline{G}_2, \tag{20}$$

whose difference gives

$$[G_{x_c} - G_{x_b}]/[x_c - x_b] = [(\overline{G}_1)_{x_c} - (\overline{G}_1)_{x_b}]/[x_c - x_b] + \tfrac{1}{2}\overline{G}_2. \tag{21}$$

From the condition of tangency and eq (6) the first and third terms of eq (21) are equal, and hence

$$(\overline{G}_1)_{x_b} = (G_1)_{x_c}. \tag{22}$$

Equations (18) and (22) are the more commonly stated conditions for phase coexistence. The condition that the tangent line lie lower than the metastable free-energy curve between requires that at each point of tangency d^2G/dx^2 be positive, and from equation (6) this is true if at each of these points $d\overline{G}_2/dx$ is positive—i.e., if the activity of hydrogen in each phase increases isothermally with increasing hydrogen content.

3. Basic Data Used

The direct measurements of the equilibrium pressures of hydrogen for the system extend from 650 to 1,373 °K and over the composition range from near $x=0$ to $x>1.7$. These data are sufficient to determine a set of the common energetic thermodynamic properties of the system in this range. However, these sets of data overlap considerably and with varying degrees of disagreement. In addition, those of the precise enthalpy data which may be considered valid, while they alone neither establish activities nor their temperature derivatives, do impose relations among the activity values at a given composition and different temperatures and also, as will be presently shown, among the temperature derivatives of activity for different compositions.

Enthalpy measurements relative to $T=273$ were made by Douglas and Victor [16] (usually at temperatures spaced at 50- or 100-deg intervals) up to $T=1{,}173$ for the compositions $x=0$, 0.324, 0.556, 0.701, 0.999, and 1.071. These measurements were all made by the drop method, and in all cases involved fairly rapid cooling in the low-temperature two-phase ($\alpha+\delta$) field, where composition equilibrium corresponds to phase reproportionation (see fig. 1). However, evidence will be shown in section 5 that phase equilibrium was approximately maintained in this field in these measurements. It would also be expected that composition equilibrium was attained for temperature intervals beginning in the one-phase field involved (the β field), and this was indicated by the high precision, regularity, and freedom from hysteresis found for most of these particular measurements (see sec. 6).

In view of the above facts, it was decided to construct the adopted consistent set of thermodynamic functions for the system largely by giving greatest weight to the hydrogen-activity data at the higher temperatures and to use the enthalpy data considered valid in order to extend the properties so derived to other temperatures and other compositions. The measurement of the highest equilibrium pressures is ordinarily subject to the smallest percentage errors, and this is often true with respect to the effects of small amounts of interfering impurities in the samples.

The hydrogen-activity data so chosen as a basis were those reported graphically by LaGrange, Dyk-

stra, Dixon, and Merten [8] at $T=1{,}073.2$ and 13 compositions ($x=0.05$ to 1), and those reported in tabular form by Edwards, Levesque, and Cubicciotti [5] for values of x of 0.650, 0.733, 0.815, and 0.894 and at 8 temperatures over the range $T=1{,}023$ to 1,173. (These points all lie in the β field.) The values of the latter authors were first all reduced to $T=1{,}073.2$ by using their smoothed temperature coefficients in the usual way. A reasonably good fit to these data was found to be given by

$$a_{2\,(1073.2)}^{\beta}=0.06084x^{1.36}+0.11251x^{8.33}, \qquad (23)$$

or

$$[(\overline{G}_2^{\beta}-G_2^{\circ})/T]_{1073.2}=6.22313\log x +4.5758\log(1+1.8493x^{6.97})-5.56334. \qquad (24)$$

The agreement with the values fit (which vary from 0.002 to 0.16 atm) is shown in table 1; over the

TABLE 1. *Deviation from eq (23) (or (24)) of observed hydrogen activities of β-ZrH_x at 1,073.2 °K*

Reference	x	$\frac{a_2(\text{obs})-a_2(\text{calcd})}{a_2(\text{obs})}\times 100$
[8]	0.05	+43
[8]	.11	−12
[8]	.19	0
[8]	.27	0
[8]	.37	−1
[8]	.46	0
[8]	.55	+1
[8]	.64	0
[5]	.650	−4
[5]	.733	0
[8]	.76	0
[5]	.815	+4
[8]	.87	0
[5]	.894	+5
[8]	.92	−4
[8]	.96	0
[8]	1.00	−8

range $x=0.19$ to 1 it averages 2 percent, which is within the precision of the measurements. Calculations of cycles of entropy and zirconium-activity which are presented in section 7 depend in part on the accuracy of eq (23) (or (24)), and show excellent consistency.

It is appropriate to examine eq (23) in the light of the fact that several observers have found a proportionality, at constant temperature and only moderately high hydrogen concentrations, between the activity a_2 and the *square* of the hydrogen concentration ("Sieverts' law"), which corresponds to an activity coefficient of *atomic* hydrogen independent of composition. Up to $x=0.5$ the last term in eq (23) contributes less than 2 percent of the total, so that the power of x is not 2 but closer to 1. Sieverts and Roell [1] measured hydrogen-pressure isotherms for beta-zirconium at 1,073° and 1,373 °K, and though their data show inferior precision compared with that of the more recent measurements fitted above, their results show an approximate proportionality of a_2 to x^2 at the higher temperature but not at the lower. It is easy to show, by substituting from eq (10) into eq (11), replacing a_2 by a single term proportional to x^n, and then differentiating partially with respect to x, that the power n is independent of T if and only if $(\overline{H}_2-H_2^{\circ})$ does not vary with x. It will in fact be found that although $(\overline{H}_2-H_2^{\circ})$ near 1,073 °K is approximately independent of x at the higher values of x, it is far from being so for $x<0.5$. The sign and magnitudes of $\partial(\overline{H}_2-H_2^{\circ})/\partial x$ in the latter region correspond to an approach to the x^2 law as the temperature rises, but for lack of enough precise data, no serious effort was made to interpolate the pressure data over the range 1,073 to 1,373 °K.

The manner of using the enthalpy data will next be considered. In the first place, it is apparent from figure 1 that in all these enthalpy measurements for the five hydride compositions the sample was cooled into the $(\alpha+\delta)$ field at 298 °K. In section 5 the following value will be derived (from eq (90)):

$$(\overline{H}_1^{\alpha+\delta}-H_1^{\circ})_{298}=4. \qquad (25)$$

This value is very small because at this temperature the composition range of the α field is very small. We may now consider $(\overline{H}_2^{\alpha+\delta}-H_2^{\circ})_{298}$. Applying eq (6) to the absolute enthalpy at any temperature and also at 298 °K, and subtracting the two, one may write

$$(\overline{H}_2-H_2^{\circ})=2[\partial(H^{\circ}-H_{298}^{\circ(\alpha+\delta)})/\partial x] +(\overline{H}_2^{\alpha+\delta}-H_2^{\circ})_{298}-(H_2^{\circ}-H_{2(298)}^{\circ}). \qquad (26)^{6}$$

The application of eq (6) to eq (16) shows that relative partial molal functions in a two-phase field at a given temperature (including $(\overline{H}_2^{\alpha+\delta}-H_2^{\circ})_{298}$) are independent of x. Consequently, if data at one temperature and composition are available for evaluating $(\overline{H}_2^{\alpha+\delta}-H_2^{\circ})_{298}$ from eq (26), then the same equation, with this value substituted, may be used to evaluate $(\overline{H}_2-H_2^{\circ})$ at other temperatures and compositions where $[\partial(H^{\circ}-H_{298}^{\circ})/\partial x]_T$ can be evaluated by suitable interpolation.

Plots of the hydrogen-pressure data of Edwards et al. [5] for the four compositions from $x=0.650$ to $x=0.894$, used above, gave without trend almost identical values which averaged $(\overline{H}_2^{\beta}-H_2^{\circ})_{1123}=-40{,}500$. Ells and McQuillan [6] measured α_2^{β} at one high concentration of hydrogen ($x=0.66$) from approximately 875 to 1,035 °K, leading to a value which when corrected to 1,123 °K by the enthalpy data gave $(\overline{H}_2^{\beta}-H_2^{\circ})_{1123}=-37{,}500$. A weighted mean was adopted:

$$(\overline{H}_2^{\beta}-H_2^{\circ})_{1123,0.7}=-39{,}500. \qquad (27)$$

For many calculations in this paper the relative enthalpy of molecular hydrogen gas has been computed from the empirical equation

$$H_2^{\circ}-H_{2(298)}^{\circ}=6.660T +2.678(10^{-4})T^2-12000T^{-1}-1969, \qquad (28)$$

which between 298 and 1,200 °K agrees within an

[6] It as assumed in eq (26) and related eqs (30–36, 39, 40) that the values of x lie in the $(\alpha+\delta)$ field at 298 °K.

average of about 3 cal mole^{-1} with the accurate values [20]. Equation (28) gives $H^\circ_{2(1123)}-H^\circ_{2(298)}=5837$. From the enthalpy of the pertinent β zirconium hydrides as formulated in section 6 (eq (92)), $2[\partial(H^\circ_{1123}-H^\circ_{298})/\partial x]=7815$. Using eq (27) and these values, eq (26) gives

$$(\overline{H}_2^{\alpha+\delta}-H^\circ_2)_{298}=-41{,}478. \quad (29)$$

Equation (29) has an uncertainty of at least 1,000 cal mole^{-1}, but the additional significant figures serve to maintain consistency in many of the subsequently derived values.

An equation equivalent to eq (26) in integral form may be derived which is more general because it indicates the energy difference between two zirconium hydrides where both x and T may differ finitely. If we consider a system of 1 g-atom of zirconium and 2 of hydrogen, and arbitrarily define the reference state as the two free elements in their standard states at a temperature of 298 °K, the increase in enthalpy when the temperature or chemical composition or both change may be called the "intrinsic enthalpy" (H').[7] The process is

$$\mathrm{Zr}(298\ ^\circ\mathrm{K})+\mathrm{H_2(g)}(298\ ^\circ\mathrm{K})=\mathrm{ZrH}_x(T)+(1-\tfrac{1}{2}x)\mathrm{H_2(g)}(T), \quad (30)$$

and

$$H'=H^\circ+(1-\tfrac{1}{2}x)H^\circ_2-H^\circ_{1(298)}-H^\circ_{2(298)}. \quad (31)$$

From eq (13)

$$H^{\circ(\alpha+\delta)}_{298}-H^\circ_{1(298)}-\tfrac{1}{2}xH^\circ_{2(298)}=(\overline{H}_1^{\alpha+\delta}-H^\circ_1)_{298}+\tfrac{1}{2}x(\overline{H}_2^{\alpha+\delta}-H^\circ_2)_{298}. \quad (32)$$

Adding eqs (31) and (32),

$$H'=(H^\circ-H^{\circ(\alpha+\delta)}_{298})+(\overline{H}_1^{\alpha+\delta}-H^\circ_1)_{298}+\tfrac{1}{2}x(\overline{H}_2^{\alpha+\delta}-H^\circ_2)_{298}+(1-\tfrac{1}{2}x)(H^\circ_2-H^\circ_{2(298)}). \quad (33)$$

This result may be applied to two compositions ZrH'_x and ZrH''_x at T' and T'' respectively. Thus for

$$\mathrm{ZrH}_{x'}(T')+\tfrac{1}{2}(x''-x')\mathrm{H_2(g)}(T')=\mathrm{ZrH}_{x''}(T'') \quad (34)$$

eq (33) leads to

$$\triangle H=(H^\circ-H^{\circ(\alpha+\delta)}_{298})_{x''}-(H^\circ-H^{\circ(\alpha+\delta)}_{298})_{x'}+\tfrac{1}{2}(x''-x')(\overline{H}_2^{\alpha+\delta}-H^\circ_2)_{298}-\tfrac{1}{2}(x''-x')(H^\circ_{2(T')}-H^\circ_{2(298)}). \quad (35)$$

In equation (26), (33), or (35), $(H^\circ_2-H^\circ_{2(298)})$ and $(\overline{H}_2^{\alpha+\delta}-H^\circ_2)_{298}$ can be evaluated from eqs (28) and (29) respectively. Partial differentiation of eq (33) with respect to x and substitution from eq (6) show that

$$(\partial H'/\partial x)_T=\tfrac{1}{2}(\overline{H}_2-H^\circ_2). \quad (36)$$

With the help of eq (32), eq (5) may be put into convenient form for relating the total and partial molal enthalpy and free-energy functions in the form in which they are expressed in this paper, as well as immediately giving the standard heat and free energy of formation of ZrH_x at temperature T. In these two cases eq (5) becomes respectively

$$H^\circ=\overline{H}_1+\tfrac{1}{2}x\overline{H}_2 \quad (37)$$

and

$$G^\circ=\overline{G}_1+\tfrac{1}{2}x\overline{G}_2. \quad (38)$$

Subtracting eq (37) from eq (32) (and remembering eq (13)) gives

$$\triangle Hf^\circ/T=(\overline{H}_1-H^\circ_1)/T+\tfrac{1}{2}x(\overline{H}_2-H^\circ_2)/T=(H^\circ-H^{\circ(\alpha+\delta)}_{298})/T-(H^\circ_1-H_{1(298)})/T-\tfrac{1}{2}x(H^\circ_2-H^\circ_{2(298)})/T+(\overline{H}_1^{\alpha+\delta}-H^\circ_1)_{298}/T+\tfrac{1}{2}x(\overline{H}_2^{\alpha+\delta}-H^\circ_2)_{298}/T, \quad (39)$$

whereas subtracting eq (38) from eq (32) (and remembering eq (15)) gives

$$\triangle Gf^\circ/T=(\overline{G}_1-G^\circ_1)/T+\tfrac{1}{2}x(\overline{G}_2-G^\circ_2)/T=(G^\circ-H^{\circ(\alpha+\delta)}_{298})/T-(G^\circ_1-H^\circ_{1(298)})/T-\tfrac{1}{2}x(G^\circ_2-H^\circ_{2(298)})/T+(\overline{H}_1^{\alpha+\delta}-H^\circ_1)_{298}/T+\tfrac{1}{2}x(\overline{H}^{\alpha+\delta}-H^\circ_2)_{298}/T. \quad (40)$$

4. Alpha-Zirconium

Pure metallic zirconium undergoes a first-order transformation from the hexagonal (α) to the high-temperature body-centered-cubic (β) lattice. The transformation temperature has been given values from 1,135 °K [21] to 1,143 °K [22, 23]. The value adopted in this paper is:

Transformation temperature of Zr=1,136 °K. (41)

Measurements of the low-temperature heat capacity of zirconium have been reported by Todd (53 to 297 °K) [24]; Skinner and Johnston (14 to 298 °K) [25]; Estermann, Friedberg, and Goldman (1.8 to 4.2 °K) [26]; Wolcott (1.2 to 20 °K) [27]; and Burk, Estermann, and Friedberg (20 to 200 °K) [28]. The heat capacities of Todd and those of Burk, Estermann, and Friedberg are in close agreement, while those obtained above 130 °K by Skinner and Johnston are about 1 percent lower. The enthalpy at high temperatures has been measured by Mixter and Dana (273 to 373 °K) [29]; Jaeger and

[7] In an earlier paper [17] the author defined an equivalent quantity and called ti the "adjusted heat content."

Veenstra (294 to 1,074 °K) [30]; Coughlin and King (298 to 1,371 °K) [31]; Redmond and Lones (273 to 1,309 °K) [32]; and Douglas and Victor (273 to 1,173 °K) [16]. Furukawa and Reilly [33] have carefully analyzed the low-temperature data and have derived a table of thermodynamic functions from 0 to 300 °K whose heat capacities approach those of Douglas and Victor at and above 300 °K. The heat-capacity curve of Douglas and Victor joins smoothly with that of Todd, but not with that of Skinner and Johnston. At 250 °K Furukawa and Reilly's table gives (in the notation of sec. 2)

$$(C_p^\circ)_{1(250)}=5.969 \tag{42}$$

and

$$(S^\circ)_{1(250)}=8.219. \tag{43}$$

Using a sample of zirconium containing a total of 0.09 percent by weight of impurities (0.015% Hf, 0.03% Fe, 0.02% C, 0.005% N, and 0.006% O), Douglas and Victor [16] precisely measured the enthalpy, relative to 273 °K, at 100-deg intervals up to 1,073 °K, and also at 1,123° and at 5-deg intervals from 1,143 to 1,173 °K. The following equation (in the notation of sec. 2) was derived to fit their data for the α form and to satisfy eq (42):

$$H_1^\circ-H_{1(298.15)}^\circ=4.0504T+5.3113\ (10^{-3})\ T^2$$
$$-4.4945\ (10^{-6})\ T^3+1.6785\ (10^{-9})\ T^4-1573.9. \tag{44}$$

The mean observed values differ from this equation by the amounts shown in table 2.

TABLE 2. *Deviation of eq (44) from observed values of α-zirconium*

Temperature	$H_1^\circ-H_{1(273.2)}^\circ$ Mean observed	Mean observed—calculated enthalpy
°K	cal mole^{-1}	cal mole^{-1}
273.2	(0)	(0)
373.2	630	+1
473.2	1284	−9
573.2	1989	+8
673.2	2686	−1
773.2	3409	0
873.2	4147	−2
973.2	4923	+9
1073.2	5708	−7
1123.2	6133	+1

For the entropy of α-zirconium, eq (43) and (44) give

$$S_1^\circ=9.32645\ \log\ T+1.06226\ (10^{-2})\ T$$
$$-6.74175(10^{-6})T^2+2.238\ (10^{-9})\ T^3-16.4145. \tag{45}$$

The thermodynamic properties of β-zirconium will be evaluated in section 7 in connection with the β field of the Zr-H system, of which it forms a part.

5. The α and $(\alpha+\delta)$ Phase Fields

The thermodynamic properties of the α and $(\alpha+\delta)$ phase fields as derived in this paper are closely related, and will be discussed together. Other parts of the Zr-H system will be similarly treated in the following two sections.

5.1. Choice of the α-Phase Eutectoid Point

Values for the eutectoid temperature, where the α, β, and δ phases of fixed compositions coexist in equilibrium, are in fair agreement as reported by various investigators. Vaughan and Bridge [10] gave 833°±10 °K, but the values most commonly reported have been closer to that of Ells and McQuillan [6], which is 820°±2 °K. In an enthalpy investigation [16], four samples transformed somewhere between 823 and 833 °K, and one sample somewhere between 813 and 823 °K. The exact temperature is probably uncertain by a few degrees owing to some sluggishness in the (all solid) transformation, but for the purposes of the calculations of this paper the following value has been adopted:

$$\text{Eutectoid temperature}=820\ °\text{K}. \tag{46}$$

Another constant evaluated empirically here is the eutectoid composition of the α phase. As indicated in figure 1, the $\alpha/(\alpha+\delta)$ and $\alpha/(\alpha+\beta)$ boundaries of different investigators [4,6,7,8,9] are in fairly good agreement. On the basis of these results the composition at 820°K selected here is

$$x_\alpha(\text{eutectoid})=0.0650. \tag{47}$$

The equilibrium properties of the $(\alpha+\delta)$ field are of course the appropriate combinations of the properties of the component phases along the two phase-field boundaries, which if known can be used to derive the two-phase-field properties. This procedure has been followed for the $(\alpha+\beta)$ field (sec. 7). If, however, more complete data are available in the two-phase field, these may be used to derive its properties even without knowing the boundaries of the field. In the present case some hydrogen-pressure data are available for the higher temperatures of the field, but not at the lower temperatures near room temperature, mainly because the equilibrium pressures are negligibly small.

5.2. Enthalpy and Related Properties

The enthalpy measurements on five well-spaced compositions in the $(\alpha+\delta)$ field [16,17] show good precision and good consistency, and will be used as the basis for extending other properties below the eutectoid temperature. These data show not only the linearity with x of isotherms expected for a two-phase field [16,17], but show also other evidence, soon to be presented, that phase equilibrium was approximately maintained during the rather rapid cooling involved in the measurements.[8] Representing an isotherm of enthalpy by

$$(H^\circ-H_{298.15}^\circ)^{\alpha+\delta}=A+Bx, \tag{48}$$

the values of A and B (referred to the experimental base temperature of 273.15 °K) were determined

[8] Even if the eutectoid temperature is really as low as 820 °K (eq (46)), the $(\alpha+\delta)$ enthalpy isotherm at 823 °K is not to be interpreted as invalid, since the samples were not heated above 823 °K in these measurements and the β phase could easily have failed to appear.

from the data by the least-square method, and are given in table 3 referred to the experimental base temperature 273.15 °K—i.e., for the equation

$$(H^\circ - H^\circ_{273.15})^{\alpha+\delta} = A' + B'x. \quad (49)$$

TABLE 3. *Isotherms of enthalpy in the $(\alpha+\delta)$ field of Zr–H*

(In cal mole^{-1} of ZrH_x)

T	A' in eq (49)	B' in eq (49)
°K		
273.15	0	0
373.15	637.5	114.0
473.15	1305.6	356.5
573.15	2041.8	694.9
673.15	2849.4	1039.7
773.15	3794.2	1410.0
823.15	4277.0	1705.8

The following equations were derived to represent A and B in eq (48) as functions of temperature (T=273 to 823)[9]:

$$A = 33.91211T - 5.051385(10^{-2})T^2 + 4.76757(10^{-5})T^3 - 1.603496(10^{-8})T^4 + 1.373028(10^{6})T^{-1} - 9.2289104(10^{7})T^{-2} - 10324.4; \quad (50)$$

$$B = 3.05464T + 5.5805(10^{-4})T^2 - 7.098895(10^{-5})T^3 + 2.608868(10^{-7})T^4 - 3.393270(10^{-10})T^5 + 1.520416(10^{-13})T^6 - 447.8. \quad (51)$$

From eqs (50) and (51), the constants in eqs (48) and (49) are related by

$$A' = A + 158.1; \quad (52)$$

$$B' = B + 19.0. \quad (53)$$

From eqs (1), (6), (8), and (48)

$$(\overline{C}_p)_1^{\alpha+\delta} = dA/dT \quad (54)$$

and

$$(\overline{C}_p)_2^{\alpha+\delta} = 2dB/dT. \quad (55)$$

From eqs (26), (28), (29), (48), and (51)

$$(\overline{H}_2^{\alpha+\delta} - H_2^\circ)/T = -40404 - 0.55072T + 8.483(10^{-4})T^2 - 1.419779(10^{-4})T^3 + 5.217736(10^{-7})T^4 - 6.78654(10^{-10})T^5 + 3.040832(10^{-13})T^6 + 12000T^{-1}. \quad (56)$$

The same properties were next formulated in the α field. Apparently no measurements of enthalpy are available except for zirconium metal (sec. 4). However, the α phases are all low in hydrogen (fig. 1), and the laws of dilute solutions should be applicable to good approximation. This involves the assumption that the enthalpy and heat-capacity isotherms are linear with x. It will presently be shown that at 273.15 °K the α field is extremely narrow; consequently, it is convenient to assume that at this temperature α-Zr is in the $(\alpha+\delta)$ field. At 820 °K eq (44) then gives

$$(H^{\circ(\alpha)}_{820} - H^{\circ(\alpha+\delta)}_{273.15})_{x=0} = 3753.0, \quad (57)$$

while eqs (47), (48), (50), (51), (52), and (53) give

$$(H^{\circ(\alpha)}_{820} - H^{\circ(\alpha+\delta)}_{273.15})_{0.0650} = 4359.8. \quad (58)$$

Thus, using eqs (52) and (53),

$$H^{\circ(\alpha)}_{820} - H^{\circ(\alpha+\delta)}_{298.15} = 3594.9 + 9316.4x. \quad (59)$$

By assuming the hydrogen vibration frequency in ZrH_2 found by Flotow and Osborne [15], 1190 cm^{-1}, the following empirical equations were derived:

$$T = 298-820: (\overline{C}_p)_2^\alpha = -5.9446 + 2.7364(10^{-2})T - 1.185(10^{-5})T^2 \quad (60)$$

$$T = 820-1136: (\overline{C}_p)_2^\alpha = 4.836 + 4.5(10^{-3})T \quad (61)$$

Since these are independent of x, by eqs (9) and (8) $(\overline{C}_p)_1^\alpha$ is identical with the heat capacity of α-Zr (from eq (44)). When the latter and eq (60) (or (61)) are substituted into eq (5) and then integrated to satisfy eq (59), we have:

$$T = 298-820: (H^{\circ(\alpha)} - H^{\circ(\alpha+\delta)}_{298.15})/T = 4.0504 + 5.3113(10^{-3})T - 4.4945(10^{-6})T^2 + 1.6785(10^{-9})T^3 - 1578.5/T + [8243.0/T - 2.9723 + 6.841(10^{-3})T - 1.975(10^{-6})T^2]x; \quad (62)$$

$$T = 820-1136: (H^{\circ(\alpha)} - H^{\circ(\alpha+\delta)}_{298.15})/T = 4.0504 + 5.3113(10^{-3})T - 4.4945(10^{-6})T^2 + 1.6785(10^{-9})T^3 - 1578.5/T + [6577.4/T + 2.418 + 1.125(10^{-3})T]x. \quad (63)$$

The application of eqs (26), (28), and (29) to eqs (62) or (63) gives respectively:

$$T = 298-820: (\overline{H}_2^\alpha - H_2^\circ)/T = -23005/T - 12.6085 + 1.3414(10^{-2})T - 3.950(10^{-6})T^2; \quad (64)$$

$$T = 820-1136: (\overline{H}_2^\alpha - H_2^\circ)/T = -26336/T - 1.828 + 1.982(10^{-3})T. \quad (65)$$

5.3. Hydrogen Activity and the $\alpha/(\alpha+\delta)$ Boundary

The thermodynamic functions $(\overline{G}_2 - G_2^\circ)/T$, giving (by eq (10)) the hydrogen equilibrium pressures,

[9] Equation (51) agrees exactly with table 3. However, owing to a small computation error, eq (50) differs slightly from the table above 473 °K (by an average of 7 cal mole^{-1}, which is within the precision of the data).

will now be formulated for the α and $(\alpha+\delta)$ fields. As discussed in section 3, these will be based on eq (23) and the pertinent thermal properties. The invariant eutectoid pressure derived in section 6 is the $(\alpha+\delta)$ value at that temperature:

$$a_{2(820)}^{\alpha+\delta}=1.0442(10^{-4}). \quad (66)$$

It is reasonable to assume that in the dilute α phases the activity of atomic hydrogen is proportional to its concentration at any temperature, and hence a_2^α is proportional to x^2, as has been observed [4]. Then from eqs (10) and (66)

$$[(\overline{G}_2^{\alpha+\delta}-G_2^\circ)/T]_{820}=-18.2174, \quad (67)$$

and, using eq (47),

$$[(\overline{G}_2^{\alpha}-G_2^\circ)/T]_{820}=9.1517\log x-7.3536. \quad (68)$$

Substitution of eq (56) into eq (11) and integrating to satisfy eq (67),

$$(\overline{G}_2^{\alpha+\delta}-G_2^\circ)/T=-40{,}403.48/T+1.26796\log T -8.4829(10^{-4})T+6000/T^2+7.098842(10^{-5})T^2 -1.739232(10^{-7})T^3+1.696622(10^{-10})T^4 -6.08162(10^{-14})T^5+22.0491. \quad (69)$$

The similar use of eqs (11), (64), and (68) gives

$$T=298\text{–}820:\ (\overline{G}_2^{\alpha}-G_2^\circ)/T=9.1517\log x -23005/T+29.02815\log T-1.34113(10^{-2})T +1.97447(10^{-6})T^2-54.2116, \quad (70)$$

while eqs (11), (65), and (68) give

$$T=820\text{–}1136:\ (\overline{G}_2^{\alpha}-G_2^\circ)/T=9.1517\log x-26336/T +4.20976\log T-1.98179(10^{-3})T+14.1221. \quad (71)$$

The $\alpha/(\alpha+\delta)$ boundary at 820 °K has been required to have a composition of $x_a=0.0650$, but no other restrictions on it have been explicitly imposed. The boundary compositions at other temperatures can be found by equating either the hydrogen activities (eqs (69) and (70)) or the enthalpies (eqs (48), (50), (51), (62)) in the two fields. The results by these two methods are compared in table 4.[10] The agreement for the two methods above 400 °K is rather striking, and gives strong support to the assumption made earlier that in the α field a_2 is proportional to x^2. If this assumption is correct, the agreement in the table indicates that phase equilibrium, especially with respect to the $\alpha/(\alpha+\delta)$ boundary, was approximately maintained in the enthalpy measurements in the $(\alpha+\delta)$ field, a result

[10] The values in the second column of the table are sensitive to the power of x assumed. With the assumption of the 820 °K value as before, the second column was recalculated with a_2^α proportional to $x^{1.75}$, but the disagreement with the third column was much worse. It may be noted, however, that the extent of disagreement is independent of the value assumed for the eutectoid hydrogen activity, for the same value was assumed in deriving eqs (69) and (70), and cancels when the two equations are set equal to each other.

TABLE 4. *The compositions of the $\alpha/(\alpha+\delta)$ boundary by two methods*

T	x_a at boundary	
	Equality of hydrogen activity	Equality of enthalpy
°K		
298.15	0.000015	0.0006
300	.000016	.0006
350	.00010	.0010
400	.00043	.0010
450	.0013	.0013
500	.0031	.0025
550	.0064	.0053
600	.0114	.0102
650	.0188	.0178
700	.0288	.0282
750	.0418	.0414
800	.0578	.0576
820	.0650	.0650

in accord with the observation of Schwartz and Mallett [9] that hydrogen diffuses in zirconium metal very rapidly at these temperatures. Aside from the small uncertainty in the value selected for 820 °K, the values in the second column of table 4 are probably more reliable than those in the third column; this is certainly true at the lowest temperatures, where the failure of the α phase to reach the final equilibrium compositions would have caused but little error in eq (56) and hence in eq (69). In this paper, however, the properties of the $(\alpha+\delta)$ field depending on the $\alpha/(\alpha+\delta)$ boundary are calculated from the third column of the table in order to avoid small discrepancies with other properties calculated from the thermal data. These discrepancies would have been minor, because the two columns of table 4 never differ by more than about 0.001 in x. For the same reason, no effort was made to adjust the $(\alpha+\delta)$ enthalpy values to make them consistent with the second-column boundary compositions.

5.4. Entropy

The absolute entropies of the various hydride compositions are calculated in this paper from those of zirconium metal (eq (45)). $\overline{S_2^\alpha}$ can be calculated from eq (4) by substituting either eqs (64) and (70) or eqs (65) and (71), depending on the temperature. Specifically, at 820 °K $S_2^\circ=38.285$, and so we get

$$\overline{S}_{2(820)}^{\alpha}=13.3187-9.1516\log x. \quad (72)$$

Since from eq (45)

$$S_{1(820)}^{0}=16.1723, \quad (73)$$

eqs (72) and (73) may be substituted into eq (7) and the integration performed from $x=0$ to x, giving

$$S_{820}^{0(\alpha)}=16.1723+8.6466x-4.5758x\log x. \quad (74)$$

The entropy may be formulated from the enthalpy by performing the integration (of eq (2)) to satisfy eq (74). When eq (63) is used for the enthalpy, the

result is

$$T=820-1136\text{: } S^{0(\alpha)}=(9.32645+5.5677x)\log T + [0.0106226+2.25(10^{-3})x]T-6.74175(10^{-6})T^2 + 2.238(10^{-9})T^3-16.4145-9.4216x-4.5758x\log x. \quad (75)$$

Equation (74) gives (in view of eqs (46) and (47))

$$S^{0(\alpha)}_{820,\,0.0650}=S^{0(\alpha+\delta)}_{820,\,0.0650}=17.0874. \quad (76)$$

At this temperature eqs (4), (56), and (69) and the value of $(S^{\circ}_2)_{820}$ give

$$\overline{S}^{\alpha+\delta}_{2(820)}=5.5207. \quad (77)$$

The substitution from eqs (76) and (77) into eq (5) then gives

$$\overline{S}^{\alpha+\delta}_{1(820)}=16.9080. \quad (78)$$

$(\overline{C}_p)^{\alpha+\delta}_1$ and $(\overline{C}_p)^{\alpha+\delta}_2$ as functions of temperature were then evaluated from eqs (50, 54) and (51, 55) respectively, and when each of these functions was substituted into the equation for the partial molal properties analogous to eq (2) and the subsequent integration was required to satisfy eq (78) or (77) respectively, the partial molal and (from eq (5)) the total entropies in the $(\alpha+\delta)$ field were completely determined. The results for the partial molal entropies are

$$\overline{S}^{\alpha+\delta}_1=78.08602\log T-0.1010277T+7.151355(10^{-5})T^2 - 2.13799467(10^{-8})T^3+6.86514(10^5)T^{-2} - 6.15260693(10^7)T^{-3}-164.9841; \quad (79)$$

$$\overline{S}^{\alpha+\delta}_2=14.06722\log T+2.2322(10^{-3})T - 2.1296685(10^{-4})T^2+6.95698132(10^{-7})T^3 - 8.483175(10^{-10})T^4+3.6489984(10^{-13})T^5 - 29.4258. \quad (80)$$

5.5. Some Partial Molal Properties With Respect to Zirconium

In the α field the partial molal relative free energy and relative enthalpy of zirconium may be found readily from those for hydrogen by integrating the Gibbs-Duhem equation (eq (9)), since zirconium in its standard state is a terminal composition ($x = 0$) of this field. Equations (70) and (71) both give the same result for the relative free energy,

$$(\overline{G}^{\alpha}_1-G^0_1)/T=-1.9872x, \quad (81)$$

and eqs (64) and (65) give the same result for the relative enthalpy,

$$(\overline{H}^{\alpha}_1-H^0_1)/T=0. \quad (82)^{11}$$

In the $(\alpha+\delta)$ field the partial molal relative free energy of zirconium is simply the values given by eq (81) along the $\alpha/(\alpha+\delta)$ boundary:

$$(\overline{G}^{\alpha+\delta}_1-G^0_1)/T=-1.9872x_{\alpha}. \quad (83)$$

The values of x_{α} are given in table 4, where, as explained earlier, those in the third column were used to obtain the tabulated values of $(\overline{G}^{\alpha+\delta}_1-G^0_1)/T$.

The partial molal relative enthalpy of zirconium in the $(\alpha+\delta)$ field may be obtained from eq (4), which in this case is

$$(\overline{H}^{\alpha+\delta}_1-H^0_1)/T=(\overline{G}^{\alpha+\delta}_1-G^0_1)/T+\overline{S}^{\alpha+\delta}_1-S^0_1, \quad (84)$$

by substituting from eqs (45), (79), and (83). For the zirconium-hydrogen system this property may be derived more directly from the enthalpies alone by what is equivalent to the "method of intercepts." From eq (8)

$$\overline{H}_1=H^0-x\partial H^0/\partial x. \quad (85)$$

By writing the same equation for 273 °K and the $(\alpha+\delta)$ field and subtracting from eq (85), we may write

$$(\overline{H}_1-H^0_1)=(H^0-H^{0(\alpha+\delta)}_{273})-x\left[\frac{\partial}{\partial x}(H^0-H^{0(\alpha+\delta)}_{273})\right]_T - (H^0_1-H^0_{1(273)})+(\overline{H}^{\alpha+\delta}_1-H^0_1)_{273}. \quad (86)$$

It was stated earlier, however, that α-Zr will be assumed to lie in the $(\alpha+\delta)$ field at 273 °K so that

$$(\overline{H}^{\alpha+\delta}_1-H^0_1)_{273}=0. \quad (87)$$

From eqs (48), (49), (52), and (53),

$$(H^{0(\alpha+\delta)}_{298}-H^{0(\alpha+\delta)}_{273})-x\left[\frac{\partial}{\partial x}(H^{0(\alpha+\delta)}_{298}-H^{0(\alpha+\delta)}_{273})\right]_T=158, \quad (88)$$

and from eq (44),

$$H^0_{1(298)}-H^0_{1(273)}=154. \quad (89)$$

Subtracting eq (89) from the sum of eqs (86), (87), and (88),

$$(\overline{H}_1-H^0_1)/T=\frac{1}{T}\left\{(H^0-H^{0(\alpha+\delta)}_{298}) - x\left[\frac{\partial(H^0-H^{0(\alpha+\delta)}_{298})}{\partial x}\right]_T-(H^0_1-H^0_{1(298)})+4\right\}. \quad (90)$$

For the $(\alpha+\delta)$ field at $T=298$, eq (90) gives the value of eq (25). Equation (90) is applicable to any phase field and any composition lying inside the $(\alpha+\delta)$ field at 298 °K. In the special case of the $(\alpha+\delta)$ field, substitution from eq (48) gives the simple result:

[11] Equation (82) follows also from eqs (11) and (81). Both equations (81) and (82) are consistent with the assumption made earlier that the α phases are ideally dilute solutions of atomic hydrogen in α-zirconium.

$$(\overline{H}_1^{\alpha+\delta}-H_1^0)/T=[A-(H_1^0-H_{1(298)}^0)+4]/T. \quad (91)$$

Values calculated from eqs (84) and (91) did not differ by more than 0.006, and were averaged for tabulation.

6. The β (Hydrogen-Rich), $(\beta+\delta)$, and δ Phase Fields

Having formulated thermodynamic properties for the $(\alpha+\delta)$ field, those formulated for the β, $\beta+\delta$, and δ fields should be consistent not only with the most reliable data for these fields but also with a single set of $\beta/(\beta+\delta)$, $\delta/(\beta+\delta)$, and $\delta/(\alpha+\delta)$ boundaries. Therefore the properties of these three fields are considered together.

An isotherm of a_2 at 1073.2 °K for the β field has already been formulated in section 3 (eq (23)). As the hydrogen concentration (x) increases, the second term in this equation becomes relatively important (several percent of the first term) in the region $x=$ 0.5 to 0.6; other properties such as the heat capacity and the heat of hydriding $(\overline{H}_2-H_2^0)$, at similar temperatures and the same general range of concentrations, show similar changes. This fact makes it convenient to treat the wide β field separately in two parts. Somewhat arbitrarily, the field has been divided in this paper by the composition selected as that of the β eutectoid phase, $x=0.57$. The properties of the β phases richer in hydrogen will be considered quantitatively in the present section, and those poorer in hydrogen, in section 7. The most appropriate dividing composition probably shifts with temperature, but the exact choice is probably not of major importance because all the important thermodynamic properties are made to have continuity at this composition.

6.1. The β Enthalpy and Other Properties ($x \geqq 0.57$)

A simple equation was selected to fit the enthalpy measurements [16] in the β field for the higher values of x:

$$x \geqq 0.57: \quad (H^{0(\beta)}-H_{298.15}^{0(\alpha+\delta)})/T=(9.664+2.144x)T +1500x-2521.1. \quad (92)$$

The values calculated from this equation are compared in table 5 with the mean observed enthalpies.[12] (The latter were actually measured relative to 273.15 °K, but have been made relative to 298.15 °K by subtracting the quantities indicated by eqs (52) and (53).)

If any of the samples was actually inside the $(\beta+\delta)$ field when measured, its enthalpy would be found to be lower than if at the same temperature it were in the β field. Measurements were made on the compositions $x=0.556$ and 0.701 also at 873.2 °K, but, contrary to figure 1, these enthalpies gave definite evidence (poor precision, large thermal hysteresis, and large negative deviations from eq (92)) that for some reason the β field had not been reached. By similar considerations the observed values in table 5 for $x=0.999$ at $T=1123.2$ and for $x=1.071$ at $T=1123.2$ and 1073.2 would be expected to fall below eq (92). The fact that the last value is only slightly lower is evidence that the preceding value (for $x=1.071$ and $T=1123.2$) probably corresponds to the β field, despite the $\beta/(\beta+\delta)$ boundary selected in figure 1. Most likely, small percentages of impurities in each sample, while corrected for additively, probably invalidated the observed enthalpy appreciably only if the impurities shifted this phase-field boundary enough to place the point erroneously in a two-phase field. The doubtful values mentioned were not used in deriving eq (92). It may be noted from table 5 that the fit is poorer and with a trend for the two lowest temperatures tabulated (up to 0.5% discrepancy), but these four points were considered insufficient justification for modifying eq (92).

TABLE 5. *Deviation from eq (92) of the mean observed enthalpies*

(For each temperature and composition the first value is the mean observed $(H^{0(\beta)}-H_{298.15}^{0(\alpha+\delta)})$ and the value in parentheses is the observed − calculated, both in cal/mole of ZrH_x.)[13]

T	$x=0.556$		$x=0.701$		$x=0.999$	$x=1.071$
°K						
923.2	8291	±6(−44)	8876	±0(+36)		
973.2	8839	(−39)	9423	(+24)		
1073.2	9971	(+8)	10528	(+13)		[11906(−16)]
1123.2					[12211(−27)]	12520(0)
1173.2	11040	(−9)	11640	(+8)	12828(0)	13118(0)

With the help of eqs (28), (29), and (92), eq (26) gives:

$$x \geqq 0.57: \quad (\overline{H}_2^{\beta}-H_2^0)/T=-36508.3/T-2.372 -2.678(10^{-4})T+12000/T^2. \quad (93)$$

When eq (93) is substituted into eq (11), and the subsequent integration is made to satisfy eq (24), there is obtained:

$$x \geqq 0.570: \quad (\overline{G}_2^{\beta}-G_2^0)/T=6.2231 \log x +4.5758 \log (1+1.8493x^{6.97}) +11.6100-36508.3/T+5.4617 \log T +2.677(10^{-4})T+6000/T^2. \quad (94)$$

Though eq (24) was derived from data up to about $x=1$, where the β field terminates at 1073 °K, eq (94) is assumed to hold up to 1200 °K and also for the slightly greater values of x (up to about 1.1) which lie in the β field above 1073 °K. An empirical equation was derived for the standard entropy of hydrogen gas from eq (28) (using eqs (1) and (2)). Since eq (28) is not quite exact, the integrated equation was adjusted to give the best fit for $T \geqq 820$:

$$T \geqq 820: \quad S_2^0=15.33532 \log T+5.356(10^{-4})T -6000/T^2-6.8288. \quad (95)$$

[12] The composition $x=0.556$ in table 5, while outside the range to which eq (92) has been restricted, is too close to $x=0.57$ to invalidate appreciably the differences "observed minus calculated" noted in the table.

[13] The tolerances attached to two of the values in the table represent not precision or estimated accuracy, but the uncertainty due to hysteresis. For these two points the temperature was approached both by heating and by cooling (in two separate series of runs). The enthalpies found were higher in the former than in the latter series by twice the stated tolerance, and the mean of the two series has been tabulated.

Substitution from eqs (93), (94), and (95) into eq (4) then gives:

$$x \geqq 0.57: \ \overline{S}_2^{\beta} = -6.2231 \log x - 4.5758 \log (1+1.8493\, x^{5.97}) + 9.8736 \log T - 20.8108. \quad (96)$$

Substituting from eqs (44) and (92) into eq (90),

$$x \geqq 0.57: \ (\overline{H}_1^{\beta} - H_1^{\circ})/T = -942.6/T + 5.6136 - 5.3113(10^{-3})T + 4.4945(10^{-6})T^2 - 1.6785(10^{-9})T^3. \quad (97)$$

Other properties to be derived for the hydrogen-rich part of the β field will depend on how the $(\beta+\delta)$ properties are formulated, because these, together with the β properties, will determine the unique composition of the β eutectoid phase with which they are consistent.

6.2. Procedure Giving Thermodynamic Consistency

Of the twelve thermodynamic functions derived and tabulated in this paper (tables 8–14), five must be continuous at each phase-field boundary: H, S, G, $\overline{G}_1$, and $\overline{G}_2$. Both relative-enthalpy and hydrogen-activity data have been obtained in the $(\beta+\delta)$ field. The enthalpy data were obtained by Douglas and Victor [16] for the compositions $x=0.701$, 0.999, and 1.071, but the values show serious inconsistencies between two of the sample compositions,[14] and therefore were given no weight in deriving properties in this field. Hydrogen-activity values in the $(\beta+\delta)$ field were reported as follows: by Edwards et al. [5] for $x=1.222$ at 973, 1,023, 1,073, 1,098, 1,123, 1,133, 1,138, and 1,148 °K; by LaGrange et al. [8] for several compositions at 843, 889, 919, 967, 1,022, and 1,073 °K. The values of the two sets of workers, which disagree somewhat at the lower temperatures, show excellent agreement as well as smooth temperature dependence at and above 1,023 °K, and were used to define the adopted values in this higher temperature range. With the complete formulation of the hydrogen activity (or $\overline{G}_2^{\beta+\delta}$) from the eutectoid temperature (820 °K) to 1,200 °K, soon to be given, the $\beta/(\beta+\delta)$ boundary was so determined as to make $\overline{G}_2^{\beta}$ and $\overline{G}_2^{\beta+\delta}$ equal along the boundary, and the values of the other four of the above five properties in the $(\beta+\delta)$ field were determined so that along the boundary they would be equal at each temperature to the corresponding β-field properties.

Representing the boundary composition at temperature T by x_β, the relative enthalpy in the $(\beta+\delta)$ field at x and T can be found by integrating eq (26) between x and x_β:

$$(H^{\circ(\beta+\delta)} - H^{\circ(\alpha+\delta)}_{298.15})/T = (H^{\circ(\beta)} - H^{\circ(\alpha+\delta)}_{298.15})_{x_\beta}/T + [\overline{H}_2^{\beta+\delta} - H_2^{\circ}) - \overline{H}_2^{\alpha+\delta} - H_2^{\circ})_{298} + (H_2^{\circ} - H_{2(298)}^{\circ})][(x-x_\beta)/2T]. \quad (98)$$

The complete determination of $(\overline{H}_2^{\beta+\delta} - H_2^{\circ})$ at the lower temperatures down to 820 °K will then complete the determination of the $(\beta+\delta)$ properties and the $\beta/(\beta+\delta)$ boundary. In particular, the composition of the eutectoid β phase will lie on this boundary, and the composition of the eutectoid δ phase will be that resulting from simultaneous solution of eqs (48) and (98) at 820 °K, the eutectoid temperature. It was decided to formulate thermodynamic properties of the Zr–H system only up to $x=1.25$, partly because there are fewer overlapping data for compositions richer in hydrogen and those that do exist show some major inconsistencies. If the eutectoid δ phase has a value of x less than 1.25, then as the temperature rises the composition $x=1.25$ passes from the $(\alpha+\delta)$ field into the δ field at some temperature (T_1), and from the δ into the $(\beta+\delta)$ field at a higher temperature (T_2). For thermodynamic consistency, it must be possible to formulate the δ-phase properties so that the five properties mentioned above agree with those of the $(\alpha+\delta)$ and $(\beta+\delta)$ fields at the eutectoid δ composition and temperature (820 °K), with the $(\alpha+\delta)$ properties at $x=1.25$ and T_1, and with the $(\beta+\delta)$ properties at $x=1.25$ and T_2.

The $(\beta+\delta)$ hydrogen-activity data above 1073 °K mentioned above indicate a value of $(\overline{H}_2^{\beta+\delta} - H_2^{\circ})$ essentially independent of temperature (approximately −51600), and in a preliminary trial the same value was assumed down to the eutectoid temperature. This assumption led, in the manner outlined above, to eutectoid compositions of approximately $x_\beta=0.54$ and $x_\delta=0.99$. The next step taken was to formulate an enthalpy function for the δ phases whose temperature derivative corresponded to a hydrogen vibration frequency of between 1050 and 1200 cm^{-1} [15] and which at the same time satisfied the $(\alpha+\delta)$ enthalpy equation (eq (48)) at the eutectoid δ point and also on the $\delta/(\alpha+\delta)$ boundary at 673 °K. With $x=1.25$, this equation was then solved simultaneously with eq (48) to determine T_1, and with eq (98) to determine T_2. To test the continuity of the other four properties at the points T_1 and T_2, entropy is an insensitive criterion, but $\overline{G}_2$ proves entirely adequate. The δ-phase enthalpy function mentioned above and eq (26) gave a value of approximately $(\overline{H}_2^{\delta} - H_2^{\circ}) = -42900$, and on substituting this value, eq (11) integrated to give for $[(\overline{G}_2^{\delta} - G_2^{\circ})/T]_{T_2,\,1.25} - [(\overline{G}_2^{\delta} - G_2^{\circ})/T]_{T_1,\,1.25}$ about 0.7 less than $[(G_2^{\beta+\delta} - G_2^{\circ})/T]_{T_2,\,1.25} - [(G_2^{\alpha+\delta} - \overline{G}_2^{\circ})/T]_{T_1,\,1.25}$. (The discrepancy of 0.7 was approximately 15% of either of the two differences.)

This serious discrepancy was practically eliminated by making two changes. The first change was to preserve the fit to the hydrogen-activity data at the higher temperatures but to assume slightly higher values of $(\overline{H}^{\beta+\delta} - H_2^{\circ})$ at the lowest temperatures

[14] The discrepancies are much larger than those found in several tests of heating-and-cooling hysteresis, and seem to be due to different locations of the $\beta/(\beta+\delta)$ boundary caused by different impurities in the two samples.

(near 820 °K). The final equations are

$$(\bar{H}_2^{\beta+\delta}-H_2^\circ)/T=$$
$$[-51678.2+3.1277(10^{-10})(1200-T)^5]/T \quad (99)$$

and (from eq (11) after substituting from eq (99))

$$(\bar{G}_2^{\beta+\delta}-G_2^\circ)/T=726592.5/T+7466.81126\log T$$
$$-5.4046582T+2.2519409(10^{-3})T^2$$
$$-6.2553915(10^{-7})T^3+7.81924(10^{-11})T^4$$
$$-19434.0399. \quad (100)$$

The additional eutectoid compositions (at 820 °K) were then found in the ways outlined above. Simultaneous solution of eqs (94) and (100) gave

$$x_\beta(\text{eutectoid})=0.570. \quad (101)$$

Using this value, simultaneous solution of eqs (48) and (98) (after substitution from eqs (50) and (51) into the former, and from eqs (28), (29), (92), and (99) into the latter) gave

$$x_\delta(\text{eutectoid})=1.171. \quad (102)$$

The effect of increasing the value of x_δ (eutectoid) from 0.99 to 1.171 was to bring the boundary temperatures T_1 and T_2 (at $x=1.25$) much closer together with the result that the discrepancy in the interval of $(\bar{G}_2^\delta-G_2^\circ)_{x=1.25}$ referred to above was now greatly reduced, but still had the same sign, and a magnitude of 0.14. To repeat the above change on an increased scale and thus to increase the eutectoid composition x_δ still further would have increased the discrepancies of the $\beta/(\alpha+\beta)$ boundary (sec. 7) but apparently without eliminating the present discrepancy in $(\bar{G}_2^\delta-G_2^\circ)_{1.25}$. This discrepancy was, however, practically eliminated by a second change which, by lowering $(\bar{H}_2^\delta-H_2^\circ)$, makes a small increase in the temperature coefficient of $(\bar{G}_2-G_2^\circ)/T$ in the δ field. This was accomplished by replacing the δ-phase enthalpy function by the simple equation

$$x=1.17 \text{ to } 1.4,\ T=790 \text{ to } 850\text{ °K}:\ (\mathrm{H}^\delta-\mathrm{H}_{298.15}^{\alpha+\delta})/T$$
$$=13.115-(4692.5+19.0x)/T. \quad (103)$$

With the use of eqs (103), (28), and (29), eq (26) now gives

$$x=1.17 \text{ to } 1.4,\ T=790 \text{ to } 850\text{ °K}:\ (\bar{H}_2^\delta-H_2^\circ)/T$$
$$=-39546.3/\mathrm{T}-6.660$$
$$-2.678(10^{-4})T+12000/T^2. \quad (104)$$

Equation (104) gives approximately $(\bar{H}_2^\delta-H_2^\circ)=-45200$, which incidentally is much closer than the preliminary value -42900 to that derived by Gulbransen and Andrew [4] from their data, -45750. The $\beta/(\beta+\delta)$ boundary on which eqs (94) and (100) give the same values of $\bar{G}_2$ is that shown in figure 1, and for convenience may be represented (to within ± 0.001 in x) by the empirical equation

$$T=820 \text{ to } 1200\text{ °K}:\ x_\beta=-1.3995+3.5169(10^{-3})T$$
$$-1.2(10^{-6})T^2+[1.19853(10^{-15})-2.87092(10^{-18})T+1.6655(10^{-21})T^2]\,[1200-T]^6. \quad (105)$$

Equation (101), when substituted into eq (94) (or (100)), gives for the eutectoid activity of hydrogen the value of eq (66) given earlier, $1.0442(10^{-4})$ atm.[15]

The heat capacity which eq (103) gives corresponds (by eqs (1) and (6)) to

$$(\bar{C}_p)_2^\delta=0, \quad (106)$$

and this deserves some comment. Though eq (103) was derived to fit only a narrow range of temperatures and compositions, no claim can be made that eq (106) is highly accurate and hence that the addition of hydrogen to the δ phases produces an intrinsic addition to the heat capacity by the vibration of the added hydrogen which is exactly offset by a reduction of the intrinsic contribution by the vibration of the zirconium. It seems not unreasonable, however, that a considerable compensation of this kind may actually exist. Equation (80) gives negative values for $\overline{S}_2^{\alpha+\delta}$ at the lowest temperatures such as 298 °K, which means that the addition of hydrogen to α-zirconium to form the coexistent δ-phases lowers the entropy at these temperatures, and hence presumably the heat capacities at all lower temperatures. In these cases it is reasonable to assume that a major result of adding the hydrogen has been to stiffen the zirconium lattice, and that this relative effect is dependent on composition as well as on temperature.

6.3. Other β Properties ($x \geqq 0.57$)

With the value of eq (101), further properties may be derived in the β field. From eqs (5), (77), and (78),

$$S^{\circ(\alpha+\delta)}_{820,\,0.570}=18.4814. \quad (107)$$

Equations (48), (50), and (51) give

$$(H^\circ-H^\circ_{298.15})^{\alpha+\delta}_{820,\,0.570}=5040.5, \quad (108)$$

and eq (92) gives

$$(H^{\circ(\beta)}-H^{\circ(\alpha+\delta)}_{298.15})_{820,\,0.570}=7260.5, \quad (109)$$

whence

$$\Delta S_{820}=2.7073 \text{ for } \mathrm{ZrH}_{0.570}(\alpha+\delta)\rightarrow \mathrm{ZrH}_{0.570}(\beta). \quad (110)$$

Adding eqs (107) and (110),

$$S^{\circ(\beta)}_{820,\,0.570}=21.1887. \quad (111)$$

For the composition $x=0.570$ eqs (92) and (111) readily give the entropy:

$$S^{\circ(\beta)}_{0.570}=25.06629\log T-51.8497. \quad (112)$$

After substituting from eqs (96) and (112), eq (7) can be used to derive the β entropies for $x>0.570$.

[15] The values indicated by the pressure measurements of Gulbransen and Andrew [4] and of Ells and McQuillan [6] seem to fall within a range of ±10 percent of this value.

This involves the integral $-2.2879\int_{0.570}^{x}\log(1+1.8493\,x^{6.97})\,dx$. Because the expansion of the integral about $x=0$ does not converge rapidly for values of x approaching unity, the following empirical equation was derived:

$$x=0.57\text{ to }1.1: -2.2879\int_{0.570}^{x}\log(1+1.8493\,x^{6.97})\,dx = 0.4202-2.12581x+3.72544x^2-2.36774x^3+0.18558x^4. \quad (113)$$

The general entropy equation then found was

$$x\geqq 0.57: S^{0(\beta)} = (22.25230+4.93681x)\log T - 46.7017 - 11.17991x+3.72544x^2-2.36774x^3+0.18558x^4-3.11155x\log x. \quad (114)$$

$\overline{S}_1^{\beta}(x\geqq 0.57)$ was calculated from eqs (5), (96), and (114).

Since from eqs (47) and (101) $ZrH_{0.0650}(\alpha)$ and $ZrH_{0.570}(\beta)$ are coexistent phases at 820 °K, eq (81) (with $x_a=0.0650$) evaluates $\overline{G}_1$ for both phases:

$$[(\overline{G}_1^{\beta}-G_1^0)/T]_{820,0.570}=-0.1292. \quad (115)$$

When eq (97) is substituted into eq (11) and the integration is made to satisfy eq (115), there is obtained for the one composition $x=0.570$

$$[\overline{G}_1^{\beta}-G_1^0)/T]_{0.570} = -942.6/T-12.92588\log T +5.3113(10^{-3})T-2.24725(10^{-6})T^2+5.595(10^{-10})T^3 +35.5312. \quad (116)$$

Equations (94) and (116) may be substituted into the Gibbs-Duhem equation (eq (9)), the integration from $x=0.570$ to higher x giving (with the help of eq (113) in integration by parts)

$$x\geqq 0.57: (\overline{G}_1^{\beta}-G_1^0)/T = 35.9017+0.77449x-3.72544x^2 +2.36774x^3-0.18558x^4-2.2879x\log(1+1.8493x^{6.97}) -942.6/T-12.92588\log T+5.3113(10^{-3})T -2.24725(10^{-6})T^2+5.595(10^{-10})T^3. \quad (117)$$

6.4. Other ($\beta+\delta$) Properties

The remaining ($\beta+\delta$) properties may be readily derived from foregoing relationships. $\overline{S}_2^{\beta+\delta}$ may be found from eqs (4), (95), (99), and (100). The entropy was found from that at the $\beta/(\beta+\delta)$ boundary ($S_{x_\beta}^{0(\beta)}$, calculated from eqs (105) and (114)) and eq (7) in the form

$$S^{0(\beta+\delta)}=S_{x_\beta}^{0(\beta)}+\tfrac{1}{2}\overline{S}_2^{\beta+\delta}(x-x_\beta). \quad (118)$$

$\overline{S}_1^{\beta+\delta}$ was calculated by substituting $S^{0(\beta+\delta)}$ and $\overline{S}_2^{\beta+\delta}$ into eq (5). $(\overline{G}_1^{\beta+\delta}-G_1^0)/T$, which is independent of x, is the β value given by eq (117) on the boundary and at the temperature in question. $(\overline{H}_1^{\beta+\delta}-H_1^0)/T$ was calculated from eq (4) from $\overline{S}_2^{\beta+\delta}$, $(\overline{G}_1^{\beta+\delta}-G_1^0)/T$, and S_1^0(eq (45)). $C_p^{0(\beta+\delta)}$ is the total derivative of eq (98) with respect to temperature (with x but not x_β independent of temperature); by eq (5) this may be broken up into the partial molal properties:

$$(\overline{C}_p)_1^{\beta+\delta}=[\partial(H^{0(\beta)}-H_{298.15}^{0(\alpha+\delta)})/\partial T]_{x_\beta}+[\partial(H^{0(\beta)}-H_{298.15}^{0(\alpha+\delta)})/\partial x]_{x_\beta}[dx_\beta/dT]-\tfrac{1}{2}x_\beta d[(\overline{H}_2^{\beta+\delta}-H_2^0)+(H_2^0-H_{2(298)}^0)]/dT -\tfrac{1}{2}[(\overline{H}_2^{\beta+\delta}-H_2^0)-(\overline{H}_2^{\alpha+\delta}-H_2^0)_{298}+(H_2^0-H_{2(298)}^0)][dx_\beta/dT]; \quad (119)$$

$$(\overline{C}_p)_2^{\beta+\delta}=d[(\overline{H}_2^{\beta+\delta}-H_2^0)+(H_2^0-H_{2(298)}^0)]/dT. \quad (120)$$

(The quantities needed in eqs (119) and (120) can be obtained from eqs (28), (29), (92), (99), and (105).)

6.5. Other δ Properties

The remaining properties in the small part of the δ field considered here (from $T=790$ to 850, and from $x=1.171$ to 1.25) were derived as follows. From eqs (90), (103), and (44),

$$x=1.17\text{ to }1.4,\ T=790\text{ to }850: (\overline{H}_1^{\delta}-H_1^0)/T = 9.0646-5.3113(10^{-3})T+4.4945(10^{-6})T^2 -1.6785(10^{-9})T^3-3114.0/T. \quad (121)$$

The following boundary points were selected as giving the best overall continuity of properties at the points:

$x=1.25$: $\delta/(\alpha+\delta)$ boundary,

$T_1=791.5$; $\delta/(\beta+\delta)$ boundary, $T_2=845.6$. (122)

At these points eqs (69) and (100) give respectively

$$[(\overline{G}_2^{\alpha+\delta}-G_2^0)/T]_{791.5,1.25}=-20.0576;$$

$$[(\overline{G}_2^{\beta+\delta}-G_2^0)/T]_{845.6,1.25}=-16.3872. \quad (123)$$

However, the integration between these two temperatures of eq (11), after substitution from eq (104) gives a corresponding increment of $(\overline{G}_2^{\delta}-G_2^0)/T$ which is 0.0203 less than that of eq (123); but by adjusting the integration constant so that the discrepancy has at the two points the same magnitude but opposite signs, the same equation then gives

$$[(\overline{G}_2^{\delta}-G_2^0)/T]_{820,1.25}=-18.0684. \quad (124)$$

From eqs (67) and (102)

$$[(\overline{G}_2^{\delta}-G_2^0)/T]_{820,1.171}=-18.2174. \quad (125)$$

By making the reasonable assumption that in this small composition range a_2^δ is proportional to some constant power of x, eqs (124) and (125) give:

$$x=1.17 \text{ to } 1.25: [(\overline{G}_2^\delta - G_2^0)/T]_{820} = 5.2281 \log x - 18.5751. \quad (126)$$

After substitution from eq (104), the general integration of eq (11) so as to satisfy eq (126) then gives:

$$x=1.17 \text{ to } 1.25,\ T=790 \text{ to } 850: (\overline{G}_2^\delta - G_2^0)/T = 5.2281 \log x - 15.2606 - 39546.3/T + 15.33532 \log T + 2.678(10^{-4})T + 6000/T^2. \quad (127)$$

From eqs (90), (103), and (44),

$$x=1.17 \text{ to } 1.4,\ T=790 \text{ to } 850: (\overline{H}_1^\delta - H_1^0)/T = 9.0646 - 5.3113(10^{-3})T + 4.4945(10^{-6})T^2 - 1.6785(10^{-9})T^3 - 3114.0/T. \quad (128)$$

From eqs (102) and (115) we have

$$[(\overline{G}_1^\delta - G_1^0)/T]_{820,\,1.171} = -0.1292. \quad (129)$$

Equations (126) and (129) may be substituted into the Gibbs-Duhem equation (eq (9)), the integration from $x=1.171$ to higher x giving

$$x=1.17 \text{ to } 1.25: [(\overline{G}_1^\delta - G_1^0)/T]_{820} = 1.1997 - 1.13526\, x. \quad (130)$$

When eq (128) is substituted into eq (11) and the latter is then integrated so as to satisfy eq (130), there is obtained

$$x=1.17 \text{ to } 1.25,\ T=790 \text{ to } 850: (\overline{G}_1^\delta - G_1^0)/T = -1.13526\, x + 62.6621 - 3114.0/T - 20.87215 \log T + 5.3113(10^{-3})T - 2.24725(10^{-6})T^2 + 5.595(10^{-10})T^3. \quad (131)$$

The partial molal entropies can be derived from eq (4). Substitution from eqs (45), (128), and (131) gives $\overline{S}_1^\delta$, and substitution from eqs (95), (104), and (127) gives $\overline{S}_2^\delta$:

$$x=1.17 \text{ to } 1.25,\ T=790 \text{ to } 850: \overline{S}_1^\delta = 30.19860 \log T + 1.13526\, x - 70.0120; \quad (132)$$

$$x=1.17 \text{ to } 1.25,\ T=790 \text{ to } 850: \overline{S}_2^\delta = 1.7718 - 5.2281 \log x. \quad (133)$$

The substitution of eqs (132) and (133) into eq (5) gives the entropy:

$$x=1.17 \text{ to } 1.25,\ T=790 \text{ to } 850: S^{o(\delta)} = 30.19860 \log T + 2.02116\, x - 2.61405\, x \log x - 70.0120. \quad (134)$$ [16]

For the composition $x=1.25$ the discrepancy at each adopted phase-field boundary between the final equations for the δ and the two-phase fields is given in table 6 for each of the five properties which should have identical values. (In each such case, the average value is tabulated.) Since continuity was required at the boundary at $x=1.171$, presumably the discrepancies would be small at the boundaries for all intervening values of x.

TABLE 6. *Discrepancies of formulated properties of* $ZrH_{1.25}$ *at the adopted phase-field boundaries*

Property	"δ"−"$(\alpha+\delta)$" at 791.5 °K	"δ"−"$(\beta+\delta)$" at 845.6 °K
$\left(H^o - H^{o(\alpha+\delta)}_{298.15}\right)/T$	+0.005	+0.007
S°	+.002	+.008
$-\left(G^o - H^{o(\alpha+\delta)}_{298.15}\right)/T$	−.002	+.001
$(\overline{G}_1 - G_1^o)/T$	−.006	+.006
$(\overline{G}_2 - G_2^o)/T$	+.010	−.010

6.6. Discussion of the δ Phase-Field Boundaries

The $\delta/(\alpha+\delta)$ and $\delta/(\beta+\delta)$ boundaries have been drawn in figure 1 through the adopted δ eutectoid point (eq (102)) and the adopted temperatures for $x=1.25$ (eq (122)). Though no effort is made in this paper to derive consistent thermodynamic properties for higher values of x, these two boundaries have been extended in figure 1 in a reasonable but empirical way. In particular, the ensemble of experimental points shown for the $\delta/(\beta+\delta)$ boundary shows wide discrepancies,[17] but the boundary drawn has been made to pass through the "hydrogen-pressure" values of Edwards et al. [5] and of LaGrange et al. [8]. The points of LaGrange et al. indicate some curvature in the boundary, but those of Edwards et al. (at seven temperatures from 973 to 1,148 °K) show a vertical boundary within the experimental error. In a previous paper [17] the author criticized a vertical boundary on thermodynamic grounds which would lead one to predict that it has a positive finite slope. The same argument still holds, but may be reexamined somewhat more quantitatively.

The hydrogen activity in a one-phase field b is of course a function of both temperature and composition, and its variation with temperature along the boundary $x_b(T)$ separating the b and $(b+c)$ fields may be written as a total derivative:

$$d \ln a_2/dT = (\partial \ln a_2/\partial T)_x + (\partial \ln a_2/\partial x)_T/(dT/dx_b), \quad (135)$$

or in the present case

$$d \ln a_2^{b+c}/dT = (\partial \ln a_2^b/\partial T)_{x_b} + (\partial \ln a_2^b/\partial x)_T/(dT/dx_b). \quad (136)$$

[16] For the eutectoid δ phase ($x=1.171$, $T=820$), eq (134) should of course give the same value of S^o as eqs (5), (79), and (80) for the $(\alpha+\delta)$ field. The two values calculated were found to differ by only 0.002. However, this is a check of thermodynamic consistency only.

[17] Relatively accentuated for higher values of x in figure 1 compared with the more usual plots of the phase diagram as temperature versus *atomic percentage* of hydrogen.

Substituting for the first two derivatives from eqs (10) and (11), eq (136) becomes

$$(\partial \ln a_2^b/\partial x)_T = (RT^2)^{-1}(dT/dx_b)[(\overline{H}_2^b - H_2^\circ) - (\overline{H}_2^{b+c} - H_2^\circ)]. \quad (137)$$

If the thermodynamic properties as formulated are consistent, regardless of how near to correct they are, they must satisfy eq (137) along every phase-field boundary. For example, the equation may be applied to the $\delta/(\alpha+\delta)$ and $\delta/(\beta+\delta)$ boundaries at $x=1.25$. In the former case the bracketed quantity in eq (137) is -3006 (from eqs (56) and (104)), and in the latter case it is $+4577$ (from eqs (99) and (104)). Since, as expected, $(\partial \ln a_2^\delta/\partial x)_T$ is positive in both cases (eq (127)), the slopes of the $\delta/(\alpha+\delta)$ and $\delta/(\beta+\delta)$ boundaries at this composition will thus be negative and positive respectively, as they are in figure 1.

The measured δ-phase isotherms of hydrogen pressure [3,5,8] are in general considerably steeper than indicated by eq (127), according to which a_2^δ is at constant temperature approximately proportional to $x^{1.14}$ (up to $x=1.25$). It may be noted furthermore that the isotherms cited usually show a more gradual change in slope,[18] as the hydrogen content changes and the sample crosses a phase-field boundary, when the latter is contiguous with the δ field than when it is contiguous with some other one-phase field. If, as seems to be the case, the heats of hydriding do not change rapidly with temperature, eq (137) indicates that at values of x considerably greater than 1.25 the far steeper $\delta/(\beta+\delta)$ boundary indicates a much greater value of $(\partial \ln a_2^\delta/\partial x)_T$ than at lower values of x, as experiment indicates. By the same reasoning, the $\delta/(\alpha+\delta)$ boundary would be expected to become much steeper as x increases. This boundary in figure 1 was drawn to pass through the points indicated by thermal-expansion studies from 293 to 673 °K [12,14], and does become somewhat steeper. If this boundary were assumed to be an equilibrium one, it would be possible to draw some conclusions about the δ-field hydrogen activities at temperatures too low for direct accurate measurements.

A sample such as $ZrH_{1.25}$ shows the interesting behavior of being in the one-phase δ field at some temperatures, but in a two-phase field at higher or lower temperatures. According to equations derived earlier (5, 50, 51, 54, 55, 103, 119, and 120), the equilibrium heat capacity increases discontinuously as the sample passes from the δ-field into either contiguous two-phase field, because a new phase of different energy starts to form at a finite rate. A simple proof may be given that the heat capacity is necessarily greater, near the boundary, in the two-phase than in the one-phase field. If $'$ and $''$ indicate respectively the one- and two-phase properties, at the boundary $G''=G'$, $S''=S'$, and so also $dG''/dT=dG'/dT$ since $S=-dG/dT$. But since *inside* the two-phase field $G''<G'$, then the G'' (T) curve for the sample must be more negatively curved than the partly metastable G' (T) curve, or $d^2G''/dT^2 < d^2G'/dT^2$. Hence $dS''/dT>dS'/dT$, and since $dS/dT=C_p/T$, it follows that $C_p''>C_p'$.

[18] This curvature of the δ-field isotherms increases the difficulty of locating the compositions of the breaks accurately, and suggests that some of the values of x selected in the references cited may be somewhat too high.

7. The β (Hydrogen-Poor) and $(\alpha+\beta)$ Phase Fields

Unlike the thermodynamic properties in the $(\alpha+\delta)$ and $(\beta+\delta)$ fields derived in sections 5 and 6, those in the $(\alpha+\beta)$ field were derived from the properties of the two adjacent one-phase fields using phase-field boundaries thermodynamically consistent with these properties. This consistency was imposed by finding two boundaries such that at each temperature $\overline{G}_2^\alpha=\overline{G}_2^\beta$ and $\overline{G}_1^\alpha=\overline{G}_1^\beta$ (eqs (18) and (22)). The α-field properties were formulated in section 5, and the β-field properties for $x\geqq 0.570$, in section 6. However, since it is assumed in this paper that $x\leqq 0.570$ in all of the $(\alpha+\beta)$ field (eq (101) and fig. 1), the pertinent β-field properties are those for the lower range of x, and are derived in the present section. This includes β-zirconium ($x=0$) from its transformation temperature, 1,136°, up to 1,200 °K.

7.1. Discussion of Thermodynamic Consistency

The thermodynamic data in the presently considered ranges of temperature and composition which were given greatest weight are as follows. Figure 1 shows, in addition to the $\alpha/(\alpha+\beta)$ and $\beta/(\alpha+\beta)$ boundaries finally arrived at in this paper, various points on these boundaries indicated by three experimental investigations [6, 8, 10]. The points from the two investigations of hydrogen pressure [6, 8] showed general agreement, but the X-ray measurements [10], which did not involve the $\alpha/(\alpha+\beta)$ boundary, indicated a much higher curve for the $\beta/(\alpha+\beta)$ boundary. The compositions of the eutectoid β phase reported by these investigators are equivalent to the following values of x: Ells and McQuillan [6], 0.47; LaGrange et al. [8], 0.50; Vaughan and Bridge [10], 0.72. Douglas and Victor's [16] measurements of the enthalpy of $Zr(\beta)$ and of $ZrH_{0.324}$ (β), when reduced to a basis of 298.15 °K by eqs (52) and (53), give the following mean values:

$$(H^{\circ(\beta)}_{1173.2} - H^{\circ(\alpha+\delta)}_{298.15})_{x=0} = 7314;$$

$$(H^{\circ(\beta)}_{1173.2} - H^{\circ(\alpha+\delta)}_{298.15})_{0.324} = 9701; \quad (138)$$

in addition, their mean observed values of $(H^{\circ(\beta)} - H^{\circ(\alpha+\delta)}_{298.15})_{0.324}$ were 8836 at $T=1073.2$ and 8004 ± 2 [19] at $T=973.2$. They actually measured the enthalpy of $Zr(\beta)$ at five temperatures over the very short temperature range 1,153 to 1,173 °K, the values varying linearly with temperature with a heat capacity averaging 9.0. Skinner's linear heat capacity-temperature equation, which is based on his enthalpy measurements of $Zr(\beta)$ from the transformation

[19] See footnote 13 (table 5).

temperature to 1,800 °K [22], gives 6.73 in the same temperature range and extrapolates to 6.46 at 1,000 °K.

Development of β-phase properties for $x \leqq 0.570$ began with the assumption of the eutectoid temperature α- and β-compositions already adopted (eqs (47) and (101)), the adopted transformation temperature of zirconium (eq (41)), and the basic relations in sections 2 and 3. In the first trial an enthalpy equation for the β region was formulated in the following way. It was required to satisfy the values of eq (138), to agree at $x=0.57$ in H and $(\partial H/\partial x)_T$ with the equation already derived for $x \geqq 0.57$ (eq (92)), and to correspond to a heat capacity independent of temperature but equaling Skinner's 1,000 °K value for $x=0$ (6.46) and Douglas and Victor's mean value for $x=0.324$ (8.48).[20] In the manner outlined later, points on the $\alpha/(\alpha+\beta)$ and $\beta/(\alpha+\beta)$ boundaries at several temperatures were then found by imposing the requirement that the two partial molal free energies be equal.

The $\beta/(\alpha+\beta)$ boundary so found lay considerably above that indicated by the hydrogen-pressure studies of Ells and McQuillan [6] and LaGrange et al. [8] and considerably below that of Vaughan and Bridge [10] (except at $x=0$, where there is general agreement). While the X-ray technique is less sensitive than the hydrogen-pressure method, it seems reasonable to conclude that unless Vaughan and Bridge made a gross misinterpretation of their data their samples actually did correspond to a boundary in the neighborhood of what they reported and that some factor such as unknown impurities accounts for the large differences from the reported hydrogen-pressure curves.[21] Nevertheless the latter two curves, although they show some differences at the lower temperatures, are in substantial agreement, and seem much more credible. In the author's derivation of the two boundaries as outlined above, the single requirement that the hydrogen activities be equal ($\bar{G}_2^{\alpha}=\bar{G}_2^{\beta}$) gives of course an infinite set of curves, one of which approximated the experimentally observed "hydrogen pressure" boundaries, but at intermediate temperatures with zirconium activities of approximately 0.94 on the α boundary and 0.97 on the β boundary. Just how sensitive these zirconium activities are to shifts under the experimental conditions of the hydrogen-pressure measurements is not apparent.

It is appropriate of course to examine critically the assumptions and basic data used by the author in deriving the boundaries. The α-field activities of hydrogen and zirconium given by eqs (70), (71), and (81), which are related by the exact Gibbs-Duhem equation,[22] are not only reasonable but are supported by the agreement in table 4 below 820 °K. An independent entropy calculation showing excellent agreement will be made later in this section, and supports the basic hydrogen-activity isotherm assumed (eq (23)). The boundaries are insensitive at the lower temperatures to the heat capacity assumed for β-zirconium. The enthalpy measurements on $ZrH_{0.324}$ were of high precision (± 5 cal mole^{-1}), the sample was of fairly high purity, and there are good reasons for believing that in the temperature range cited above (973 to 1,173 °K) the sample was entirely in the one-phase β field and hence not subject to the uncertainties caused by phase reproportionation. Nor did it seem justified to modify eq (92) for the "hydrogen-rich" β enthalpies. In fact, it seems clear that enthalpies corrected additively for small amounts of impurities may still be seriously in error in multiphase fields owing to improper phase compositions, but reliable in one-phase fields. In several attempts it was found impossible to reformulate the β-phase enthalpies for $x \leqq 0.570$ with the restrictions mentioned above and still obtain a credible approximately monotonic function which had an appreciable effect on the derived $\alpha/(\alpha+\beta)$ and $\beta/(\alpha+\beta)$ boundaries. Furthermore, the choice of a somewhat lower value of the eutectoid β composition would do some violence to the fit which led to eq (101) without leading to a much better fit to the experimental "hydrogen-pressure" $\beta/(\alpha+\beta)$ boundaries. This is because the latter suggest a boundary slope near the eutectoid temperature which is several times less steep than that required by eq (137).

7.2. The β Properties ($x \leqq 0.57$)

In order to derive a thermodynamically consistent set of properties in the range of temperature and composition under consideration ($T>820$, $x<0.570$), it was decided to give approximately equal weight to the hydrogen-pressure results [6, 8] and the enthalpy data [16] by making such changes in the latter as would lead to a derived $\beta/(\alpha+\beta)$ boundary approximately halfway between the experimental "hydrogen-pressure" boundary and that derived above. A new β-field enthalpy function was derived by the procedure described earlier except that the heat capacity of $Zr(\beta)$ was raised from 6.46 to 7.76 and that of $ZrH_{0.324}$ (β) was raised from 8.48 to 9.00:[23]

$$x \leqq 0.570\text{: } (H^{\circ(\beta)}-H^{\circ(\alpha+\beta)}_{298.15})/T=7.763+2.144x +90.047x^4-126.382x^5 +(4990.1x-109834.5x^4+147541.6x^5-1793.8)/T. \quad (139)$$

From the temperature derivative of eq (139), eqs (6) and (8) give the partial molal heat capacities:

$$x \leqq 0.570\text{: } (\bar{C}_p)_1^{\beta}=7.763-270.141x^4+505.528x^5; \quad (140)$$

$$x \leqq 0.570\text{: } (\bar{C}_p)_2^{\beta}=4.288+720.376x^3-1263.82x^4. \quad (141)$$

From eqs (44), (90), and (139):

[20] Douglas and Victor's value of 9.0 for β-Zr, which is greater than they found for $ZrH_{0.324}$, is not precise because of the short temperature range, and may be too high if the small amount of oxygen and nitrogen (0.065 atom %) raised the transformation temperature above 1,153 °K [6].

[21] Ells and McQuillan [6] concluded, e.g., that oxygen as an impurity raises this boundary.

[22] The boundaries are insensitive to the eutectoid hydrogen pressure used as an integration constant.

[23] By retaining the values of eq (138), the enthalpies of $ZrH_{0.324}$ below 1,173 °K were varied by many times what seems the probable uncertainty of the observed values. However, this procedure had the desired effect of increasing $(\partial H^{\beta}/\partial x)_T$ at the lower temperatures near the phase-field boundary.

$$x \leqq 0.570\text{: } (\overline{H}_1^{\beta} - H_1^{\circ})/T$$
$$= (-215.3 + 329503.5x^4 - 590166.4x^5)/T$$
$$+ 3.7126 - 270.141x^4 + 505.528x^5 - 5.3113(10^{-3})T$$
$$+ 4.4945(10^{-6})T^2 - 1.6785(10^{-9})T^3. \quad (142)$$

From eqs (26), (28), (29), and (139):

$$x \leqq 0.570\text{: } (\overline{H}_2^{\beta} - H_2^{\circ})/T = -2.372 + 720.376x^3 - 1263.82x^4$$
$$+ (-29528.1 - 878676x^3 + 1475416x^4)/T$$
$$- 2.678(10^{-4})T + 12000/T^2. \quad (143)$$

By substituting from eq (143) in eq (11), integrating to satisfy eq (24), and adding a small correction term "Δ" (a function of x only) which will be presently evaluated (eq (151)), there is obtained

$$x \leqq 0.570\text{: } (\overline{G}_2^{\beta} - G_2^{\circ})/T$$
$$= 6.22313 \log x + 4.5758 \log (1 + 1.8493x^{6.97})$$
$$+ 5.1053 + 5845.8474x^3 - 10194.2788x^4$$
$$+ (-29528.1 - 878676x^3 + 1475416x^4)/T$$
$$+ (5.46177 - 1658.73778x^3 + 2910.07193x^4) \log T$$
$$+ 2.678(10^{-4})T + 6000/T^2 + \Delta. \quad (144)$$

On substitution from eqs (95), (143), and (144), eq (4) gives (with $\log (1 + 1.8493x^{6.97})$ expanded to one term):

$$x \leqq 0.570\text{: } \overline{S}_2^{\beta} = -6.22313 \log x - 3.675x^{6.97}$$
$$- 14.3061 - 5125.4714x^3 + 8930.4588x^4$$
$$+ (9.87355 + 1658.73778x^3 - 2910.07193x^4) \log T - \Delta. \quad (145)$$

The entropy will next be found. From eq (45) the entropy of α-zirconium at the transformation temperature is

$$S^{0(\alpha)}_{1136,\, x=0} = 18.7293. \quad (146)$$

Equations (44) and (139) give for the heat of transformation of zirconium

$$(H^{\circ(\beta)} - H^{\circ(\alpha)})_{1136,\, x=0} = 937.1. \quad (147)$$

Adding the corresponding entropy of transformation to eq (146),

$$S^{0(\beta)}_{1136,\, x=0} = 19.5542. \quad (148)$$

The entropy at 1,136 °K and any value of x up to 0.570, found from eq (7) by integrating from $x=0$ to x after substituting from eqs (145) and (148), is

$$x \leqq 0.570\text{: } S^{0(\beta)}_{1136} = 19.5542 + 9.28232x - 3.11156x \log x$$
$$- 0.23x^{7.97} - 7.17464x^4 + 3.9083x^5 - \tfrac{1}{2}\int_0^x \Delta dx. \quad (149)$$

When, using the heat capacity from eq (139), eq (2) is integrated to satisfy eq (149), the result is

$$x \leqq 0.570\text{: } S^{\circ(\beta)} = (17.87508 + 4.93677x$$
$$+ 207.3422x^4 - 291.0072x^5) \log T - 35.0610$$
$$- 5.80139x - 3.11156x \log x - 0.23x^{7.97}$$
$$- 640.6838x^4 + 893.0459x^5 - \tfrac{1}{2}\int_0^x \Delta dx. \quad (150)$$

The way in which eq (150) was derived indicates no value of Δ other than zero. With $\Delta = 0$, the equation gives for $x = 0.570$ values of entropy which are higher than those of eq (112) by 0.016 at all temperatures. To make the two equations agree, Δ was arbitrarily chosen to be

$$\Delta = -0.13 \log (x/0.570) \quad (151)$$

in eqs (144), (145), (149), and (150). Agreement with the value of eq (148) is maintained, and for $x = 0.57$ eqs (94) and (144) still agree. Since eq (151) changes the calculated values of hydrogen activity by only 3 percent for $x = 0.2$ and by less for higher values of x, the agreement with the observed values as tabulated in table 1 is still good and within the experimental error.

Equations (112) and (150) (with $\Delta = 0$) both depend on the entropy of zirconium metal at 820 °K, but were otherwise derived by different paths of composition- and temperature-change from this common point. The small disagreement of 0.016 noted above is thus a good check on some of the data entering the derivations, particularly on the basic hydrogen-activity equation (eq (23)) since this equation enters into the derivation of eq (150) only. However, some of the thermal data assumed affect both equations to comparable extents. Specifically, the close agreement is no real check on the β enthalpy functions (eqs (139) and (143)), nor on the exact choice of the eutectoid β composition (eq (101)), for to these it is rather insensitive.

When eq (144) (with Δ from eq (151)) is substituted into the Gibbs-Duhem relation (eq (9)) and the integration is required to satisfy eq (116), there is obtained

$$x \leqq 0.570\text{: } (\overline{G}_1^{\beta} - G_1^{\circ})/T = 22.3595 - 1.32311x$$
$$- 2192.19277x^4 + 4077.7115x^5 - 1.607x^{7.97} + 1.6x^{14.94}$$
$$+ (-215.3 + 329503.5x^4 - 590166.4x^5)/T$$
$$+ (-8.54863 + 622.02667x^4 - 1164.02877x^5) \log T$$
$$+ 5.3113(10^{-3})T - 2.24725(10^{-6})T^2$$
$$+ 5.595(10^{-10})T^3. \quad (152)$$

For $x = 0$ and $T = 1136$, this equation gives $+0.004$. This value should be zero, since 1,136 °K has been assumed to be the transformation temperature of zirconium. $\overline{S}_1^{\beta}$ for $x \leqq 0.570$ can readily be found from eq (4) or (5) using equations already given (45, 142, and 152).

7.3. Derived $(\alpha+\beta)$ Boundaries

Points x_α and x_β on the $\alpha/(\alpha+\beta)$ and $\beta/(\alpha+\beta)$ boundaries as determined by the formulations for the α and β fields given in this paper were then calculated at several temperatures, and are listed in table 7. This was done by requiring the respective partial molal free energies to be equal at the boundary compositions at the temperature in question (eqs (71), (81), (144), (151), and (152)). The compositions at the eutectoid temperature had already been determined (eqs (47) and (101)). The boundaries meet at the transformation temperature of zirconium. The solid $\alpha/(\alpha+\beta)$ and $\beta/(\alpha+\beta)$ boundaries in figure 1 were drawn through the points in table 7, except that they were allowed to deviate slightly from the 1,000 °K points, meeting as straight lines at $T=1136$ and $x=0$. LaGrange et al. [8] have pointed out that the two boundaries are required thermodynamically to meet at this point with a difference in slope equal to the heat of transformation of zirconium divided by RT^2. In the notation of the present paper this relation is

$$\left(\frac{dx_\alpha}{dT}-\frac{dx_\beta}{dT}\right)_{1136,\,x=0}=\left(\frac{H^{0(\beta)}-H^{0(\alpha)}}{RT^2}\right)_{1136,\,x=0}, \quad (153)$$

and is true provided the activity of diatomic hydrogen is proportional to x^2 in both solid solutions. Despite eq (23), this is a reasonable assumption for very dilute solutions, and the two boundaries have been drawn in figure 1 so as to meet with slopes satisfying eq (153) with the heat of transformation of eq (147). At the higher temperatures the procedure of this section in defining the boundaries becomes increasingly sensitive to errors in the data, and no calculations of this nature were attempted above 1,000 °K.

TABLE 7.—*Calculated boundary compositions of the $(\alpha+\beta)$ phase field*

T	x_α	x_β
°K		
820	0.0650	0.570
850	.0696	.535
865.3	.0717	.500
873.2	.0727	.472
900	.0747	.355
950	.0745	.259
956.6	.0741	.250
1000	.0708	.202
1136	.0000	.000

7.4. The $(\alpha+\beta)$ Properties

The values of $(\overline{G}_1^{\alpha+\beta}-G_1^0)/T$ and $(\overline{G}_2^{\alpha+\beta}-G_2^0)/T$ are of course the values at the boundaries given by the equations just cited. The enthalpy function and the entropy, $(H^{0(\alpha+\beta)}-H^{0(\alpha+\delta)}_{298.15})/T$ and $S^{0(\alpha+\beta)}$, are given by eq (16) after substituting from eqs (63), (75), (139), (150), and (151) and table 7. $\overline{S}_2^{\alpha+\beta}$ and $\overline{S}_1^{\alpha+\beta}$ were calculated from eqs (6) and (5) respectively. $(\overline{H}_1^{\alpha+\beta}-H_1^0)/T$ and $(\overline{H}_2^{\alpha+\beta}-H_2^0)/T$ were then obtained from eq (4). The latter function was also calculated from eq (26), which takes the form

$$(\overline{H}_2^{\alpha+\beta}-H_2^0)/T=$$
$$[2/T(x_\beta-x_\alpha)][(H^{0(\beta)}-H^{0(\alpha+\delta)}_{298})_{x_\beta}-(H^{0(\alpha)}-H^{0(\alpha+\delta)}_{298})_{x_\beta}]$$
$$+(\overline{H}_2^{\alpha+\delta}-H_2^0)_{298}/T-(H_2^0-H^0_{2(298)})/T. \quad (154)$$

The values calculated by the two methods differed (owing to small computational inconsistencies) by 0.007 on the average, and the mean was tabulated.[24]

The heat capacity in the $(\alpha+\beta)$ field was formulated by substituting the α and β enthalpies (given by eqs (63) and (139) into eq (16) and then taking the total derivative with respect to temperature. For simplicity replacing $(H^{0(\alpha)}-H^{0(\alpha+\delta)}_{298})_{x_\alpha}$ by "H^α" and $(H^{0(\beta)}-H^{0(\alpha+\delta)}_{298})_{x_\beta}$ by "H^β" and omitting the subscripts x_α and x_β, the result is

$$C_p^{0(\alpha+\beta)}=\left(\frac{\partial H^{\alpha+\beta}}{\partial T}\right)_x$$
$$=\left[\frac{x_\beta-x}{x_\beta-x_\alpha}\right]\left[\frac{\partial H^\alpha}{\partial T}+\left(\frac{\partial H^\alpha}{\partial x}-\frac{H^\beta-H^\alpha}{x_\beta-x_\alpha}\right)\frac{dx_\alpha}{dT}\right]$$
$$+\left[\frac{x-x_\alpha}{x_\beta-x_\alpha}\right]\left[\frac{\partial H^\beta}{\partial T}+\left(\frac{\partial H^\beta}{\partial x}-\frac{H^\beta-H^\alpha}{x_\beta-x_\alpha}\right)\frac{dx_\beta}{dT}\right]. \quad (155)$$

The phase-field boundary slopes in eq (155) may be replaced in terms of more common thermodynamic functions. Since

$$\overline{G}_2^{\alpha+\beta}=\overline{G}_2^\alpha=\overline{G}_2^\beta, \quad (156)$$

we have

$$\frac{d(\overline{G}_2^{\alpha+\beta}-G_2^0)/T}{dT}=\frac{\partial(\overline{G}_2^b-G_2^0)/T}{\partial T}$$
$$+\frac{\partial(\overline{G}_2^b-G_2^0)/T}{\partial x}\frac{dx_b}{dT}, \quad (157)$$

where b is either α or β. dx_α/dT and dx_β/dT may be substituted into eq (155) from eqs (157). If the temperature derivatives appearing in eq (157) are replaced from eq (11), some simplification is achieved by substituting for the resulting partial molal enthalpies from eqs (26) and (154). Equation (155) finally becomes

$$C_p^{0(\alpha+\beta)}=\left[\frac{x_\beta-x}{x_\beta-x_\alpha}\right]\left[\frac{\partial H^\alpha}{\partial T}+2\left(\frac{\partial H^\alpha}{\partial x}-\frac{H^\beta-H^\alpha}{x_\beta-x_\alpha}\right)^2\Big/T^2\frac{\partial}{\partial x}\left(\frac{G_2^\alpha-G_2^0}{T}\right)\right]$$
$$+\left[\frac{x-x_\alpha}{x_\beta-x_\alpha}\right]\left[\frac{\partial H^\beta}{\partial T}+2\left(\frac{\partial H^\beta}{\partial x}-\frac{H^\beta-H^\alpha}{x_\beta-x_\alpha}\right)^2\Big/T^2\frac{\partial}{\partial x}\left(\frac{\overline{G}_2^\beta-G_2^0}{T}\right)\right]. \quad (158)$$

The partial molal heat capacities can be found from eq (158) by using eq (5).

[24] As a further check, the values of $(\overline{H}_1^{\alpha+\beta}-H_1^0)/T$ and $(\overline{H}_2^{\alpha+\beta}-H_2^0)/T$ agreed approximately with those estimated from eq (11).

The procedure outlined in this section is generally applicable to determining the phase-field boundaries and the thermodynamic properties of two-phase fields from the properties of the adjoining one-phase fields. In the present case, there is considerable uncertainty in the $(\alpha+\beta)$ properties because of uncertainty in the exact locations and shapes of the boundaries, and this is particularly true of the heat capacity, which eq (155) shows to be highly dependent on the slopes of the boundaries. However, as noted earlier, small changes in the one-phase properties often have large effects on the calculated boundaries. For this reason, due consideration of direct evidence as to the positions of the boundaries can serve in a treatment of the present type to define the properties of the neighboring one-phase fields more accurately.

TABLE 8. *Thermodynamic functions for zirconium*, Zr

T in deg K, thermodynamic functions in cal (deg K)$^{-1}$ mole^{-1}. Subscript 1 refers to Zr(α). Subscript 2 refers to H_2(g).

$(\overline{C}_p)_1 = C_p^\circ \quad \overline{S}_1 = S^\circ \quad \overline{S}_2 = -(\overline{G}_2 - G_2^\circ)/T = \infty$

T	Phases present	$\frac{H^\circ - H^\circ_{298.15}}{T}$	C_p°	S°	$\frac{G^\circ - H^\circ_{298.15}}{T}$	$\frac{\overline{H}_1^\circ - H^\circ_1}{T}$	$\frac{\overline{G}_1 - G_1^\circ}{T}$	$\frac{\overline{H}_2 - H_2^\circ}{T}$	$(\overline{C}_p)_2$
298.15	α	0	6.197	9.290	−9.290	0	0	−86.12	1.16
300	α	0.038	6.205	9.329	−9.291	0	0	−85.62	1.20
350	α	.934	6.404	10.301	−9.367	0	0	−74.13	2.18
400	α	1.628	6.572	11.167	−9.539	0	0	−65.39	3.10
450	α	2.186	6.712	11.949	−9.763	0	0	−58.49	3.97
500	α	2.644	6.830	12.663	−10.019	0	0	−52.90	4.78
550	α	3.030	6.931	13.319	−10.289	0	0	−48.25	5.52
600	α	3.359	7.020	13.926	−10.567	0	0	−44.32	6.21
650	α	3.643	7.102	14.491	−10.848	0	0	−40.95	6.84
709	α	3.893	7.182	15.020	−11.127	0	0	−38.02	7.40
750	α	4.115	7.265	15.519	−11.404	0	0	−35.44	7.91
791.5	α	4.282	7.340	15.912	−11.629	0	0	−33.53	8.29
800	α	4.315	7.357	15.990	−11.675	0	0	−33.16	8.36
820	α	4.390	7.396	16.172	−11.782	0	0	−32.32	8.53
845.6	α	4.482	7.451	16.400	−11.919	0	0	−31.30	8.64
850	α	4.497	7.461	16.439	−11.942	0	0	−31.13	8.66
865.3	α	4.550	7.496	16.573	−12.023	0	0	−30.55	8.73
891.5	α	4.637	7.561	16.797	−12.160	0	0	−29.60	8.85
900	α	4.665	7.584	16.869	−12.204	0	0	−29.31	8.89
950	α	4.822	7.729	17.283	−12.461	0	0	−27.67	9.11
956.6	α	4.842	7.751	17.337	−12.494	0	0	−27.46	9.14
1000	α	4.972	7.904	17.684	−12.712	0	0	−26.18	9.34
1050	α	5.116	8.111	18.074	−12.958	0	0	−24.83	9.56
1089.9	α	5.204	8.258	18.312	−13.108	0	0	−24.05	9.70
1100	α	5.258	8.357	18.457	−13.199	0	0	−23.59	9.79
1136	α	5.359	8.560	18.729	−13.370	0	0	−22.76	9.95
1136	β	6.18	7.76	19.55	−13.37	0.82	0	−28.66	4.29
1150	β	6.20	7.76	19.65	−13.45	.80	−0.01	−28.35	4.29
1200	β	6.27	7.76	19.98	−13.71	.73	−.04	−27.29	4.29

TABLE 9. *Thermodynamic functions for* ZrH_{0-25}

T in deg K, thermodynamic functions in cal (deg K)$^{-1}$ mole^{-1}. Subscript 1 refers to Zr(α). Subscript 2 refers to H_2(g).

T	Phases present	$\frac{H^\circ - H^\circ_{298.15}}{T}$	C_p°	S°	$\frac{G^\circ - H^\circ_{298.15}}{T}$	$\frac{\overline{H}_1 - H_1^\circ}{T}$	$(\overline{C}_p)_1$	$\overline{S}_1$	$\frac{\overline{G}_1 - G_1^\circ}{T}$	$\frac{\overline{H}_2 - H_2^\circ}{T}$	$(\overline{C}_p)_2$	$\overline{S}_2$	$\frac{\overline{G}_2 - G_2^\circ}{T}$
298.15	$\alpha+\delta$	0	6.54	9.27	−9.27	0.02	6.32	9.31	−0.00	−139.12	1.71	−0.29	−107.62
300	$\alpha+\delta$	0.04	6.54	9.31	−9.27	.02	6.32	9.34	−.00	−138.29	1.74	−.28	−106.76
350	$\alpha+\delta$	.98	6.78	10.33	−9.35	.02	6.42	10.33	−.00	−119.20	2.86	+.07	−86.95
400	$\alpha+\delta$	1.73	7.11	11.26	−9.53	.02	6.58	11.19	−.00	−104.73	4.24	.54	−72.02
450	$\alpha+\delta$	2.35	7.51	12.12	−9.77	.03	6.81	11.98	−.00	−93.32	5.57	1.12	−60.36
500	$\alpha+\delta$	2.89	7.94	12.93	−10.05	.04	7.12	12.71	−.00	−84.07	6.56	1.76	−51.03
550	$\alpha+\delta$	3.37	8.39	13.71	−10.35	.08	7.51	13.41	−.01	−76.44	7.05	2.41	−43.38
600	$\alpha+\delta$	3.80	8.85	14.46	−10.66	.13	7.97	14.08	−.02	−70.06	7.03	3.03	−37.01
650	$\alpha+\delta$	4.21	9.32	15.19	−10.98	.21	8.48	14.74	−.04	−64.69	6.75	3.58	−31.62
700	$\alpha+\delta$	4.59	9.86	15.90	−11.30	.31	9.01	15.39	−.06	−60.09	6.76	4.08	−27.00
750	$\alpha+\delta$	4.97	10.53	16.60	−11.63	.43	9.53	16.03	−.08	−56.07	8.00	4.58	−23.00
800	$\alpha+\delta$	5.34	11.48	17.31	−11.97	.55	10.00	16.66	−.11	−52.41	11.86	5.20	−19.49
820	$\alpha+\delta$	5.50	11.99	17.60	−12.10	.61	10.17	16.91	−.13	−50.98	14.54	5.52	−18.22
820	$\alpha+\beta$	6.49	9.99	18.59	−12.10	.26	7.56	16.56	−.13	−40.26	19.43	16.24	−18.22
850	$\alpha+\beta$	6.64	11.60	18.97	−12.34	.24	6.88	16.82	−.14	−38.15	37.74	17.19	−16.81
900	$\alpha+\beta$	7.18	17.32	19.90	−12.73	+.07	3.96	17.09	−.15	−31.22	106.89	22.53	−14.80
950	$\alpha+\beta$	7.61	14.82	20.74	−13.13	−.08	5.26	17.35	−.15	−25.53	76.19	27.08	−13.27
956.6	$\alpha+\beta$	7.66	14.94	20.84	−13.18	−.10	5.29	17.39	−.15	−24.86	77.14	27.62	−13.10
956.6	β	7.66	8.53	20.84	−13.18	+1.23	7.20	18.72	−.15	−35.49	10.61	16.99	−13.10
1000	β	7.70	8.53	21.22	−13.52	1.15	7.20	19.04	−.20	−33.80	10.61	17.46	−11.56
1050	β	7.74	8.53	21.64	−13.90	1.06	7.20	19.39	−.25	−32.03	10.61	17.98	−9.96
1100	β	7.77	8.53	22.03	−14.26	0.96	7.20	19.72	−.30	−30.42	10.61	18.47	−8.50
1136	β	7.80	8.53	22.31	−14.51	.89	7.20	19.95	−.33	−29.35	10.61	18.82	−7.54
1150	β	7.80	8.53	22.41	−14.61	.86	7.20	20.04	−.34	−28.96	10.61	18.95	−7.18
1200	β	7.84	8.53	22.77	−14.94	.76	7.20	20.35	−.38	−27.61	10.61	19.40	−5.98

8. Tables of Thermodynamic Functions

The common integral and differential thermodynamic properties were calculated as described previously in this paper, and are listed in tables 8–14 for zirconium and several compositions of zirconium hydride (ZrH_x). In addition, table 15 gives the properties of ideal "normal" hydrogen gas (H_2, 25% para and 75% ortho) [20], which are closely related to those of the Zr-H system. The tables cover evenly spaced compositions of ZrH_x with $x=0$, 0.25, 0.50, 0.75, 1.00, and 1.25; in addition, the composition $x=0.57$ is also included in the tabulation, partly because this composition is of special interest as the assumed β-phase eutectoid composition, and partly because the β-field properties are separately formulated on both sides of this composition. In conformity with the conventions used throughout this paper, temperatures are in degrees Kelvin and the thermodynamic properties are given in defined thermochemical calories per degree per mole of ZrH_x (or H_2, in table 15). The temperatures tabulated, which begin with 298.15 °K, run every 50° from 300 to 1,200 °K except that the eutectoid temperature, 820 °K, and the transformation temperature, 1,136 °K, are included in all the tables because of some interest in these particular isotherms. In addition, each table includes

TABLE 10. *Thermodynamic functions for* $ZrH_{0.50}$

T in deg K, thermodynamic functions in cal (deg K)$^{-1}$ mole^{-1}. Subscript 1 refers to Zr(α). Subscript 2 refers to H_2(g).

T	Phases present	$\frac{H^\circ-H^\circ_{298.15}}{T}$	C_p°	S°	$\frac{G^\circ-H^\circ_{298.15}}{T}$	$\frac{\overline{H}_1-H_1^\circ}{T}$	$(\overline{C}_p)_1$	$\overline{S}_1$	$\frac{\overline{G}_1-G_1^\circ}{T}$	$\frac{\overline{H}_2-H_2^\circ}{T}$	$(\overline{C}_p)_2$	$\overline{S}_2$	$\frac{\overline{G}_2-G_2^\circ}{T}$
298.15	α+δ	0	6.75	9.23	−9.23	0.02	6.32	9.31	−0.00	−139.12	1.71	−0.29	−107.62
300	α+δ	0.04	6.76	9.28	−9.23	.02	6.32	9.34	−.00	−138.29	1.74	−.28	−106.76
350	α+δ	1.03	7.14	10.34	−9.32	.02	6.42	10.33	−.00	−119.20	2.86	+.07	−86.95
400	α+δ	1.82	7.64	11.33	−9.51	.02	6.58	11.19	−.00	−104.73	4.24	.54	−72.02
450	α+δ	2.50	8.21	12.26	−9.76	.03	6.81	11.98	−.00	−93.32	5.57	1.12	−60.36
500	α+δ	3.10	8.76	13.15	−10.06	.04	7.12	12.71	−.00	−84.07	6.56	1.76	−51.03
550	α+δ	3.64	9.27	14.01	−10.38	.08	7.51	13.41	−.01	−76.44	7.05	2.41	−43.38
600	α+δ	4.12	9.73	14.84	−10.72	.13	7.97	14.08	−.02	−70.06	7.03	3.03	−37.01
650	α+δ	4.57	10.17	15.64	−11.06	.21	8.48	14.74	−.04	−64.69	6.75	3.58	−31.62
700	α+δ	4.99	10.70	16.41	−11.42	.31	9.01	15.39	−.06	−60.09	6.76	4.08	−27.00
750	α+δ	5.40	11.53	17.17	−11.78	.43	9.53	16.03	−.08	−56.07	8.00	4.58	−23.00
800	α+δ	5.82	12.97	17.96	−12.14	.55	10.00	16.66	−.11	−52.41	11.86	5.20	−19.49
820	α+δ	6.00	13.80	18.29	−12.28	.61	10.17	16.91	−.13	−50.98	14.54	5.52	−18.22
820	α+β	8.34	12.42	20.62	−12.28	.26	7.56	16.56	−.13	−40.26	19.43	16.24	−18.22
850	α+β	8.54	16.32	21.12	−12.59	.24	6.88	16.82	−.14	−38.15	37.74	17.19	−16.81
865.3	α+β	8.72	22.57	21.46	−12.74	.22	5.74	16.94	−.14	−36.72	67.33	18.09	−16.14
865.3	β	8.72	10.51	21.46	−12.74	2.55	6.68	19.26	−.14	−46.02	15.35	8.78	−16.14
900	β	8.79	10.51	21.87	−13.08	2.41	6.68	19.52	−.24	−43.93	15.35	9.39	−14.37
950	β	8.88	10.51	22.44	−13.56	2.24	6.68	19.88	−.37	−41.19	15.35	10.22	−12.07
1000	β	8.96	10.51	22.98	−14.02	2.07	6.68	20.23	−.48	−38.72	15.35	11.00	−10.02
	β												
1050		9.04	10.51	23.49	−14.46	1.91	6.68	20.55	−.57	−36.49	15.35	11.75	−8.19
1100	β	9.10	10.51	23.98	−14.88	1.75	6.68	20.86	−.66	−34.46	15.35	12.47	−6.54
1136	β	9.15	10.51	24.32	−15.17	1.64	6.68	21.08	−.71	−33.11	15.35	12.97	−5.45
1150	β	9.16	10.51	24.45	−15.29	1.59	6.68	21.16	−.73	−32.61	15.35	13.16	−5.05
1200	β	9.22	10.51	24.90	−15.68	1.44	6.68	21.44	−.80	−30.92	15.35	13.81	−3.70

TABLE 11. *Thermodynamic functions for* $ZrH_{0.57}$

T in deg K, thermodynamic functions in cal (deg K)$^{-1}$ mole^{-1}. Subscript 1 refers to Zr(α). Subscript 2 refers to H_2(g).

T	Phases present	$\frac{H^\circ-H^\circ_{298.15}}{T}$	C_p°	S°	$\frac{G^\circ-H^\circ_{298.15}}{T}$	$\frac{\overline{H}_1-H_1^\circ}{T}$	$(\overline{C}_p)_1$	$\overline{S}_1$	$\frac{\overline{G}_1-G_1^\circ}{T}$	$\frac{\overline{H}_2-H_2^\circ}{T}$	$(\overline{C}_p)_2$	$\overline{S}_2$	$\frac{\overline{G}_2-G_2^\circ}{T}$
298.15	α+δ	0	6.81	9.22	−9.22	0.02	6.32	9.31	−0.00	−139.12	1.71	−0.29	−107.62
300	α+δ	0.04	6.82	9.26	−9.22	.02	6.32	9.34	−.00	−138.29	1.74	−.28	−106.76
350	α+δ	1.04	7.24	10.34	−9.31	.02	6.42	10.33	−.00	−119.20	2.86	+.07	−86.95
400	α+δ	1.85	7.79	11.35	−9.50	.02	6.58	11.19	−.00	−104.73	4.24	.54	−72.02
450	α+δ	2.54	8.40	12.30	−9.76	.03	6.81	11.98	−.00	−93.32	5.57	1.12	−60.36
500	α+δ	3.16	8.99	13.22	−10.06	.04	7.12	12.71	−.00	−84.07	6.56	1.76	−51.03
550	α+δ	3.71	9.52	14.10	−10.39	.08	7.51	13.41	−.01	−76.44	7.05	2.41	−43.38
600	α+δ	4.22	9.98	14.95	−10.73	.13	7.97	14.08	−.02	−70.06	7.03	3.03	−37.01
650	α+δ	4.68	10.40	15.76	−11.09	.21	8.48	14.74	−.04	−64.69	6.75	3.58	−31.62
700	α+δ	5.10	10.94	16.55	−11.45	.31	9.01	15.39	−.06	−60.09	6.76	4.08	−27.00
750	α+δ	5.52	11.81	17.33	−11.82	.43	9.53	16.03	−.08	−56.07	8.00	4.58	−23.00
800	α+δ	5.96	13.38	18.14	−12.18	.55	10.00	16.66	−.11	−52.41	11.86	5.20	−19.49
820	α+δ	6.15	14.31	18.48	−12.34	.61	10.17	16.91	−.13	−50.98	14.54	5.52	−18.22
820	β	8.85	10.89	21.19	−12.34	2.21	9.66	18.51	−.13	−47.10	4.29	9.41	−18.22
850	β	8.93	10.89	21.58	−12.65	2.21	9.66	18.86	−.21	−45.53	4.29	9.56	−16.55
900	β	9.04	10.89	22.20	−13.17	2.20	9.66	19.41	−.34	−43.16	4.29	9.80	−14.02
950	β	9.13	10.89	22.79	−13.66	2.19	9.66	19.93	−.45	−41.04	4.29	10.03	−11.74
1000	β	9.22	10.89	23.35	−14.13	2.18	9.66	20.42	−.56	−39.14	4.29	10.25	−9.69
1050	β	9.30	10.89	23.88	−14.58	2.15	9.66	20.90	−.67	−37.41	4.29	10.46	−7.82
1100	β	9.37	10.89	24.39	−15.02	2.12	9.66	21.35	−.77	−35.85	4.29	10.66	−6.12
1136	β	9.42	10.89	24.74	−15.32	2.09	9.66	21.66	−.84	−34.80	4.29	10.80	−4.98
1150	β	9.44	10.89	24.87	−15.43	2.08	9.66	21.78	−.86	−34.42	4.29	10.86	−4.56
1200	β	9.50	10.89	25.33	−15.84	2.03	9.66	22.19	−.95	−33.11	4.29	11.04	−3.12

the temperature at which the derived properties indicate that the particular composition crosses a phase-field boundary, with properties being tabulated for both the fields which meet at that boundary. Except for the properties of hydrogen gas and for those of α-zirconium which were not derived from those of the zirconium hydrides, the values of the properties have been rounded off to two decimal places as being more in keeping with their uncertainties in general.

9. References

[1] A. Sieverts and E. Roell, Zirconium, thorium, and hydrogen, Z. anorg. allgem. Chem. **153,** 289–308 (1926).

[2] M. N. A. Hall, S. L. H. Martin, and A. L. G. Rees, Solubility of hydrogen in zirconium and zirconium-oxygen solid solutions, Trans. Faraday Soc. **41,** 306–316 (1945).

[3] E. A. Gulbransen and K. F. Andrew, Crystal structure and thermodynamic studies on the zirconium-hydrogen alloys, J. Electrochem. Soc. **101,** 474–480 (1954).

[4] E. A. Gulbransen and K. F. Andrew, Solubility and decomposition pressures of hydrogen in alpha-zirconium, J. Metals **7,** 136–144 (1955).

TABLE 12. *Thermodynamic functions for* $ZrH_{0.75}$

T in deg K, thermodynamic functions in cal (deg K)$^{-1}$ mole^{-1}. Subscript 1 refers to Zr(α). Subscript 2 refers to H_2(g).

T	Phases present	$\frac{H^\circ-H^\circ_{298.15}}{T}$	C_p°	S°	$\frac{G^\circ-H^\circ_{298.15}}{T}$	$\frac{\overline{H}_1-H_1^\circ}{T}$	$(\overline{C}_p)_1$	$\overline{S}_1$	$\frac{\overline{G}_1-G_1^\circ}{T}$	$\frac{\overline{H}_2-H_2^\circ}{T}$	$(\overline{C}_p)_2$	$\overline{S}_2$	$\frac{\overline{G}_2-G_2^\circ}{T}$
298.15	α+δ	0	6.97	9.20	−9.20	0.02	6.32	9.31	−0.00	−139.12	1.71	−0.29	−107.62
300	α+δ	0.04	6.98	9.24	−9.20	.02	6.32	9.34	−.00	−138.29	1.74	−.28	−106.76
350	α+δ	1.07	7.49	10.35	−9.28	.02	6.42	10.33	−.00	−119.20	2.86	+.07	−86.95
400	α+δ	1.91	8.17	11.40	−9.48	.02	6.58	11.19	−.00	−104.73	4.24	.54	−72.02
450	α+δ	2.65	8.90	12.40	−9.75	.03	6.81	11.98	−.00	−93.32	5.57	1.12	−60.36
500	α+δ	3.31	9.58	13.37	−10.06	.04	7.12	12.71	−.00	−84.07	6.56	1.76	−51.03
550	α+δ	3.91	10.16	14.32	−10.41	.08	7.51	13.41	−.01	−76.44	7.05	2.41	−43.38
600	α+δ	4.45	10.61	15.22	−10.77	.13	7.97	14.08	−.02	−70.06	7.03	3.03	−37.01
650	α+δ	4.94	11.01	16.08	−11.15	.21	8.48	14.74	−.04	−64.69	6.75	3.58	−31.62
700	α+δ	5.39	11.55	16.92	−11.53	.31	9.01	15.39	−.06	−60.09	6.76	4.08	−27.00
750	α+δ	5.83	12.53	17.74	−11.92	.43	9.53	16.03	−.08	−56.07	8.00	4.58	−23.00
800	α+δ	6.30	14.45	18.61	−12.31	.55	10.00	16.66	−.11	−52.41	11.86	5.20	−19.49
820	α+δ	6.51	15.62	18.98	−12.47	.61	10.17	16.91	−.13	−50.98	+14.54	+5.52	−18.22
820	β+δ	8.41	23.55	20.87	−12.47	5.88	33.12	22.19	−.13	−60.00	−25.52	−3.50	−18.22
850	β+δ	8.98	25.08	21.76	−12.78	6.56	31.21	23.35	−.35	−58.86	−16.36	−4.24	−16.08
891.5	β+δ	9.71	23.77	22.93	−13.22	7.25	26.40	24.73	−.68	−56.99	−7.03	−4.79	−13.32
891.5	β	9.71	11.27	22.93	−13.22	2.20	9.66	19.68	−.68	−43.55	+4.29	+8.65	−13.32
900	β	9.72	11.27	23.04	−13.32	2.20	9.66	19.78	−.70	−43.16	4.29	8.69	−12.91
950	β	9.80	11.27	23.65	−13.84	2.19	9 66	20.30	−.82	−41.04	4.29	8.92	−10.63
1000	β	9.88	11 27	24.22	−14.35	2.18	9.66	20.80	−.94	−39.14	4.29	9.14	−8.58
1050	β	9.94	11.27	24.78	−14.83	2.15	9.66	21.27	−1.04	−37.41	4.29	9.35	−6.71
1100	β	10.00	11.27	25.30	−15.30	2.12	9.66	21.72	−1.14	−35.85	4.29	9.55	−5.00
1136	β	10.04	11.27	25.66	−15.62	2.09	9.66	22.03	−1.21	−34.80	4.29	9.69	−3.87
1150	β	10.06	11.27	25.80	−15.74	2.08	9.66	22.15	−1.23	−34.42	4.29	9.75	−3.44
1200	β	10.11	11.27	26.28	−16.17	2.03	9.66	22.56	−1.32	−33.11	4.29	9.93	−2.01

TABLE 13. *Thermodynamic functions for* $ZrH_{1.00}$

T in deg K, thermodynamic functions in cal (deg K)$^{-1}$ mole^{-1}. Subscript 1 refers to Zr(α). Subscript 2 refers to H_2(g).

T	Phases present	$\frac{H^\circ-H^\circ_{298.15}}{T}$	C_p°	S°	$\frac{G^\circ-H^\circ_{298.15}}{T}$	$\frac{\overline{H}_1-H_1^\circ}{T}$	$(\overline{C}_p)_1$	$\overline{S}_1$	$\frac{\overline{G}_1-G_1^\circ}{T}$	$\frac{\overline{H}_2-H_2^\circ}{T}$	$(\overline{C}_p)_2$	$\overline{S}_2$	$\frac{\overline{G}_2-G_2^\circ}{T}$
298.15	α+δ	0	7.18	9.16	−9.16	0.02	6.32	9.31	−0.00	−139.12	1.71	−0.29	−107.62
300	α+δ	0.04	7.20	9.20	−9.16	.02	6.32	9.34	−.00	−138.29	1.74	−.28	−106.76
350	α+δ	1.11	7.85	10.36	−9.25	.02	6.42	10.33	−.00	−119.20	2.86	+.07	−86.95
400	α+δ	2.00	8.70	11.46	−9.46	.02	6.58	11.19	−.00	−104.73	4.24	.54	−72.02
450	α+δ	2.80	9.60	12.54	−9.74	.03	6.81	11.98	−.00	−93.32	5.57	1.12	−60.36
500	α+δ	3.52	10.40	13.59	−10.07	.04	7.12	12.71	−.00	−84.07	6.56	1.76	−51.03
550	α+δ	4.18	11.04	14.62	−10.44	.08	7.51	13.41	−.01	−76.44	7.05	2.41	−43.38
600	α+δ	4.77	11.49	15.60	−10.83	.13	7.97	14.08	−.02	−70.06	7.03	3.03	−37.01
650	α+δ	5.30	11.85	16.53	−11.23	.21	8.48	14.74	−.04	−64.69	6.75	3.58	−31.62
700	α+δ	5.78	12.39	17.43	−11.64	.31	9.01	15.39	−.06	−60.09	6.76	4.08	−27.00
750	α+δ	6.26	13.53	18.32	−12.06	.43	9.53	16.03	−.08	−56.07	8.00	4.58	−23.00
800	α+δ	6.78	15.93	19.26	−12.48	.55	10.00	16.66	−.11	−52.41	11.86	5.20	−19.49
820	α+δ	7.02	17.44	19.67	−12.65	.61	10.17	16.91	−.13	−50.98	+14.54	+5.52	−18.22
820	β+δ	7.79	20.36	20.44	−12.65	5.88	33.12	22.19	−.13	−60.00	−25.52	−3.50	−18.22
850	β+δ	8.29	23.04	21.23	−12.94	6.56	31.21	23.35	−.35	−58.86	−16.36	−4.24	−16.08
900	β+δ	9.11	22.60	22.55	−13.44	7.35	25.37	24.97	−.75	−56.58	−5.52	−4.85	−12.78
950	β+δ	9.77	20.60	23.72	−13.95	7.75	20.07	26.19	−1.16	−54.08	+1.07	−4.96	−9.79
1000	β+δ	10.27	19.04	24.73	−14.46	7.89	16.68	27.13	−1.56	−51.58	4.72	−4.80	−7.08
1050	β+δ	10.66	17.99	25.63	−14.97	7.88	14.76	27.89	−1.94	−49.20	6.47	−4.52	−4.62
1080.9	β+δ	10.86	17.46	26.15	−15.28	7.83	13.97	28.31	−2.17	−47.80	6.98	−4.32	−3.22
1080.9	δ	10.86	11.81	26.15	−15.28	2.13	9.66	22.62	−2.17	−36.43	4.29	+7.06	−3.22
1100	δ	10.88	11.81	26.36	−15.48	2.12	9.66	22.79	−2.21	−35.85	4.29	7.14	−2.59
1136	δ	10.91	11.81	26.74	−15.83	2.09	9.66	23.10	−2.28	−34.80	4.29	7.28	−1.45
1150	δ	10.92	11.81	26.88	−15.96	2.08	9.66	23.22	−2.30	−34.42	4.29	7.33	−1.03
1200	δ	10.96	11.81	27.38	−16.42	2.03	9.66	23.63	−2.39	−33.11	4.29	7.52	+0.41

[5] R. K. Edwards, P. Levesque, and D. Cubicciotti, Solid solution equilibria in the zirconium-hydrogen system, J. Amer. Chem. Soc. **77,** 1307–1311 (1955).
[6] C. E. Ells and A. D. McQuillan, A study of the hydrogen-pressure relationships in the zirconium-hydrogen system, J. Inst. Metals **85,** 89–96 (1956).
[7] M. W. Mallett and W. M. Albrecht, Low-pressure solubility and diffusion of hydrogen in zirconium, J. Electrochem. Soc. **104,** 142–146 (1957).
[8] L. D. LaGrange, L. J. Dykstra, J. M. Dixon, and U. Merten, A study of the zirconium-hydrogen and zirconium-hydrogen-uranium systems between 600 and 800°, J. Phys. Chem. **63,** 2035–2041 (1959).
[9] C. M. Schwartz and M. W. Mallett, Observations on the behavior of hydrogen in zirconium, Trans. Amer. Soc. Metals **46,** 640–651 (1954).
[10] D. A. Vaughan and J. R. Bridge, High-temperature X-ray diffraction investigation of the Zr-H system, J. Metals **8,** 528–531 (1956).
[11] R. E. Rundle, C. G. Shull, and E. O. Wollan, The crystal structure of thorium and zirconium dihydrides by X-ray and neutron diffraction, Acta Cryst. **5,** 22–26 (1952).
[12] R. L. Beck, Thermophysical properties of zirconium hydride, Trans. Amer. Soc. Metals **54,** 556–564 (1962).
[13] L. Espagno, P. Azou, and P. Bastien, Dilatometric study of the system zirconium-hydrogen, Compt. rend. **247,** 1199–1202 (1958).
[14] L. Espagno, P. Azou, and P. Bastien, Dilatometric study of the zirconium-hydrogen system between ambient and 500°, Compt. rend. **248,** 2003–2005 (1959).
[15] H. E. Flotow and D. W. Osborne, Heat capacities and thermodynamic functions of ZrH_2 and ZrD_2 from 5 to 350°K and the hydrogen vibration frequency in ZrH_2, J. Chem. Phys. **34,** 1418–1425 (1961).
[16] T. B. Douglas and A. C. Victor, Heat content of zirconium and of five compositions of zirconium hydride from 0 to 900 °C, J. Research NBS **61,** 13–23 (1958) RP2878.
[17] T. B. Douglas, The zirconium-hydrogen system: some thermodynamic properties from a heat content study, J. Amer. Chem. Soc. **80,** 5040–5046 (1958).
[18] S. L. H. Martin and A. L. G. Rees, Interpretation of the solubility of hydrogen in zirconium, Trans. Faraday Soc. **50,** 343–352 (1954).

TABLE 14. *Thermodynamic functions for* $ZrH_{1.25}$

T in deg K, thermodynamic functions in cal (deg K)$^{-1}$ mole^{-1}. Subscript 1 refers to Zr(α). Subscript 2 refers to H_2(g).

T	Phases present	$\frac{H^\circ-H^\circ_{298.15}}{T}$	C_p°	S°	$\frac{G^\circ-H^\circ_{298.15}}{T}$	$\frac{\overline{H}_1-H_1^\circ}{T}$	$(\overline{C}_p)_1$	$\overline{S}_1$	$\frac{\overline{G}_1-G_1^\circ}{T}$	$\frac{\overline{H}_2-H_2^\circ}{T}$	$(\overline{C}_p)_2$	$\overline{S}_2$	$\frac{\overline{G}_2-G_2^\circ}{T}$
298.15	$\alpha+\delta$	0	7.39	9.12	−9.12	0.02	6.32	9.31	−0.00	−139.12	1.71	−0.29	−107.62
300	$\alpha+\delta$	0.05	7.42	9.17	−9.12	.02	6.32	9.34	−.00	−138.29	1.74	−.28	−106.76
350	$\alpha+\delta$	1.15	8.21	10.37	−9.22	.02	6.42	10.33	−.00	−119.20	2.86	+.07	−86.95
400	$\alpha+\delta$	2.10	9.23	11.53	−9.34	.02	6.58	11.19	−.00	−104.73	4.24	.54	−72.02
450	$\alpha+\delta$	2.95	10.29	12.68	−9.73	.03	6.81	11.98	−.00	−93.32	5.57	1.12	−60.36
500	$\alpha+\delta$	3.73	11.23	13.81	−10.08	.04	7.12	12.71	−.00	−84.07	6.56	1.76	−51.03
550	$\alpha+\delta$	4.45	11.92	14.92	−10.47	.08	7.51	13.41	−.01	−76.44	7.05	2.41	−43.38
600	$\alpha+\delta$	5.09	12.37	15.98	−10.89	.13	7.97	14.08	−.02	−70.06	7.03	3.30	−37.01
650	$\alpha+\delta$	5.66	12.70	16.98	−11.32	.21	8.48	14.74	−.04	−64.69	6.75	3.58	−31.62
700	$\alpha+\delta$	6.18	13.24	17.94	−11.76	.31	9.01	15.39	−.06	−60.09	6.76	4.08	−27.00
750	$\alpha+\delta$	6.69	14.53	18.89	−12.20	.43	9.53	16.03	−.08	−56.07	8.00	4.58	−23.00
791.5	$\alpha+\delta$	7.15	16.77	19.73	−12.57	.53	9.93	16.55	−.11	−53.02	10.94	5.08	−20.05
791.5	δ	7.15	13.12	19.73	−12.57	2.91	13.12	18.94	−.11	−56.82	0.00	1.26	−20.05
800	δ	7.22	13.12	19.87	−12.65	2.94	13.12	19.08	−.15	−56.29	.00	1.26	−19.44
820	δ	7.36	13.12	20.19	−12.83	3.01	13.12	19.40	−.22	−55.09	.00	1.26	−18.07
845.6	δ	7.53	13.12	20.59	−13.06	3.09	13.12	19.80	−.32	−53.64	.00	+1.26	−16.39
845.6	$\beta+\delta$	7.53	20.64	20.59	−13.06	6.49	31.62	23.18	−.32	−59.05	−17.56	−4.16	−16.39
850	$\beta+\delta$	7.60	20.99	20.70	−13.10	6.56	31.21	23.35	−.35	−58.86	−16.36	−4.24	−16.08
900	$\beta+\delta$	8.39	21.91	21.94	−13.55	7.35	25.37	24.97	−.75	−56.58	−5.52	−4.85	−12.78
950	$\beta+\delta$	9.07	20.74	23.10	−14.02	7.75	20.07	26.19	−1.16	−54.08	+1.07	−4.96	−9.79
1000	$\beta+\delta$	9.63	19.63	24.13	−14.50	7.89	16.68	27.13	−1.56	−51.58	4.72	−4.80	−7.08
1050	$\beta+\delta$	10.08	18.80	25.07	−14.99	7.88	14.76	27.89	−1.94	−49.20	6.47	−4.52	−4.62
1100	$\beta+\delta$	10.46	18.03	25.93	−15.46	7.78	13.56	28.55	−2.31	−46.98	7.15	−4.20	−2.38
1136	$\beta+\delta$	10.69	17.45	26.50	−15.81	7.68	12.87	28.98	−2.56	−45.49	7.32	−3.97	−0.89
1150	$\beta+\delta$	10.77	17.22	26.71	−15.94	7.64	12.62	29.13	−2.66	−44.94	7.35	−3.88	−.34
1200	$\beta+\delta$	11.02	16.39	27.42	−16.40	7.47	11.76	29.65	−2.98	−43.06	7.41	−3.56	+1.53

TABLE 15. *Ideal-gas thermodynamic functions for normal hydrogen,* H_2 *(25 percent para, 75 percent ortho)*

T in deg K, thermodynamic functions in cal (deg K)$^{-1}$ mole^{-1}

T	$\frac{H^\circ-H^\circ_{298.15}}{T}$	C_p°	S°	$\frac{G^\circ-H^\circ_{298.15}}{T}$	T	$\frac{H^\circ-H^\circ_{298.15}}{T}$	C_p°	S°	$\frac{G^\circ-H^\circ_{298.15}}{T}$
298.15	0	6.891	31.209	−31.209	845.6	4.537	7.108	38.502	−33.965
300	0.043	6.894	31.252	−31.209	850	4.551	7.110	38.539	−33.988
350	1.026	6.951	32.321	−31.295	865.3	4.596	7.120	38.666	−34.070
400	1.769	6.975	33.251	−31.482	891.5	4.671	7.136	38.879	−34.208
450	2.347	6.987	34.072	−31.725	900	4.695	7.142	38.946	−34.251
500	2.813	6.993	34.809	−31.996	950	4.825	7.180	39.334	−34.509
550	3.192	7.001	35.477	−32.285	956.6	4.841	7.185	39.384	−34.543
600	3.511	7.009	36.085	−32.574	1000	4.944	7.220	39.702	−34.758
650	3.780	7.021	36.647	−32.867	1050	5.052	7.261	40.055	−35.003
700	4.011	7.037	37.168	−33.157	1080.9	5.116	7.291	40.267	−35.151
750	4.214	7.057	37.653	−33.439	1100	5.154	7.309	40.395	−35.241
791.5	4.363	7.077	38.034	−33.671	1136	5.223	7.343	40.631	−35.408
800	4.392	7.081	38.110	−33.718	1150	5.249	7.357	40.721	−35.472
820	4.458	7.092	38.285	−33.827	1200	5.337	7.406	41.035	−35.698

[19] G. G. Libowitz, The nature and properties of transition metal hydrides, J. nuclear materials **2,** 1–22 (1960).
[20] J. Hilsenrath, C. W. Beckett, W. S. Benedict, L. Fano, H. J. Hoge, J. F. Masi, R. L. Nuttall, Y. S. Touloukian, and H. W. Woolley, Tables of thermal properties of gases, NBS Circ. 564, pp. 290–292 (U.S. Government Printing Office, Washington, D.C. Nov. 1, 1955).
[21] F. D. Rossini, D. D. Wagman, W. H. Evans, S. Levine, and I. Jaffe, Selected values of chemical thermodynamic properties, NBS Circ. 500, p. 718 (U.S. Government Printing Office, Washington, D.C., 1952).
[22] G. B. Skinner, Thermodynamic and structural properties of zirconium, Ph.D. Dissertation, Ohio State Univ., Columbus, Ohio, 1951.
[23] J. L. Scott, A calorimetric investigation of zirconium, titanium, and zirconium alloys from 60 to 960° C, A.E.C. Report ORNL–2328, Oak Ridge Natl. Lab., Oak Ridge, Tenn., 1957.
[24] S. S. Todd, Heat capacities at low temperatures and entropies of zirconium, zirconium nitride, and zirconium tetrachloride, J. Am. Chem. Soc. **72,** 2914–2915 (1950).
[25] G. B. Skinner and H. L. Johnston, Low temperature heat capacities of inorganic solids. VIII. Heat capacity of zirconium from 14 to 300° K, J. Am. Chem. Soc. **73,** 4549–4550 (1951).
[26] I. Estermann, S. A. Friedberg, and J. E. Goldman, The specific heats of several metals between 1.8° and 4.2° K, Phys. Rev. **87,** 582–588 (1952).
[27] N. M. Wolcott, The atomic heats of titanium, zirconium, and hafnium, Phil. Mag. [8] **2,** 1246-1254 (1957).
[28] D. L. Burk, I. Estermann, and S. A. Friedberg, The low temperature specific heats of titanium, zirconium, and hafnium, Z. physik. Chem. (Neue Folge, Frankfurt) **16,** 183–193 (1958).
[29] W. G. Mixter and E. S. Dana, Specific heats of zirconium, silicon, and boron, Liebigs Ann. Chem. **169,** 388–392 (1873).
[30] F. M. Jaeger and W. A. Veenstra, The exact measurement of the specific heats of solid substances at high temperatures. VII. The calorimetric behavior of zirconium, Rec. trav. chim. **53,** 917–932 (1934).
[31] J. P. Coughlin and E. G. King, High-temperature heat contents of some zirconium-containing substances, J. Am. Chem. Soc. **72,** 2262–2265 (1950).
[32] R. F. Redmond and J. Lones, Enthalpies and heat capacities of stainless steel (316), zirconium, and lithium at elevated temperatures, A.E.C. Report ORNL–1342, pp. 3–20, Oak Ridge Natl. Lab., Oak Ridge, Tenn., 1952.
[33] G. T. Furukawa and M. L. Reilly, National Bureau of Standards, Washington, D.C., private communication, 1 January 1961.

(Paper 67A5–230)

JOURNAL OF RESEARCH of the National Bureau of Standards—A. Physics and Chemistry
Vol. 67A, No. 5, September–October 1963

Heat of Oxidation of Aqueous Sulfur Dioxide With Gaseous Chlorine

Walter H. Johnson and John R. Ambrose [1]

(June 5, 1963)

The heat of oxidation of aqueous sulfur dioxide with gaseous chlorine has been determined by calorimetric methods. The results correspond to the reaction:

$$Cl_2(g) + SO_2 \cdot 2500\ H_2O + 2502\ H_2O = H_2SO_4 \cdot 2500\ H_2O + 2(HCl \cdot 1250\ H_2O),$$
$$\Delta H(25\ ^\circ C) = -77.28 \pm 0.14\ \text{kcal/mole}.$$

The heat of formation of aqueous sulfuric acid (in 2500 moles of water) has been calculated to be −213.92 kcal/mole.

1. Introduction

An investigation of the heats of solution and oxidation of sulfur dioxide to sulfuric acid using bromine as the oxidizing substance was recently made at the University of Lund, Sweden [1].[2] Although the data on the heats of solution of sulfur dioxide were in substantial agreement with the previous data [2] the calculated heat of formation of sulfuric acid differed by approximately 0.3 kcal/mole from the results obtained in several recent determinations [3, 4, 5, 6]. Because the heat of formation of sulfuric acid seems to be well substantiated it seemed probable that the discrepancy must be attributed to the data on the heat of formation of hydrobromic acid. It seemed desirable, therefore, to make a new determination of the heat of oxidation of sulfur dioxide using chlorine as the oxidizing agent. The combined data would be indicative of the consistency between the data on hydrochloric and hydrobromic acid as well as that between the data on sulfur dioxide and sulfuric acid. An error of 0.15 kcal/mole in the heat of formation of hydrobromic acid could account for the apparently high value obtained for the heat of formation of sulfuric acid obtained from the heat of oxidation of sulfur dioxide with bromine.

2. Materials

2.1. Iodine Solution

The 0.1 N iodine solution was prepared by dissolving 12.7 g of resublimed iodine in a concentrated solution containing 80 g of iodate-free potassium iodide and diluting to 2 liters. The solution was protected from light by covering the bottle with aluminum foil. Removal of the solution from the bottle was by means of a siphon. The solution was standardized against arsenious oxide, NBS standard sample 83b. Weight burets were used for all titrations.

2.2. Thiosulfate Solution

The 0.05 N sodium thiosulfate solution was prepared by adding 25 g of reagent-grade sodium thiosulfate pentahydrate and 0.2 g of sodium carbonate to 2 liters of water. The concentration of the solution was determined by comparison with the 0.1 N iodine solution.

2.3. Sulfur Dioxide Solution

A mass-spectrometric analysis of the gaseous sulfur dioxide was performed by E. E. Hughes of the Applied Analytical Research Section of the Analytical and Inorganic Chemistry Division. The analysis gave the following results in mole percent: 98 SO_2, 1.3 CO, 0.4 N_2, and 0.2 CS_2. The 0.15 M sulfur dioxide solution was prepared by passing the gas through 4 liters of distilled water from which air and CO_2 had been removed by boiling. A slight excess of SO_2 was added. This excess was later removed by passing a stream of nitrogen through the solution while stirring which also removed most of the CO and CS_2 impurities. The solution was protected from light by covering the bottle with aluminum foil. A slight pressure of nitrogen was maintained over the solution; removal from the bottle was by means of a siphon. The concentration of the solution was determined by adding a 50 ml portion to an excess of standard iodine solution and titrating the excess iodine with sodium thiosulfate solution.

2.4. Chlorine

The chlorine was taken from a cylinder of gas certified by the manufacturer to have a purity of not less than 98 percent. Noncondensible gases were removed by pumping with the cylinder immersed in liquid nitrogen. Before each calorimetric experiment about a liter of gas was removed which tended to reduce the amount of any volatile impurities.

[1] Present address: 211 74th St., Virginia Beach, Va.
[2] Figures in brackets indicate the literature references at the end of this paper.

691-886—63——3

2.5. Sulfuric and Hydrochloric Acid Solutions

The solutions of sulfuric and hydrochloric acid were prepared from reagent-grade materials and sealed into weighed sample bulbs. The concentrations were determined by breaking some of the bulbs into water and titrating with standard alkali solution.

3. Apparatus

The glass calorimeter was, except for minor changes, the same as that previously described [7]. The Teflon bearings were removed and the stirrer shaft was supported by ball bearings placed above the calorimeter head. An O-ring seal was fitted on the head to prevent leakage of gas around the stirrer shaft. A capillary inlet tube replaced the usual bulb-crushing apparatus. This tube passed through the calorimeter head and terminated at a point about 1 cm above the screw-type propeller. A capillary exit tube projected through the calorimeter head into the vapor space above the solution. Although the metal parts were not in contact with the solution, they were coated with paraffin to prevent corrosion by the moist vapors.

Calorimeter temperatures were measured to ± 0.00005 °C by means of a glass-sheathed platinum resistance thermometer, a G-2 Mueller bridge and a high-sensitivity galvanometer. Timing of the experiments was by reference to the NBS standard second signals.

The calorimeter system was calibrated by means of electrical energy using a method which has been described [8] except that a more precise method was used to determine the time of the heating interval, and the source of the electrical energy was a constant voltage electronic power supply which was fed by a saturation transformer. During the heating period a small current passed through a 60,000-ohm resistance to ground. Upon closing the heater circuit, the positive pulse, resulting from the increase in potential across a 10,000-ohm portion of the 60,000-ohm resistor, served to trigger the start-channel of an electronic gating counter which was connected to a 10 kc standard frequency. When the heater circuit was opened the resulting negative pulse served to trigger the stop-channel of the counter. It was possible with this apparatus to determine the duration of the heating period to ± 0.0001 sec, although a precision of ± 0.01 sec would have been adequate.

The calorimeter was modified slightly for determination of the heats of mixing of the hydrochloric and sulfuric acids in the final sulfur dioxide solution. This involved the substitution of a bulb-crushing apparatus for the gas-inlet tube and the closing of the exit tube.

4. Unit of Energy and Atomic Weights

The unit of energy used in these calculations is the absolute joule obtained as the product of absolute volts, absolute amperes and mean solar seconds. The conventional thermochemical calorie is taken as equal to 4.1840 absolute joules. All atomic weights have been taken from the 1961 table of international atomic weights based on carbon-12 [9].

5. Procedure

One hundred cubic centimeters of 0.15 *M* sulfur dioxide were added to 400 cm^3 of air-free water (at 22 °C) in the calorimeter vessel which was then covered and weighed. The calorimeter was then assembled, placed in a thermostat, the glass thermometer was inserted and the stirrer attached. The thermostat was adjusted to 25.0 °C and regulated within ± 0.001 °C; the stirring rate was approximately 500 rpm by a reducing pulley from a synchronous motor. Nitrogen was passed through the inlet tube at about 100 cm^3/min for about 5 min to remove the bulk of the oxygen in the air space in the calorimeter. The calorimeter was then preheated to about 23.5 °C and approached a steady thermal state after a drift-period of about 15 min. Calorimeter temperatures were then determined at 2-min intervals during the initial rating period. Chlorine was then introduced through the inlet tube at about 30 cm^3/min until the desired calorimeter temperature (25 °C) was reached; the flow of chlorine was then interrupted and the connecting tube was flushed with nitrogen. During the experiment the exit tube was connected to a bubbling vessel which contained a measured quantity of standard iodine solution; a slight positive pressure (1 mm) was thus maintained in the calorimeter vessel. Calorimeter temperatures were observed at 1-min intervals during the reaction period and were continued at 2-min intervals during a final 20-min rating period with the calorimeter in a steady thermal state.

Aliquot portions of the resulting calorimetric solution were taken to determine the final concentration of sulfur dioxide by titration with iodine and the quantity of chloride by precipitation as silver chloride. The quantity of sulfur dioxide in the bubbling vessel was determined by titration of the excess iodine with standard thiosulfate solution. The initial concentration of sulfur dioxide was calculated from these data.

Two series of experiments were performed to determine the heats of mixing of the components in the final solution resulting from the reaction of chlorine with aqueous sulfur dioxide. The first series was to determine the heat of mixing of aqueous hydrochloric acid with the aqueous sulfur dioxide. The second series involved the heat of mixing of aqueous sulfuric acid with the sulfur dioxide-hydrochloric acid solution. The procedure differed somewhat in the heat-of-mixing experiments from that used in the sulfur dioxide-chlorine experiments in that each experiment was preceded by a calibration. This was possible since the temperature rise in each case was only about 0.05 °C. The calibration consisted of an initial rating period, a heating period, and a final rating period. The final rating period of the calibration then became the initial rating period of the heat-of-mixing experiment. At the end of this period the sample bulb was broken;

since the temperature effect was complete within 30 sec, no separate reaction period was required and the subsequent temperature observations comprised the final rating period. The corrected temperature rise was determined by extrapolation of the initial and final time-temperature curves according to the method of Dickinson [10]. The concentration of sulfur dioxide in the final solution was determined in each case by titration with iodine solution.

6. Results and Discussion

The results of the electrical calibration experiments on the calorimetric system used for the heat of reaction of chlorine with aqueous sulfur dioxide are given in table 1. ΔRc is the corrected temperature rise of the calorimetric system [11] as measured on the platinum thermometer; E_e is the quantity of electrical energy introduced into the system; ΔE_s is the deviation in the heat capacity of the actual system from that of the "standard" system as calculated from the mass of solution; and E_s is the energy equivalent of the "standard" calorimeter system. The uncertainty interval has been taken as twice the standard deviation of the mean.

TABLE 1. *Results of the electrical calibration experiments*

Experiment	ΔRc	E_e	ΔE_s	E_s
	Ohm	*j*	*j/ohm*	*j/ohm*
1	0.160953	3713.03	+2.1	23071.1
2	.133728	3085.40	+3.7	23075.9
3	.099719	2301.69	+0.4	23082.2
4	.125095	2886.83	0.0	23077.1
5	.124301	2868.88	−0.4	23079.7
6	.123887	2858.87	+1.2	23077.6
Mean				23077.3
Standard deviation of the mean				±1.53

TABLE 2. *Results of the experiments on the reaction of chlorine with aqueous sulfur dioxide*

Experiment	ΔRc	ΔE_s	SO_2(f)	SO_2(g)	q(dil)	Cl_2	$-\Delta H$(25 °C)
	Ohm	*j/ohm*	*mmoles*	*mmole*	*j*	*mmoles*	*kj/mole*
1	0.153058	−1.1	3.156	0.0030	+8.03	11.006	321.64
2	.136404	0.0	4.107	.0058	−0.17	9.796	321.32
3	.126626	−0.2	5.845	.0025	+2.18	9.074	322.28
4	.107620	+0.5	7.210	.0028	+9.12	7.761	321.18
5	.121110	−0.1	5.891	.0034	+2.51	8.733	320.32
6	.132806	−0.9	5.094	.0032	+2.18	9.536	321.61
Mean							321.39
Standard deviation of the mean							±0.26

The results of the experiments on the reaction of gaseous chlorine with the aqueous sulfur dioxide solution are given in table 2. The heat evolved in the calorimetric process, q, is obtained as the product of ΔRc and $(E_s+\Delta E_s)$. The column designated SO_2(f) gives the analytically determined quantity of SO_2 remaining in the final calorimetric solution. The column designated SO_2(g) gives the quantity of SO_2 carried from the calorimeter by flushing with nitrogen during the reaction period. The quantity q(dil) is a correction applied to make the concentrations of the individual components in the actual final solution correspond to the concentrations given in reaction (1). It includes corrections for the heats of vaporization of the sulfur dioxide and water carried out of the solution by flushing with nitrogen. The quantity of reaction was determined by the amount of chlorine, determined analytically as chloride, in the final calorimetric solution. The heat of reaction given in table 2 corresponds to the process:

$$Cl_2(g)+(1.560\ SO_2+2964\ H_2O)=[2\ HCl+H_2SO_4+0.560\ SO_2+2962\ H_2O]$$
$$\Delta H\ (25\ °C)=-76.81\ \pm 0.13\ \text{kcal/mole}. \quad (1)$$

The assigned uncertainty has been taken as the square root of the sum of the squares of the uncertainty intervals for the calibration experiments, the reaction experiments, and estimated values for all other known sources of error.

The results of the experiments on the heat of mixing of aqueous hydrochloric acid with aqueous sulfur dioxide are given in table 3. The energy due to the crushing of the sample bulb was shown through separate experiments to be completely negligible. The heat of solution given in table 3 corresponds to the process:

$$HCl\cdot 6.708\ H_2O+(0.201\ SO_2+1577\ H_2O)=[HCl+0.201\ SO_2+1583.7\ H_2O]$$
$$\Delta H(25\ °C)=-1.625\ \pm 0.02\ \text{kcal/mole}. \quad (2)$$

TABLE 3. *Results of the experiments on the heat of mixing of aqueous hydrochloric acid with aqueous sulfur dioxide*

Experiment	ΔRc	E	q	q(dil)	HCl(aq)	$-\Delta H$(25 °C)
	Ohm	*j/ohm*	*j*	*j*	*mmoles*	*kj/mole*
1	0.005661	23190	131.28	+0.32	19.216	6.85
2	.005538	23155	128.23	+0.16	18.508	6.94
3	.004798	23210	111.36	−0.21	16.485	6.74
4	.005132	23201	119.07	0.00	17.610	6.76
5	.004987	23208	115.74	−0.14	17.072	6.77
6	.004720	23176	109.39	−0.27	16.204	6.74
Mean						6.80
Standard deviation of the mean						±0.03

TABLE 4. *Results of the experiments on the heat of mixing of aqueous sulfuric acid with the aqueous sulfur dioxide-hydrochloric acid solution*

Experiment	ΔRc	E_s	q	q(dil)	H_2SO_4(aq)	$-\Delta H$(25 °C)
	Ohm	*j/ohm*	*j*	*j*	*mmoles*	*kj/mole*
1	0.004509	23169	104.47	+2.85	9.771	10.98
2	.004044	23171	93.70	−2.18	8.647	10.58
3	.004286	23161	99.27	+0.38	9.213	10.82
4	.004418	23172	102.37	+2.01	9.584	10.89
5	.003918	23144	90.68	−3.14	8.319	10.52
Mean						10.76
Standard deviation of the mean						±0.089

The results of the experiments on the heat of mixing of aqueous sulfuric acid with the hydrochloric acid-sulfur dioxide solution are given in table 4. The resulting heat of solution corresponds to the process:

$$H_2SO_4 \cdot 11.37\,H_2O + [0.386SO_2 + 1.423\,HCl + 3033.2\,H_2O] = [H_2SO_4 + 1.423\,HCl + 0.386\,SO_2 + 3044.6\,H_2O]$$
$$\Delta H(25\ ^\circ C) = -2.57 \pm 0.04 \text{ kcal/mole.} \quad (3)$$

The consistency of the data in tables 3 and 4 indicate that small differences in concentration do not affect the results beyond the limits of experimental error. The results given for eqs (1), (2), and (3) were therefore corrected to the stoichiometry specified in eqs (4), (5), and (6) by assuming that in each case only the reference component was present in water. Equations (1), (2), and (3) were combined with the heats of dilution of sulfur dioxide [1], sulfuric acid [2, 12], and hydrochloric acid [2], to obtain the processes:

$$Cl_2(g) + 2(SO_2 \cdot 2500\,H_2O) + 2502\,H_2O = [H_2SO_4 \cdot 2500\,H_2O + 2(HCl \cdot 1250\,H_2O) + SO_2 \cdot 2500\,H_2O]$$
$$\Delta H(25\ ^\circ C) = -75.92 \pm 0.13 \text{ kcal/mole } Cl_2. \quad (4)$$

$$2(HCl \cdot 1250\,H_2O) + (SO_2 \cdot 2500\,H_2O) = [2(HCl \cdot 1250\,H_2O) + SO_2 \cdot 2500\,H_2O]$$
$$\Delta H(25\ ^\circ C) = 0.25 \pm 0.02 \text{ kcal/mole HCl.} \quad (5)$$

$$H_2SO_4 \cdot 2500\,H_2O + [SO_2 \cdot 2500\,H_2O + 2(HCl \cdot 1250\,H_2O)] = [H_2SO_4 \cdot 2500\,H_2O + SO_2 \cdot 2500\,H_2O + 2(HCl \cdot 1250\,H_2O)]$$
$$\Delta H(25\ ^\circ C) = 0.86 \pm 0.04 \text{ kcal/mole } H_2SO_4. \quad (6)$$

The appropriate combination of eqs (4), (5), and (6) yields the process:

$$Cl_2(g) + SO_2 \cdot 2500\,H_2O + 2502\,H_2O(liq) = H_2SO_4 \cdot 2500\,H_2O + 2(HCl \cdot 1250\,H_2O)$$
$$\Delta H(25\ ^\circ C) = -77.28 \pm 0.14 \text{ kcal/mole.} \quad (7)$$

The heat of formation of aqueous sulfuric acid may be obtained from eq (7) together with data on the heats of formation of water and of aqueous hydrochloric acid [2], and the heat of formation of aqueous sulfur dioxide [1]:

$$S_{rhombic} + 2O_2(g) + H_2(g) + 2500\,H_2O = H_2SO_4 \cdot 2500\,H_2O$$
$$\Delta H(25\ ^\circ C) = -213.92 \pm 0.17 \text{ kcal/mole.} \quad (8)$$

The heat of formation of aqueous sulfuric acid was determined in a similar manner by the reaction of liquid bromine with aqueous sulfur dioxide [1] and -214.20 ± 0.11 kcal/mole was obtained for the process corresponding to eq (8). The heat of formation of $H_2SO_4 \cdot 115\,H_2O$ has been determined by several independent calorimetric determinations using rotating-bomb techniques [3, 4, 5, 6]; the mean of these determinations gives the heat of formation as -212.20 ± 0.10 kcal/mole and it appears that this value is well established. By taking 1.81 kcal/mole for the heat of dilution [2] the value obtained for the heat of formation of $H_2SO_4 \cdot 2500\,H_2O$ is -214.01 kcal/mole. The excellent agreement of the present investigation with this value would seem to indicate a high degree of consistency in the data on HCl, SO_2, and H_2SO_4. The discrepancy of 0.33 kcal obtained in the results with bromine [1] may possibly be due to an error in the heat of formation of aqueous hydrobromic acid.

The combination of eq (7) with the data of Johnson and Sunner [1] yields:

$$\tfrac{1}{2}\,Cl_2(g) + HBr \cdot 1250\,H_2O = \tfrac{1}{2}\,Br_2(liq) + HCl \cdot 1250\,H_2O$$
$$\Delta H(25\ ^\circ C) = -10.90 \text{ kcal/mole.} \quad (9)$$

By taking -68.3149 kcal/mole for the heat of formation of water [2], -79.90 for the heat of formation of $SO_2 \cdot 2500\,H_2O$ [1], and -214.01 for the heat of formation of $H_2SO_4 \cdot 2500\,H_2O$ we calculate -39.90 kcal/mole for the heat of formation of $HCl \cdot 1250\,H_2O$ according to eq (7). This is in excellent agreement with the selected "best" value of -39.92 kcal/mole [2]. The substitution of this value in eq (9) gives -29.00 kcal/mole for the heat of formation of $HBr \cdot 1250\,H_2O$ whereas the selected "best" value is given as -28.81 kcal/mole [2] and indicates a discrepancy of 0.19 kcal.

Sunner [13] is conducting an investigation of the heat of reaction of chlorine with aqueous arsenious oxide. The results of that investigation together with a similar determination using bromine [14] should give additional evidence regarding the consistency between the data on hydrogen bromide and hydrogen chloride.

7. References

[1] W. H. Johnson and S. Sunner, Acta Chem. Scand. (in press).
[2] F. D. Rossini, D. D. Wagman, W. H. Evans, S. Levine, and I. Jaffe, Selected values of chemical thermodynamic properties, NBS Circ. 500 (U.S. Government Printing Office, Washington 25, D.C., 1952).
[3] J. P. McCullough, S. Sunner, H. L. Finke, W. N. Hubbard, M. E. Gross, R. E. Pennington, J. F. Messerly, W. D. Good, and Guy Waddington, J. Am. Chem. Soc. **75,** 5075 (1953).
[4] S. Sunner and B. Lundin, Acta Chem. Scand. **9,** 832 (1955).
[5] D. W. Scott, J. P. McCullough, W. N. Hubbard, J. F. Messerly, I. A. Hossenlopp, F. R. Frow, and Guy Waddington, J. Am. Chem. Soc. **78,** 5463 (1956).
[6] W. D. Good, J. L. Lacina, and J. P. McCullough, J. Am. Chem. Soc. **82,** 5589 (1960).
[7] W. H. Johnson, A. A. Gilliland, and E. J. Prosen, J. Research NBS **63A,** (Phys. and Chem.) No. 2, 161 (1959).
[8] E. J. Prosen, W. H. Johnson, and F. Y. Pergiel, J. Research NBS **62,** 43 (1959) RP2927.
[9] Report of Commission on Atomic Weights, Compt. rend. 21st Conf. IUPAC, Montreal, p. 281–327 (1961).
[10] H. C. Dickinson, Bull. BS **11,** 187 (1915).
[11] E. J. Prosen, Chapter 6 in "Experimental Thermochemistry," F. D. Rossini, ed. (Interscience Publishers, Inc., New York, N.Y., 1956).
[12] J. E. Kunzler and W. F. Giauque, J. Am. Chem. Soc. **74,** 3472 (1952).
[13] S. Sunner, private communication.
[14] L. Bjellerup, S. Sunner, and I. Wadsö, Acta Chem. Scand. **11,** 1761 (1957).

(Paper 67A5–231)

JOURNAL OF RESEARCH of the National Bureau of Standards—A. Physics and Chemistry
Vol. 67A, No. 5, September–October 1963

Thickness of Adsorbed Polystyrene Layers by Ellipsometry[1, 2]

Robert R. Stromberg, Elio Passaglia, and Daniel J. Tutas

(June 5, 1963)

The adsorption of polystyrene from cyclohexane below the theta temperature onto chrome ferrotype plate was studied by means of ellipsometry (polarization spectrometry). In this technique changes in the state of polarization of polarized light are measured upon reflection from a film-covered surface. The measurements were carried out in situ and permitted determination of the thickness and refractive index of the swollen polymer film at the solid-solution interface. A concentration range of 0.18 to 9.7 mg/ml was studied for polymer with a molecular weight of 76,000. The thickness of the adsorbed film increased with increasing solution concentration, reaching a plateau for most of the concentration range studied. The average thickness at this plateau was approximately 210 Å. The adsorbed film was highly swollen, consisting of about 12 g/100 ml of polymer for most of the concentration range. The amount adsorbed was determined to be approximately 2.25×10^{-4} mg/cm^2 at the plateau. Comparison of the radius of gyration of polystyrene in solvent is made to the results obtained.

1. Introduction

One important aspect concerning the adsorption of polymers from dilute solution onto solid surfaces that has not yet been resolved is the conformation of the polymer molecule at the interface. Early experiments on the adsorption of polymers on solid surfaces indicated that the entire polymer molecule did not contact the surface. It was proposed that the polymer is attached at a number of locations along the chain, joined by loops extending into the solution [1].[3] This model has been widely accepted, but the number and sizes of the attached portions of the polymer chain and the sizes of the loops have not been determined.

The theoretical treatment developed by Simha, Frisch, and Eirich [2] for the adsorption of flexible macromolecules predicts a molecular conformation characterized by attachment of the molecule at relatively few locations and long chain loops extending into the solution. The sizes of these loops increase with the square root of the molecular weight. A different theoretical treatment has recently been published by Silberberg [3]. A conformation is predicted in which short stretches of segments are attached to the adsorbent surface, connected by short loops extending into the solution. The lengths of these loops are independent of the molecular weight. The shape of the molecule at the interface according to this latter treatment is dependent only on the adsorption energy and certain steric factors.

Two rather widely divergent theories, therefore, have been advanced. One results in a description of polymer adsorption characterized by relatively few attachments per polymer molecule and a rather thick adsorbed layer of what is probably a very highly solvated polymer, attached to the surface. The other leads to a film that would be of much higher density, relatively close to the surface, with many attachments per polymer molecule, thus allowing the molecule to uncoil on the surface from its conformation in the solution.

The experimental evidence concerning the thickness and conformation of the attached polymer layer is also conflicting. The apparent reduction in the diameters of fine capillary viscometer tubes has been attributed to adsorption of polymers on the walls and the thickness of the adsorbed polymer film has been calculated from such measurements [4, 5, 6, 7, 8]. These studies all indicate a thick polymer film. Adsorption studies of polymers such as poly(vinyl acetate) on metal oxide surfaces have shown that sufficient polymer is adsorbed to indicate a thick film [9]. It was estimated that enough polymer was adsorbed to correspond to a film 10 to 40 molecules thick if the molecules were to lie flat. Application of the Simha, Frisch, and Eirich theory to the adsorption of rubber onto carbon black indicated only a few attachments per molecule [10].

Other measurements, however, have indicated that the polymer molecule may be much more closely associated with the adsorbent surface, resulting in much thinner films. Surface potential measurements on the adsorption of poly(vinyl acetate) on chrome ferrotype surfaces have indicated that the polymer uncoils almost completely until a monolayer is formed, resulting in a rather thin film [11]. Once this layer is formed it was postulated that additional polymer is deposited to build a thicker layer. This finding was supported by rate experiments with the same type of polymer and surface [12]. The adsorption of polyesters on polar surfaces such as glass and silica showed that relatively small amounts were adsorbed for these systems, corre-

[1] Presented in part at American Chemical Society Meeting, Los Angeles, Calif. April 1963.
[2] Supported, in part, with funds provided by the Army Research Office (Durham).
[3] Figures in brackets indicate the literature references at the end of this paper.

sponding to 2 to 5 layers on the glass, depending on the solvent used, and to one layer on the silica, if the polymer molecule were considered to lie flat [13]. A study of the adsorption of butyl rubber and polyisobutylene on carbon black led the investigators to the conclusion that both long and short polymers lie flat on the external surface of the carbon black [14]. Infrared spectrophotometry was used in a more direct approach to the measurement of the number of poly(alkyl methacrylate) units on silica [15]. It was reported that a relatively large number of groups were attached to the silica, inferring a relatively flattened molecule.

Thickness measurements carried out by the same authors by a sedimentation velocity method gave a film thickness of about 25 Å for one polymer and 210 Å for another. Experimental data on the adsorption of polystyrene on carbon [16] appeared to fit a simplified isotherm of Frisch and Simha [17] better if the number of anchor segments per polymer molecule was chosen to be 50 rather than 1, again inferring a flattened molecule.

The present paper reports the results of a study of the thickness and refractive index in situ of the layer of polystyrene adsorbed on chrome surfaces from cyclohexane. The measurement of the thickness and refractive index was carried out by the technique of ellipsometry (polarization spectrometry). From the refractive index the concentration of polymer in the swollen film can be calculated, and from this and the thickness, the amount of polymer adsorbed per unit area is obtained.

2. Measurement

2.1. Theory

In many ways ellipsometry is a very suitable technique for the measurement of the thickness and refractive index of an adsorbed film. Under the correct experimental conditions it is possible to measure the thickness of a thin film to within a few Angstrom units and at the same time determine the refractive index of that film to the third decimal place. It is also possible to carry out these measurements on the adsorbed film over a period of time while the film is in its swollen state in contact with the solution. Unfortunately, as will be seen below, when the refractive index of the film is close to that of the solution, the experimental precision is lowered.

The basic principles of ellipsometry are based on the original equations of Drude [18] and have been reviewed by Winterbottom [19]. Although the actual measurements with the ellipsometer are not particularly difficult, the calculations required for an exact solution of the equations are complex and very lengthy. Most of the work reported to date on the ellipsometer has been carried out using either some approximation to the solution of the equations or, more frequently, some empirical calibrations such as step wedges of barium stearate—stearic acid. Neither of these approaches was suitable to the problem of polymer adsorption. Therefore, a computational method that permitted the use of the exact equations was developed and programmed for an electronic computer [20]. The ease of the computations permitted determination of the optical constants of the specific adsorption surface immediately prior to adsorption of polymer, thus permitting increased accuracy in the determination of the properties of the films.

The method of ellipsometry is based on the measurement of changes in the state of polarization of light upon reflection from a surface. The pertinent equations are well known [18, 19] and the method has recently been reviewed [20], so that only enough detail will be given here to make the method clear.

For the purpose of analysis of reflection, the polarization vector of the light is resolved into components in the plane of incidence and in the normal to the plane of incidence (the plane of the surface). Upon reflection from the surface, the relative amplitudes and phases of the two components will be changed, so that incident linearly polarized light will be reflected in general as elliptically polarized light. For a bare surface, (i.e., one with no film) the reflection coefficient for the component in the plane of incidence, r^p, and for the component in the plane of the surface, r^s, are given by,

$$\left.\begin{aligned} r^p &= \frac{n_2 \cos \varphi_1 - n_1 \cos \varphi_2}{n_2 \cos \varphi_1 + n_1 \cos \varphi_2} \\ r^s &= \frac{n_1 \cos \varphi_1 - n_2 \cos \varphi_2}{n_1 \cos \varphi_1 + n_2 \cos \varphi_2} \end{aligned}\right\} \tag{1}$$

where n_2 is the refractive index of the surface, n_1 is the refractive index of the surrounding medium, and φ is the angle of incidence. For a metal, n_2 is complex. The ratio of the reflection coefficients, ρ, is the basic equation of ellipsometry,

$$\rho = \frac{r^p}{r^s} = \tan \psi e^{i\Delta} \tag{2}$$

in which $\tan \psi$ is the relative amplitude reduction and Δ is the relative phase difference of the two components.

The ellipsometer measures Δ and ψ. From these measurements, the real and imaginary parts of the complex refractive index of the surface medium may be calculated.

For a film-covered surface, the total reflection coefficients, R^p and R^s, are given by

$$\left.\begin{aligned} R^p &= \frac{r_{12}^p + r_{23}^p \exp D}{1 + r_{12}^p r_{23}^p \exp D} \\ R^s &= \frac{r_{12}^s + r_{23}^s \exp D}{1 + r_{12}^s r_{23}^s \exp D} \end{aligned}\right\} \tag{3}$$

where r_{12} and r_{23} are the reflection coefficients at the film-medium and film-substrate interfaces respectively, and D is given by

$$D = -4\pi i n_2 \cos \phi_2 \, d_2/\lambda \tag{4}$$

where n_2 is the refractive index of the film, d_2 its thickness, ϕ_2 the angle of incidence on the substrate surface, and λ is the wavelength of light. The ratio of reflection coefficients is again represented by

$$\rho=\frac{R^p}{R^s}=\tan\psi e^{i\Delta}. \tag{5}$$

It is clear that ψ and Δ will be complex functions of n_1, n_2, n_3, d_2, λ_1, ϕ_1, and ϕ_2. In principle, if all these parameters are known except n_2 and d_2, these may be calculated from the observed values of ψ and Δ, when n_2 is real.

The method in principle is as follows. By measurement of ψ and Δ on a bare surface under a liquid, n_3 (complex for a metal) is determined. Adsorption is carried out on the surface, and Δ and ψ measured again. By the use of eq (5), n_2 and d_2 can be obtained as described in the section, "Computational Method." The ellipsometer does not measure ψ and Δ directly; they are, however, easily obtained from instrumental readings (20).

2.2. Multiple Reflections

The sensitivity and accuracy of ellipsometry is dependent upon the refractive index differences between the film and the surrounding medium [20]. The closer the refractive index of the film to that of the immersion medium, the larger the range of thicknesses and refractive indexes that will fit within experimental error. This is a very important consideration and limitation to the study of adsorbed polymer films in situ, for the film can be expected to be highly swollen with solvent and have a refractive index near that of the solvent. However, multiple reflections may be used in order to improve the sensitivity of the measurements. Although ellipsometry has in general been restricted to one reflection, the use of 8 reflections for the measurement of the adsorption of water vapor on metals in a gaseous environment has been reported [21].

The reflection coefficient for n reflections is

$$\rho_n=\rho^n \tag{6}$$

where ρ is the reflection coefficient for a single reflection. From eq (5)

$$\rho_n=(\tan\psi)^n e^{in\Delta} \tag{7}$$

where ψ and Δ are the values used in eq (5), and hence

$$\tan\psi=(\tan\psi_n)^{1/n} \tag{8}$$

and

$$\Delta=\frac{\Delta_n}{n}. \tag{9}$$

The values of ψ and Δ are determined directly from the measured values of ψ_n and Δ_n by eqs (8) and (9), respectively.

It is assumed that the error in measuring Δ_n and ψ_n is a constant independent of the number of reflections, and experimentally this appears to be the case for not too many reflections. If the error in Δ_n is $\delta\Delta$, it is clear from eq (9) that the error in the Δ used in the computations is $\frac{\delta\Delta}{n}$ if measurements are made with n reflections.

From the error in ψ, it may readily be shown that

$$\delta\psi=\frac{1}{n}\frac{[(\tan\psi)^{2n}+1](\tan\psi)^{1-n}}{\tan^2\psi+1}\delta\psi_n. \tag{10}$$

It might be mentioned that for total internal reflection, $\tan\psi$ is unity and this expression reduces to

$$\delta\psi=\frac{1}{n}\delta\psi_n. \tag{11}$$

Therefore, for this special case as much improvement in precision is effected in ψ as in Δ by multiple reflections. For the more normal case of reflection from a metallic surface, $\tan\psi$ is approximately $\frac{1}{2}$, and we obtain

$$\delta\psi=\frac{1}{5n}\frac{1+2^{2n}}{2^{n-1}}\delta\psi_n. \tag{12}$$

For a large number of reflections it is apparent that the error in ψ increases, i.e., $\delta\psi_1$ becomes less than $\delta\psi_n$, and multiple reflections become a hindrance rather than a help. However, for three reflections, $\delta\psi_1\simeq\delta\psi_3$, and nothing is lost. Moreover, the precision of Δ is improved by a factor of 3. For the type of surfaces used here, ψ is less sensitive to film thickness than is Δ, so that the latter is the more critical quantity. For these reasons three reflections was the optimum number for the type of measurements carried out here. All the work reported in this paper was carried out with three reflections.

2.3. Computational Method

Equation 5 cannot be solved in a closed form for the refractive index, n, and the thickness, d. The solution of this equation is described in detail in reference 20. Equation 5 may be recast into the form,

$$C_1(\exp D)^2+C_2(\exp D)+C_3=0 \tag{13}$$

where D is given by eq (4), and C_1, C_2, and C_3 are complex coefficients, containing as parameters all the experimental quantities, including Δ and ψ.

All these parameters are known, except for n_2, the refractive index of the film. If a value for n_2 is assumed, eq (13) may be solved to yield two values of exp D. From these two values, eq (4), and the assumed value of n_2, two values of d, the film thickness are obtained. If the assumed value of n_2 is not the "correct" value, both these calculated values of d will be complex. If the assumed value of n_2 is the "correct" value, one of these thicknesses will have

no imaginary part. This thickness and the corresponding refractive index are taken to be the "true" values of the thickness and refractive index of the film.

The procedure, then, is as follows. A value of n_2 is assumed, and using it a value for d is calculated. If this is complex, another value of n_2 is assumed and the calculation repeated. This is continued until a real value of d is obtained. On an electronic computer the procedure is quite simple.

In practice, errors in the measured values of Δ and ψ will cause uncertainty in both n_2 and d. This is handled in the following manner. When a complex value of d is calculated as above from an assumed value of n_2, the imaginary part is discarded and the real part used to calculate values of Δ and ψ (Δ_{cal} and ψ_{cal}), from eq (5). These values of Δ_{cal} and ψ_{cal} are then compared to the experimentally observed values of Δ and ψ, (Δ_{exp} and ψ_{exp}). In general, there will be a difference between the calculated and experimental quantities since the imaginary part of the complex thickness was discarded. This procedure is continued until the difference between the experimental and calculated values of Δ and ψ is within preassigned error limits. The corresponding range of values of n_2 and d are taken to be the possible range of refractive index and thickness for the film. The values of n_2 and d for which the difference between the calculated and experimental values of Δ and ψ is zero will be called here the "best-fit" values.

The error limits, as determined from numerous experiments, were found to be $\pm 0.02°$ for the measurement of ψ and $\pm 0.04°$ for Δ. The use of triple reflection lowers the error in Δ to 0.013° and does not affect the error in ψ. However, even with these reduced error limits, the range of uncertainty in both n_2 and d, due to the small differences in refractive index between that of the film and that of the polymer solution, is still significant for the problem studied here.

3. Experimental Procedure

3.1. Materials

The polystyrene used was kindly supplied by Dr. H. W. McCormick of the Dow Chemical Company and had been prepared by the anionic polymerization of styrene. (Dow's sample No. S 102, $\overline{M}w/\overline{M}n = 1.05$). For most of the work reported here the polymer described above was fractionated by conventional precipitation methods to remove any possible high and low molecular weight "tails." The molecular weight of the fractionated polymer determined by intrinsic viscosity was 76,000, using the relation $\log [\eta] = -4.021 + 0.744 \log M$ [22][4]. Some of the work reported here was carried out using the unfractionated polymer as received. The results using this unfractionated polymer will be so labeled when discussed. The molecular weight of the polymer as determined by Dow was $\overline{M}w = 82{,}500$, $\overline{M}n = 78{,}500$ [23].

[4] Fractionation and molecular weight by Warren H. Grant, NBS.

The solvent, cyclohexane, was freshly distilled prior to use. Measurements were carried out in a temperature-controlled room maintained at 24 °C, which is 11 degrees lower than the Flory theta temperature for this system. The concentrations studied ranged from 0.18 to 9.7 mg/ml.

3.2. Surface Preparation

The adsorption experiments were carried out on highly reflecting chrome surfaces. The samples themselves were 1x2 cm rectangles cut from commercial ferrotype plate. These were cleaned by immersion in warm sulfuric acid-chromic acid cleaning solution, followed by thorough rinsing in hot distilled water, then by drying at 100 °C. Immediately prior to use the slides were passed three times through a gas-oxygen flame, and immersed while still warm in solvent in the adsorption cell. The entire cleaning procedure was carried out usually within an hour of use. This procedure always resulted in hydrophilic surfaces; slides that remained in the laboratory air for short periods of time soon became hydrophobic.

3.3. Technique

The surfaces were prepared as described in the experimental section and placed, while still warm, into a cell containing the solvent, cyclohexane. Two slides were prepared and set in a cell as shown in figure 1. The light entered and left normal to the cell windows. The angle of incidence was 70°, the wavelength of light, 5461 Å. The upper slide was set on two gage blocks thus providing a level constant height from the lower reflecting surface. The assembly was placed on the ellipsometer stage and Δ and ψ determined for the triple reflection situation shown. As will be discussed later, the optical constants varied somewhat over a slide and to an even larger extent between slides. The optical constants calculated from the Δ and ψ determined for triple reflections were therefore an average of the optical constants for the three locations at which reflection actually took place.

After these measurements were carried out on the bare surface, the solvent was removed by hypodermic syringe and a polymer solution added. The Δ and ψ values for the film-covered surface were then determined as a function of time at the same locations. The determination of the properties of the adsorbed film was therefore actually a difference measurement. In the case of desorption, the solu-

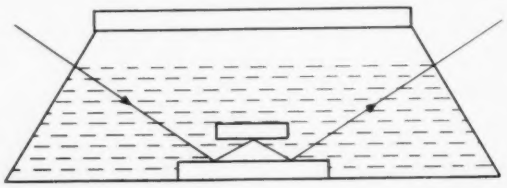

FIGURE 1. *Schematic drawing of adsorption cell showing two chrome slides arranged for triple reflection of the polarized light beam.*

tion was removed from the cell after an adsorption study by means of a hypodermic syringe, and solvent added. This procedure was repeated three times and then measurements started.

4. Results

The thickness and refractive index of the adsorbed film are determined directly from the experimental measurements as described above. The refractive index increment, dn/dc, was obtained experimentally for a range of concentrations up to polymer concentrations of approximately 9 percent polystyrene in cyclohexane. The relationship between percent of polymer and refractive index was found to be linear and a value of 0.168 ml/g was obtained. Using the molar refraction relationships of Lorentz and Lorenz, and assuming additivity of specific volumes, a linear relation was also obtained for the range of swollen film concentrations studied here, resulting in a value of 0.163 ml/g. Both values were also very close to that determined experimentally [24] for a more dilute concentration range. Thus, from the refractive index of the film, the concentration of the polymer in the film can be determined. The product of this concentration and the thickness of the film gives the amount of polymer adsorbed per unit area. The experimental value 0.168 ml/g was used.

The calculations used here assume a uniform film with no refractive index gradients. This is equivalent to assuming that the polymer segment density is uniform throughout the film. This is almost certainly not the case and, in fact, Forsman and Hughes [25] have indicated that to a first approximation the segment density in the direction normal to the surface is a sum of two Gaussian curves. While it is difficult to assess the exact type of average that the assumption of a uniform film assumes, it may be seen from eq (4) that the average quantities are probably given by

$$\bar{n}_2\bar{d}\cos\phi_2 = \int_0^\infty n_2(z)\cos\varphi_2 dz \qquad (14)$$

where $\bar{n}_2$ and $\bar{d}$ are the average quantities, and $n_2(z)$ and $\cos\varphi_2$ are both functions of z, the distance from the surface.

Measurements on the adsorption of polystyrene from cyclohexane solution onto the chrome surfaces were carried out for a concentration range of 0.18 to 9.7 mg/ml. There was, obviously, only negligible change in solution concentration as a result of this adsorption. Some typical individual measurements of the thickness of the swollen adsorbed layer in contact with the solution taken over a period of time are shown in figures 2 to 5. The symbols on these figures represent the "best-fit" values, while the vertical lines represent the range of thicknesses consistent with the experimental error of each individual measurement, as described in the section on Measurement.

The points shown in figure 2, obtained at a solution concentration of 0.18 mg/ml, were obtained in three runs, on three different sets of slides. Two sets

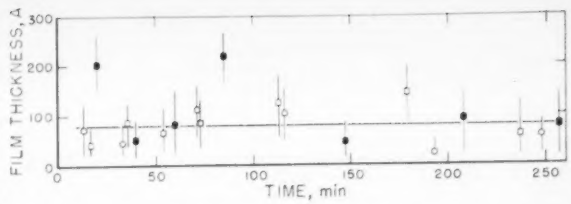

FIGURE 2. *Thickness of swollen adsorbed film of polystyrene versus time of exposure to a solution for solution concentration of 0.18 mg/ml.*

The three different sets of points were obtained on three different sets of slides.
○, Fractionated polymer
□, ■, Unfractionated polymer

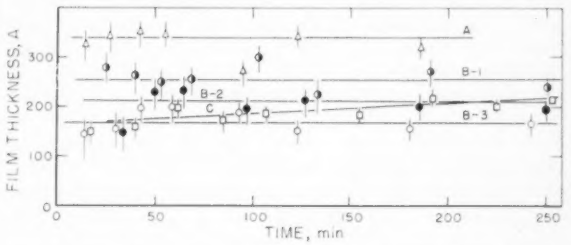

FIGURE 3. *Thickness of swollen adsorbed layer of polystyrene versus time of exposure to a solution for solution concentration of approximately 3.5 mg/ml.*

Curves A and B obtained with fractionated polymer, curve C obtained with unfractionated polymer. Curves B–1, B–2, and B–3 obtained from measurements on different locations on the same set of slides. Curves A and C obtained from different sets of slides.
Fractionated polymer; solution concentration 3.50 mg/ml.
△, Curve A
◑, Curve B–1
●, Curve B–2
○, Curve B–3
Unfractionated polymer; solution concentration 3.32 mg/ml.
□, Curve C

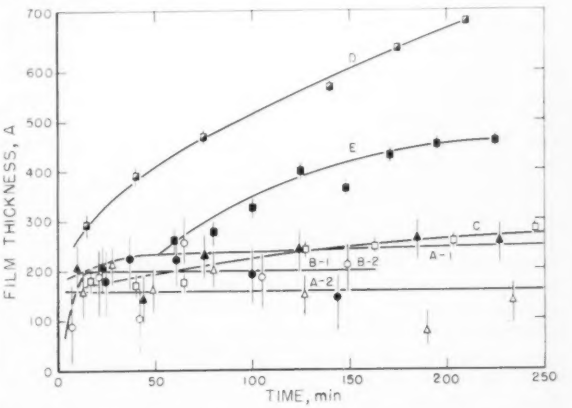

FIGURE 4. *Thickness of swollen adsorbed layer of polystyrene versus time of exposure to a solution for solution concentration of 5.00 mg/ml.*

Curves A–1 and A–2 refer to measurements made on different portions of the same set of slides. The same notation applies to Curves B–1 and B–2. Curves A and B were obtained using fractionated samples, curves C, D, and E using unfractionated.
▲, Curve A–1
△, Curve A–2
●, Curve B–1
○, Curve B–2
□, Curve C
◑, Curve D
■, Curve E

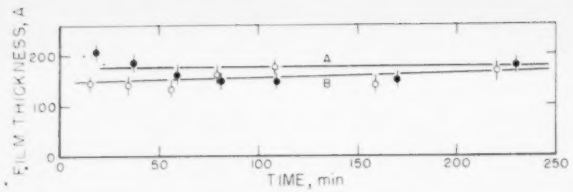

FIGURE 5. *Thickness of swollen adsorbed layer of polystyrene versus time of exposure to a solution for solution concentration of 9.76 mg/ml.*

Both curves were obtained using fractionated polymer and each represents a different set of slides.
●, Curve A
○, Curve B

were obtained using unfractionated polymer, and one using the fractionated sample. As can be observed from this figure, at this concentration there is no significant difference in the calculated thickness of the adsorbed swollen film obtained using either different sets of slides or fractionated or unfractionated polymer. The curve drawn represents an average for all the individual "best-fit" points obtained from all three runs. This average thickness is seen to be approximately 80 Å, and almost certainly less than 120 Å. The thickness did not appear to change with time over the time range studied.

The thicknesses shown in figure 3, obtained for a concentration of approximately 3.5 mg/ml (the exact concentration for each run is given in the caption for the figure) indicate a dependence of the thickness on the specific characteristics of the surface. Curves A and B were obtained using fractionated polymer, curve C using unfractionated material. Each curve for the fractionated polymers represents the average of the "best-fit" values for that particular run. Curves B–1, B–2, and B–3 are the results of measurements made at three different locations on the same set of slides. Thickness curves that differed from each other were obtained at the different locations on the same set of slides as well as on the different slides. This is taken as an indication that the individual locations studied differed from each other, perhaps in the number of adsorption sites available.

It can be observed from figure 3 that the curve obtained with the unfractionated polymer fell within the limits of the fractionated material, although the thickness of the unfractionated material appeared to increase somewhat with time, while the other curves appear to be flat. However, a comparison with the adsorbance [5] in figure 7 shows that more polymer was actually deposited from the unfractionated polymer, as seen by curve C. Although the swollen film thicknesses seen in figure 3 are about the same for fractionated and unfractionated polymer, the concentration of polymer in the unfractionated swollen polymer film was appreciably higher, resulting in the curve C shown in figure 7. Examination of figure 6 shows that there was no significant difference between the adsorbances for the fractionated and unfractionated samples that were measured at the lower concentration of 0.178 mg/ml.

The thickness results obtained for the concentration of 5.00 mg/ml are shown in figure 4. In this case curves A–1 and A–2 were obtained from different portions of one set of slides, and curves B–1 and B–2 from another set of slides. All four of these determinations were carried out with fractionated polymer. The averages of the "best-fit" values range from about 160 to 240 Å. In the examples shown in this figure, the differences in thicknesses measured from one location on one set of slides to another location on the same set of slides was greater than the differences from one set of slides to another. Curves C, D, and E were obtained using unfractionated polymer. Curves D and E represent thicknesses that are much greater than those obtained with the fractionated polymer and that continue to increase with time. It should be noted that the range of uncertainty is much less for the thicker films than for the thinner. Curve C is seen not to differ appreciably from those obtained with the fractionated material. The amounts adsorbed for this solution concentration (shown in fig. 8), again indicate that much more polymer is deposited from the unfractionated material, although the swollen film may have approximately the same thickness as the fractionated polymer.

Figure 5 shows the results of the thickness measurements obtained with a solution concentration of 9.7 mg/ml. In this case, both of the runs using fractionated polymer resulted in thickness measurements that were quite similar to each other. The thicknesses obtained were somewhat smaller than had been obtained with the lower concentrations. The range of uncertainty was decreased because of the increased polymer concentration in the adsorbed layer. The behavior of the unfractionated polymer at this concentration is not shown in the figure, but it was similar to that shown for the 5 mg/ml concentration in figure 4.

Figures 6 to 9 represent the individual calculated adsorbances for the same solution concentrations used for figures 2 to 5. The symbols used for the individual points and the lettering of the curves are identical on both sets of curves for the same solution concentration. The amount adsorbed is a function of the refractive index and thickness of the swollen film. As the calculated thickness of the swollen film varies with the assumed refractive indexes, the value of the adsorbance is relatively independent of the uncertainties that are inherent in the determination of the swollen film thicknesses. Differences in the amounts adsorbed for swollen films of approximately the same thickness represent, of course, different densities of the polymer films.

Figure 6 obtained for the concentration of 0.178 mg/ml, shows that for this relatively dilute concentration the adsorbance for fractionated and unfractionated polymer was virtually the same. This is probably due to the fact that there was no precipitation of unfractionated polymer. Figure 7 shows the amounts adsorbed for the solution concentration of

[5] We use the term *adsorbance* to denote the amount adsorbed per unit area, in mg/cm².

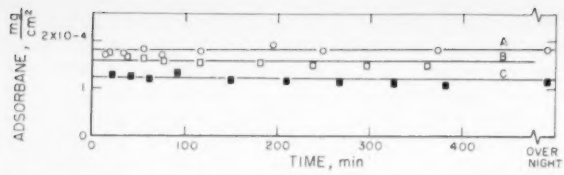

FIGURE 6. *Adsorbance of polystyrene for solution concentration of 0.18 mg/ml.*

The symbols on this figure represent the runs using the identical symbols used in figure 2.

○, Fractionated polymer
□, ■, Unfractionated polymer

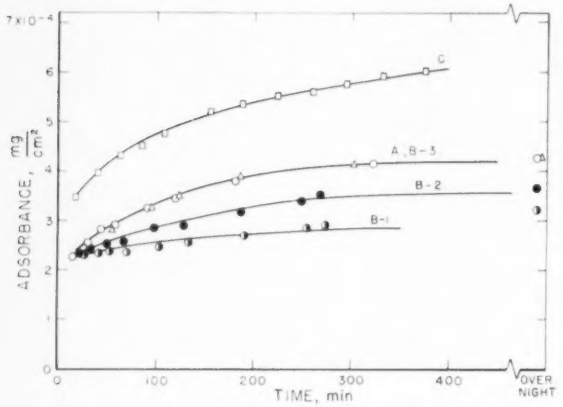

FIGURE 7. *Adsorbance of polystyrene for solution concentration of approximately 3.5 mg/ml.*

The designation of the curves by letter and the symbols used correspond to those used in figure 3.

Fractionated polymer; solution concentration, 3.50 mg/ml
△, Curve A
◑, Curve B-1
●, Curve B-2
○, Curve B-3
Unfractionated polymer; solution concentration, 3.32 mg/ml.
□, Curve C

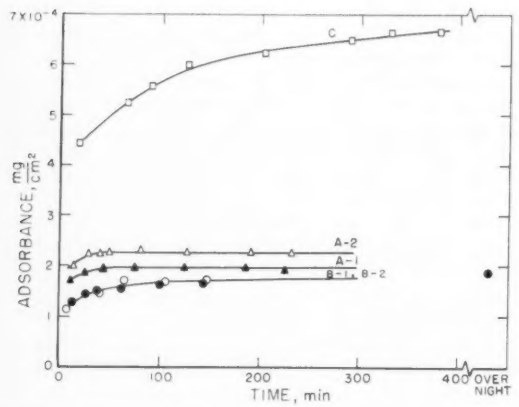

FIGURE 8. *Adsorbance of polystyrene for solution concentration of 5.00 mg/ml.*

The designation of the curves by letter and the symbols used correspond to those used in figure 4. Curves A and B represent fractionated sample, curve C unfractionated.

▲, Curve A-1
△, Curve A-2
●, Curve B-1
○, Curve B-2
□, Curve C

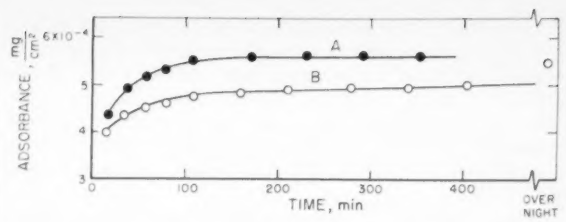

FIGURE 9. *Adsorbance of polystyrene for solution concentration of 9.76 mg/ml.*

Both curves were obtained using fractionated polymers and the lettering of the curves and the symbols used are identical with that used in figure 5.

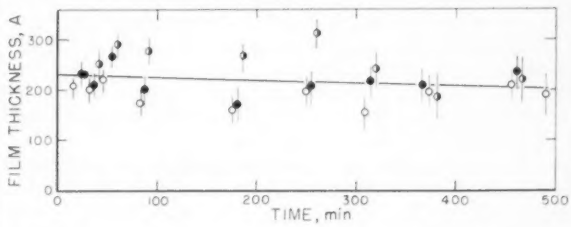

FIGURE 10. *Desorption: Thickness of adsorbed polystyrene layer versus time of exposure of film to solvent.*

Films adsorbed from solution concentration of 3.50 mg/ml.
◑, Curve B-1
●, Curve B-2
○, Curve B-3

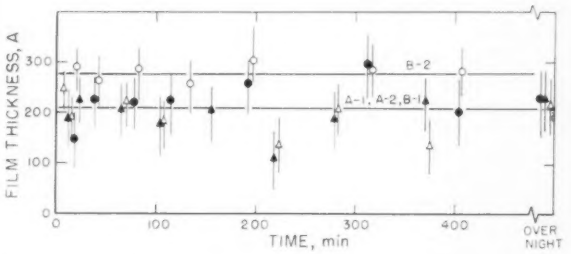

FIGURE 11. *Desorption: Thickness of adsorbed polystyrene layer versus time of exposure of film to solvent.*

Films adsorbed from solution concentration of 5.00 mg/ml.
▲, Curve A-1
△, Curve A-2
●, Curve B-1
○, Curve B-2

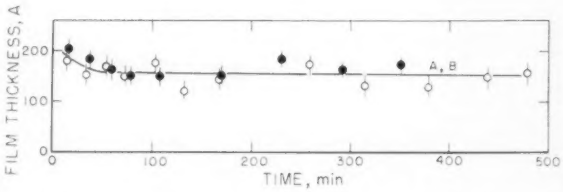

FIGURE 12. *Desorption: Thickness of adsorbed polystyrene layer versus time of exposure of film to solvent.*

Films adsorbed from solution concentration of 9.76 mg/ml.
●, Curve A
○, Curve B

3.5 mg/ml. The arrangement of the curves is observed to be different from that shown in figure 3, with the quantities ranging from about 2.8×10^{-4} to 4.2×10^{-4} mg/cm² for the fractionated polymer. As mentioned earlier, the quantity deposited for the unfractionated material, curve C, does not fall with the group of curves obtained for the fractionated polymer.

The adsorbances obtained for the 5 mg/ml concentration are given in figure 8, and range from about 1.8×10^{-4} to 2.3×10^{-4} mg/cm². The arrangement of the curves with respect to each other is again seen to be somewhat different than that for the solvated films represented in figure 4. A more definite increase in quantity with time is observed during the early portion of the adsorption than was evident from the solvated film thicknesses. As the solution concentration increases, the difference between the fractionated and unfractionated polymer solutions becomes increasingly more apparent. Curve C is seen to be very different from the other samples, although the swollen film thicknesses were similar. The other unfractionated curves shown in figure 4 are not given but would be much greater in amounts deposited. Although the thicknesses of the swollen films for the solution concentration 9.7 mg/ml shown in figure 5 are relatively small, the quantities given in figure 9 are quite high, ranging from about 4.9×10^{-4} to 5.6×10^{-4} mg/cm².

The desorption of polystyrene was studied by the same technique and resulted in swollen film thicknesses that were not appreciably different from those obtained during adsorption. Typical results are shown in figures 10, 11, and 12. Curves B–1, B–2, and B–3 in figure 10 are approximately the same thickness or only slightly less than that shown by the curves in figure 3. The desorption curves shown in figure 11 show a slightly increased thickness over those shown in the adsorption isotherms in figure 4. In the case of the most concentrated solution studied, the desorption curves shown in figure 12 are almost identical with the adsorption curves shown in figure 5.

5. Discussion

It was observed that there was considerable variation in the thickness of the adsorbed polymer film. It appears that for most of the range of concentrations studied more variation was caused for the fractionated polymer by the differences in the particular surface studied than by changes in solution concentration. Further, it was observed that there were no large changes in the thickness of the adsorbed film with time, several minutes being required before the initial measurements were made. If the average thicknesses for each run at a specific concentration are then averaged for that concentration, the points represented by the open circles in figure 13 are obtained. The curve drawn through these points, therefore, represents the average of the individual "best-fit" point averages for the concentration range studied. It is observed that the average thickness of the swollen polystyrene film on the chrome surface is about 200 Å for most of the concentration range given. The value of thickness obtained at the lowest concentration appears to be significantly lower than the remainder. The desorption thickness values, obtained from fewer runs, are also given, and are seen not to differ appreciably from the adsorption curve.

This work was carried out at a temperature below the theta temperature. The increased thicknesses and amounts of unfractionated polymer deposited probably are caused by precipitation of a portion of polymer with a molecular weight higher than 76,000. This is especially indicated by the increasing differences between fractionated and unfractionated polymer as the concentration increases.

Figure 14 shows the concentration of polymer in the adsorbed film for the fractionated sample. The points are the averages of several runs, obtained in the same manner as those in figure 13. It is observed that the film contains about 12 g of polymer per 100 ml of solution for most of the concentration range. The film adsorbed from the 9.7 mg/ml concentration contained approximately 30 percent polymer. It is possible that as the solution concentration increases, a multilayer adsorption occurs. This was not evidenced by the film thickness measurements, but an intertwining of polymer chains may occur at high solution concentrations, retaining the same film thickness, but greatly increasing the amount of polymer in the layer. There is also an indication that the percentage of polymer in the film is greater at low solution concentrations. In this case, the film thickness was lower than the remainder of the

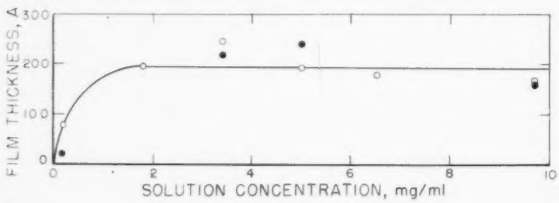

FIGURE 13. *Average swollen film thickness as a function of solution concentration.*

The points represent the averages of several measurements.
○, Adsorption thicknesses.
●, Desorption thicknesses—film adsorbed from solution concentration shown, but measured in contact with solvent.

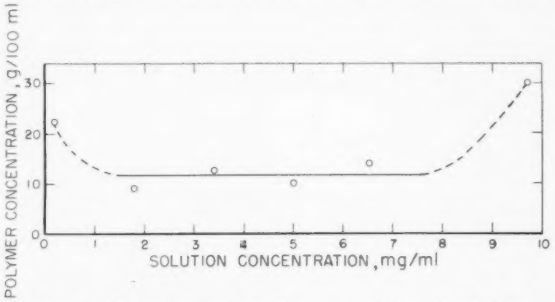

FIGURE 14. *Concentration of polymer in swollen adsorbed film as a function of solution concentration.*

The points represent averages of several runs.

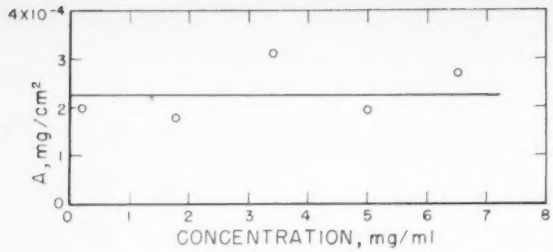

FIGURE 15. *Adsorption isotherm obtained from ellipsometer data.*

Points represent averages of individual runs.

concentration range and it is possible that a thinner, more tightly bound film is first formed, similar to the situation proposed by Gottlieb [11].

From the data obtained here, the amount of polymer adsorbed can be calculated and an isotherm constructed. This is shown in figure 15. Not shown on this figure is the amount of material adsorbed at the solution concentration of 9.7 mg/ml. The amount calculated for this concentration was about 5.2×10^{-4} mg/cm². As discussed above, this large amount may be caused by multilayer adsorption. The remainder of the isotherm shows a plateau, extending for the entire range of concentrations studied, with the exception of the 9.7 mg/ml concentration, at about 2.25 mg/m².

Although a different molecular weight polystyrene was used, the results reported here are considerably lower than the 1500 Å calculated by Öhrn [4] for glass, or similar large values obtained by Fendler, Rohleder, and Stuart [7]. Our results are also much lower than the effective thickness of approximately 5000 Å obtained by Tuijnman and Hermans [6] for poly(vinyl acetate) on glass, or that calculated by Takeda and Endo [8] for poly(vinyl chloride) on glass. All of these measurements were carried out by viscosity measurements and the effective thickness average obtained by such a technique is undoubtedly quite different from that obtained by the method described here. It is not expected that the differences between the chromium-chromium oxide and glass surfaces are sufficiently great to account for the large differences in the thicknesses ascribed to the film.

The possibility of a two-stage adsorption as advanced by Gottlieb [11] could not be verified or disproved. The thicknesses found here are similar to the 210 Å reported by Fontana and Thomas [15] for the adsorption of a copolymer of stearyl methacrylate and *N*-vinyl-2-pyrrolidone on silica, although they also reported a 25 Å thickness for an alkyl methacrylate on silica.

It is of interest to compare the values obtained from these measurements with the root-mean-square distance of an element from the center of gravity. The radius of gyration for polystyrene in a poor solvent is approximately 83 Å for the molecular weight used here [26]. If the amount adsorbed is taken from figure 15 to be approximately 2.25 mg/m², then, assuming hexagonal packing of a "monolayer", the centers of the molecules are calculated to be 88 Å apart. A model consistent with this dimension would be one with almost complete interpenetration of the random coils. It would be of great interest, of course, to relate the measurement of a thickness of 200 Å, as measured by the ellipsometer, to these considerations. However, until more is known about the type of average determined by the ellipsometer, and a realistic model for the adsorbed polymer molecule developed, this cannot be done.

At first glance it appears that our results are somewhat more consistent with the theoretical treatments of Simha, Frisch, and Eirich [2] than with that of Silberberg [3] who predicts a rather flat adsorbed molecule with only short loops extending into the solution for situations where there is a multitude of available sites. It seems apparent that in the system studied here, the loops are extending very far into the solution, unless there is first adsorbed a tightly bound layer and what is being observed here is some multilayer adsorption on top of this layer. However, if one considers that the adsorbent surface is a highly polar oxide surface and that polystyrene is not a very polar molecule, there would be, therefore, only relatively few sites available for adsorption, yielding another situation described by Silberberg.

The authors express their appreciation to Frank McCrackin of the National Bureau of Standards for his helpful suggestions regarding the triple reflection technique, and to Harold Steinberg of NBS for some of the early experimental work.

6. References

[1] E. Jenckel and B. Rumbach, Z. Elektrochem. **55,** 612 (1951).
[2] R. Simha, H. L. Frisch, and F. R. Eirich, J. Phys. Chem. **57,** 584 (1953); H. L. Frisch and R. Simha, ibid. **58,** 507 (1954); H. L. Frisch, ibid. **59,** 633 (1955); H. L. Frisch and R. Simha, J. Chem. Phys. **24,** 652 (1956).
[3] A. Silberberg, J. Phys. Chem. **66,** 1872 (1962); A. Silberberg, ibid. **66,** 1884 (1962).
[4] O. E. Öhrn, J. Polymer Sci. **17,** 137 (1955).
[5] M. M. Hugue, M. Fishman, and D. A. I. Goring, J. Phys. Chem. **63,** 766 (1959).
[6] C. A. F. Tuijnman and J. J. Hermans, J. Polymer Sci. **25,** 385 (1957).
[7] H. G. Fendler, H. Rohleder, and H. A. Stuart, Makromol. Chem. **18,** 383 (1955).
[8] M. Takeda and R. Endo, J. Phys. Chem. **60,** 1202 (1956).
[9] J. Koral, R. Ullman, and F. R. Eirich, J. Phys. Chem. **62,** 541 (1958).
[10] G. Kraus and J. Dugone, Ind. and Eng. Chem. **47,** 1809 (1955).
[11] M. H. Gottlieb, J. Phys. Chem. **64,** 427 (1960).
[12] C. Peterson and T. K. Kwei, J. Phys. Chem. **65,** 1330 (1961).
[13] R. R. Stromberg, A. R. Quasius, S. D. Toner, and M. S. Parker, J. Research NBS **62,** 71 (1959) RP2933.
[14] J. S. Binford, Jr., and A. L. Gessler, J. Phys. Chem. **63,** 1376 (1959).
[15] B. J. Fontana and J. R. Thomas, J. Phys. Chem. **65,** 480 (1961).
[16] H. L. Frisch, M. Y. Hellman, and J. L. Lundberg, J. Polymer Sci. **38,** 441 (1959).
[17] H. L. Frisch and R. Simha, J. Chem. Phys. **27,** 702 (1957).

[18] P. Drude, Ann. Physik. **272,** 532 (1889); ibid. **272,** 865 (1889); ibid. **275,** 481 (1890).
[19] A. B. Winterbottom, Optical studies of metal surfaces, The Royal Norwegian Scientific Society Report No. 1, 1955, published by F. Bruns, Trondheim, Norway.
[20] F. L. McCrackin, E. Passaglia, R. R. Stromberg, and H. L. Steinberg, J. Research NBS 67A (Phys. and Chem.) No. 4, 363 (1963).
[21] F. P. Bowden and W. R. Throssell, Proc. Royal Soc. London **209A,** 297 (1951).
[22] W. R. Krigbaum and P. J. Flory, J. Polymer Sci. **11,** 37 (1953).
[23] J. F. Rudd, J. Polymer Sci. **44,** 459 (1960).
[24] J. H. O'Mara and D. McIntyre, J. Phys. Chem. **63,** 1435 (1959).
[25] W. Forsman and R. E. Hughes (private communication).
[26] P. J. Flory, Principles of polymer chemistry, p. 618 (Cornell Univ. Press, 1953).

(Paper 67A5–232)

JOURNAL OF RESEARCH of the National Bureau of Standards—A. Physics and Chemistry
Vol. 67A, No. 5, September–October 1963

Melting Temperature and Change of Lamellar Thickness with Time for Bulk Polyethylene

James J. Weeks

(April 11, 1963)

The melting temperature of linear polyethylene has been obtained as a function of the time and temperature of crystallization. Recrystallization was minimized by a special melting procedure. By interpreting the melting points as characteristic of a given lamellar thickness, it was found that the thickness of crystals of appreciable age increased linearly with the logarithm of their time of existence. The lowest melting (i.e., thinnest) lamellae in a given specimen may be assumed to have either existed for only a short period of time, or to have been impeded in their growth in the chain direction, and they were found to have an estimated thickness close to that predicted by recent kinetic theories of polymer crystal growth with chain folding.

1. Introduction

Linear polyethylene is known to crystallize from its melt into lamellar structures which range in thickness from less than one hundred to several hundred angstroms [1–5][1]. The extreme thinness of these lamellar crystals causes their melting points to be depressed below the equilibrium melting temperature, T_m^o, by amounts which are easily measurable. Thus, one can use the observed range of melting temperatures to obtain information concerning the distribution of lamellar thicknesses in a crystallized specimen.

Theoretical studies [6, 7] have indicated that the lamellar thickness ("step height") of a growing polymer crystal should initially be equal to l_g^*, the thickness of the critical-size nucleus for maximum growth rate. Since a crystal with this dimension would melt only slightly above the crystallization temperature, T_x, and since polyethylene is known to melt approximately midway between T_x and T_m^o [8], one concludes that the crystals have thickened subsequent to their original formation from the melt [9]. The exact relationship between l, the step height of a mature lamella, and l_g^* is of interest in connection with an extrapolation method for obtaining T_m^o [8] as well as for a detailed understanding of polymer crystal growth as controlled by nucleation mechanisms.

In this paper, the melting temperatures of the lamellae, or portions thereof, in a given specimen are reported as a function of the time and temperature of crystallization. By assuming that the melting temperature of linear polyethylene depends primarily on the lamellar thickness, one may correlate an observed melting point with the thickness of a lamella which was formed at a known temperature. However, in doing this, certain precautions must be taken to minimize changes in the crystal geometry prior to actual melting. Some of the factors that may affect the observed melting range of a sample are mentioned in the next section, and the extent to which these factors influence the choice of a melting procedure is indicated.

[1] Figures in brackets indicate the literature references at the end of this paper.

2. Factors Affecting the Observed Melting Temperature

2.1. Recrystallization

The melting of unstable crystalline regions of small size followed by the crystallization of the newly formed melt on existing stable nuclei is termed *recrystallization* in this paper. The occurrence of recrystallization makes it very difficult to obtain the complete distribution of melting points which characterize the crystals present in a given sample [10]. Polyethylene samples that are crystallized by quenching or slow cooling from the melt to room temperature will have crystallized to a considerable extent at high degrees of undercooling from T_m^o. Since crystallization at low growth temperatures produces very thin lamellae, such samples will contain a large fraction of low-melting crystals. These low-melting crystals will produce much crystallizable liquid and myriad nucleation sites if the specimens are warmed slowly through the melting range. Simultaneous melting and recrystallization at high growth temperatures will bias the observed melting curve toward the higher melting temperatures [8, 11]. As pointed out by Chiang and Flory [12], recrystallization in polyethylene is minimized by crystallizing at elevated temperatures.

The need to avoid recrystallization, or continued isothermal crystallization after a fixed time, has led to the adoption of a melting procedure wherein the sample is transferred from T_x directly into a bath at a higher temperature where the spherulitic growth rate is negligibly slow. In selecting this temperature, one should bear in mind that recrystallization can more rapidly produce crystalline material than can ordinary isothermal crystallization from the melt at the same growth temperature. This has been clearly demonstrated by Gubler, Rabesiaka, and

Kovacs [13] and probably is a result of the larger number of nuclei (unmelted regions of the lamellae) that are present in a sample undergoing recrystallization.

2.2. Isothermal Thickening of the Lamellae

The increase of the lamellar thickness of polyethylene crystals that may occur on storage at constant temperature is called *isothermal thickening*. It is presumed to take place without previous melting of the crystallites and, to a first approximation, not to increase the volume of the crystal but only its thickness. A similar slow-thickening process, wherein the lamellae are not melted, can of course take place while a specimen is being warmed.

Since the crystals of polyethylene do not possess a minimum surface free energy per unit volume when they are first formed during a crystallization process, there is a thermodynamic driving force which tends to increase the thickness of the crystals and thereby minimize the total free energy. The minimum total free energy of a single polyethylene crystal of specified volume could be achieved only if the lateral area of the crystal were about eight times as great as the chain-fold surface area (the ratio of the surface energies is about four to one [9]). No macroscopic single crystals have been observed having a shape approaching the equilibrium shape; thus, one may assume that the tendency for increasing the step height exists at all temperatures below the melting point, including T_x.

As a result of an increase in thickness, the melting point, T_m, of a crystal will be raised. Thus, one expects to find higher values of T_m for samples which are isothermally crystallized for longer periods of time if the thickening process can take place at T_x in an observable interval of time. Information on the temperature and time dependence of the thickening process has been obtained in this study. Details of the molecular motions involved in the thickening process are not dealt with here. This has, however, been discussed by Reneker [14], who proposes that the requisite chain motion is accomplished by the diffusion of point dislocations along the chain.

By warming polyethylene very slowly, other investigators [12, 15, 16] have attempted to form crystals that melt at or very near to T_m^o. Such a procedure utilizes the processes of recrystallization and isothermal thickening to attain thick lamellae, and thus high melting points. However, polyethylene's extremely slow crystal growth rate at temperatures above about 133 °C (where the growth nucleus is large) limits the effectiveness of recrystallization in producing high-melting material, and, as will be seen in section 5.1, isothermal thickening tends to become increasingly ineffective with longer annealing times because of a logarithmic time dependence.

2.3. Rate of Heat Transfer

Another factor that must be taken into consideration in devising the melting procedure is the heat transfer rate in the particular specimens at hand.

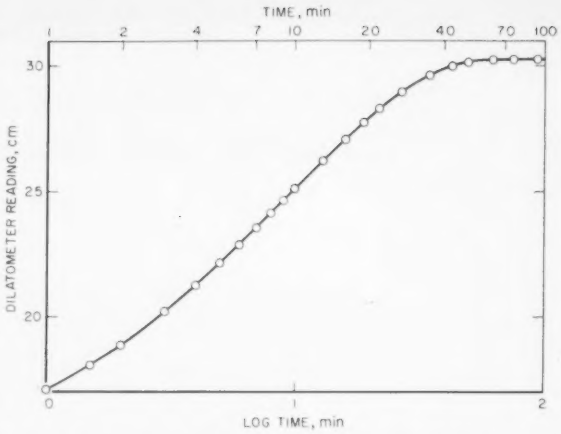

FIGURE 1. *Rate of melting of a ca. 3g polyethylene sample crystallized in mercury dilatometer in 125.0 °C bath for 125 min and then transferred to a 135.20 °C bath.*

With the nearly spherical 3 g samples used in this study, more than one hour is needed to achieve a static volume when a highly crystallized sample is transferred from T_x to a temperature at which almost all of its crystalline regions will melt. Figure 1 shows the rate of melting of a sample crystallized in a 125.0 °C bath for 125 min when it is transferred into a bath at 135.20 °C. Temperature measurements with a thermocouple in the sample have shown that thermal equilibrium is not achieved until the material attains a constant volume. The principal causes of the long time needed to reach temperature equilibrium in the sample are the high heat of fusion and low thermal conductivity of polyethylene.

If the melting of a specimen is accomplished by heating it through its melting range at a given rate, the temperature inside the sample will lag behind the bath temperature by an amount dependent on the sample size and geometry, the rate of heating, the degree of crystallinity, and the distribution of melting points. When using the melting procedure given in section 3, the rate of heating was the most critical factor for a given sample, the error in T_m being approximately 27 min times the warming rate in degrees per minute for any rate less than 0.040 deg/min.

Possibly heat transfer is not the only reason for the slowness of the melting at a fixed temperature near the maximum melting point. If one allows sufficient time for the achievement of a static volume part way through the melting range and then raises the temperature slightly, one finds that melting continues for a considerably longer interval than should be necessary in order to reach thermal equilibrium. Matsuo [17], Chiang and Flory [12], and others have noted the same effect.

2.4. Other Factors

The phenomena mentioned thus far all tend to cause the observed melting temperature to be greater than it should be for the proper characterization of

the original crystallization conditions. On the other hand, two factors may be mentioned which could enter during the course of an investigation and cause the melting points to be lower than the correct values. One is the absorption of solvent. This difficulty was avoided in the present case by the use of mercury-filled dilatometers. The other is decomposition of the polymer. Evidently there was enough anti-oxidant present in the material studied to prevent degradation in spite of repeated heating to 177 °C. No change in the liquid volume occurred with time; nor was there any significant shift of the crystallization isotherm after repeated melting runs. Thus, barring decompositon and diluent absorption, the procedure which gives the lowest T_m for a given crystallized specimen would seem to be the best one to reflect the size of the crystals as formed under the initial growth conditions.

Whether or not the presence of linear polyethylene of low molecular weight affects the distribution of observed melting points is not known. It appears from the work of Chiang and Flory [12] that unfractionated Marlex 50 does have a larger proportion of low melting crystalline regions than does a fractionated specimen. However, it is possible that much of this difference results from the different times and temperatures required to crystallize the various samples to a high degree.

3. Experimental Detail

The material used in this investigation was an unfractionated linear polyethylene (Marlex 50), obtained in the form of small pellets from the Phillips Chemical Company of Bartlesville, Okla. It was used as received except for washing with water and acetone and drying.

Crystallization and melting were carried out in a typical mercury-filled dilatometer. About 3 g of material were used in a 5 ml spherical bulb. The dilatometer capillary was nominally 2 mm in diameter and the height of the meniscus was estimated to the nearest 0.1 mm.

Three Silicone oil bath thermostats were utilized for any given experiment. One bath was for the initial melting of the sample. A temperature of 177 °C for a period of 10 min was found to be sufficient to remove all measurable crystallinity from the sample. No change in the crystallization isotherm was observed as a result of varying the initial melting temperature between 150 and 200 °C. (The crystallization is almost entirely of heterogeneous or pseudohomogeneous origin.) After melting the sample, the dilatometer was transferred to a crystallization bath maintained at $T_x \pm 0.02$ °C by a mercury thermoregulator. Time was measured after the sample had been in the T_x bath for 5 min. After enough time had elapsed to produce the desired crystallinity, the sample was transferred directly to the melting bath which was controlled to a set temperature ± 0.01 °C by a thermistor connected to a bridge circuit. Generally, the melting experiment was begun at a starting temperature just slightly (0.1 to 0.6 °C) below the anticipated melting point in order to avoid recrystallization. A period of 1 hr was allowed at the starting temperature so that nearly all of the crystals which were unstable at that temperature would be melted. Thereafter, the temperature was raised in increments of 0.18° each 30 min until the sample was completely melted. Variations from this scheme were occasionally employed in order to study particular effects.

The temperatures of the baths were measured by a calibrated platinum resistance thermometer. Mercury-in-glass thermometers were found to be unsatisfactory for measuring the bath temperatures because of condensation of the mercury in portions of the capillary above the bath liquid level.

The range of crystallization temperatures employed was 125.0 to 130.0 °C except for a few isolated experiments. The extremely long time required to achieve high crystallinity limited the number of experiments above 130 °C. By the use of a differential thermocouple in one of the dilatometers, it was found that self-heating of the *circa* 3 g specimen during crystallization prevented extension of this range to lower temperatures. Table 1 gives the magnitude of the self-heating near the center of the dilatometer at various times during the crystallization.

The degree of crystallinity, χ, was obtained from the specific volume of the sample, $\overline{V}$, by using the relation $\chi=(\overline{V}_l-\overline{V})/(\overline{V}_l-\overline{V}_c)$ where $\overline{V}_l=1.1484+9.33\times10^{-4}T(°C)$ is the measured liquid specific volume and $\overline{V}_c=0.9940+3.18\times10^{-4}T(°C)$ is an approximation to Swan's crystal specific volume as obtained from X-ray studies [18].

TABLE 1. *Self-heating during crystallization of circa 3 g polyethylene specimens in mercury dilatometer*

Bath temperature	Differential temperature	Time of crystallization	Degree of crystallinity
°C	°C	min	
125.00	0.69	12	0.10
	[a] 1.05	23	.29
	0.13	100	.63
126.25	.59	35	.10
	[a] .77	58	.29
	.54	99	.50
127.50	.26	119	.10
	[a] .33	168	.27
	.21	278	.50
128.75	.06	520	.10
	[a] .09	730	.26

[a] Maximum differential temperature during the crystallization.

4. Results of the Melting Studies

The melting temperature customarily reported for a polymeric sample is the highest observed melting point in the distribution of melting points—the last detectable melting point. Obviously, the temperature obtained by this method will vary with the sensitivity of the detector used to observe the presence of crystallinity. When one is interested in determining the effect of crystallization time on the distribution of melting points, the last detectable

melting point should not be used; since, for a given distribution in a sample of very low χ, the last detectable melting point will be much nearer to the median point than it will be in a sample of high χ. In order to prevent the fixed and finite sensitivity of the measuring instrument from biasing the melting points for samples of different χ, it has been found to be convenient to normalize the distribution of melting points. This may be accomplished by comparing melting points where the same fraction, p, of originally crystallized material remains unmelted. When melting points are being obtained from plots of sample volume against temperature, the most accurate T_m (p) correspond to $p \cong 0.01$. Very low values of p do not give precise melting points because the sample volume asymptotically approaches the liquid volume. Large p melting points have to be avoided, especially for samples crystallized at low T_x, since recrystallization may occur and significantly alter the fraction melted. In addition, when larger amounts of crystal are undergoing fusion, the temperature of the material is nonuniform, and it is difficult to determine the exact temperature of the crystallites melting at a given instant.

Typical melting runs for obtaining T_m (p), for $p=0.01$, using one dilatometer at one crystallization temperature, are shown in figure 2. As may be seen, the accuracy of selecting the melting point when 1 percent of the originally formed crystals remain unmelted drops somewhat at very low χ (see left-hand curve in fig. 2). The T_m (0.01) values, corrected for melting rate by the relation given in section 2.3, are reported in table 2 and are plotted in figure 3 as a function of the logarithm of the crystallization time in minutes. These T_m (0.01) melting points clearly show that the high-temperature side of the distribution of melting points is displaced to higher temperatures as the crystallization time is increased.

A comparison of the time scale in figure 3 with that in figure 4, where the crystallization isotherms are plotted, reveals that the change of slope in T_m (0.01) versus log t (stage 1→stage 2) occurs at roughly the same time that the isotherm reaches χ_w, the beginning of stage II or secondary crystallization. However, it is not certain that the onset of stage II in a crystallization isotherm, which is a result of massive impingement of spherulites [9], is actually closely connected with the onset of stage 2 in the T_m versus log t plot. The apparent increase of the slope for samples crystallized into stage II (dashed lines in fig. 3) with an increase of T_x was confirmed by crystallization of a sample at 125.0 °C for 120 min followed by annealing at 120.0 °C for various lengths of time. The rate of increase of T_m (0.01) with log time of crystallization was found to be 0.05 deg/decade at 120.0 °C, which is almost a factor of 4 smaller than the rate measured at 125.0 °C for samples crystallized into stage II.

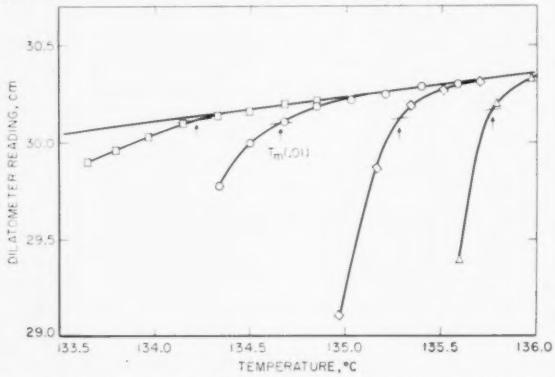

FIGURE 2. *Typical melting curves for samples crystallized in a bath at 126.25 °C.*

The crystallization times are −□−33 min, −○−70 min, −◇−305 min, and −△−9,960 min. The arrows locate the melting temperature where one percent of the original crystallinity remains ($p=.01$).

TABLE 2. *The observed melting temperature of polyethylene when 1 percent of the original crystallinity remains*

Crystallization temperature	Time of crystallization	Warming rate	T_m (0.01)
°C	min	deg/min	°C
125.00–126.05	120	0.006	134.73
	1,204	.006	135.02
	10,000	.012	135.19
126.25–127.02	30	.003	133.99
	33	.006	134.06
	45	.006	134.24
	70	.006	134.50
	120	.006	134.83
	305	.006	135.12
	950	.006	135.29
	3,820	.006	135.51
	9,960	.006	135.61
	34,200	.006	135.76
127.50–127.83	87	.006	134.55
	95	.006	134.62
	135	.006	134.73
	191	.006	134.94
	330	.006	135.27
	920	.006	135.55
	1,040	.000	135.54
	1,040	.000	135.54
	3,890	.006	135.78
128.75–128.84	465	.004	135.35
	745	.006	135.55
	745	.006	135.59
	970	.006	135.72
	970	.006	135.76
	1,410	.006	135.89
	5,300	.006	136.29
130.00	2,820	.006	136.04
	2,930	.007	136.00
	3,800	.019	136.17
	4,320	.007	136.27
	4,330	.000	136.24
	5,280	.019	136.42
	5,380	.006	136.38
	6,680	.006	136.48
	9,650	.006	136.73
	9,910	.007	136.67
	10,200	.030	136.74
	19,800	.019	137.01
	21,200	.006	136.94

In order to obtain the variation of $T_m(p)$ with time of crystallization for some values of p greater than 0.01, the entire melting range of several samples crystallized at 130.0 °C was recorded. Heating of the bath was carried out at an average rate of 0.019 deg/min. This high crystallization temperature minimizes interference from recrystallization and permits the melting to take place in a short period of time relative to the time at T_x. Two of the normalized distributions of observed melting points are shown in figure 5, where corrections have been made for the heating rate and the amount of material melted.

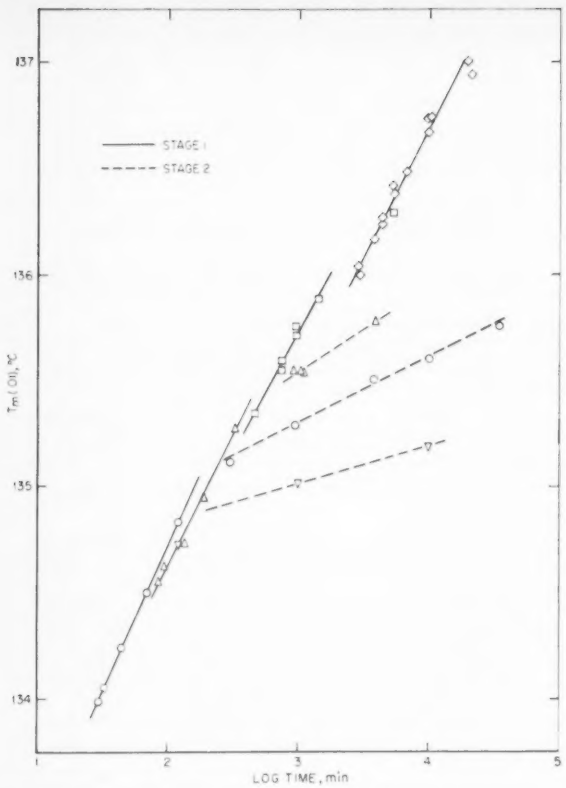

FIGURE 3. *The observed melting temperature, where one percent of the original crystallinity remains, plotted against the logarithm of the crystallization time for various crystallization bath temperatures:* —▽—*125.0°* —○—*126.2°* —△—*127.5°* —□—*128.8°, and* —◇—*130.0 °C.*

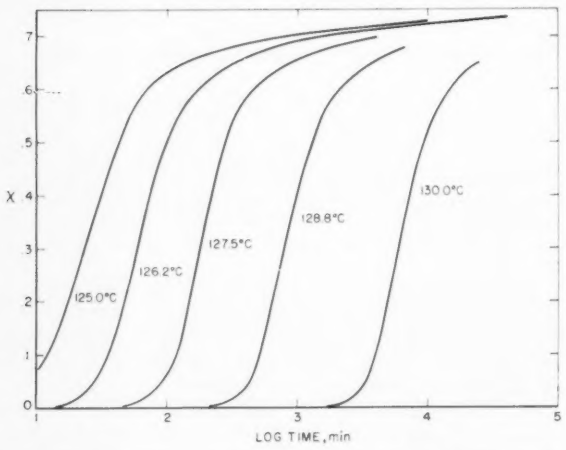

FIGURE 4. *Crystallization isotherms for samples crystallized in baths at the various temperatures shown on the plot.*

The following induction times, t_i, for the beginning of crystallization were observed: at 125.0 °C, none; at 126.2 °C, 7 min; at 127.5 °C, 15 min; at 128.8 °C, 90 min; and at 130.0 °C, 450 min.

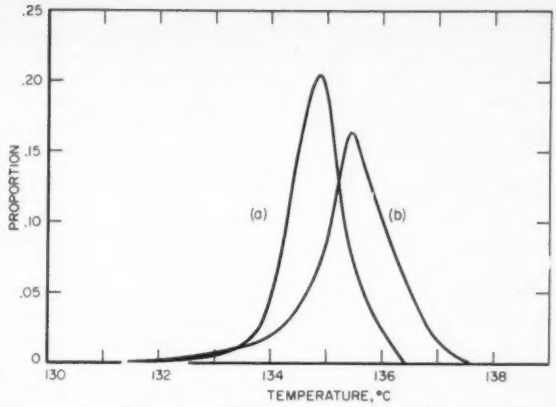

FIGURE 5. *Normalized distributions of the observed melting temperatures of two samples crystallized at 130.0 °C for (a) 3800 min (χ=0.081) and (b) 19,800 min (χ=0.635).*

5. Interpretation and Discussion of T_m

5.1. Estimation of Lamellar Thickness

The depression from T_m^0 of the melting point of a highly crystalline linear polymer of high molecular weight has been attributed generally to imperfections in the crystals. These may be interior defects, or high energy surfaces, or both. On the assumption that the predominant cause of the depression is the high surface-to-volume ratio, which is known to exist as a result of the lamellar habit, one may estimate the step height of mature crystals which melt at T_m. The relation between the melting point depression, $T_m^0 - T_m$, and the thickness, l, is given by the thermodynamic formula [6, 8, 19]

$$l = \frac{2\sigma_e T_m^0}{\Delta h_f (T_m^0 - T_m)} \tag{1}$$

where σ_e is the free energy of formation of the lamellar surface and Δh_f is the bulk heat of fusion. In deriving this relation, the assumptions are made that (a) the other two dimensions of the crystal are large compared to l and (b) the heat capacities of liquid and solid polyethylene are approximately equal in the region of observed melting points.

In order to apply eq (1) to calculate l from T_m, it is necessary to estimate T_m^0 and $\sigma_e/\Delta h_f$. Values of T_m^0 of 141 and 143 °C have recently been obtained by other investigators [20, 21, 22] who extrapolated the melting points of the normal paraffins to infinite chain length. A value of T_m^0 equal to 142 °C is used in the following analysis. Eby and Brown's measurements [21, 22] of the low angle X-ray spacings and corresponding melting points of several Marlex 50 specimens provide an estimate of $\sigma_e/\Delta h_f$. This quantity comes from the slope of a plot of T_m against $1/l$ according to a rearrangement of eq (1). A value of $\sigma_e/\Delta h_f$ equal to 2.04×10^{-8} cm was obtained from the results of their measurements, using the smaller of the two low angle spacings as a measure of the lamellar thickness. Geil has shown that this smaller spacing corresponds to the actual lamellar thickness as measured by electron microscopy [5, 23]. (Using

Quinn and Mandelkern's value of Δh_f [16], as revised in reference [12], we have $\Delta h_f = 2.80 \times 10^9$ erg/cm^3, which gives $\sigma_e = 57$ erg/cm^2 from the previous ratio.) The work of Eby and Brown on Marlex 50, which directly relates T_m and l, thus quite directly permits melting point data to be translated into values of the lamellar thickness.

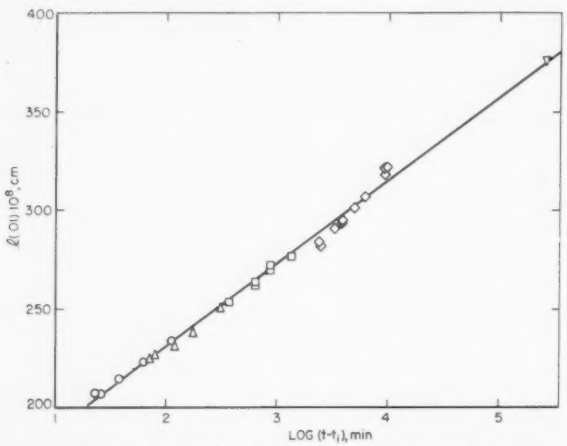

FIGURE 6. *Estimated lamellar thickness as a function of the logarithm of the time of crystallization of the samples (stage I data).*

Melting points shown in figure 3 were used with eq (1) to obtain the estimates of l. The crystallization bath temperatures were −○−126.2°, −△−127.5°, −□−128.8°, −◇−130.0°, and −▽−131.5 to 133.0 °C.

Estimates of $l(p)$ for $p = .01$ have been obtained from the T_m (.01) listed in table 2. Figure 6 shows a plot of the $l(.01)$ as a function of the time of crystallization. Only values from stage 1 on a T_m versus log t plot are given in the figure. (One additional point is included from an eight-month crystallization, during which T_x increased from 131.5 to 133.0 °C. At the time of melting, χ had reached about 0.30.) Here the induction time, t_i, for the appearance of visible crystallinity has been subtracted from the crystallization time as measured from the time the sample reaches its liquid volume at T_x. For specimens with a crystallization time of less than 200 min, it was necessary to make a small correction for the change of lamellar thickness which occurred subsequent to the crystallization time and prior to the time of melting at T_m (0.01). This correction will be considered in section 5.3.

The $l(p)$ values for $p = 0.01$ were obtained by using a value for $\sigma_e/\Delta h_f$ which was calculated from melting point and low angle X-ray measurements on mature polyethylene crystals. If the value of σ_e (equal to 49 erg/cm^2 [9]) derived from kinetic studies on the nucleation and growth of polyethylene spherulites had been used to obtain l, then the estimated l values would have been 14 percent smaller.

As figure 6 illustrates, the values of l vary linearly, to a good approximation, with the logarithm of the time of crystallization. Hirai et al. [24] and Fisher and Schmidt [25] have found by X-ray diffraction that the long period of polyethylene single crystals, which were grown from solution, increases in a similar manner during annealing. The latter authors also found a similar logarithmic time dependence for the thickening of lamellae in quenched bulk polyethylene which had been annealed at various temperatures. These observations imply that there was initially a rather rapid increase in the thickness of both the melt-grown and solution-grown crystals that occurred prior to the experimentally measured time.

5.2. Model for the Thickening Process

Hirai et al. [24] have proposed a nucleation-type model for the thickening of lamellae that leads to an approximately linear increase in l with log t. They make the observation that a nucleation barrier must be surmounted in order for lamellar thickening to lower the free energy of a crystal of given fixed volume. Below we summarize this approach in slightly revised form. Taking the dimensions of a surface nucleus to be x on each side and g in height, one has for the change in free energy of a crystal of thickness l,

$$\Delta F = 4xg\sigma - 2x^2 g\sigma_e/l \tag{2}$$

because of the local increase in thickness at the nucleation site and corresponding local decrease in basal area. Here σ is the free energy of formation of the lateral surface per unit area. The location of the minimum in the free energy surface, ΔF^*, is independent of g but its value is proportional to g; thus, the increase in l should be accomplished by steps of only 2.54 Å at a time.[2] After a critical value of x has been exceeded, the increase in thickness is assumed to be propagated rapidly over a rather large area. Just how large an area might depend on external impingements, strain terms, or other complex factors. By differentiation of ΔF with respect to x, one finds

$$\Delta F^* = (2g\sigma^2/\sigma_e)l = Cl \tag{3}$$

Thus, as an elementary approximation, one has

$$\frac{dl}{dt} = Ae^{-Cl/kT}. \tag{4}$$

(Hirai et al. calculate that $dl/dt = A' \exp(-Cl/2kT)$, but, by a more rigorous derivation based on the method of Turnbull and Fisher [26], Lauritzen [27] has shown that the correct exponent is given by eq (4).)

At this point we mention that an equation identical in form to eq (4) has been obtained by Peterlin [28] on the assumption that there exists an energy barrier of height nE for the lengthwise translation of a chain of n carbon atoms to an adjacent crystal lattice site. The rate at which this motion could occur is $dn/dt = A'' \exp(-nE/kT)$. Since $l = 1.27 \times 10^{-8} n$(cm), this equation is similar in form to eq (4). Hirai

[2] This assumes a lengthwise translation of 5.08 Å by one chain in order to reform the fold with the same configuration that it had previously. A translation of half this amount may be possible but would produce a higher energy fold.

assumes that the barrier to lengthwise translation is independent of the crystal thickness. (This point will be re-examined later.)

Integration of eq (4) gives

$$l = B \log \frac{AC}{kT} + B \log (t - t_0 + \tau_0), \tag{5}$$

where $B = 2.3\ kT/C$ and $\tau_0 = (kT/AC)\ \exp(l_g^* C/kT)$. It is supposed that a crystal born at time t_0 initially has a thickness equal to l_g^*. When $t - t_0$ is large compared to τ_0—which is the case in the experimentally accessible time range—then

$$l \simeq B \log \frac{2.3A}{B} + B \log (t - t_0), \tag{6}$$

or alternatively

$$l \simeq l_g^* + B \log \frac{t - t_0}{\tau_0}. \tag{6a}$$

Equation (6) may be put in terms of the crystallization time, rather than the existence time, of the crystal by noting that the age of any fraction, p, of the crystals in a given sample crystallized to χ_f at time t_f (equal to $t - t_i$) is greater than or equal to $t_f - t_0$, where t_0 is the time at which $\chi = \chi_0 = p\chi_f$. If there is a monotonic dependence of melting temperature on age as a consequence of isothermal thickening, then the crystals that melt at temperatures higher than $T_m(p)$ will have formed earlier than time t_0. Thus, $t_f - t_0$ is the estimated age of a crystal melting at $T_m(p)$. To a good approximation the isotherms in figure 4 are given by the equation [29]

$$\chi = \chi_w [1 - e^{-Z(t - t_i)^3/\chi_w}], \tag{7}$$

where Z is a constant for a given isotherm. This corresponds to the growth of heterogeneously nucleated spheres. From this equation

$$t_0 = q^{1/3} t_f, \tag{8}$$

where $q = \log (1 - \chi_0/\chi_w)/\log (1 - \chi_f/\chi_w)$.

Substitution for t_0 in eq (6) gives

$$l \simeq B \log \frac{2.3A}{B} + B \log (1 - q^{1/3}) + B \log t_f. \tag{9}$$

since t_f is the crystallization time. A slightly poorer but more convenient approximation results if the "free growth rate," $\chi = Z(t - t_i)^3$, is assumed in place of eq (7). In this case,

$$l \simeq B \log \frac{2.3A}{B} + B \log (1 - p^{1/3}) + B \log t_f. \tag{10}$$

Average values of the parameters A, B, and C may be calculated from the plot in figure 6 by use of eq (10). The slope gives $B = 43.3 \times 10^{-8}$ cm; A is found to be 7.8×10^{-6} cm/sec; and C is 2.94×10^{-7} erg/cm for $T = 400$ °K. Taking g as equal to 2.54×10^{-8} cm, one may obtain $\sigma^2/\sigma_e = 5.8$ erg/cm^2 from the magnitude of C. This value of 5.8 for σ^2/σ_e may be compared to the value of 3.0 that has been obtained from parameters for the nucleation and growth of polyethylene crystals [9]. Various assumptions can be advanced to account for the difference in σ^2/σ_e values, for example: (a) other barriers to the formation of the nucleus, such as that proposed by Peterlin for the lengthwise translation ("sliding diffusion") of the chains, (b) the existence of restraints on the thickening process (see section 5.4), and (c) the fact that the lateral surface of the nucleus, which presumably rises only 2.54 Å above the surrounding crystal, is not typical of the lateral surface of either a primary nucleus or a growth nucleus. The extent to which these factors may be operative is not known, but it is likely that the barrier for lengthwise translation of the chains is dependent on l. This translation barrier will probably be more temperature dependent than the nucleation barrier; if it were, it could explain the strong temperature dependence of B that Fisher and Schmidt [25] observed. They found that the magnitude of B increased by a factor of 3 in the range 120 to 130 °C. The data in figure 6 also indicate a positive temperature coefficient for B. The 130 °C points give a value of $B = 64 \times 10^{-8}$ cm ($\sigma^2/\sigma_e = 3.9$ erg/cm^2) and $A = 6.5 \times 10^{-8}$ cm/sec when treated by themselves. When both the nucleation and translation barriers are controlling the thickening rate, the quantity B is given by $2.92kT\sigma_e/(10^8 E\sigma_e + 2.54\ g\ \sigma^2)$. If E decreases with increasing temperature as the lattice expands, then the nucleation barrier would be the limiting rate controlling factor at high temperatures while the translation barrier might be the limiting factor at very low temperatures.

5.3. Change of During Melting

Of necessity, samples crystallized at T_x, and then melted using the procedure followed here, contain crystals that have existed for a greater time interval than that measured at T_x. In order to determine the amount of lamellar thickening that occurred during the melting process, a polyethylene sample was crystallized in a 126.25 °C bath for 42 min, then transferred to a bath at 133.64 °C, where it was stored for a time interval t_s, and then melted at a rate of 0.006 deg/min. By repeating the procedure, the data given in table 3 were obtained. Values of

TABLE 3. *Melting temperature of polyethylene sample stored at 133.64 °C for various lengths of time* [a]

Time of storage, t_s	Total melting time, t_m	Corrected $T_m(0.01)$ [b]	$l(.01)$
min	*min*	*°C*	*cm*
(not stored)	91	134.30	220.0×10^{-8}
23	148	134.25	218.5
148	328	134.34	221.0
903	1143	134.91	239.0
9,906	10,331	136.16	290.0

[a] The sample was initially crystallized in a 126.25 °C bath for 42 min.
[b] T_m (0.01) observed minus 0.16 °C heating rate correction.

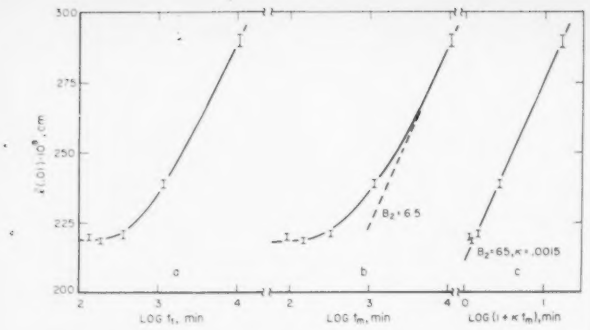

FIGURE 7. *The estimated lamellar thickness, l (.01), for a polyethlene sample crystallized in 126.25 °C bath for 42 min and then melted in time interval* t_m:

7a. *Plotted against the logarithm of the total time of crystallization plus melting,* t_t;

7b. *Plotted against log* t_m;

7c. *Plotted against log* $(1+\kappa t_m)$ *where* κ *is a constant equal to 0.0015.*

l (0.01) were derived from the T_m (0.01) by use of eq (1). These values are plotted in figure 7a as a function of the logarithm of the total time of crystallization plus melting, t_t. This plot is not suitable for determining the change in l during melting. A probable explanation of the shape of the curve in figure 7a may be found from a consideration of the effect of a change in the parameters A and B as the temperature is changed from T_x to one near T_m (0.01). Assume that a lamella is crystallized at T_x for a time (t_1-t_0) where the thickening rate is

$$\frac{dl}{dt}=A_1e^{-2.3l/B_1};\ l_g^*<l<l_1,\ t_0<t<t_1. \tag{11}$$

After this time the crystallite is transferred to a higher temperature where it thickens at a rate

$$\frac{dl}{dt}=A_2e^{-2.3l/B_2};\ l>l_1,\ t>t_1. \tag{12}$$

When eqs (11) and (12) are integrated and combined one obtains

$$l-l_1=B_2\log\{1+\kappa(t-t_1)\} \tag{13}$$

where $\kappa=(2.3A_2/B_2)[(2.3A_1/B_1)(t_1-t_0+\tau_0)]^{-B_1/B_2}$ and

$$\tau_0=(B_1/2.3A_1)\exp 2.3l_g^*/B_1$$

which is negligible compared to t_1-t_0.

According to eq (13), a plot of l versus log $(t-t_1)$ will give a curve whose slope approaches B_2 when $t-t_1>>\kappa^{-1}$. Such a plot is shown in figure 7b where B_2 has been estimated to be about 65×10^{-8} cm. When B_2 is known, κ may be estimated from a plot such as that given in figure 7c. The data imply a κ of about 0.0015. Once B_2 and κ have been determined, eq (13) may be used to obtain the change in l (0.01) that occurs during the melting procedure (by successive approximation until B_1 is known). In this way corrections were applied to the l(0.01) which were crystallized for less than 200 min, as was mentioned in section 5.1. The maximum correction was 7.5×10^{-8} cm.

All of the quantities in κ have been estimated except for A_2. Using $\kappa=0.0015$, $B_1=43\times10^{-8}$ cm, $B_2=65\times10^{-8}$ cm, and $A_1=7.8\times10^{-6}$ cm/sec, one finds that $A_2=2.4\times10^{-5}$ cm/sec. This is about the same change in A with temperature that Hirai et al. have found for the annealing of polyethylene single crystals [24].

5.4. The Distribution of Step Heights and Restraints to Isothermal Thickening

The nucleation theory of lamellar thickening successfully accounts for the time dependence of the values of l estimated from the T_m (0.01); however, it does not, in itself, provide a complete explanation of the distributions of melting points shown in figure 5. This may be shown by obtaining the $l(p)$ for $p=0, .1, .2, \ldots, 1.0$ from the entire melting curves and the corresponding values of $t-t_0$ from the 130.0 °C crystallization isotherm, assuming a perfect positive correlation between age and melting temperature. These l values are plotted in figure 8. (They have been adjusted slightly so that the l(0.01) fall exactly on the l versus log t curve of figure 6.) According to eq (6) all of the $l(p)$ points should fall on the same curve. This curve should be essentially a straight line, when $t-t_0>100$ min, having a slope B equal to 43.3×10^{-8} cm. It has been drawn as a solid line in figure 8 and is labeled $p=0.01$. Three points of interest are apparent in the plot: (i) about 80 percent of sample (a) has $l(p)$ which give a slope similar to the l(0.01) but which are displaced to lower values (see dashed line); (ii) the l(0) points imply a much greater slope than

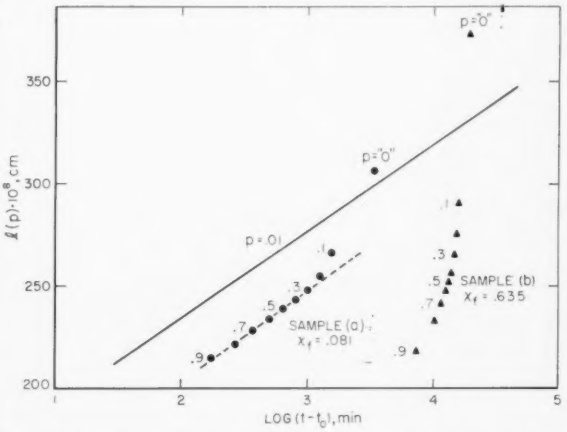

FIGURE 8. *Estimated crystal thickness from* $T_m(p)$ *for the two distributions shown in figure 5 as a function of the logarithm of the estimated existence time of the crystals.*

Sample (a) crystallized at 130.0° for 3800 min, ●; sample (b) crystallized at the same temperature for 19,800 min, ▲.

do the $l(0.01)$ points; and (iii) the $l(p)$ for sample (b) fall much below the solid line except for $l(0)$. These effects are thought to be the result of two factors which have not been treated in deriving eq (6); namely, the existence of a distribution of step heights around l_g^* when crystals are first formed from the melt and the existence of restraints to normal lamellar thickening.

Lauritzen and Hoffman [6, 27] have considered the distribution of step heights of growing chain-folded crystals and have found that the probability distribution may be represented by

$$F(l) \cong \gamma^2 (l - l_{gm}) e^{-\gamma(l - l_{gm})} \qquad (14)$$

to an approximation sufficient for the present purpose. Here $l_{gm} = 2\sigma_e/\Delta f$ where Δf is the bulk free energy of fusion, $\gamma = 2b_0\sigma/kT$ (which is taken as a constant), and b_0 is the width of a chain. By assuming that crystals are generated according to $\chi = Z(t - t_i)^3$ with a distribution of step heights given by eq (14), Lauritzen [27] has found the following relation for crystals that have thickened according to eq (4) in a sample crystallized for time $t_f = t - t_i$ when $t >> \tau_0$:

$$l' = \frac{2.3}{\gamma} \log \frac{3}{p} + \frac{2.3}{\gamma} \log \frac{2\lambda^3\gamma \left[l' - l_{gm} - B \log \left(1 + \frac{t_f}{\tau_0} \right) \right]}{(\gamma+\lambda)(\gamma+2\lambda)(\gamma+3\lambda)} + \lambda^3 \frac{8\gamma^3 + 36\gamma^2\lambda + 44\gamma\lambda^2 + 12\lambda^3}{(\gamma+\lambda)^2(\gamma+2\lambda)^2(\gamma+3\lambda)^2} + l_{gm} - B \log \tau_0 + B \log t_f. \qquad (15)$$

Here λ equals $2.3/B$. This equation holds for $p < \sim 0.02$ and may be compared at low p with a modification of eq (10), namely,

$$l = B \log (1 - p^{1/3}) + \frac{2}{\gamma} + l_{gm} - B \log \tau_0 + B \log t_f. \qquad (16)$$

The more detailed treatment by Lauritzen shows that $l(0.01)$ should be essentially a linear function of log $(t - t_i)$ as has been observed in figure 6. However, eq (15) shows a stronger dependence of l on p than does eq (16) for low values of p. In order to demonstrate a qualitative agreement between the $l(p)$ values for low p shown in figure 8 and those values predicted by eq (15), we note that the dilatometers used in this study have a fixed limit of sensitivity of about 0.25 mg of polyethylene crystal. This is equivalent to a degree of crystallinity of about 0.00008 and means that the so-called "$p=0$" values in figure 8 actually are $p = 0.00008/0.081 = 0.001$ and $p = 0.00008/0.635 = 0.00013$ for samples (a) and (b), respectively. Now one may compare the change in the $l(p)$ predicted by eqs (15) and (16) with that observed experimentally. This is done in table 4 by computing $l(p) - l(.02)$ for several values of p. It is seen that the variation of l with p shown by sample (a) agrees well with that predicted by eq (15).

TABLE 4. *Comparison of* l(p)—l(0.02) *observed with tha predicted by eqs (15) and (16)*

p	$l(p) - l(.02)$ by eq (15)	$l(p) - l(.02)$ by eq (16)	Observed $l(p) - l(.02)$	
			Sample (a)	(b)
	cm	*cm*	*cm*	*cm*
0.01	4.4×10^{-3}	1.4×10^{-3}	5.5×10^{-3}	10.0×10^{-3}
[a].0010	19.1	4.0	17.5	----------
[b].00013	31.5	5.0	----------	53.5

[a] p="0" for sample (a).
[b] p="0" for sample (b).

From the foregoing consideration of the effect of a distribution of step heights on $l(p)$ in a crystalline specimen, one may suppose that in a low χ sample the T_m (p) for large p generally reflect the melting of crystals initially formed near the average of the step-height distribution. At lower values of p, fewer and fewer crystals remain in the sample so that the observed melting points correspond to the larger crystals in the original distribution. The strong dependence of l on p for low values of p thus explains the strong upswing in $l(p)$ for $p < 0.1$ that is seen in figure 8 and which is a result of the "tail" on the melting curves (see figure 2). This "tail" on the melting curve near the liquidus is due primarily to the corresponding tail on the high end of the $F(l)$ distribution, which persists at all ages.

The fact that the $l(p)$ for high p in sample (b) fall appreciably below the $p=0.01$ curve may be interpreted as showing the existence of restraints to normal isothermal thickening of the lamellae. These restraints are probably of varying degree, but they may also vary with χ (the stage of development of the "spherulites"). They can be visualized to occur as the result of external impingement of adjacent lamellae, which may be most severe in regions of secondary surface nucleation, branching, spiral dislocation, or numerous interlamellar tie molecules; and/or they may result from internal build-up of strain associated with the large mass transport required for lamellar thickening at constant volume. Irrespective of the cause, the existence of restraints to normal thickening would destroy the prefect correlation between age and melting point which was assumed in obtaining the coordinates for the points in figure 8. Because of the possibility of residual restraints on the thickening process, the true value of B—estimated previously from the slope of $l(0.01)$ versus log t—may be greater than that shown in figure 6, but the similarity of this slope with that defined by high p-values of l for sample (a) suggests that B is not appreciably biased by restraints.

From the foregoing, it is reasonable to suppose that the transition from stage 1 to stage 2 on a T_m or l versus log t plot (compare figs. 3 and 6) is a result of retardation to thickening in the c crystallographic direction of the older lamellae in the spherulites. Conversely, the transition from stage I to stage II in a crystallization isotherm is thought to result from retardation to growth in the a and b directions, e.g., impingements of lamellae at spherulite boundaries.

5.5. Estimates of l_g^* from $T_m(1.0)$

Of particular interest is the fact that the smallest estimated values of l, which were obtained from the complete melting curves of samples crystallized at 130.0 °C, are close to the value of l_g^* predicted by theories for polymeric crystal growth with chain folding [6, 7] if the "thermodynamic" value of the surface free energy is employed (σ_e=57 erg/cm^2). Similar observations have been made for other crystallization temperatures as are shown in table 5.

TABLE 5. *Comparison of* $l(1.0)$ *with the theoretical value of a growth nucleus of critical size,* l_g^*

Crystallization temperature	Time of crystallization	(1.0)	[a] l_g^*
°C	min	cm	cm
125.00–126.05	120	113×10^{-8}	$111–117\times10^{-8}$
	120	107	(94–99)
	[b] 120	100	
130.00	3800	158	152
	5280	168	(128)
	19,800	160	
131.60–133.00	288,000	218	174–199
			(146–167)

[a] The values of l_g^* are calculated as $l_g^*=\frac{2\sigma_e T_m^0}{\Delta h_f(T_m^0-T_x)}+\frac{kT_x}{b_0\sigma}$

after Lauritzen and Hoffman [6], where k is Boltzmann's constant and b_0 is the width of a chain. The values T_m^0=415 °K, σ_e=57 erg/cm^2, σ=12 erg/cm^2 [9], $\Delta h_f=2.8\times10^9$ erg/cm^3, and $b_0=4.1\times10^{-8}$ cm were used. The range of l_g^* values shown refers to the temperature range in the first column. Similar results are obtained using Price's formulation of l_g^* [7]. Values in parentheses calculated with σ_e=49 erg/cm^2 from kinetic data [9].

[b] Three heating rates were used to melt the preceding samples; namely, 0.030, 0.060, and 0.120 deg/min.

The discrepancy that appears at the highest crystallization temperature could imply that some thickening of the $l(1.0)$ has occurred during the very long storage at T_x.

The crystals melting at $T_m(1.0)$ are assumed to be the thinnest (and therefore lowest melting) of all those in the specimen because of a short time of existence and/or a very highly impeded thickening. It is conceivable that they could be low melting because of a defective internal structure as a result of the incorporation of short branches into the crystal. But Keith [30] has found that branched structures tend to be rejected at the growing boundary. The crystals in samples that have been crystallized slowly to a low χ should be especially free from internal defects.

There is a strong implication from the logarithmic time dependence of the lamellar thickness, together with the values found for $l(1.0)$, that polyethylene crystals are initially formed in a growth process having a thickness near that of the theoretical critical-size growth nucleus, l_g^*. This thickness evidently increases very rapidly at first, at a rate inversely proportional to $(t\text{-}t_0+\tau_0)$, and eventually gives a thickness of approximately 2 l_g^* in the region that is experimentally accessible for study by low-angle X-ray diffraction or by electron microscopy of surface replicas.

5.6. Extrapolation of T_m Versus T_x To Obtain T_m^0

The experimentally measured increase in T_m with increasing crystallization time, when interpreted as in increase of lamellar thickness, helps to elucidate the extrapolation procedure proposed by Hoffman and Weeks [8] for obtaining T_m^0. In the application of this method one assumes that the thicknesses of the larger mature lamellae (in samples crystallized to a given value of χ and then melted without recrystallization) are dependent only on the crystallization temperature and may be closely approximated by βl_p^*, where β is a constant and l_p^* is equal to $4\sigma_e/\Delta f$. As an example, if one obtains the crystallization times of samples crystalized to a χ of 0.10 from the isotherms in figure 4 and determines the corresponding values of l from figure 6, then one finds that β increases from 0.98 to 1.04 in the temperature range 126.5 to 130.0 °C. A similar change in β occurs using $l(0)$ instead of $l(0.01)$ values. The increasing value of β causes an appreciable error in the estimate of T_m^0=145.5 °C that is obtained by linear extrapolation of $T_m(0)$ versus T_x to the intersection with the line $T_m(0)=T_x$.

It appears that, for polyethylene, a better extrapolation for obtaining T_m^0 than the one suggested by Hoffman and Weeks is one based on eq (1), where the observed melting point is plotted as a function of the reciprocal of the lamellar thickness. When Eby and Brown's data [21, 22] are plotted in this manner, one obtains a value of T_m^0 of about 143.5 °C by extrapolation of either of the two long spacings which they report. If p=0.50 melting points are used instead of the last detectable melting points, then the estimate of T_m^0 is about 1.5 degrees lower. The T_m (0.50) probably correspond more closely to the l's obtained from low-angle X-ray diffraction than do the last detectable melting points. This is consistent with the value T_m^0=142 °C used in the preceding sections and corresponds well with the value obtained from extrapolation of paraffin data.

5.7. Summary of the Analysis

Eby and Brown's [21, 22] experimental verification of eq (1) has shown that the principal cause of a sample's melting below T_m^0 is the thinness of its lamellar crystals. Their measurements provide a value for $\sigma_e/\Delta h_f$, but other estimates of σ_e [9] and Δh_f [16] could have been used just as well for estimating lamellar thickness from the melting point. A study of the melting temperature of polyethylene specimens has shown that isothermal thickening occurs and that it has a logarithmic time dependence. On the basis of a nucleation model of the thickening process, about half of the observed rate of change of l is accounted for between 125 and 130 °C. Another contributing factor is presumed to result from a barrier (to the lengthwise translation of the chains) that depends on chain length [28]. There is evidence to show that this barrier decreases with increasing temperature, allowing substantially more than one half of the rate of change of l to be explained by the

nucleation model near and above 133 °C. When the theory is extended by the inclusion of a distribution of step heights around l_g^*, one can quantitatively attribute the entire distribution of melting points, observed for a sample of low χ, to differences in the ages of the crystallites. However, as the degree of crystallinity increases, it is evident that something restrains a fraction of the crystals from thickening at their normal rate. This impeded fraction increases with the time of crystallization until, for the samples crystallized into stage II, even the last one percent of the crystals exhibit a diminished thickening rate. Values of l_g^* close to those predicted by recent theories of growth with chain folding are obtained from T_m (1.0) data. An estimate of T_m^0 (equal to 142 °C) has been obtained from Eby and Brown's data by the use of eq (1).

The author thanks Dr. J. D. Hoffman for suggesting a study of the melting temperature of polyethylene and also for his helpful criticism of this manuscript. Appreciation is expressed to Dr. J. I. Lauritzen, Jr., for permission to use some of his unpublished derivations and for his interest in many aspects of the theory.

6. References

[1] G. C. Claver, Jr., R. Buchdahl, and R. L. Miller, J. Polymer Sci. **20,** 202 (1956).
[2] E. W. Fisher, Z. Naturforsch. **12a,** 753 (1957).
[3] H. Hendus, Ergeb. Exakt. Naturw. **31,** 331 (1959).
[4] C. Sella and J. J. Trillat, Compt. Rend. **248,** 410 (1959).
[5] P. H. Geil, *Polymer Single Crystals* to be published by John Wiley and Sons, Inc., 440 Park Ave. So., New York 16, New York.
[6] J. I. Lauritzen, Jr. and J. D. Hoffman, J. Research NBS **64a,** 73 (1960).
[7] F. P. Price, J. Chem. Phys. **35,** 1884 (1961).
[8] J. D. Hoffman and J. J. Weeks, J. Research NBS **66A,** 13 (1961).
[9] J. D. Hoffman and J. J. Weeks, J. Chem. Phys. **37,** 1723 (1962).
[10] B. Wunderlich, Abstracts of the Polymer Div. Meeting of the Am. Chem. Soc., Atlantic City (1962). To be published in Polymer.
[11] S. Matsuoka and C. J. Aloisio, J. Appl. Polymer Sci. **4,** 116 (1960).
[12] R. Chiang and P. J. Flory, J. Am. Chem. Soc. **83,** 2857 (1961).
[13] M. Gubler, J. Rabesiaka, and A. J. Kovacs, to be published.
[14] D. H. Reneker, J. Polymer Sci. **59,** S 39 (1962).
[15] L. Mandelkern, M. Hellmann, D. W. Brown, D. E. Roberts, and F. A. Quinn, Jr., J. Am. Chem. Soc. **75,** 4093 (1953).
[16] F. A. Quinn, Jr., and L. Mandelkern, J. Am. Chem. Soc. **80,** 3178 (1958).
[17] H. Matsuo, personal communication.
[18] P. R. Swan, J. Polymer Sci. **42,** 525 (1960).
[19] B. Wunderlich, J. Chem. Phys. **29,** 1395 (1958).
[20] M. G. Broadhurst, J. Chem. Phys. **36,** 2578 (1962).
[21] R. K. Eby and R. G. Brown, Bull. Am. Phys. Soc. **7,** 241 (1962).
[22] R. K. Eby and R. G. Brown, J. Appl. Phys., to be published.
[23] P. H. Geil, Bull. Am. Phys. Soc. **7,** 206 (1962).
[24] N. Hirai, Y. Yamashita, T. Mitsuhata, and Y. Tamura, Rep. Res. Lab. Surface Sci., Fac. Sci. Okayama Univ. **2,** 1 (1961).
[25] E. W. Fisher and G. Schmidt, Angew. Chem. Internat. Edit. **1,** 488 (1962).
[26] D. Turnbull and J. C. Fisher, J. Chem. Phys. **17,** 71 (1949).
[27] J. I. Lauritzen, Jr., unpublished.
[28] A. Peterlin, to be published.
[29] L. Mandelkern, SPE Journal **15** (1959).
[30] H. D. Keith, personal communication.

(Paper 67A5–233)

JOURNAL OF RESEARCH of the National Bureau of Standards—A. Physics and Chemistry
Vol. 67A, No. 5, September–October 1963

Precise Coulometric Titrations of Potassium Dichromate

George Marinenko and John K. Taylor

(June 10, 1963)

A method has been developed for the precise assay of potassium dichromate by constant-current coulometric titration with ferrous ions generated at a platinum cathode. It is shown that one-half gram samples of the dichromate can be titrated with a standard deviation of 0.003 percent.

1. Introduction

This paper reports results of a continuing investigation to evaluate coulometric methods of analysis and to develop highly precise and accurate analytical methods for important materials, based upon this technique. Earlier papers described the coulometric titrations of acids and bases [1] [1] and of halides [2]. The present research is concerned with a typical oxidation-reduction titration, the analysis of potassium dichromate.

The application of constant-current coulometric titrations to the analysis of dichromate is not novel [3, 4, 5], but highly precise and accurate results have not been reported. The method developed in the present investigation consists of the reduction of dichromate with electrogenerated ferrous ion. The technique and procedure have been refined to permit results reliable to a few parts in 100,000, which are about two orders of magnitude better than those reported by previous investigators.

2. General Considerations

The conditions for 100-percent efficient generation of ferrous ion at a platinum cathode are readily obtained from current density versus potential studies of the supporting electrolyte alone and with several additions of ferric ion. This technique has been employed by Lingane and co-workers for the evaluation of the current efficiency of generation of ceric ion [6] and of titanous ion [7].

The results of a study of the reduction of ferric ion at a platinum cathode are shown in figure 1. Such curves are readily and quickly obtained by the use of an X–Y recorder in which the potential of the platinum electrode with reference to a saturated calomel electrode is recorded on the X-axis while the voltage drop across a standard resistor in series with the electrolysis cell is recorded on the Y-axis. The latter values are related to current density from knowledge of the value of the resistor and the area of the electrode used. By manually varying the potential applied to the electrolysis cell, the curves relating current density to electrode potential are quickly obtained.

In figure 1, curve 1 represents the data obtained for the supporting electrolyte, 2 M sulfuric acid. Curves 2, 3, and 4 represent the data obtained on successive additions of ferric ion to the acid. The estimation of the current-efficiency for the generation of ferrous ion is illustrated by the following examples.

Consider the solution represented by curve 2. At a current density of 2 ma/cm², the potential of the platinum electrode was found to be about −0.39 v (point C). At the same potential, the current density for the electrode immersed in the supporting electrolyte alone was 0.3 ma/cm². The fraction of current producing ferrous ions is evidently (2.0−0.3)/2.0

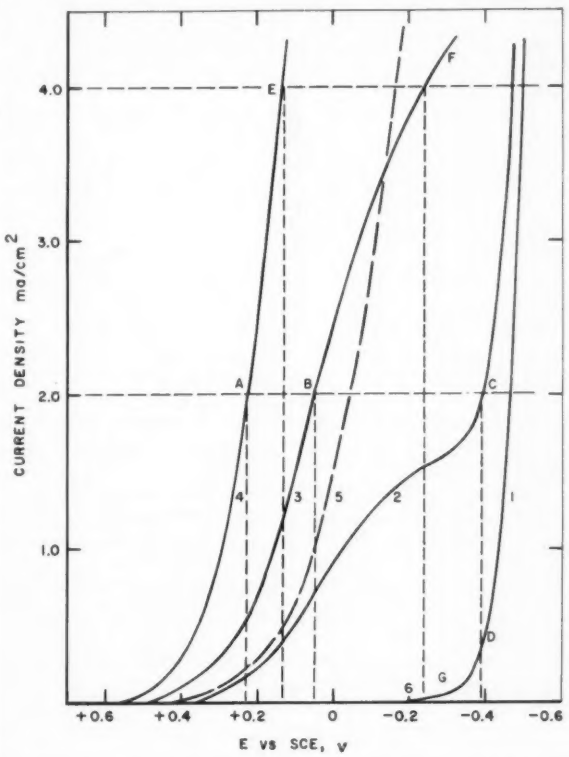

FIGURE 1. *Current density, potential curves for the reduction of ferric ion at platinum cathode.*

1. 2M H_2SO_4
2. 2M H_2SO_4; 0.01 M Fe^{+++}
3. 2M H_2SO_4; 0.03 M Fe^{+++}
4. 2M H_2SO_4; 0.2 M Fe^{+++}
5. 2M H_2SO_4; 0.2 M Fe^{+++}; 1 M H_3PO_4

[1] Figures in brackets indicate the literature references at the end of this paper.

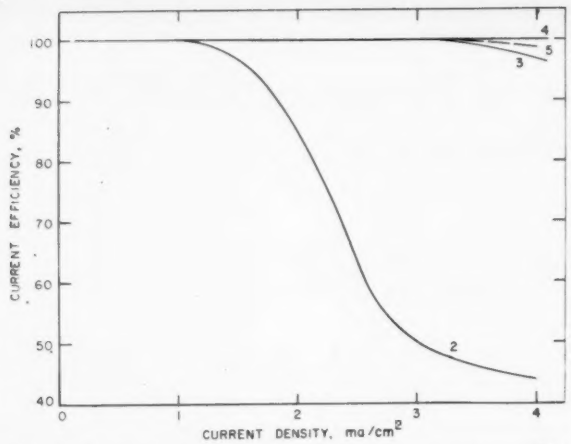

FIGURE 2. *Current density, efficiency diagram for electrogeneration of ferrous ion at platinum cathode.*

2. 2M H_2SO_4; 0.01 M Fe^{+++}
3. 2M H_2SO_4; 0.03 M Fe^{+++}
4. 2M H_2SO_4; 0.2 M Fe^{+++}
5. 2M H_2SO_4; 0.2 M Fe^{+++}; 1 M H_3PO_4

or 0.85 corresponding to a current efficiency of 85 percent. For the same current density, the projections of points B and A from curves 3 and 4, respectively, on curve 1 indicate no current due to reduction of the supporting electrolyte and a resulting current efficiency of reduction of ferric ion of essentially 100 percent.

At a current density of 4 ma/cm², solution 3 was reduced at a potential of about −0.24 v (point F) and this potential was obtained at a current density of 0.05 ma/cm² for the supporting electrolyte alone (point G). The efficiency of reduction of solution 3 under this condition would be (4.0−0.05)/4.0=0.99. The projection of point E indicates a negligible current due to reduction of the supporting electrolyte and 100 percent efficiency for reduction of solution 4.

From calculations like those described above, the curves shown in figure 2 were plotted. It is evident that solutions more concentrated than 0.01 *M* with respect to ferric ion in a supporting electrolyte of 2 *M* sulfuric acid can be reduced with a current efficiency of 100 percent, provided the current density is less than 1.2 ma/cm².

It is also indicated in figure 1 that the presence of phosphoric acid is not essential for theoretically efficient reduction of ferric ion to ferrous ion, as has been reported by previous investigation [3]. In fact, it is evident that presence of phosphoric acid lowers the limiting current-density for efficient reduction of ferric ion.

The conditions selected for this work consisted in the pregeneration of ferrous ion from a solution 0.4 *M* with respect to ferric ion, in a supporting electrolyte of 2 *M* sulfuric acid, at current densities never exceeding 0.6 ma/cm². The pregeneration technique, described later, reduced the ferric ion concentration to 0.3 *M* but this was well above the limit for efficient generation of ferrous ion.

The end points of these titrations were determined amperometrically using a polarized platinum indicator anode and a saturated calomel electrode as the nonpolarizable reference cathode. Using this electrode system the current-voltage curves shown in figure 3 were obtained. An applied-potential of +0.85 v is midway on the diffusion-current plateau for the reaction $Fe^{++} \rightarrow Fe^{+++} + e^-$. In actuality, this plateau is not completely flat; however, this voltage corresponds to a region where the indicator current is the least dependent on the applied voltage.

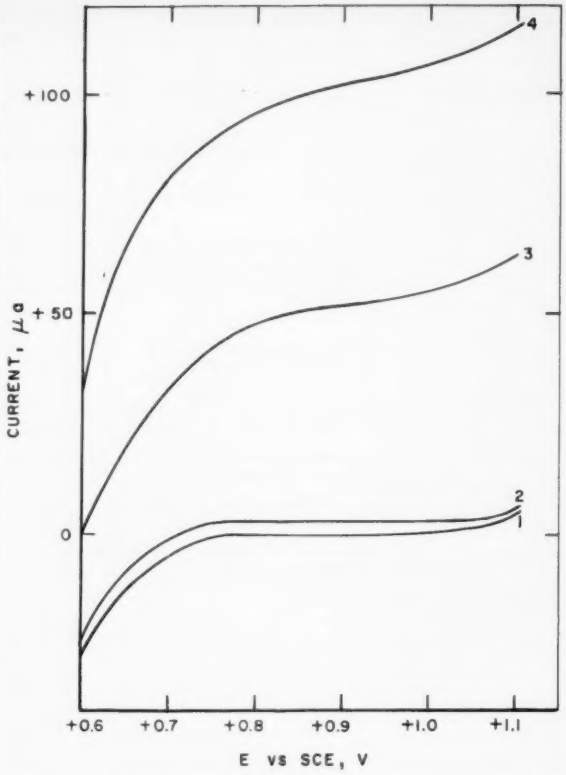

FIGURE 3. *Current, potential curves for oxidation of ferrous ion at a polarized platinum electrode.*

1. 2*M* H_2SO_4; 0.5 *M* Fe^{+++}; 40 μeq $K_2Cr_2O_7$
2. 2*M* H_2SO_4; 0.5 *M* Fe^{+++}; 40 μeq Cr^{+++}; 0.5 μeq Fe^{++}
3. 2*M* H_2SO_4; 0.5 *M* Fe^{+++}; 40 μeq Cr^{+++}; 10 μeq Fe^{++}
4. 2*M* H_2SO_4; 0.5 *M* Fe^{+++}; 40 μeq Cr^{+++}; 20 μeq Fe^{++}

From studies of Anson [8, 9], it is evident that the oxide film which is formed on platinum affects the behavior of the ferrous-ferric couple at the electrode. According to him, the reduction of such a film is easily accomplished by ferrous ion in a sulfuric acid medium. If such a film were not removed prior to generation of ferrous ion, it would cause positive errors in the final analysis of oxidant, dichromate in the present case. Taking precautions to avoid such interferences, the electrodes (both the indicator anode and the generator cathode) were pretreated by immersion for 10 min in a chromic acid solution with subsequent rinsing, followed by a 10 min immersion in 0.1 *M* ferrous ammonium sulfate solution in 2 *M* H_2SO_4. Thus the electrode surfaces were freshly "reactivated" prior to each titration.

All calculations were based on the 1961 C^{12} atomic weight scale [10]. From it the molecular weight of $K_2Cr_2O_7$, which was used, was calculated to be 294.191$_8$.

The value of the faraday constant which was used in the calculations was 96,487.2 coul/g-equiv (based on the determination of D. N. Craig et al. [11] and corrected to the C^{12} atomic weight scale).

3. Apparatus and Procedure

3.1. Apparatus

The titration cell used in this work was similar to the one described in a previous communication [2]. The anode and cathode compartments are separated by a connecting tube containing a series of porous glass frits to provide two intermediate sections. Tubes sealed to the tops of these sections permit application of suction or pressure to fill or empty the compartments. A silicic acid gel plug, prepared by gelation of sodium silicate solution with sulfuric acid, was formed on the fine-porosity disk of the anode compartment to eliminate flow of electrolyte. The plug remained for long periods of time without degeneration provided it was kept wet with supporting electrolyte.

A piece of corrugated platinum foil (5 cm×16 cm) served as the generator cathode. The anode was constructed from sheet lead (12 cm×10 cm×0.2 cm) which was contoured to fit the anode compartment of the cell.

The electrical circuit was the same as used previously [1, 2]. The current was adjusted manually to maintain the IR drop across a standard resistor constant and equal to the voltage of a saturated standard cell. Because the dummy resistance only approximated that of the electrolytic cell, a momentary initial imbalance was invariably observed. Such imbalances were small and corrected quickly so that they could not affect the titrations by more than 0.00001 percent.

The saturated standard cell and the standard resistor used in this work were calibrated by the appropriate sections of the Bureau. Although the resistor was placed in a thermostated oil-bath there was always a slight temperature rise of the resistor due to heat dissipation. The correction for this temperature change was applied using the mean value of the resistor for a given titration and the temperature coefficient for manganin.

The time was measured by means of a 10 kc-quartz crystal controlled time interval meter (TIM) whose calibration was checked with respect to standard frequency signals of WWV; the calibration was found to be accurate to at least 1 ppm.

Near the equivalence point of the titration, it was more convenient to pass current increment-wise using a commercially-available constant-current coulometric source. The current and timing accuracy of this apparatus were calibrated and the *It* product was found to be accurate to ±0.005 percent. Since the fraction of the total titration performed with this instrument was of the order of 0.0005, the errors encountered as a result of the use of this equipment were negligible.

The amperometric indicator system consisted of a platinum foil electrode (1 cm² in area) and a saturated calomel electrode with a 3-percent agar-agar gel in 0.1 *N* potassium chloride in a salt bridge. A recording polarograph was used as the source of applied emf (0.85 v) between these two electrodes and also as the microammeter for measuring or recording the indicator current.

All weighings were done on a 20 g capacity microbalance of the single-arm, constant-load type and were precise to ±0.003 mg. All weighings were corrected for air buoyancy.

3.2. Procedure

The material used in this work was potassium dichromate NBS standard sample 136b. Visual examination revealed an occasional dark-colored crystal which may or may not contribute a certain amount of inhomogeneity to the sample. The material was dried at 110 °C for 24 hr and cooled in a desiccator for a period of about 4 hr before weighing.

One-half gram samples contained in a platinum boat were weighed by the method of substitution using a calibrated 500 mg tantalum weight. Sample weights agreed with the nominal value and with each other within 3 mg. The difference between the mass of the sample and the calibrated mass was determined on the optical scale of the balance. The weighed samples were transferred from the boat into 30-ml weighing bottles and stored in a desiccator until used.

The weighings were done in sets, each representing a number of samples weighed on the same day. Measurements were made of air temperature, barometric pressure, and relative humidity during the weighings and the appropriate corrections for air bouyancy were applied.

The supporting electrolyte was prepared in advance and was 0.4 *M* with respect to ferric ion and 2 *M* with respect to sulfuric acid. Ferric ammonium sulfate, reagent grade salt, or electrolytically oxidized ferrous ammonium sulfate served as the source of the ferric ion.

The anode and cathode compartments were filled with 100 ml of 2 *M* sulfuric acid and 120 ml of supporting electrolyte, respectively. At this point, about 1 ml of 0.005 *N* potassium dichromate was delivered into the cathode compartment to remove traces of ferrous ion and to facilitate the pretitration step described later.

Dissolved air was removed from the catholyte by purging with nitrogen gas that was introduced through the coarse frit of the side compartment adjacent to the cathode compartment. The nitrogen used for this purpose was pretreated by passing it through a heated copper-filled tube to remove oxygen and successively through towers containing acidified potassium permanganate, ferrous ammonium sulfate, and supporting electrolyte, respectively.

After purging, the catholyte was permitted to flow into the intermediate compartments to the

extent that it would just cover the bottom of each compartment, thus establishing electrolytic contact between the cathode and anode compartments. This was accomplished by application of suction to each intermediate compartment.

The catholyte was then pretitrated by passage of increments of current equivalent to 0.200 μeq, using the 0.643 ma current range of the coulometric power supply. At the conclusion of each increment, the indicator current was observed. This was small and essentially constant up to the equivalence point, exhibited a curvature in the vicinity of the equivalence point, and became a linear function of the ferrous ion concentration with slope of about 5.0 μa/μeq beyond the equivalence point. This linear portion was extrapolated graphically and its intersection with the zero-current line was taken as the end point.

After completion of the pretitration, the intermediate compartments were rinsed by repeated emptying and filling with catholyte by applying suction or nitrogen pressure as required. The walls of the cathode compartment and its cover were rinsed by withdrawing catholyte using a syringe in which a glass tip replaced the hypodermic needle. The tip was bent so that the expelled catholyte would wash down all parts of the cathode chamber. The final reading of the indicator current was then taken from which the amount of over-titration of the pretitration step was determined.

The intermediate compartments of the cell were then filled with catholyte and ferrous ion was electrogenerated at constant current using the high precision circuit and the TIM. The amount of ferrous ion generated was a predetermined quantity sufficient to reduce about 99.95 percent of the dichromate in a given sample.

After the generation of this major portion of ferrous ion, a dry funnel was inserted into the cover of the cathode compartment through an auxiliary opening which was stoppered with a piece of glass rod during the time of generation of ferrous ion. The stem of this funnel reached slightly below the level of the liquid in the cell. The weighing bottle containing the weighed sample was inverted into the funnel and lightly tapped, so that all visible crystals of the dichromate were delivered into the cell. A complete dissolution of sample took place in about 5 min after delivery into catholyte. Following dissolution of sample the intermediate compartments were successively emptied by applying nitrogen pressure until only the bottoms of these compartments were wetted enough to make the electrical contact between the anolyte and the catholyte. The compartment which is adjacent to the cathode compartment was rinsed several more times, by permitting the catholyte to flow into it, and by forcing the same out with nitrogen pressure. This was done because a perceptible amount of ferrous ion diffused into that compartment during the course of its generation. Thus, it required more than one rinse to remove all ferrous ion which was entrapped in the glass frits. The second compartment contained an imperceptible amount of ferrrous ion.

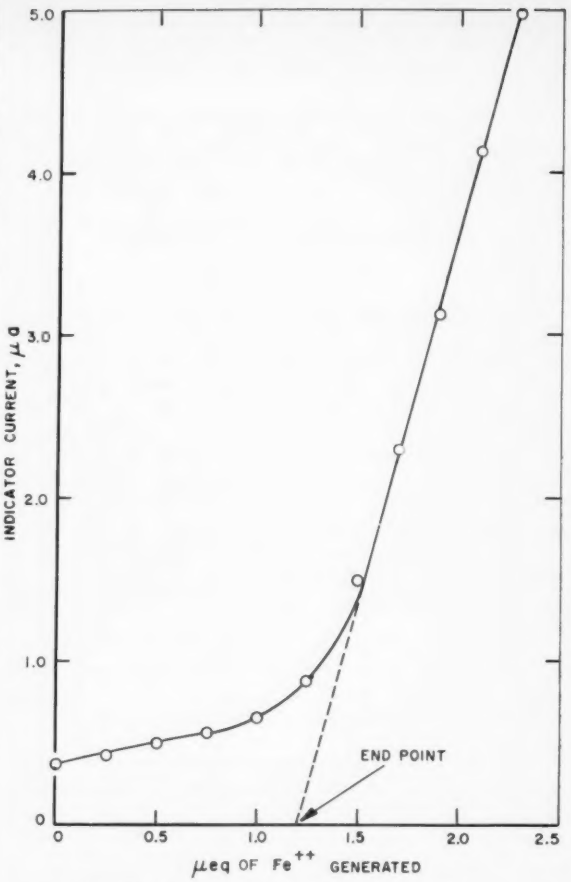

FIGURE 4. *Typical end-point determination.*

At this point the titration was continued incrementwise, using the coulometric current source as in the case of pretitration. When the first rise of the indicator current was observed, the cell walls, the cell cover, and the intermediate compartments were rinsed as already described, and the weighing bottle which originally contained the sample and the delivery funnel were rinsed with catholyte withdrawn from the cell by the syringe. This procedure was repeated after each succeeding increment The extrapolation of the indicator current line, where it becomes a straight line function of the ferrous ion concentration was again taken as the end point at the point where it intersects the zero current line. A typical end-point determination is shown in figure 4.

It is obvious that the amount of ferrous ion equivalent to the dichromate is the amount generated to the end point plus the excess which was generated in pretitration.

4. Design of Experiments

In the initial stages of this investigation it became evident that there was a definite effect associated with the history of the supporting electrolyte. Re-

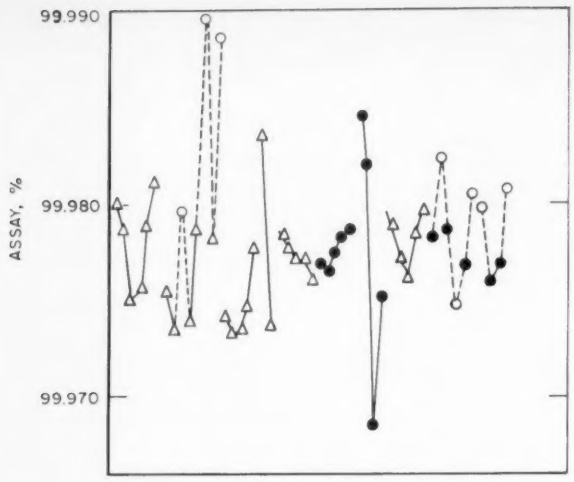

FIGURE 5. *The sequence of experiments.*

△, previously used electrolyte
○, untreated electrolyte
●, electrolyte, treated by alternate reduction and oxidation

sults obtained with a fresh electrolyte appeared to be slightly yet appreciably higher than when a sample was added to an electrolyte previously used for an analysis. To verify this effect and also to detect any possible systematic errors varying with time, the analytical program outlined in the following was adopted.

Samples were weighed in sets consisting of two to six members, all weighings being made within a period of an hour or two. These samples were titrated sequentially using pretreated electrolyte except that nine samples were withdrawn in a random manner for analysis in untreated electrolyte.

The pretreated electrolyte consisted of solution that had been previously used in a coulometric titration of dichromate, or one in which a number of repeated reductions and oxidations had been performed. This latter procedure was accomplished by reduction of the supporting electrolyte (in the same electrolysis cell) for about 500 sec with a 100 ma current followed by reversal of the current. This procedure was repeated several times. The platinum electrode which was used for this pretreatment was "reactivated" as already described between each current reversal. After the final oxidation there was a small amount of ferrous ion present that had not undergone electrolytic oxidation. This residual amount was oxidized by addition of dilute solution of dichromate until the diffusion current of the ferrous ion reached a very low value (e.g., 0.5 μa).

The sequence of experiments is shown in figure 5.

5. Results

The results for titrations of ten sets of samples in pretreated supporting electrolyte are given in columns 2 to 11 of table 1. Set XI is composed of a number of samples taken from the sets as indicated by the vacant spots labeled "c" in the table.

The average value for the assay of this material using pretreated electrolyte is 99.977_2 percent with the standard deviation of all measurements being 0.002_9 percent. The significantly higher value of 99.982 percent was obtained from samples titrated in the untreated supporting electrolyte. These samples also showed a higher standard deviation of 0.0049 percent.

The results of table 1 are plotted with respect to analytical sequence in figures 5 and 6. The results for a given series are interconnected. Dashed lines are drawn to show the time relationship for samples determined in the untreated electrolyte and emphasize that their results were not used in computing the average line nor the standard deviation limits. No significant trends with respect to time both with respect to sets and for the entire sequence are evident.

The difference between results with pretreated and untreated supporting electrolyte is obvious. Undoubtedly, some reducible impurity was present in the supporting electrolyte the kinetics of reduction of which is slow, so that it was not completely removed by the pretitration procedure. On the other hand, a longer electrolytic pretreatment and/or higher concentrations of ferrous ion had the beneficial effect in removing this impurity.

It is recommended that for titrations of potassium dichromate in which high accuracy is a serious consideration, the supporting electrolyte should be

TABLE I. *Summary of results*

Sample number	Assay										
	Set I [a]	Set II [a]	Set III [a]	Set IV [a]	Set V [a]	Set VI [a]	Set VII [a]	Set VIII [a]	Set IX [a]	Set X [a]	Set XI [b]
1	99.980_0	99.975_5	99.974_2	99.983_5	99.978_5	99.976_9	99.984_6	99.978_9	(c)	(c)	99.979_7
2	99.978_8	99.973_6	99.973_4	99.973_7	99.977_7	99.976_6	99.982_0	99.977_1	99.978_3	99.976_0	99.989_6
3	99.975_1	(c)	99.973_5	----------	99.977_2	99.977_5	99.968_5	99.976_4	(c)	99.976_9	99.988_6
4	99.975_7	99.973_9	99.974_7	----------	99.977_1	99.978_4	99.975_2	99.978_5	99.978_7	(c)	[d]100.000_1
5	99.978_9	99.978_7	99.977_8	----------	99.976_2	99.978_7	----------	99.979_6	(c)	----------	99.982_8
6	99.981_2	(c)	----------	----------	----------	----------	----------	----------	99.976_9	----------	99.974_8
7	----------	99.978_3	----------	----------	----------	----------	----------	----------	(c)	----------	99.980_5
8	----------	(c)	----------	----------	----------	----------	----------	----------	----------	----------	99.979_9
9	----------	----------	----------	----------	----------	----------	----------	----------	----------	----------	99.980_9
Average	99.978_3	99.976_9	99.974_7	99.978_6	99.977_3	99.977_6	99.977_6	99.978_1	99.978_0	99.976_5	99.982_1
Standard deviation for each set	0.002_4	0.002_4	0.001_8	0.004_9	0.000_9	0.000_9	0.006_0	0.001_3	0.001_0	0.000_5	0.004_9
Overall average	99.977_2, $\sigma=0.002_9$										

[a] Pretreated supporting electrolyte.
[b] Untreated supporting electrolyte.
[c] Samples taken to be titrated in Set XI.
[d] Not included in the average.

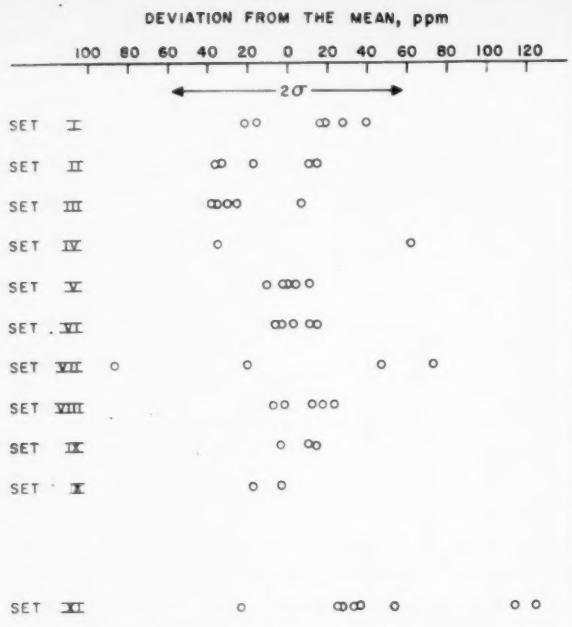

FIGURE 6. *Precision of analysis.*

Set number XI is separated as it was not included into calculation of the mean.

pretreated either by repeated reduction and oxidation, or by titrating a sizable sample in the electrolyte and disregarding the first result.

The precision of the method is high, in that a standard deviation of only 0.002_9 percent, or 29 ppm, was obtained. The accuracy of the method is more difficult to evaluate in that pure reference materials are not available for calibration purposes.

The assay value, 99.977_2 percent, is in good agreement with the certified oxidizing power, 99.98 percent, for standard sample 136b, which is given in the provisional certificate of the National Bureau of Standards dated June 30, 1961.

This certified value is based upon comparison with predecessor samples 136 and 136a, the former having been standardized with respect to pure iron and arsenious oxide. The present sample 136b was also standardized with respect to uranium metal of high purity and the provisionally certified value of 99.98 ± 0.01 percent represents the reliability of the value based on both analytical uncertainty and the agreement of cross-checks in which such factors as uncertainties in atomic weights are involved.

In view of the agreement of the coulometric results with other analytical data, and the fact that the conditions were such that theoretical current efficiency should have been realized, it is concluded that the accuracy of the results is consistent with the analytical uncertainty.

6. Discussion

This investigation emphasizes the high precision and accuracy that can be attained in constant-current coulometry. In common with the acidimetric and argentimetric titrations already reported, the determination of oxidants to a few parts in one-hundred thousand has been accomplished and uncertainties of only a few parts in a million are a definite possibility.

Coulometric methods are absolute methods in that the results depend directly upon the reliability of measured quantities. This is in contrast to many analytical methods which are comparative in principle, in that an unknown is compared with a material of known composition.

The factors affecting the precision and accuracy of coulometric titrations have been discussed in previous papers [1, 2]. In the present work, much effort was expended to minimize all errors to produce results of high reliability. An attempt has been made to evaluate the precision of all measurements involved. These are summarized in the following:

Weighings were precise to about 3 μg, which amounts to 0.0006 percent in the case of 0.5 g samples and uncertainties in the buoyancy corrections did not exceed 0.0003 percent. Manual control of the current was maintained within a 0.5 cm galvanometer deflection which would amount to 0.00015 percent. Timing errors are not believed to exceed 0.0001 percent for the 10,000—second period of electrolysis. Uncertainties in the current due to temperature fluctuation of the standard resistor were no more than 0.00007 percent, while endpoint uncertainties may have amounted to about 0.02 μeq which represents 0.0002 percent in a 10-meq sample. On the basis of these estimates an overall precision of 0.0008 percent should have been attained, which is about one-third of the standard deviation of the results.

There are of course other sources of error, magnitudes of which are difficult to estimate. Such indeterminate errors include mechanical losses due to transfer of sample, spray losses, and residual amounts of oxygen in the cell. Errors due to inhomogeneity of sample could be considerable since small samples (0.5 g) of incompletely purified material (99.98 percent purity) were used. Efforts were made to minimize some of the indeterminate errors by the washing procedure already described and by pretreatment of the electrolyte.

The stability of the generating current was greatly improved by the pregeneration technique, and this was the reason for its adoption. In preliminary work, it was found that the current became quite unsteady when about 30 percent of a 10 meq sample of dichromate which had been added directly to the supporting electrolyte was reduced. Potential measurements showed that the cathode potential shifted abruptly at this point from that of the dichromate-chromic couple to that of the ferric-ferrous couple. Undoubtedly, due to concentration polarization effect, the primary electrode reaction changed from the reduction of dichromate to reduction of ferric ion, well in advance of the stoichiometric end point. The transition was too rapid to adjust for by manual means and consequently large uncertainties were introduced. The pregeneration of

the ferrous ion as already described eliminates this uncertainty.

Another improvement in precision of the end-point determination resulted from the pretitration technique. Some uncertainty was introduced by small but measurable variations in the current prior to the complete reduction of dichromate (residual current). However, by alternate reduction and oxidation in the region of the end point, it became evident that extrapolations of the linear residual-current curve to zero current gave reliable values for a sample added to one previously titrated, and the pretitration technique described earlier was adopted. Also, it was hoped that this procedure would eliminate blank corrections, but it was soon discovered that a pretreatment of the supporting electrolyte was required as well.

7. Conclusions

This investigation has shown that potassium dichromate can be titrated coulometrically with precision and accuracy which is equal to or exceeds that obtainable by the most careful conventional methods of chemical analysis. The method has further advantage in that the reagent is generated in situ which eliminates some of the cumbersome techniques of the conventional chemical analysis. The amount of this generated reagent is measured in terms of physical quantities—current, time, and the faraday constant, all of which are more precisely and accurately measurable than the certification of conventional standard reference materials.

It has also conclusively shown that a pretreatment technique is required for supporting electrolyte if the results of highest obtainable degree of accuracy and precision are desired.

The authors are grateful to J. Cameron of the Statistical Engineering Section for help in the statistical analysis of the data.

8. References

[1] J. K. Taylor and S. W. Smith, J. Research NBS **63A** (Phys. and Chem.) No. 2, 153 (1959).
[2] G. Marinenko and J. K. Taylor, J. Research NBS **67A** (Phys. and Chem.) No. 1, 31 (1963).
[3] W. D. Cooke and N. H. Furman, Anal. Chem. **22,** No. 7, 896 (1950).
[4] W. D. Shults II, P. F. Thomason, and M. T. Kelley, Anal. Chem. **27,** No. 11, 1750 (1955).
[5] K. Rawley and E. H. Swift, Anal. Chem. **26,** No. 2, 373 (1954).
[6] J. J. Lingane and F. C. Anson, Anal. Chim. Acta **16,** 165 (1957).
[7] J. J. Lingane and J. H. Kennady, Anal. Chim. Acta **15,** 465 (1956).
[8] F. C. Anson, Anal. Chem. **33,** No. 7, 934 (1961).
[9] F. C. Anson, Anal. Chem. **33,** No. 7, 939 (1961).
[10] International Union of Pure and Applied Chemistry, Preliminary Report of the Commission on Atomic Weights.
[11] D. N. Craig, J. I. Hoffman, C. A. Law, and W. J. Hamer, J. Research NBS **64A** (Phys. and Chem.) No. 5, 381 (1960).

(Paper 67A5–234)

691-886—63——5

JOURNAL OF RESEARCH of the National Bureau of Standards—A. Physics and Chemistry
Vol. 67A, No. 5, September-October 1963

Resolution Limits of Analyzers and Oscillatory Systems

Edith L. R. Corliss

(June 5, 1963)

This paper considers the resolution limits of those analyzers and oscillatory systems whose performance may be represented by a second-order differential equation. The "signal uncertainty" product $\Delta f \cdot \Delta t$ is shown to be controlled by the ability of a system to indicate changes in energy content. The discussion refers the functioning of the system to a signal space whose coordinates are energy, frequency, and time. In this signal space, the product of the resolution limits, $U = (\Delta E/E_0)\ (\Delta f/f_0)\ (\Delta t/T_0)$ is the volume of a region within which no change of state in the system may be observed. Whereas the area element $\Delta f \cdot \Delta t$ is freely deformable, no operations upon either Δf or Δt can further the reduction of the energy resolution limit. Thus U is irreducibly fixed by the limiting value of $\Delta E/E_0$. By considering the effects of noise upon $\Delta E/E_0$, and thus upon U, the paper demonstrates the rise of statistical features as signal-to-noise ratios decrease.

Functional relationships derived from $\Delta E/E_0$ and U are tabulated. These equations facilitate computation of the limits of observable changes of state in a system, and they provide guidance for the design of experiments to apportion the uncertainties of measurement of transient phenomena as advantageously as possible. A reference bibliography and appendices giving somewhat detailed proofs are included.

The basis of this paper is the consideration that the indication of most instruments used in measurement represents either the storage of energy or the flow of power. The least changes that the instruments can indicate, therefore, are controlled by the smallest discernible change in energy storage or power flow.

The subject of the resolution limits of measuring instruments in terms of the least amounts of frequency change and the least time interval in which a change may be detected have been treated by several authors, among whom one may cite as examples Gabor, Kharkevich, and Brillouin—and, while this paper was being revised, Pimonow.[1] The present author has also discussed this relationship for scanning analyzers, and indicated that there were circumstances in which limitations were introduced by the presence of a least discernible increment of power or energy.[2] These papers (ref. 2) are quoted, in addition to the prior work, by Pimonow.

Gabor pointed out, by analogy to quantum theory, that there was a "quantum" of information that could be described by the product of differentials representing the least discriminable increment of frequency that could be observed in an increment of time. This relation arose from the application of the Fourier transform to relate an increment of time to its corresponding increment in the frequency domain. The product

$$\Delta f \cdot \Delta t \approx 1$$

was defined by Gabor as the "Logon." The fact that, as he says, the product is "of the order of unity" is a consequence of the particular normalization he used in computing the Fourier transform for Gaussian pulses. A similar relation was presented by Brillouin, but as he computed Δt in terms of the half-powers of brief, symmetrical pulses, he found a somewhat different normalization factor, and obtained

$$\Delta f \cdot \Delta t = \frac{1}{4\pi}.$$

Kharkevich adopted a somewhat more general expression for this equation, also in terms of a normalized Fourier transform, by first writing

$$\Delta f \cdot \Delta t = A$$

and computing A for pulses of various forms. He remarked that A might differ if other criteria were chosen, but related A only to the form of the signal. Further, he pointed out that A is independent of the damping of the system.

The studies by Gabor, Kharkevich, and Brillouin were all carried out for essentially noiseless systems. This paper, on the other hand, does not normalize for unit energy, but considers the energy storage and dissipation in systems whose performance may be described by a linear differential equation of the second order. Thus, by dealing with the energy stored as well as with the time and frequency we are able to study the response of a system to signals other than variously shaped pulses of unit energy, and to signals in noise as well as to noiseless systems.

We can also consider, in this way, the case which has been omitted from the previous work: the response of the system which may in itself have a "least count"[3] or inherent internal noise.

[1] D. Gabor, Theory of communication, J. Inst., Elec. Eng. **93**, Part III (1946), 429–457; A. A. Kharkevich, Spectra and Analysis, Translated and published by Consultants Bureau, New York (1960); L. Brillouin, Science and Information Theory, 2d edition, published by the Academic Press, New York (1962); L. Pimonow, Vibrations en Régime Transitoire, Dunod, Paris (1962). (This book has a very extensive bibliography.)

[2] Limitations on rapid signal analysis, J. Wash. Acad. Sci. **45**, 359–360 (1955); Transients in signal analysis, J. Wash. Acad. Sci. **46**, 305–307 (1956); Uniform transient error, J. Research NBS **61**, 25–30 (1958) RP2879.

[3] The term "least count" is chosen here by analogy to a term describing the limitation in a metering system: the least increment that can be read on the meter.

We introduce the means for taking into account the presence of noise with a signal, internal noise in an analyzer, or the least discernible indication of the analyzer (which may be a step limitation—such as a digital step, or a reading limit) by discussing the limits of the analyzer's performance as being fixed by the least change in energy storage, ΔE, that can be resolved under the circumstances of analysis. Several conditons may combine to fix the value of ΔE. For example, an analyzer having appreciable self-noise may be used to detect a signal in noise. As a rule, the internal and external noise sources in that case would be incoherent, and the sum of the noise energies stored in the analyzer from those sources would fix the value of ΔE.

The system for which this discussion is carried out is a system whose working may be described by a linear differential equation of the second order. This behavior is common to many physical systems occurring in nature, and to many instruments used to observe natural phenomena. All of these systems share the same properties, because they are properties inherent in the differential equation that describes them. By virtue of the second-order term, they may be seen to be capable of storing oscillatory energy reversibly. They will respond with a sinusoidal output after excitation by shock or noise. Under sinusoidal excitation, they will respond selectively to excitation of various frequencies.

Systems to be discussed in this paper are those in which the storage of energy occurs in the coordinates describing the system: these systems are described by a second-order differential equation with constant coefficients; i.e., the system parameters are not affected by the energy storage process. By invoking the Boltzmann-Ehrenfest adiabatic principle,[4] it is also possible to apply many of these equations to systems in which energy is stored by a change of parameters. However, this matter has not been investigated in detail.

Although most of the systems to which the second-order differential equation is applicable take part in time-varying phenomena, there is nothing inherent that restricts the equation to functions of time. Certain spatial distributions also may be described by the equation—such as the magnetization on magnetic tape, some types of optical images, and some diffraction effects. Thus, although this paper will deal with application of the equation to time-varying phenomena, its conclusions are also applicable, with a judicious choice of variables, to spatial distributions.

For the sake of a coherent structure upon which to base this paper, we choose a mechanical system of inertia, M, dissipation (proportional to velocity) D, and coefficient of restitution, k. This system has a single degree of freedom, along the coordinate x, and its force-free behavior is given by solutions of the homogeneous equation:

$$M\ddot{x}+D\dot{x}+kx=0.$$

[4] M. Greenspan, Simple derivation of the Boltzmann-Ehrenfest adiabatic principle, J. Acoust. Soc. Am. **27**, 34-35 (1955). The adiabatic principle states that for a system excited by a change in parameters, the ratio of energy content to resonant frequency is a constant.

When energy is stored in the system, it is dissipated at a mean rate which bears a constant relationship to the amount of energy stored. This constant is a function of the parameters of the system. In terms of dissipation, the constant is frequently expressed by the relative damping, γ, the ratio of the damping of the system to the critical damping for no oscillation. A reciprocal quantity, the "figure of merit," Q, is commonly used in communication problems. These two constants are related through the equation:

$$\gamma=\frac{1}{2Q}.$$

Because we are more concerned here with storage than with dissipation, the quantity Q will be used in the discussion.

The conventional definition for Q applies when the system is driven at its resonance frequency; at other frequencies the ratio of the storage of energy to the rate of dissipation depends upon the driving frequency. When the system is free of excitation, the conventional definition of Q again applies. This value of Q will be denoted as Q_0, to distinguish it from the more general definition of Q to be applied in the appendix. Defining as the natural frequency of the system the quantity f_0, which is the natural frequency of the system in the absence of damping,

$$f_0=\frac{1}{2\pi}\sqrt{\frac{k}{M}}$$

and

$$Q_0=\frac{\text{Peak energy stored at the natural frequency}}{\text{Energy dissipated per cycle at the natural period}}$$

In terms of the parameters of the system, this definition of Q_0 is equivalent to the ratio:

$$Q_0=\frac{2\pi f_0 M}{D}=\frac{k}{2\pi f_0 D}=\frac{\sqrt{kM}}{D}.$$

The differential equations for the transient and driven response of the system can be expressed in terms of Q_0, D, and f_0. For the force-free equation:

$$\frac{\ddot{x}}{2\pi f_0}+\frac{\dot{x}}{Q_0}+2\pi f_0 x=0$$

and, for the driven response of the system to a sinusoidal force of amplitude A and frequency f:

$$\frac{\ddot{x}}{2\pi f_0}+\frac{\dot{x}}{Q_0}+2\pi f_0 x=\frac{A}{Q_0 D}\,e^{j2\pi ft}.$$

Letting the ratio of the driving frequency to the natural undamped frequency be represented by

$$\phi=f/f_0$$

we can write down the phase relation between the driving force and the resulting motion. The phase

angle, θ, when the steady-state condition has been attained is given by

$$\theta=\tan^{-1}\frac{\phi}{Q_0(1-\phi^2)}$$

and the energy stored in the steady-state condition is given by:

$$E_s=\frac{A^2}{2D}\cdot\frac{Q_0}{2\pi f_0}\cdot\frac{1}{Q_0^2(1-\phi^2)^2+\phi^2}.$$

The application of the Fourier transform can be considered to be tantamount to referring the behavior of the system to one or the other of two mutually perpendicular planes: The steady-state condition is described by the representation of the state of the system in the energy versus frequency plane and it of necessity deals with the steady state because the variable, time, is not involved. The transient behavior of the system is represented in the energy versus time plane. It is easier to understand that this is orthogonal to the frequency representation if we omit the normalization often used, of choosing the unit of time in terms of the natural period of the system. Nevertheless, it is more convenient to express the behavior of a system in terms relative to its natural parameters, and for the sake of simplicity of equations, much of the discussion will be related to the natural properties of the system.

Three properties serve to specify the behavior of an analyzer described by a second-order differential equation: its undamped natural frequency, f_0, its figure of merit, Q_0, and its "least count," ΔE, the least energy change that can be resolved by the system. The changes in energy content of the system may be thought of as taking place within the signal space bounded by the energy-time and energy-frequency planes, and the representation of the behavior of the system as a function of time or of frequency may be considered as projections upon the principal planes. Since the actual use of the system as an analyzer is never wholly steady-state or completely broadband, the actual process of analysis may be considered as taking place in some plane within the signal space bounded by the principal planes. Depending upon the information sought, the plane of the analyzer will be close to one or the other of the principal planes.

Ordinarily, an analyzer indicates a running time average over the energy, E_s, stored in it. For steady-state signals the indication becomes proportional to the input power; for signals of very brief duration the analyzer responds ballistically and thus gives an indirect indication of energy. The limit of resolution is fixed by the least change in energy storage, ΔE, that can be resolved under the circumstances of analysis. In this discussion we shall be dealing with incremental ratios. As the differential will always be considered jointly with the total energy stored over the same time interval, it will be possible in general to discuss ratios of incremental power, ΔW, to input power, W_0, or incremental energy, ΔE, to energy stored, E_s, interchangeably.

As a function of time, the building up and decay of the energy stored within the system are exponential processes. Therefore it proves convenient to describe the behavior of the system in terms of an exponential variable. Thus, to express the changes in energy storage, we choose an exponential coefficient, α. The energy resolution limit, $\Delta E/E_0$, may be expressed in terms of α through the following definition: If the initial amount of energy stored in the analyzer is E_0, and the minimum change of energy that can be discerned is ΔE, then in terms of the exponential variable α the equivalent statement is that the energy content must decrease to an amount $(e^{-\alpha})$ times its original value for the change to be at least equal to the minimum change discernible. Expressed as an equation, this limit is given by $\Delta E=(1-e^{-\alpha})E_0$ for energy, and in the many cases in which we are dealing with energy flow through the system, alternatively as $\Delta W=(1-e^{-\alpha})W_0$ for power. From the definition of α in terms of ΔE and E_0, it is evident that:

$$\alpha=-ln\left(1-\frac{\Delta E}{E_0}\right).$$

However, it is not along the time axis alone that α proves such a convenient function. Because of the close relation between exponential and angle functions, it also yields simple equations for the behavior of the system as a function of frequency. For the foregoing reasons, we shall describe the manner in which the independent variable, the energy increment ΔE, influences the resolution limits in frequency and time in terms of the variable α, and we will then return to consideration of what the equations describing these resolution limits mean in terms of ΔE. We will also discuss special types of noise conditions that may give rise to the irreducible increment that ΔE represents.

The conditions under which α sets the resolution limit along the time axis are derived from considering the system to contain an amount of energy E_0 at time $t=0$, and at that instant and for some time subsequent to that, to be free of any driving force. The resolution limit along the time axis is fixed by the least time interval, Δt, during which the system is capable of changing its energy storage by the factor, $e^{-\alpha}$. This corresponds to dissipating at least the discernible energy increment, ΔE, during the time Δt. The resolution limit stated in terms of the natural period of the system, T_0, is thus given by $\Delta t/T_0$.

When a system of this sort is used as an analyzer, the time interval over which the observation takes place must be of sufficient length for some change to be indicated. Thus the observation interval, $\Delta\tau$, must equal or exceed the least time interval Δt. (In the previous papers cited in reference 2, the observation interval $\Delta\tau$ was used in place of the least time increment Δt. Use of the least time increment converts several previously found inequalities to equations.)

It is a very close approximation (see appendix 1) to consider only the exponential factor in the decay of energy in the system. The oscillatory terms

arising from the sinusoidal nature of the dissipation process are always relatively minor. Thus, regardless of the precise initial conditions,

$$\left.\frac{E}{E_0}\right|_{(t=\Delta t)} = e^{-\alpha} \approx \exp\left(-\frac{2\pi}{Q_0}\cdot\frac{\Delta t}{T_0}\right)$$

and, therefore, the resolution limit along the time axis, expressed in terms of the natural undamped period of the system is

$$\frac{\Delta t}{T_0} \approx \frac{\alpha Q_0}{2\pi}.$$

From this equation one can see that the ratio of α to Δt is twice the real coordinate of the poles of the system on a Nyquist diagram.

The system is selective with respect to the sinusoidal frequency of the driving force which acts as a source for the energy it stores. This makes it suitable for the detection of sinusoidal frequencies falling within its range of response, or a group of similar systems with different f_0's may be used in the analysis of the components of complex signals. For this purpose, the observation takes place in a plane approximating the energy-frequency plane. Along the frequency axis, one may speak of a frequency resolution limit in this sense: If one knows the natural frequency f_0 to which an analyzer is tuned, then a maximum indication of energy storage for a steady-state sinusoidal signal corresponds to a signal in the vicinity of f_0. Until the energy storage has changed by an amount in excess of ΔE or, when expressed as a relative proportion, a factor in excess of $\Delta E/E_0$, the departure from maximum indication is not observable. The change in frequency required to produce this effect, Δf, corresponds to the frequency resolution limit $\Delta f/f_0$.

As one can see from the equation for the energy stored in the steady-state condition, the response of the system to a sinusoidal frequency other than its natural undamped frequency is diminished to a fraction, F, of the maximum energy that would be stored at the natural frequency. Expressed in terms of the ratio of the frequency of the driving force to the natural undamped frequency of the system ($f/f_0=\phi$), the fraction is

$$F = \frac{1}{\phi^2 + Q_0^2(1-\phi^2)^2}.$$

The frequency limits for the region Δf surrounding f_0 are found by solving for the condition $e^{-\alpha}=F$. Solving for the upper and lower frequency limits, f_b and f_a, for which the energy stored in the resonating system is a fraction $e^{-\alpha}$ of the peak response yields the expression:

$$\frac{f_b^2 - f_a^2}{f_0^2} = \frac{2}{Q_0}\sqrt{(e^{\alpha}-1)+\frac{1}{4Q_0^2}}.$$

And to a very close approximation, the frequency resolution limit comes out as:

$$\frac{\Delta f}{f_0} = \sqrt{\frac{(e^{\alpha}-1)}{Q_0}}$$

when Δf is defined as $(f_b - f_a)$.

The foregoing discussion may now be summarized in geometrical form by reference to a three-dimensional figure in signal space. The limits of resolution of an analyzer may be represented by an irreducible region in a three-dimensional space that must be exceeded before any information about a signal can be found. This space is shown in figure 1. As one can see from the equations, the figure of merit, Q_0, enters into the resolution limits for time and frequency in a complementary way. Thus, it determines the relative proportions between the resolution limits $\Delta f/f_0$ and $\Delta t/T_0$. One may therefore apportion the relative uncertainties in frequency and time to suit the requirements of an experiment whenever one can control the Q of a system. This process is discussed more fully in "Uniform Transient Error" (see footnote 2). But the product of the resolution limits, the "uncertainty equation" depends in irreducible fashion upon α.

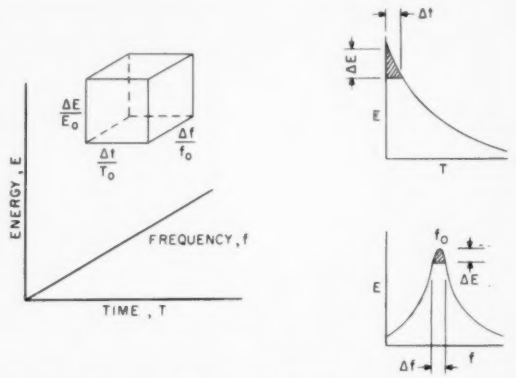

FIGURE 1. *Resolution limits making up the indication limit,* U. T_0 is the period corresponding to f_0, the natural undamped frequency of the system. E_0 is the maximum sinusoidal energy stored.

Thus the signal uncertainty equation, expressed in terms of α, turns out to be

$$\Delta f \cdot \Delta t = \frac{1}{2\pi}\sqrt{(e^{\alpha}-1)}$$

where α is related to ΔE through the definition of the least change ΔE that may be observed in the total stored energy E_0.

The basic form of the resolution equations results from substitution for the exponential coefficient, α, in the equations already derived:

$$\frac{\Delta t}{T_0} = -\frac{Q_0}{2\pi}\ln\left(1-\frac{\Delta E}{E_0}\right)$$

$$\frac{\Delta f}{F_0} = \frac{1}{Q_0}\sqrt{\frac{\frac{\Delta E}{E_0}}{\left(1-\frac{\Delta E}{E_0}\right)}}$$

$$\Delta f \cdot \Delta t = \frac{1}{\pi} \sqrt{\frac{\Delta E}{E_0}} \cdot \frac{1}{\sqrt{1-\frac{\Delta E}{E_0}}} \, ln \, \frac{1}{\sqrt{1-\frac{\Delta E}{E_0}}}$$

The volume corresponding to the irreducible limits in signal space, a quantity here defined as the "indication limit," can be computed from the signal uncertainty equation. It is defined by the triple product of the resolution limits along the three axes,

$$U = \frac{\Delta E}{E_0} \cdot \frac{\Delta t}{T_0} \cdot \frac{\Delta f}{f_0},$$

and it is just the volume of the elementary figure shown in figure 1. Its computation might at first glance appear to be somewhat redundant to the signal uncertainty equation. In fact, its functional form permits factoring the expression for U into components that have an interesting connotation in physical measurements.

Thus, since:

$$U = \frac{\Delta E}{E_0} \cdot \frac{\Delta f}{f_0} \cdot \frac{\Delta t}{T_0} \approx \frac{\Delta W}{W_0} \cdot \frac{\Delta f}{f_0} \cdot \frac{\Delta t}{T_0}$$

the magnitude of U expressed in terms of the variable, α, is

$$U = \frac{\alpha e^{-\alpha}}{2\pi} (e^{\alpha} - 1)^{3/2}$$

and U is given in terms of the energy resolution limit, $\Delta E/E_0$, by:

$$U = \frac{1}{2\pi} \cdot \left(\frac{\frac{\Delta E}{E_0}}{1-\frac{\Delta E}{E_0}} \right)^{3/2} \cdot \left[-\left(1-\frac{\Delta E}{E_0}\right) ln \left(1-\frac{\Delta E}{E_0}\right) \right].$$

It should be noted that the indication limit U and the signal uncertainty relation $\Delta f \cdot \Delta t$ depend only upon the energy resolution limit. The energy resolution limit is an independent variable and cannot be reduced by operations altering the function of the system along the f and t axes: for instance, changing the Q_0 of the system.

For a system operating at its optimum, the irreducible energy or power increment for the system would be set by the noise energy stored in the system. This noise energy may be due to Brownian motion in the system, for example. Noise of external origin may be present with the driving signal. In the general case the intrinsic and extrinsic noise powers will not be coherent, and the total noise energy stored in the system may usually be considered as the sum of contributions.

The prior papers relating the resolution limits to the relative amounts of signal and noise present (see footnote 2) were based upon a derivation subject to the restriction that the signal-to-noise ratio be high. In those papers, the relationship found was

$$\Delta f \cdot \Delta \tau \geq \frac{(S/N)^{-3/2}}{2\pi}$$

where S and N were signal and noise powers, respectively, and where the use of the observation interval $\Delta \tau$ rather than the limiting time increment Δt made the relation an inequality.

Such a restriction was, in fact, not required. A tractable and useful expression for the product $\Delta f \cdot \Delta t$ can be derived, valid for all values of S/N.

In the case where both signal and noise energy are stored, the total energy present in the system is $E_0 = S+N$. An increment in the signal energy stored (or in the input signal power) can be detected only if it equals or exceeds the minimum energy increment the system is capable of indicating. From this definition and the definition of the exponential factor, α:

$$\frac{\Delta S}{S+N} \geq \frac{\Delta E}{E_0} = \frac{\Delta W}{W_0} = (1-e^{-\alpha}).$$

And, where the least energy increment is controlled by the noise energy stored; $\Delta E \rightarrow N$: or, very nearly

$$\frac{\Delta E}{E_0} = \frac{N}{S+N}.$$

Thus, where the limit of detection is set by the noise energy:

$$\alpha = ln \frac{N+S}{S}$$

from which the signal uncertainty becomes:

$$\Delta f \cdot \Delta t = \frac{1}{2\pi} \sqrt{\frac{N}{S}} \cdot ln \left(1+\frac{N}{S}\right).$$

For high values of S/N, this expression approaches the limit $(1/2\pi)\ (S/N)^{-3/2}$, a result found previously (see footnote 2).

An especially interesting interpretation can be made from the form of the expression for the indication limit, U, when it is written in terms of the signal-to-noise ratio.

$$U = \frac{(S/N)^{-3/2}}{2\pi} \cdot \left(\frac{-S/N}{1+S/N} \, ln \, \frac{S/N}{1+S/N} \right).$$

The first factor can be recognized to be the expression for the signal uncertainty, $\Delta f \cdot \Delta t$, when the signal-to-noise ratio is high. The term in parentheses also has a recognizable functional form, and in fact it is possible to relate it to the limiting probability of information transfer.

To facilitate discussion, the factor N may be cleared from the fractions in the term, giving it the form: $-S/(S+N)\ ln\ S/(S+N)$. As one can see from the series expansion for the natural logarithm, this product approaches the value N/S for large values of S relative to N, and the indication limit then is merely the trivial product of the reciprocal of the signal-to-noise ratio multiplied by the signal uncertainty function. It is quite another matter as $S/N \rightarrow 0$. Then the indication limit may be con-

sidered to consist of two meaningful terms: one is the same signal uncertainty function that has already been derived for high signal-to-noise ratios (see footnote 2) (i.e., for ΔE small *re* E_0); the other is a modulating function that we will now proceed to relate to statistical matters.

Where one is dealing with the statistical presence of noise and signal, the long-time average signal-to-noise ratio may be described in terms of expected values. The following definition of expected value is taken from a textbook on statistics.[5] "The expected value of a random variable or any function of a random variable is obtained by finding the average value of the function over all possible values of the variable . . . . This is the *expected value*, or *mean value* of x. It is clear that the same result would have been obtained had we merely multiplied all possible values of x by their probabilities and added the results . . . we might reasonably expect the average value of x in a great number of trials to be somewhere near the expected value of x."

A special case that is quite common experimentally is one in which the level distributions of signal and noise are precisely the same. If one has either a signal or noise, the probability of the signal being P, then it follows that the probability of the noise is $(1-P)$. If the signal and noise have the same level distribution, G, the modulating term

$$\frac{S}{N+S}\,ln\,\frac{S}{N+S}\rightarrow\frac{P\cdot G}{P\cdot G+(1-P)\cdot G}\,ln\,\frac{P\cdot G}{P\cdot G+(1-P)\cdot G}$$

and thus the term that modulates the signal uncertainty function can be seen to reduce to the form $-PlnP$, where P is the probability of signal occurrence. From very simple considerations, therefore, the limit of detection is shown to be related directly here to a limiting probability of information transfer—a quantity usually derived in information theory by considering signals and noise to be made up of equal-sized unit impulses.

It is interesting that this point was arrived at in the reverse direction by Woodward and Davies.[6] They started with the $PlnP$ term from Shannon's information function and demonstrated from considering the signals and noise in radar detection that the quantity P was related to the signal-to-noise ratio for radar signals.

However, the modulating term in its original form, in terms of S and N, may be seen to represent a generalization of the function defined in information theory as the channel capacity, H. This form is more closely related to the ordinary formulation describing the entropy of a system in terms of the probability distribution of energy states within it.[7]

[5] A. M. Mood, Introduction to the Theory of Statistics, p. 91. (McGraw-Hill Book Co., New York, N.Y., 1950).

[6] P. M. Woodward and I. L. Davies, A theory of radar information, Phil. Mag. Series 7, **41**, 1001-1017 (1950).

[7] Max Born, Natural Philosophy of Cause and Chance, The Clarendon Press, Oxford (1949), cf, especially the discussions of probability and entropy; Claude Shannon and Warren Weaver, The Mathematical Theory of Communication, University of Illinois Press. Urbana, Ill. (1949).

The question of whether a signal is detected in the presence of noise depends upon what the investigator chooses to consider a reasonable limiting probability in deciding whether a signal has been detected. A preponderance of only 1 percent above random distribution would correspond to a much smaller signal-to-noise ratio than would 90 percent. In fact, the common definition that gives the limit of detection as a signal-to-noise ratio of unity corresponds directly to setting the criterion for the limiting probability of detection at 50 percent.

For the case $N=S$, the "$-PlnP$" term becomes $-\frac{1}{2}\,ln\,\frac{1}{2}$ and the indication limit becomes:

$$U_1=\frac{1}{2\pi}\left(-\frac{1}{2}\,ln\,\frac{1}{2}\right)=\frac{ln2}{4\pi}$$

for which the signal uncertainty function is:

$$\Delta f\cdot\Delta t=\frac{ln2}{4\pi}.$$

These are the limiting forms also where signals and noise are transmitted as "bits."

Thus far we have discussed noise from the standpoint of the noise energy stored in the system. This energy is, so far as the actual storage in the system is concerned, not distinguishable from energy stored that might be derived from purely sinusoidal excitation. If all excitation were withdrawn, and the system left in the force-free state, the energy in it would be dissipated in the usual exponential decay, and the oscillations during the decay would be essentially of frequency f_0, providing the system had moderate energy storage capacity ($Q_0>1$).

Therefore, unless we have some other means for distinguishing among the sources of the energy stored in the system—such as, for example, knowledge of the spectral character of pulsed signals applied to the system—or knowledge of the amount of energy found present in the system when it is considered to be free of any known source, we are left to regard as signal that part of the energy stored in the system that was produced by a sinusoidal signal of power S_f. The remaining driving sources, of more or less broad spectral distribution, would in general be classified as noise.

If the system is being driven at its natural frequency, its output signal will be $Q_0/2\pi$ times its input, for Q_0 is 2π times the ratio of the energy stored to the energy dissipated during the cycle. At any other driving frequency, the energy stored will be weighted by the response, ρ, which relates the energy stored to the power supplied to the system.

$$\rho=\frac{Q_0/2\pi f_0}{f^2/f_0^2+Q_0^2(1-f^2/f_0^2)^2}.$$

Suppose the noise within the system arises from a source whose spectral distribution is given by the power density function, N_f. The system will store energy with a weighting factor of ρ.

The total energy stored in the system due to ex-

citation by noise will then be found from the integral:

$$N=\int_0^\infty N_f \rho d\omega.$$

Although we have discussed the behavior of the system in terms of cycles per second, the quantity we have designated as Q_o is defined directly in terms of the ratio of the energy stored to the energy dissipated *per radian*. As the parameter of the function we are integrating is Q_o, we must choose the dimensionally similar variable in order to carry out the integration correctly. Thus we must integrate with respect to ω rather than f. This point is given in detail because it is an instance of the dimensionality of angles recently pointed out by C. H. Page.[8]

This integral may be evaluated easily for noise of constant energy per unit bandwidth in cycles per second; the result is then [9]

$$N=\frac{\pi N_f}{2}$$

and it is independent of Q_o because the energy storage capacity of the system and its bandpass for noise are affected in a complementary fashion by changes in the figure of merit.

For several other types of noise, an approximate equivalent white noise coefficient, n_f, can be defined, for which the foregoing equations remain applicable. Given a noise whose spectral distribution is $\nu(f)$, a mean value "equivalent" white noise per unit bandwidth may be computed from the equation:

$$n_f=\frac{\int_{f_a}^{f_b} \nu(f)df}{\int_{f_a}^{f_b} df}.$$

Obviously if $\nu(f)$ equals a constant, then n_f is the familiar "White Noise" coefficient. However, for several other types of noise the mean-value integration yields an equivalent n_f, which may be treated as a constant, with rather low residual error resulting from this approach. This can be seen from the fact that the system is selective with respect to the frequency components of the power sources from which it stores energy. Thus the restriction is only that the spectral distribution be changing *slowly* in the frequency region immediately surrounding f_o. For the following noise distributions, the residual terms discarded amount, in the worst case, to no more than 12½ percent of the approximate value:

For the noise distributions shown in the left-hand column, the respective mean values are shown in the right-hand column:

$$\nu(f)=k\cdot f \qquad n_f=\frac{k}{2}(f_b+f_a)$$

$$\underset{\text{(constant energy/octave)}}{\nu(f)=k/f} \qquad n_f=\frac{k \ln f_b/f_a}{(f_b-f_a)}$$

where, for this purpose, f_b and f_a are taken as the upper and lower half-energy limits of the response weighting function, ρ.

One can use the foregoing to predict the ratio of energy stored from the sinusoidal excitation to the energy stored from the source of noise. Thus the effective signal-to-noise ratio in terms of energy stored in the system is given by:

$$S/N=\frac{2S_i\rho}{\pi n_f f_0}.$$

The signal-to-noise ratio will be a maximum if the frequency of the sinusoidal excitation is just equal to the natural undamped frequency of the system. (For this condition, $\rho=Q_0/2\pi$.) The maximum ratio is:

$$S_0/N=\frac{S_i Q_0}{\pi^2 n_f f_0}.$$

The foregoing derivation has meaning also with respect to any system described by a second-order differential equation in which some event of brief duration occurs. A quantity directly analogous to the indication limit may be computed. In this instance, the expressions relate the resolution limits that bound the occurrence of the event, specifying the least increments of energy, frequency and time within which the event can take place.

Further, the limiting energy increment, ΔE, need not be formed by noise. For example, in a pulse-height system it would correspond to the smallest step in pulse height that might be indicated. As another example, an atomic system described by a second-order differential equation might have ΔE subject to quantum limitations.

Summary

The incremental limits, resolution limits, and indication limit for the performance of any system that is described by a second-order differential equation may be computed from considering the manner in which the system stores and dissipates energy, subject only to the restriction that the system be capable of storing oscillatory energy reversibly. As these limits are inherent in the mathematical properties of second-order differential equations, they are applicable to other types of systems by analogy.

The results of the discussion presented here are summarized in table 1. The relations tabulated apply to conditions that may be observed so long as the observation interval exceeds ¼π times the natural period of the system. The first line of table 1 summarizes the equations in terms of the basic energy resolution limit, $\Delta E/E_0$. The second line gives the same results expressed as functions of the exponential quantity α, and its inherent advantage

[8] C. H. Page, Physical entities and mathematical representation, J. Research NBS **65B** (Math. and Math. Phys.) No. 4, 227–235 (1961).

[9] D. Bierens de Haan, Nouvelles Tables D'Intégrales Définies, eq (6) p. 47 (Edition 1867, reprinted 1939).

Basic Variables:			Resolution Limits:	
$\frac{\Delta E}{E_o}$	α	S/N	$\Delta f/f_o$	$\Delta t/T_o$
$\frac{\Delta E}{E_o}$	$-\ln(1-\frac{\Delta E}{E_o})$	$\frac{1-\frac{\Delta E}{E_o}}{\frac{\Delta E}{E_o}}$	$\frac{1}{Q_o}\sqrt{\frac{\frac{\Delta E}{E_o}}{1-\frac{\Delta E}{E_o}}}$	$-\frac{Q_o}{2\pi}\ln(1-\frac{\Delta E}{E_o})$
$1-e^{-\alpha}$	α	$\frac{1}{e^{\alpha}-1}$	$\frac{\sqrt{e^{\alpha}-1}}{Q_o}$	$\frac{\alpha Q_o}{2\pi}$
$\frac{1}{S/N+1}$	$\ln\frac{S/N+1}{S/N}$	S/N	$\frac{1}{Q_o\sqrt{S/N}}$	$\frac{Q_o}{2\pi}\ln\frac{S/N+1}{S/N}$
$\frac{\pi^2 n_f f_o}{S_i Q_o + \pi^2 n_f f_o}$	$\ln(1+\frac{\pi^2 n_f f_o}{S_i Q_o})$	$\frac{S_i Q_o}{\pi^2 n_f f_o}$	$\frac{1}{Q_o}\sqrt{\frac{\pi^2 n_f f_o}{S_i Q_o}}$	$\frac{Q_o}{2\pi}\ln(1+\frac{\pi^2 n_f f_o}{S_i Q_o})$

Uncertainty Relation:	Indication Limit:
$\Delta f\,\Delta t$	U
$\frac{1}{\pi}\sqrt{\frac{\Delta E}{E_o}}\cdot\frac{1}{\sqrt{1-\frac{\Delta E}{E_o}}}\ln\frac{1}{\sqrt{1-\frac{\Delta E}{E_o}}}$	$\frac{1}{2\pi}\left(\frac{\frac{\Delta E}{E_o}}{1-\frac{\Delta E}{E_o}}\right)^{3/2}\left[-(1-\frac{\Delta E}{E_o})\ln(1-\frac{\Delta E}{E_o})\right]$
$\frac{\alpha}{2\pi}\sqrt{e^{\alpha}-1}$	$\frac{\alpha e^{-\alpha}}{2\pi}(e^{\alpha}-1)^{3/2}$
$\frac{1}{2\pi\sqrt{S/N}}\ln\frac{S/N+1}{S/N}$	$\frac{(S/N)^{-3/2}}{2\pi}\cdot\left[-\frac{S/N}{S/N+1}\ln\frac{S/N}{S/N+1}\right]$
$\frac{1}{2\pi}\sqrt{\frac{\pi^2 n_f f_o}{S_i Q_o}}\ln(1+\frac{\pi^2 n_f f_o}{S_i Q_o})$	$\frac{1}{2\pi}\left[\frac{\pi^2 n_f f_o}{S_i Q_o}\right]^{3/2}\cdot\left[-\frac{S_i Q_o}{\pi^2 n_f f_o + S_i Q_o}\ln\frac{S_i Q_o}{\pi^2 n_f f_o + S_i Q_o}\right]$

TABLE 1. *Resolution limits of analyzers and oscillatory systems expressed in several alternative variables.*

as a means of expressing $\Delta E/E_0$ can be seen from the greater simplicity of the equations in α. The third line summarizes the equations for the condition that $\Delta E/E_0$ is limited by the noise energy stored with the signal. The last line is the formulation of the noise-limited case in terms of the input powers of sinusoidal signal and noise, where the noise power can be expressed as noise energy per cycle.

The derivations sketched in the text are presented in detail in a series of appendices for those cases where it is felt this presentation will prove informative.

It is not feasible to relate each idea in this paper to a specific item in the literature. However, there are numerous papers that bear some relation to the material in this paper. A classified bibliography of some of these papers is therefore included at the end of this paper for the convenience of persons working on related problems. (The reader may also wish to consult the bibliography in Pimonow's book, see footnote 1.)

In this work I have benefited greatly by numerous discussions with Chester H. Page and Richard K. Cook. For several very enlightening remarks I am grateful to William H. Huggins and C. G. M. Fant. For a very helpful discussion on the dimensional properties of Q, and for painstaking checking of derivations, I should like to acknowledge the help of my colleague, Joseph Tant Priestley. To a number of my colleagues, friends, and visitors who have sat patiently discussing this problem with me while I was working it out, I should like to take this opportunity of extending my thanks.

This work was sponsored by the Office of Naval Research and also supported in part by the National Bureau of Standards.

Appendix 1. Energy Storage and Dissipation

For a system whose properties are described by a second-order differential equation, subjected to a driving force of amplitude A, the differential equation becomes:

$$M\ddot{x}+D\dot{x}+kx=Ae^{j\omega t}.$$

The equation may be rewritten in terms of parameters related to the undamped natural frequency and figure of merit of the system. The relative frequency, ϕ, replaces the quantities f and ω by ϕf_0 and $\phi\omega_0$ respectively. The equation resulting from this substitution is

$$\frac{Q_0}{\omega_0}\ddot{x}+\dot{x}+\omega_0 Q_0 x=\frac{A}{D}e^{j\phi\ \omega_0 t},$$

where, of course, the ratio k/M is ω_0^2.

The system responds to the force by motion of amplitude B, whose phase relative to A is given by the angle Θ.

$$\Theta=\tan^{-1}\frac{\phi}{Q_0(1-\phi)^2}$$

and the absolute value of the square of the amplitude is

$$|B^2|=\frac{A^2}{\omega_0^2 D^2}\cdot\frac{1}{Q_0^2(1-\phi^2)^2+\phi^2}.$$

The conventional definition for the quantity we represent here by Q_0 is given in terms of the natural undamped period of the system. For a sinusoidal driving force, one may have more use for the energy dissipated per cycle of the driving force, and in general the exciting force will not necessarily be alternating at the natural frequency of the system.

We wish to extend the definition of Q for a system when it is being excited at frequencies other than its natural frequency. There are several alternative definitions ordinarily given for the quantity we designate here as Q_0.

$$Q_0=\frac{\text{Peak energy stored}}{\text{Mean energy dissipated per radian fraction of the natural period}}$$

$$=2\pi\frac{\text{Peak energy stored}}{\text{Energy dissipated per cycle of the natural period}}$$

$$=\omega_0\frac{\text{Peak energy stored}}{\text{Mean rate of power dissipation}}$$

The second definition is commonly given because the amount of energy dissipated in a single cycle can be computed without finding a mean value. For our purposes, the third alternative gives the most direct approach to a generalized definition of Q.

The peak energy stored in the system under steady-state excitation is given by:

$$E_s=\frac{A^2}{2D}\cdot\frac{M}{D}\cdot\frac{1}{Q_0^2(1-\phi^2)^2+\phi^2}$$

and the mean rate of power dissipation is

$$\overline{W}_D=\frac{A^2}{2D}\cdot\frac{\phi^2}{Q_0^2(1-\phi^2)^2+\phi^2}.$$

The term ω_0 in the third alternative of the definition for Q_0 may be rewritten as $2\pi/T_0$, where T_0 is the natural period of the system.

Let us denote by Q_f the ratio of peak energy stored to the energy dissipated during one cycle of the driving frequency. The period of the driving frequency is $T=T_0/\phi$ and the resultant equation for Q_f becomes

$$Q_f=Q_0/\phi.$$

However, when a system is subjected to excitation by a complex group of driving forces, the only consistent period over which to compute the energy dissipated is the natural period of the system. For one frequency component of the complex signal, whose frequency is ϕ times the natural frequency of the system, the system stores and dissipates energy during excitation as though it had a Q given by:

$$Q_\phi=\frac{Q_0}{\phi^2}.$$

Note that either of these more general definitions of Q reverts to Q_0 for excitation at the natural frequency of the system. These expressions show that the ratio of energy stored by the system to the energy dissipated is a rather smooth function of frequency. The familiar frequency-selective action of the system is in fact shown by the amount of energy stored in the system under excitation by a sinusoidal force of a given *amplitude*, and is a consequence of the material lowering of impedance in the vicinity of the resonant frequency of the system.

The exponential decay of the energy stored in the system after cessation of the driving force takes place at a frequency very near to the natural undamped frequency of the system. Owing to the dissipation, the frequency is lowered by the factor

$$\delta=\sqrt{1-\frac{1}{4Q_0^2}}.$$

Thus the time scale of the decay is most closely expressed by the figure of merit, Q_0.

The exponential factor α has been defined from the exponential envelope of the decay of the energy stored in the system after the driving force was withdrawn. This is an approximation in that no account is taken of the instantaneous phase of the energy stored in the system at the instant when the driving force ceased. In fact, this is no gross approximation, as one can see by inspection of the equation that describes the process. Letting x_a and x_b represent the amplitudes of the sine and cosine

terms representing the coordinates of the system at $t=0$:

$$E_s=\frac{\pi Q_0 D}{T_0}\,e^{-\frac{2\pi}{Q_0}\frac{t}{T_0}}\left\{(x_a^2+x_b^2)+\frac{1}{4Q_0}\left[\frac{x_a^2-x_b^2}{Q_0}-4\delta x_a x_b\right]\cos\frac{4\pi\delta t}{T_0}+\frac{1}{4Q_0}\left[\frac{x_a x_b}{Q_0}+4\delta(x_a^2-x_b^2)\right]\sin\frac{4\pi\delta t}{T_0}\right\}.$$

As the first term is the square of the modulus of the system coordinate at $t=0$, it is independent of time. The remaining terms, which form the modulus of a double-frequency component, represent minor variations from exponential decay of the energy stored in the system. The main term is a sum of squares, whereas the modulus of the double-frequency component contains the difference of x_a^2 and x_b^2 and the product $x_a x_b$. Neither the difference nor the product can exceed the sum of the squares, and they are further diminished by a factor of $1/Q_0$ or smaller, depending upon the initial conditions. The magnitudes of the double-frequency terms depend upon the conditions at $t=0$, but they are always fairly unimportant. The situation is shown graphically in figure 2.

The discussion can be carried one step further: As the energy in a force-free system can only be dissipated, dE_s/dt is not positive during any part of the decay. Therefore, the slope of the modulated exponential curve is never greater than zero.

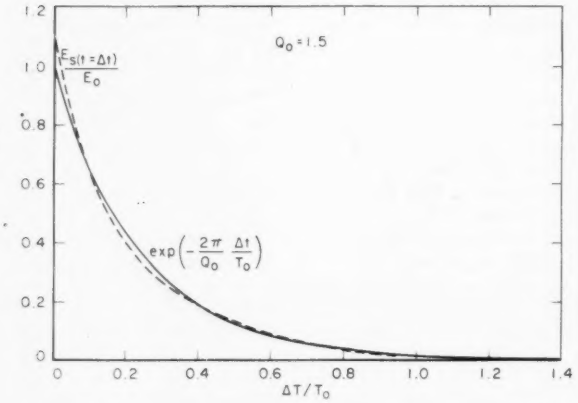

FIGURE 2. *Decay of the energy in an oscillatory system for* Q *of* $1\frac{1}{2}$

It is these minor variations that we omit by working only with the exponential decay. They are too minor to represent for values of Q in excess of 2.

Appendix 2. Noise

Noise can be considered as the result of a number of sinusoidal components acting simultaneously. The steady-state storage of noise energy in the system can be computed because the energy dissipated will be equal to the energy supplied.

Usually, when we speak of noise of constant power per unit bandwidth, we imply that the driving force amplitude is described by the equation:

$$\frac{A^2}{2D}=n_f f.$$

Since the power dissipation in the system at its resonant frequency is given by $W_D=A_0^2/2D$, the parameter n_f has the dimensions of energy per cycle.

At the frequency of resonance for the system, the energy stored is

$$E_0=\frac{Q_0}{2\pi f_0}\cdot n_f f_0.$$

For a driving force of a given magnitude, the peak energy stored by the system at any frequency is related to the peak energy stored at the frequency of its natural resonance by the fraction, F:

$$F=\frac{1}{Q_0^2(1-\phi^2)^2+\phi^2}.$$

The total noise energy stored is found by integrating over this function. The parameter Q_0 is defined for energy dissipated per radian. Therefore the weighting for the noise energy stored is

$$\int_0^\infty E\cdot F\,d\omega.$$

The integration may be stated in terms of the variable, ϕ, by making the substitution $d\omega=\omega_0 d\phi=2\pi f_0 d\phi$. After some rearrangement of terms, the noise energy stored in the system is given by:

$$N=\frac{1}{Q_0}\int_0^\infty\frac{n_f d\phi}{1+2\left(\frac{1}{2Q_0^2}-1\right)\phi^2+\phi^4}.$$

Under circumstances for which n_f may be removed from the integration, the remainder of the integral becomes merely $(\pi Q_0)/2$, so that $N=(\pi n_f)/2$. For a sinusoidal input signal of average power $\overline{W}_s$, at the resonance frequency of the system, the maximum ratio of signal energy stored to noise energy stored is given by:

$$S/N=\frac{Q_0\overline{W}_s}{\pi^2 n_f f_0}.$$

In general, n_f would be some function of frequency $\nu(f)$, and the evaluation of the noise weighting integral would be more difficult. However, since the systems we are dealing with are somewhat selective, there are some other noise distributions for which a useful "equivalent white noise coefficient" can be approximated. We have defined an equivalent white noise coefficient as the mean value of the noise function over the passband of the system.

For the type of noise that may be described by $\nu(f)=kf$ the mean-value integration gives:

$$n_f = \frac{k}{2}(f_b + f_a).$$

The range of values of $\nu(f)$ is $k(f_b - f_a)$ whereas the "equivalent" n_f is $(k/2)(f_b + f_a)$. The ratio of the range of values for $\nu(f)$ to the computed value for n_f represents an extreme estimate for the error made in using n_f. It represents the situation for a flat weighting of the noise components, whereas the system is actually selective and gives most weight to components in the vicinity of f_0. This extreme estimate yields the ratio:

$$\frac{\nu(f_b) - \nu(f_a)}{n_f} = \frac{2(f_b/f_a - 1)}{(f_b/f_a + 1)}.$$

For systems with a Q of 3 or higher, the response of the system falls away rapidly from the peak response, and the ratio f_b/f_a is very nearly unity when f_a and f_b are taken as the one-half power points. For the half-power points at $Q=3$ this error estimate represents the fraction 1/3, but half the total integrated energy stored in the system is stored within the range of frequencies *between* f_a and f_b; the other half arises from the remainder of the frequency range between zero and infinity.

(See appendix 3 for derivation of the energy stored within restricted ranges of frequency.)

For $\nu(f) = k/f$, the equivalent white noise concentration, n_f, is given by:

$$n_f = \frac{k \ln f_b/f_a}{f_b - f_a}.$$

It is necessary here to apply l'Hôpital's Rule to see that this equation is valid even for high values of Q because as $f_b \to f_a$, it simply approaches the limit $n_f = k/f_a$. Thus, as it should, the mean value, n_f, approaches the value $\nu(f_0)$, as the range over which the mean value is computed decreases.

For low values of Q, the question of the error introduced by substituting the mean value for the actual function is again limited at worst to the ratio that the range of values of $\nu(f)$ bears to the mean value n_f. Thus, for the function $\nu(f) = k/f$.

$$\frac{\nu(f_b) - \nu(f_a)}{n_f} = \frac{(f_b/f_a - 1)^2}{\frac{f_b}{f_a} \ln \frac{f_b}{f_a}}.$$

Because of the relatively slow change of the logarithm as a function of its argument, this range always represents a fairly small error.

In summary, we have shown that an equivalent white noise figure can be derived from the mean value of several noise functions, and that substitution of an n_f derived from the mean value of $\nu(f)$ in place of the white noise constant does not lead to serious error. Thus the relations derived in this paper for ordinary white noise are applicable to a number of other noise functions as well.

Appendix 3. Distribution of Energy Versus Frequency, and the Noise Integral

By patterning the integration upon the polynomial used in equations 6 and 7 on page 47 in the tables of Bierens de Haan, we can compute the fraction of the total noise power taken up by the system between any pair of fractional-power points in the frequency range, and the fraction of the total noise energy that is stored within the frequency range bounded by any pair of fractional energy points.

For the system, the mean rate of power dissipation is given by:

$$\overline{W}_D = \frac{\frac{A^2}{2D}\phi^2}{Q_0^2(1-\phi^2)^2 + \phi^2}$$

The energy stored is given by:

$$E_s = \frac{\frac{A^2}{2D} \cdot \frac{Q_0}{2\pi f_0}}{Q_0^2(1-\phi^2)^2 + \phi^2}$$

At the natural resonance frequency of the system, $\phi^2 = 1$, and thus, when expressed as a fraction of the response at the natural frequency, the relative power and relative energy functions become independent of the driving force. Choosing for convenience to express the fractional response as a reciprocal (e.g., 2 for the one-half power, etc.) for fractional energy,

$$F_E = Q_0^2(1-\phi^2)^2 + \phi^2$$

and, for fractional power,

$$F_W = \frac{Q_0^2(1-\phi^2)^2 + \phi^2}{\phi^2}.$$

One can then solve these equations to find at what relative frequency limits the system has a given fractional response. This procedure yields, for the frequency range between the fractional energy points, the *approximate* result:

$$\frac{f_b - f_a}{f_0} = \frac{\sqrt{F_E - 1 + 1/4Q_0^2}}{Q_0}$$

and, for the frequency range between the fractional power points, the *exact* solution:

$$\frac{f_2 - f_1}{f_0} = \frac{\sqrt{F_W - 1}}{Q_0}.$$

The approximation needed in solving for the fractional energy points arises from the fact that the system has finite energy storage capacity at zero frequency, whereas it has zero energy storage capacity at infinite frequency. The power dissipation capacity of the system is, however, zero at both extremes of the frequency range, and the func-

tion of power dissipation versus the logarithm of the frequency is symmetrical. Except for systems of low energy-storage capacity, the asymmetry of the energy storage function is negligible. (Its influence on $\Delta f/f_0$ is discussed in appendix 4.)

Within the frequency range between any two fractional energy limits, the noise energy stored is given by:

$$N_E=\frac{n_f}{Q_0}\int_{\phi_a=f_a/f_0}^{\phi_b=f_b/f_0}\frac{d\phi}{1+2\left(\frac{1}{2Q_0^2}-1\right)\phi^2+\phi^4}.$$

This integral can be divided into partial fractions, and the separated integrals give angle functions, from which the combined result is

$$N_E=\frac{n_f}{Q_0}\cdot\frac{Q_0}{2}\tan^{-1}\frac{-2\sqrt{F_E-1+1/4Q_0^2}}{(F_E-1)\sqrt{1-F_E/Q_0^2}}$$

The radical in the denominator becomes imaginary for the condition in which the energy storage at zero frequency exceeds the value of F_E chosen for the frequency limit.

The power taken up by the system between the frequency limits representing various fractional power points is given by the integral:

$$W_f=\frac{2\pi n_f f_0}{Q_0^2}\int_{\phi_1=f_1/f_0}^{\phi=f_2/f_0}\frac{\phi^2 d\phi}{1+2\left(\frac{1}{2Q_0^2}-1\right)\phi^2+\phi^4}$$

$$=\frac{\pi n_f f_0}{Q_0}\cdot\tan^{-1}\frac{2\sqrt{F_W-1}}{2-F_W}$$

where ϕ_1 and ϕ_2 are the limits of relative frequency corresponding to the fractional powers whose reciprocal is F_W. This equation requires no approximation.

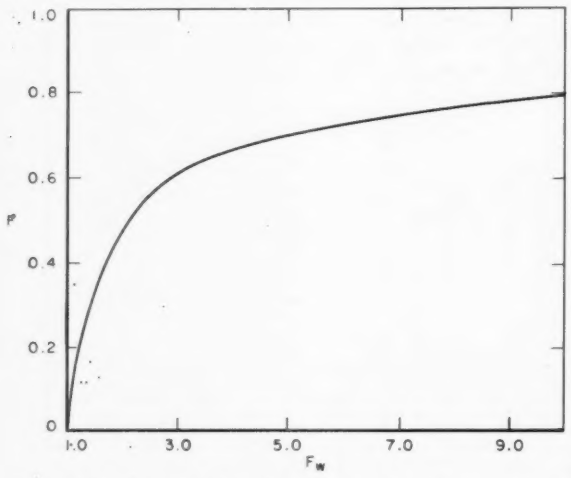

FIGURE 3. *Fraction of total energy stored for various relative response limits.*

The graphical result of this integration is shown in figure 3. The stored energy derived from noise power between the frequency limits representing various fractional power points is presented as a fraction of the total storage for the complete spectrum.

These integrals between finite limits may also be applied to evaluating the storage and dissipation of energy derived from band-limited sources.

Appendix 4. Frequency Resolution Limit

The approximation that leads to computation of $\Delta f/f_0$ has interesting connotations in physical problems. One of the terms discarded represents an asymmetry in the function describing the energy response of the system as a function of frequency. This term becomes appreciable only for systems of low energy-storage capacity ($Q\longrightarrow\frac{1}{2}$), but its computation permits a quantitative estimate to be made as to the limits within which the equations derived in this paper are applicable.

The boundaries of the frequency resolution limit, $\Delta f/f_0$, are those for which the energy storage is less than the maximum steady-state storage by the limiting energy increment, ΔE. This condition may be found from solutions of the equation:

$$e^{-\alpha}=\frac{1}{Q_0^2(1-\phi^2)^2+\phi^2}.$$

A convenient method is to rewrite the equation as:

$$(\phi^2-1)^2+(\phi^2-1)/Q_0^2-(e^\alpha-1)/Q_0^2=0$$

and to solve for the quantity (ϕ^2-1). The two roots can be written as

$$d_1=(\phi_1^2-1)=(f_1/f_0-1)(f_1/f_0+1)$$
$$d_2=(\phi_2^2-1)=(f_2/f_0-1)(f_2/f_0+1)$$

Let

$$\Delta f_1=f_0-f_1;\qquad \Delta f_2=f_2-f_0.$$

Then the limiting frequency increment is given by:

$$\Delta f=\Delta f_1+\Delta f_2.$$

The asymmetry between the limits f_1 and f_2 relative to f_0 may be defined as:

$$A_s=\frac{\Delta f_1-\Delta f_2}{2f_0}.$$

From these definitions:

$$\frac{\Delta f}{f_0}=\frac{d_2-d_1}{2(1-A_s)}.$$

The solution for the quantity (ϕ^2-1) yields, as the roots:

$$d_1=\frac{-1}{2Q_0^2}-\frac{1}{Q_0}\sqrt{(e^\alpha-1)+1/4Q_0^2}$$

$$d_2=\frac{-1}{2Q_0^2}+\frac{1}{Q_0}\sqrt{(e^\alpha-1)+1/4Q_0^2}$$

By applying the definitions for Δf_1, Δf_2 and A_s to the roots d_1 and d_2, the value of A_s is found to be

$$A_s=1-\sqrt{1-\frac{1}{4}\left(\frac{\Delta f}{f_0}\right)^2-\frac{1}{2Q_0^2}}.$$

No approximation has been used to this point. However, the second and third terms under the radical are much smaller than the first. When they are removed from the radical, by approximation:

$$A_s\approx\frac{1}{8}\left(\frac{\Delta f}{f_0}\right)^2+\frac{1}{4Q_0^2}$$

Now, in the expression for $\Delta f/f_0$ the term $(1-A_s)$ appears in the denominator. A_s is composed of terms that are quite small relative to unity, so that a series approximation of one term is sufficient, and we may place it in the numerator, obtaining:

$$\frac{\Delta f}{f_0}=\frac{1}{Q_0}\sqrt{e^\alpha-1+\frac{1}{4Q_0^2}}\,(1+A_s).$$

Inspection of this expression shows that a further simplifying approximation may be made in A_s, for it is clear that the term $(e^\alpha-1)$ is also rather small. Clearly the term in A_s that contains the square of $\Delta f/f_0$ will in general be less than half as large as $1/4Q_0^2$. Thus, the major term in A_s is just the quantity $1/4Q_0^2$. We have discarded this quantity from the equations shown in the text.

In order to find the limitations that bound the application of the equations given in the text, we must find the conditions under which the term $1/4Q_0^2$ is indeed small.

When Q_0 is taken as large as permitted by the least time interval in which an observation may take place, the relation between the resolution limit along the time axis and the energy resolution limit is

$$\frac{\Delta t}{T_0}=\frac{\alpha Q_0}{2\pi}$$

and, thus, in the limit:

$$\frac{1}{4Q_0^2}=\frac{\alpha^2T_0^2}{16\pi^2\Delta t^2}.$$

The approximation for $\Delta f/f_0$ will be poorest for the condition under which the discarded term is largest re $(e^\alpha-1)$. From this limiting condition, we can find the bounds imposed upon the least time interval for which these derivations are applicable. Let

$$\frac{\alpha^2T_0^2}{16\pi^2\Delta t^2}\div(e^\alpha-1)=M\,\frac{\alpha^2}{(e^\alpha-1)}$$

where M represents the terms that do not contain α. Differentiating the right-hand term with respect to α and setting it equal to zero, one finds two solutions, the trivial one of $\alpha=0$, and the equation

$$(\alpha-2)\,e^\alpha+2=0.$$

A graphical solution gives as the most unfavorable condition, $\alpha=1.6$.

This solution represents a condition in which $\Delta E/E_0$ would be very large; in fact, where noise is the limitation, the condition implies a signal-to-noise ratio of approximately 0.2. For this limit:

$$(e^\alpha-1)=e^{1.6}-1=4.$$

Thus, for a precision limit of about 12½ percent, we require only that the product $\alpha^2M<1$, or:

$$2.56\cdot\left(\frac{T_0}{\Delta T}\right)^2\cdot\frac{1}{16\pi^2}<1.$$

For times of observation comparable to one full period and even less, and in almost any condition in which $Q_0>1$, the term under the radical sign that we have discarded is in fact negligible.

Reference Bibliography

1. On the General Problems of Signal Detection

F. Zernike, Die natürliche Beobachtungsgrenze der Stromstärke, Z. Physik **40,** 628–636 (1926–27).

R. V. L. Hartley, Transmission of information, Bell System Tech. J. **7,** 535–563 (1928).

R. B. Barnes and S. Silverman, Brownian motion as a natural limit to all measuring processes, Rev. Mod. Phys. **6,** 162–192 (1934). (This paper has an extensive reference bibliography.)

D. Gabor, Theory of communication, J. Inst. Electr. Eng. **93,** pt III, 429–457 (1946).

S. Goldman, Frequency analysis, modulation, and noise (McGraw-Hill Book Company, New York, N.Y., 1948).

C. Shannon and W. E. Weaver, The mathematical theory of communication (University of Illinois Press, 1949).

S. O. Rice, Statistical properties of a sine wave plus random noise, Bell System Tech. J. **28,** 109–157 (1949).

J. L. Lawson and G. E. Uhlenbeck, Threshold signals (McGraw-Hill Book Co., New York, N.Y., 1950).

P. M. Woodward and I. L. Davies, A theory of radar information, Phil. Mag., Series 7, **41,** 1001–1017 (1950).

D. Gabor, Communication theory and physics, Phil. Mag., Series 7, **41,** 1161–1187 (1950).

S. O. Rice, Communications in the presence of noise—probability of error for two encoding schemes, Bell System Tech. J. **29,** 60–93 (1950).

P. Selgin, Harmonic output of the synchronous rectifier, J. Research NBS **47,** 427–432 (1951), RP 2267.

C. W. Harrison, Experiments with linear prediction in television, Bell System Tech. J. **31,** 764–783 (1952).

G. F. Montgomery, A comparison of amplitude and angle modulation for narrow-band communication of binary-coded messages in fluctuation noise, Proc. IRE **42,** 447–454 (1954).

G. F. Montgomery, Message error in diversity frequency-shift reception, Proc. IRE **42,** 1184–1187 (1954).

E. L. Kaplan, Signal-detection studies, with applications, Bell System Tech. J. **34,** 403–437 (1955).

2. Transients

F. M. Lewis, Vibration during acceleration through a critical speed, Trans. ASME APM–54–24, 253–261 (1932).

M. F. Gardner and J. L. Barnes, Transients in linear systems (John Wiley & Sons, New York, N.Y., 1942 (Reprinted 1945) Volume 1.

G. S. Brown and D. P. Campbell, Principles of servomechanisms (John Wiley & Sons, New York, N.Y., 1948).

F. K. Harris, Electrical measurements (John Wiley & Sons, New York, N.Y., 1952).

C. H. Page, Physical mathematics (D. Van Nostrand Co., New York, N.Y., 1955).

3. Power Spectra

W. R. Bennett, Spectra of quantized signals, Bell System Tech. J. 27, 446–471 (1948).

J. W. Tukey, The sampling theory of power spectrum estimates, Symposium on Applications of Autocorrelation Analysis to Physical Problems, Woods Hole, Massachusetts, 47–67 (13–14 June 1949).

C. B. Feldman and W. R. Bennett, Band width and transmission performance, Bell System Tech. J. **28,** 490–595 (1949).

C. H. Page, Instantaneous power spectra, J. Appl. Phys. **23,** 103–106 (1952).

H. Gamo, A theory of signal analysis in the frequency-time domain, J. Acoust. Soc. Japan **9,** 154–165 (1953).

C. H. M. Turner, On the concept of an instantaneous power spectrum, and its relationship to the autocorrelation function, J. Appl. Phys. **25,** 1347–1351 (1954).

S. S. L. Chang, On the filter problem of the power-spectrum analyzer, Proc. IRE **42,** 1278–1282 (1954).

R. B. Blackman and J. W. Tukey, The measurement of power spectra, Reprinted from the Bell System Tech. J. **37** (Dover Publications, Inc., New York, N.Y., 1958).

L. Pimonow, Théorie et pratique de l'analyse des vibrations en régime transitoire, Annales des Télécommunications **13,** 100–111 and 125–152 (1958).

P. Deman, Spectre instantané et analyse du signal simultanément en fréquences et en temps, Annales des Telecommunications **14,** 21–32 (1959).

A. A. Kharkevich, Spectra and analysis (translated and published by Consultants Bureau, New York, N.Y., 1960).

L. Brillouin, Science and Information Theory, IInd ed, (Academic Press, New York, N.Y., 1962).

4. Filters and Instruments Using Filters

J. J. Markham, The analysis of acoustic signals by means of the self-consistent spectrum, J. Acoust. Soc. Am. **20,** 95–98 (1948).

G. Hok, Response of linear resonant systems to excitation of a frequency varying linearly with time, J. Appl. Phys. **19,** 242–250 (1948).

N. F. Barber and F. Ursell, The response of a resonant system to a gliding tone, Phil. Mag. **39,** 345–361 (1948).

R. C. Mathes, A. C. Norwine, and K. H. Davis, The cathode ray sound spectroscope, J. Acoust. Soc. Am. **21,** 527–537 (1949).

O. O. Gruenz, Jr., and L. O. Schott, Extraction and portrayal of pitch of speech sounds, J. Acoust. Soc. Am. **21,** 487–495 (1949).

J. Marique, The response of RLC resonant circuits to EMF of sawtooth varying frequency, Proc. IRE **40,** 945–950 (1952).

M. C. Herrero, Resonance phenomena in time-varying circuits, Tech. Report No. 69, Electronics Research Laboratory, Stanford University (1953).

W. R. Bennett, The correlatograph, Bell System Tech. J. **32,** 1173–1185 (1953).

H. W. Batten, R. A. Jorgensen, A. B. MacNee, and W. W. Peterson, The response of a panoramic analyzer to CW and pulse signals, Proc. IRE **42,** 948–956 (1954).

J. K. Grierson, A technique for the rapid analysis of whistlers, Proc. IRE **45,** 806–811 (1957).

T. J. Higgins and H. W. Enomoto, A critical study of the effects of steepness of pulse fronts on the response of L–C ladder networks, University of Wisconsin Engineering Experiment Station, Reprint No. 303, Reprinted from Proceedings National Electronics Conference, Vol. XII (1956).

E. L. R. Corliss, Uniform transient error, J. Research NBS **61,** 25–30 (1958) RP 2879.

G. Fant, Acoustic analysis and synthesis of speech with applications to Swedish, Ericsson Techniques No. 1, 1959. (This paper has an extensive treatment of the time-delay in the response of filters, and it is written in English.)

J. Klapper and C. M. Harris, On the response and approximation of Gaussian filters, IRE Trans. Audio **AU–7,** 80–87 (1959).

5. Noise

D. Slepian, Fluctuations of random noise power, Bell System Tech. J. **37,** 163–184 (1958).

W. Freiburger and U. Grenander, Approximate distributions of noise power measurements, Quarterly of Applied Mathematics **17,** 271–283 (1959).

(Paper 67A5–235)

JOURNAL OF RESEARCH of the National Bureau of Standards—A. Physics and Chemistry
Vol. 67A, No. 5, September–October 1963

Synthesis, Purification, and Physical Properties of Seven Twelve-Carbon Hydrocarbons

Thomas W. Mears, Connie L. Stanley, Edward L. Compere, Jr.,[1] and Frank L. Howard

(April 12, 1963)

As part of a program to determine accurately the heats of combustion of specialized fuels in the kerosene range, seven hydrocarbons, biphenyl, bicyclohexyl, cyclohexylbenzene, *n*-hexylbenzene, *n*-hexylcyclohexane, 1-cyclopentylheptane, and *n*-dodecane were synthesized or purified from commercial material. Physical constants were determined on the purified samples. These materials may have use as secondary standards for heat of combustion measurements.

1. Introduction

These syntheses and purifications are a part of the project concerned primarily with heats of combustion and other properties of kerosene-like fuels. For certain specific applications it is necessary not only to know the heat of combustion of bulk lots of material but to have very exact knowledge of this property for individual portions of the bulk immediately before use. As an aid to the precise determination of these heats of combustion, it was decided to synthesize a series of typical hydrocarbons.

Since the fuels of interest are either kerosenes per se or hydrocarbon mixtures boiling in the kerosene range, it was decided that the materials synthesized should have molecular weight encompassed by the kerosene range and the hydrocarbon types represented should be those present in some or all commercial kerosenes. Since most kerosenes distill between 175 and 260 °C, it was decided that the most characteristic hydrocarbons would be those containing 12 carbon atoms. Therefore, 7 hydrocarbons of different structures, but all containing 12 carbon atoms, were selected for synthesis and purification. Three classes of compounds containing 12 carbon atoms typical of hydrocarbons found in kerosenes were not included, namely, dimethyldecalins, dimethyltetralins, and dimethylnaphthalenes, as they either boil above the kerosene range or are present only in small amounts.

2. Synthesis and Purification of the Hydrocarbons

The hydrocarbons were, in general, synthesized by modifications of techniques used earlier [2, 3][2] these methods involved the synthesis of an appropriate carbinol, the dehydration of this carbinol to an olefin or a mixture of olefins, and the catalytic hydrogenation of the olefins to paraffins.

The liquid hydrocarbons were purified by fractional distillation. Two types of distillation apparatus were used. One was a 6 ft by 1 in. column described by Whitmore and Lux [4] packed with 3/16-in. glass helices. The head was a modification of the Whitmore-Lux type designed by Howard [5]. These columns had an efficiency of 25 to 30 theoretical plates at atmospheric pressure and were used largely in the separation and purification of intermediates. The other column was a 3 ft by 25 mm Podbielniak "Heli-grid" column [6] having an efficiency of about 85 theoretical plates at atmospheric pressure, and was used for the final distillations. Both columns were equipped to operate at reduced pressures.

2.1. Purification of Biphenyl

Biphenyl, obtained by purchase,[3] had a purity of 99.86 to 99.88 mole percent [1, 7] and was further purified by the single crystal technique of Horton and Glasgow [8, 9].

The biphenyl was distilled into the crystallization tube and sealed under its own vapor pressure. The tube was then lowered slowly into a bath containing two immiscible liquids at different temperatures. The upper liquid was a silicone oil heated to 95 °C, the lower liquid was ethylene glycol held at 45 °C. The interface between these two liquids provided a sharp, plane boundary between the two temperature zones. As the sample passed from the warmer to the cooler zone, the biphenyl slowly crystallized with the impurities concentrating in the liquid phase. The rate of crystallization was ½ to 1½ in. per day with a total time of 10 to 25 days for a single crystallization. The crystallization tubes were so designed that the small amount of residual liquor remaining near the end of a crystallization could be removed without exposing the main sample to air. The crystal could then be melted and the process repeated. Each sample was crystallized three times.

The purity of these samples was determined by a modification of the freezing point method of Glasgow,

[1] Present address: Michigan College of Mining & Technology, Houghton, Mich.

[2] Figures in brackets indicate the literature references at the end of this paper.

[3] Distillation Products Industries, Rochester, New York.

Streiff, and Rossini [10]. The freezing points, 68.931 °C to 68.951 °C, correspond to purities of 99.92 to 99.96 mole percent [7].

2.2. Purification of Cyclohexylbenzene

Cyclohexylbenzene was obtained by purchase [4] and purified by fractional distillation at a pressure of 60 mm Hg using the "Heli-grid" column. Fractions of approximately 50 ml each were collected and the refractive indices determined. The individual fractions were grouped into cuts largely on the basis of uniformity of refractive indices. The data shown in figure 1 are typical of the three distillations of cyclohexylbenzene. The physical properties measured on cuts E and F are given in table 1. Cuts C and D were subsequently hydrogenated to bicyclohexyl (see section 2.3.).

Other methods of purification were attempted. One was the slow, fractional melting of solidified cyclohexylbenzene and separation in a specially designed basket centrifuge [11]. The crystals were placed in the basket of the centrifuge which was held at a temperature near the melting point of the crystals. The basket was rotated rapidly and, as the crystals slowly melted, the liquid was thrown from the basket and collected into fractions. The refractive index and freezing point of each fraction were determined. This method was not satisfactory, probably because of the relatively low heat of fusion of cyclohexylbenzene, or possibly the formation of solid solutions. A second method used was chromatographic adsorption on alumina. Commercial cy-

[4] Matheson, Coleman & Bell Division, The Matheson Co., Inc., East Rutherford, N.J.

TABLE 1. *Distillation of cyclohexylbenzene*
Charge: 3700 ml of crude cyclohexylbenzene

Cut	Fraction No.	Head temperature °C at 60 mm Hg	Refractive index at 20 °C	Volume
				ml
A	1–7	146.4–156.5	1.5174–1.5226	314
B	7–14	156.5–156.6	1.5228–1.5244	356
C	15–22	156.6–156.6	1.5246–1.5253	304
D	23–34	156.6–156.6	1.5251–1.5256	354
[a]				
E	35–39	155.8–155.9	1.5262–1.5262	259
F	40–72	155.9–156.2	1.5262–1.5263	1663
G	73	156.2–159.5	1.5285	42
[b]				

[a] Distillation interrupted.
[b] The distillation was terminated because biphenyl clogged the takeoff and condenser.

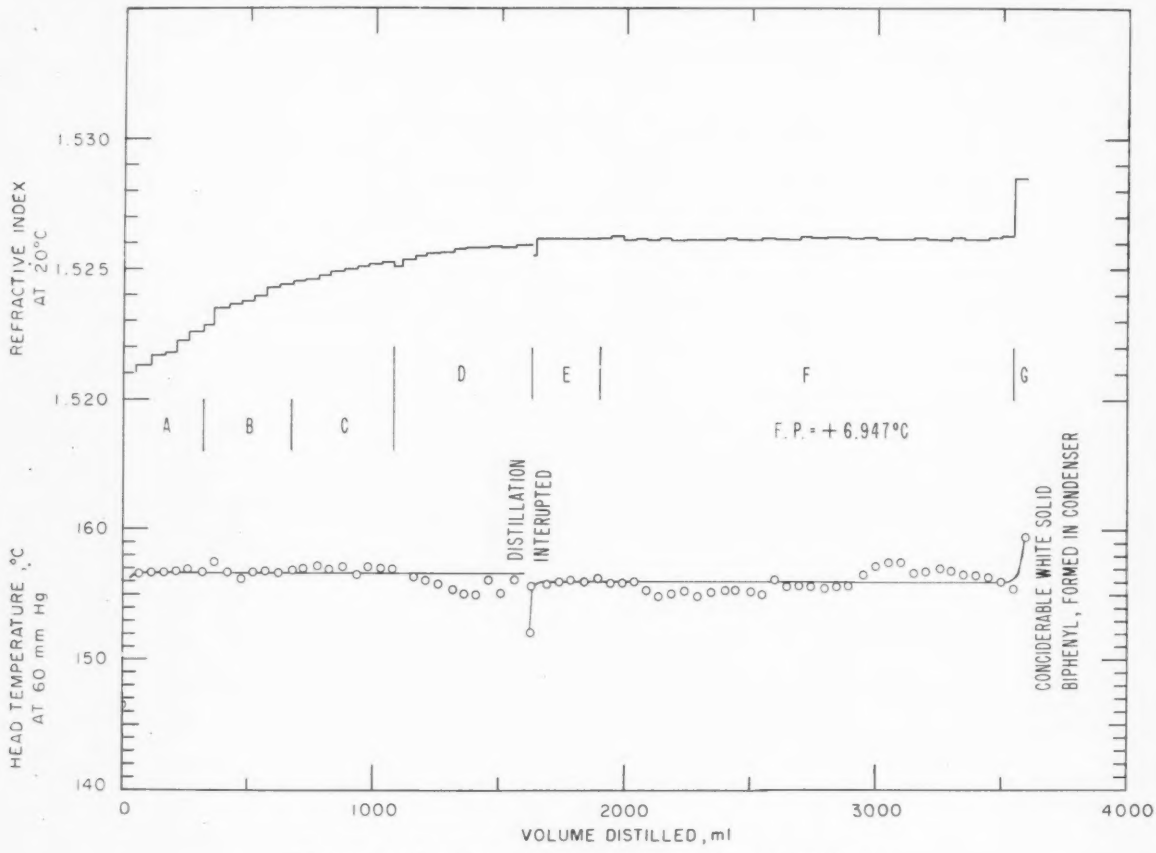

FIGURE 1. *Distillation of cyclohexylbenzene, charged—3750 ml.*

clohexylbenzene of 92 percent purity, when passed once through an alumina column, showed a 2.5 to 3.0 percent increase in purity of some of the eluent fractions. Material which had been previously purified by fractionation and crystallization to a purity of 98.65 percent was improved to 99.12 percent in one pass and to 99.24 percent in a second pass. These improvements, however, were accompanied by a high loss of material. Attempts to apply silica gel chromatography to the purification of this material proved completely unproductive.

2.3. Synthesis and Purification of Bicyclohexyl

Bicyclohexyl was prepared by catalytic hydrogenation of selected fractions from the distillations of cyclohexylbenzene. The fractions used for hydrogenation were those immediately preceding the material collected as purified cyclohexylbenzene. The hydrogenation was carried out using nickel-on-kieselguhr catalyst at 180 °C ± 10 °C and an initial pressure of about 1850 lb/in.^{2}

The hydrogenated hydrocarbon was filtered to remove the catalyst and percolated through silica gel prior to distillation. The material boiling at 148.5 to 150 °C at 58 mm Hg with refractive indices at 20 °C of 1.4796 to 1.4797 (uncorr.) was collected as bicyclohexyl. The product was again percolated through silica gel and certain physical properties were measured.

2.4. Synthesis and Purification of 1-Cyclopentylheptane

The 1-cyclopentylheptane was prepared in two ways. In the first, 1-heptyl-1-cyclopentanol was synthesized. Magnesium turnings, (53 g, 2.2 moles) were covered with ether and 296 g (2.2 moles) of *n*-heptyl chloride in 500 ml of ether was slowly added. This was followed by the slow addition of 168 g (2 moles) of cyclopentanone in 200 ml of ether. After the mixture had been stirred for 2 to 3 hr, it was hydrolyzed and the ether removed in the usual manner. The products from several runs were combined and distilled at reduced pressure. However, only a small amount of 1-heptyl-1-cyclopentanol (bp 91 to 92 °C at 3 mm Hg, n_D^{20} 1.4604 [12]) was isolated. This was due to the extensive dehydration that took place during distillation. The partially dehydrated material was distilled rapidly at atmospheric pressure to give a fraction boiling between 218 and 220 °C. This material contained a considerable amount of the carbinol along with the olefin resulting from the dehydration. An approximate estimate of the combined yield of these compounds is 20 percent. The low yield is probably due to the ease with which cyclopentanone tautomerizes to the enol form. The carbinol-olefin product was passed over alumina at 300 °C to complete the dehydration.

To conduct the synthesis by another path, 1-cyclopentyl-1-heptanol was prepared from cyclopentylmagnesium bromide and *n*-heptaldehyde in a similar manner. The Grignard reagent was prepared by reacting 328 g (2.2 moles) of cyclopentyl bromide with 53.5 g (2.2 moles) of magnesium turnings in 600 ml of dry ether. To this was added 228 g (2 moles) of redistilled *n*-heptaldehyde (bp 152 to 157 °C) in 270 ml of ether. The usual procedure of hydrolysis, washing, drying, and removal of the ether was followed. The residues from 14 runs (28 moles of *n*-heptaldehyde) were combined and distilled in two charges in the glass-helix packed column. The major fractions were 1-heptanol (bp 102.4 to 113.4 °C at 50 mm Hg, n_D^{20} 1.4260 to 1.4242) 1300 g, and 1-cyclopentyl-1-heptanol (bp 168 to 170 °C at 60 mm Hg, n_D^{20} 1.4606 to 1.4611) 1944 g. The reduction of *n*-heptaldehyde by the Grignard reagent to 1-heptanol accounts for 41 percent of the aldehyde used. The yield of 1-cyclopentyl-1-heptanol was 38 percent.

The 1-cyclopentyl-1-heptanol was dehydrated by passage over alumina at 265 to 300 °C. Approximately 90 percent of the theoretical quantity of water was recovered. The crude olefin was washed, dried, and distilled in the glass-helix packed column. The material distilling between 132 and 134 °C at 54 mm Hg (n_D^{20} 1.4565 to 1.4571), was collected as the mixed 1-cyclopentylheptenes. The fractions of higher boiling point and refractive index containing undehydrated carbinol were recycled through the dehydration apparatus. The overall yield was 84 percent.

The incompletely dehydrated material from the reaction of *n*-heptylmagnesium chloride and cyclopentanone was also dehydrated over alumina at 265 to 300 °C. The olefin mixture was hydrogenated with nickel-on-kieselguhr catalyst at 130 °C and hydrogen pressure not exceeding 1200 lb/in.^{2} The hydrogenation proceeded smoothly up to a point of partial hydrogenation after which no more hydrogen was absorbed. In order to complete the hydrogenation it was necessary to raise the temperature to 160 °C and the pressure to 2000 lb/in.^{2} The hydrogenated product was washed, dried, and percolated through a silica gel column.

The 1-cyclopentylheptane was purified by fractionation on a 3-foot "Heli-grid" [5] column under approximately 50 mm Hg pressure. The purification was made difficult by a small amount of an unidentified material with a boiling point near that of the product. This made it necessary to redistill the heart cuts of several distillations before obtaining a sample of satisfactory purity. The final distillation gave material boiling 142.1 to 142.9 °C at 50 mm Hg.

2.5. Synthesis and Purification of *n*-Hexylbenzene

Normal-hexylbenzene was prepared by a method similar to that used in the synthesis of 1-cyclopentylheptane. Sufficient *n*-hexylbenzene was prepared so that a part of it could be further hydrogenated to *n*-hexylcyclohexane. In a typical run a Grignard reagent was prepared by the reaction of 415 g (2.75 moles) *n*-amyl bromide (bp 127 to 129 °C) in 800 ml of ether with 66.9 g (2.75 moles) of magnesium turnings. To this was slowly added 265 g (2.5 moles) of benzaldehyde in 250 ml of ether. During the course of the reaction, it was necessary to add ether

to keep the reaction fluid. After the addition was complete the reaction mixture was refluxed for 2 hr, and hydrolyzed with saturated ammonium chloride solution. The ether layer was siphoned off and the aqueous layer extracted four times with ether. The ether extracts were combined, dried, and the ether removed by distillation.

The crude products from four Grignard reactions (9 moles of benzaldehyde) were combined and distilled under reduced pressure in the glass-helix packed column. The fractions boiling at 172 °C at 50 mm Hg, n_D^{20} 1.5064 to 1.5048 [13], were collected as 1-phenyl-1-hexanol. The yield was 1264 g (7.1 moles) which represents 79 percent yield on the basis of benzaldehyde used; a total of 4.5 kg was prepared.

The 1-phenyl-1-hexanol was successfully dehydrated over alumina at temperatures ranging from 270 to 315 °C. Since the dehydration resulted in some movement of the double bond to produce a series of close-boiling olefins no attempt was made to isolate individual compounds. The crude olefin mixture was separated from residual carbinol compounds by distillation under reduced pressure (10 to 20 mm Hg) using a short Vigreaux column. The entire lot of mixed phenylhexenes was hydrogenated over nickel-on-kieselguhr catalyst at 120 °C and pressures up to 1600 lb/in.^{2} and the amount of hydrogen fed into the reactor was measured. Under these conditions, the absorption of hydrogen ceased upon the saturation of the olefinic double bond without attacking the benzenoid nucleus. Distillation of the *n*-hexylbenzene in the "Heli-grid" column under reduced pressure gave several fractions boiling from 132 to 133 °C at 47 mm Hg, n_D^{20} 1.4866 to 1.4867. A portion of this material was reserved as *n*-hexylbenzene and the balance along with selected foreruns was further hydrogenated to *n*-hexylcyclohexane.

2.6. Synthesis and Purification of *n*-Hexylcyclohexane

Normal hexylcyclohexane was prepared by the hydrogenation of *n*-hexylbenzene (5) using nickel-on-kieselguhr catalyst. The temperature of the hydrogenator was raised to 180 to 190 °C and the peak pressures were about 2100 lb/in.^{2} The hydrogenated product was percolated through silica gel and distilled.

Distillation of the product in the 3 ft "Heli-grid" column under reduced pressure gave two principal cuts: cut C (bp 144 to 147 °C at 65 mm Hg, n_D^{20} 1.4471 to 1.4469), 867 ml; and cut D (bp 147 °C at 65 mm Hg, n_D^{20} 1.4468 to 1.4465), 707 ml. Both cuts were percolated through silica gel and their freezing points determined. Cut C gave a freezing point of −47.51 °C and was reserved as "best" material. Cut D was less pure with a freezing point of −51.77 °C.

2.7. Synthesis and Purification of *n*-Dodecane

n-Dodecane was prepared by the hydrogenation of the olefins obtained from the dehydration of lauryl alcohol. Lauryl alcohol (1-dodecanol) was dehydrated by passage over alumina at 350 to 375 °C with a yield for a single pass of about 80 percent. The organic liquid was washed, dried, and fractionated through a short, helix-packed, distilling column. The material boiling from 210 to 215 °C was collected as mixed dodecenes; and the residue was recycled through the dehydration apparatus. The overall yield of olefin based on dodecanol consumed was about 88 percent.

The mixed dodecenes were hydrogenated with nickel-on-kieselguhr catalyst at 140 °C and initial hydrogen pressures of 1800 lb/in.^{2} The *n*-dodecane was freed from nickel and percolated through silica gel. The final product was fractionated in the glass-helix-packed column. The fractions boiling at 126 °C at 50 mm, n_D^{20} 1.4218 to 1.4219 were collected as *n*-dodecane.

3. Determination of Physical Properties

Physical properties and purities were determined on the best samples of each hydrocarbon, and the values obtained are given in table 2. Boiling points, densities, and refractive indices were determined by the procedures described by Mears et al. [3]. The constant temperature apparatus was maintained within ±0.02 °C during the measurement of density and refractive indices.

The freezing points and purities were determined where possible by the method of Glasgow, Streiff, and Rossini [10]. The freezing point curves obtained using the monocyclic hydrocarbons with long side chains gave purity values which seemed incompatible with estimates of purity based on other properties. For this reason the estimates of purities of 1-cyclopentylheptane, *n*-hexylcyclohexane, and *n*-hexylbenzene were determined from vapor-phase chromatograms. In each case only one peak was noted.

TABLE 2. *Physical properties of hydrocarbons prepared*

Hydrocarbon	Hydrocarbon class	Freezing point	Boiling point at 760 mm Hg	dt/dp at 760 mm Hg	Refractive index		Density		Purity
					at 20° C	at 25° C	at 20° C	at 25° C	
		°C	°C	°C/mm	n_D	n_D	g/ml	g/ml	mole percent
Biphenyl	Bicyclic aromatic	+68.95							99.96
Cyclohexylbenzene	Naphthenic aromatic	+6.99	240.12	0.0525	1.52633	1.52303	0.94272	0.93874	99.83
Bicyclohexyl	Bicyclic naphthene	+3.63	239.04	.0555	1.47995	1.47768	.88619	.88249	99.96
n-Hexylbenzene	Alkylaromatic	[a] −63.5	225.77	.0563	1.48668	1.48445	.85802	.85428	(b)
n-Hexylcyclohexane	Naphthene	−47.51	224.78	.0572	1.44600	1.44459	.80817	.80452	(b)
1-Cyclopentylheptane	Naphthene	−61.04	223.92	.0560	1.44231	1.43993	.80132	.79778	(b)
n-Dodecane	Paraffin	−9.71	216.26	.0557	1.42174	1.41955	.74901	.74535	99.52

(a) See section 3 of text.
(b) These hydrocarbons were analyzed by vapor-phase chromatography. In each case only one peak was noted.

It has been observed earlier in this laboratory that the freezing points of long-chain normal hydrocarbons, notably *n*-hexadecane, are a poor criterion of purity. This phenomenon has been studied in the past; Broadhurst [14] has reviewed these studies and developed a general qualitative theory of solid phase behavior of normal paraffin hydrocarbons.

An unusual behavior was also encountered in the case of the melting point of the *n*-hexylbenzene. A number of melting points were determined of the same or similar samples, no two of which gave the same value. The following are values on one fraction: 1. one sample, −63.484° and −63.566 °C three days apart; 2. another sample, −63.502° and −63.538 °C the same day, one in the morning and one in the afternoon. It is possible that a solid phase transition takes place in the immediate vicinity of freezing (melting) point.

The authors express their appreciation to the following persons who carried out various assignments in this work: Donald Adams, Roy L. Alexander, Anthony Grimaldi, John McAuley, August Kushta, George S. Saines, John VandeCastle, and James A. Walker. Thanks are also due Avery T. Horton for the use of his crystallization apparatus and instructions for carrying out this type of purification, and to R. T. Leslie for preparing and evaluating the vapor-phase chromatograms.

4. References

[1] J. Timmermans, Physico-chemical constants of pure organic compounds (Elsevier Publishing Co., Inc., New York, N.Y., 1950).
[2] F. L. Howard, T. W. Mears, A. Fookson, P. Pomerantz, and D. B. Brooks, J. Research NBS **38,** 365 (1947) RP1779.
[3] T. W. Mears, A. Fookson, P. Pomerantz, E. H. Rich, C. S. Dussinger, and F. L. Howard, J. Research NBS **44,** 299 (1950) RP2079.
[4] F. C. Whitmore and A. R. Lux, J. Am. Chem. Soc. **54,** 3451 (1932).
[5] F. L. Howard, Anal. Chem. **19,** 144 (1947).
[6] W. J. Podbielniak, Ind. Eng. Chem., Anal. Ed. **13,** 639 (1941).
[7] A. J. Streiff, L. H. Shultz, A. R. Hulme, J. A. Tucker, N. C. Krouskop, and F. D. Rossini, Anal. Chem. **29,** 361 (1957).
[8] A. T. Horton and A. R. Glasgow, J. Research NBS (in press).
[9] A. T. Horton, U.S. Patent 2,754,180, July 10, 1956.
[10] A. R. Glasgow, A. J. Streiff, and F. D. Rossini, J. Research NBS **35,** 355 (1945).
[11] F. D. Rossini, B. J. Mair, and A. J. Streiff, Hydrocarbons from Petroleum, p. 177 (Reinhold Publishing Co., New York, N.Y., 1953).
[12] A. F. Plat'e, Compt. rend. acad. sci. U.S.S.R. **24,** 269 (1939).
[13] W. C. Davies, R. S. Cison, and W. J. Jones, J. Chem. Soc. (**1930**) 468.
[14] M. G. Broadhurst, J. Research NBS **66A** (Phys. and Chem.), No. 3, 241 (1962).

(Paper 67A5–236)

JOURNAL OF RESEARCH of the National Bureau of Standards—A. Physics and Chemistry
Vol. 67A, No. 5, September–October 1963

Reactions of Polyfluorobenzenes With Nucleophilic Reagents [1]

Leo A. Wall, Walter J. Pummer, James E. Fearn, and Joseph M. Antonucci

(June 10, 1963)

Nucleophilic reactions of hexafluorobenzene and related polyfluorobenzenes were studied in detail. Reaction of hexafluorobenzene with hydroxides, alcoholates, aqueous amines, and organolithium compounds led to the substitution of one or more fluorine atoms. The structures of the products were determined, using near infrared and nuclear magnetic resonance spectra. Fluorine is replaced more readily than chlorine, bromine, iodine, or other groups. In the majority of the products in which two of the fluorines in hexafluorobenzene were replaced, the substituting groups were para to each other. However, depending on the reagents other orientation effects were noted. The reaction mechanisms were a function of reagents and conditions. The most prevalent mechanism is presumably the displacement of a fluoride anion by another anion, probably via the formation of transition complexes of different lifetimes. However, simple ionization or attack by neutral species may occur under some conditions. The diazotization and oxidation of pentafluoroaniline were also investigated.

1. Introduction

Hexafluorobenzene [1, 2, 3, 4] [2] and other highly fluorinated benzene derivatives [5] have been synthesized in recent years by several methods. These substances are very inert chemically and extremely stable to heat and radiation [6, 7, 8]. Hexafluorobenzene has not, to date, been reported to react with electrophilic reagents. Exceedingly drastic acidic conditions have been required to halogenate further tetrafluoro- and pentafluoro benzene [9, 10, 11, 12]. Hexafluorobenzene will add chlorine [1, 2, 4] and is readily attacked by free radicals [13].

Like hexachlorobenzene [14], hexafluorobenzene would be expected to react with bases. Strong nucleophilic reagents will displace fluorine from the aromatic ring. The strong inductive effect of the electronegative fluorine atoms should produce highly positive ring-carbon atoms. Unlike hexachlorobenzene, which is a high-melting solid poorly soluble in organic solvents, hexafluorobenzene is a liquid and is soluble in many solvents. Hence, the latter compound readily reacts with many bases in appropriate solvents. Under pressure at elevated temperatures, aqueous systems have also been used successfully with hexafluorobenzene.

The reactions of hexafluorobenzene and many of its monosubstituted derivatives with various nucleophilic reagents will be described in this paper. The chief reagents utilized were alkali-metal hydroxides, alcoholates, amines, and organolithium compounds. In general, these reagents replace fluorine in preference to bromine or iodine, for example, in reactions with bromo- and iodo-pentafluorobenzene. This is in accord with previously observed results on nucleophilic reactions [15, 16]. With 1-chloro-3,4,5,6-tetrafluorobenzene, the chlorine atom can, however, be replaced preferentially by a hydrogen atom [17]. The reaction is carried out with hydrogen over a palladium catalyst at 280 °C.

Many of the reactions studied are informative of the directional effects created by groups other than a fluorine atom in an otherwise completely fluorinated benzene ring. Very meager information of this nature has been available previous to this work. Nuclear magnetic-resonance spectroscopy was used as the primary method for determining molecular structure. Infrared spectra, particularly in the near-infrared, were also of assistance in determining structure, especially in the case of the *ortho* hydroxyl compounds.

2. Reactions of Hexafluorobenzene

2.1. Reactions With Hydroxides

It has been found that polyfluoroaromatic phenols can be prepared readily by the following type of reaction:

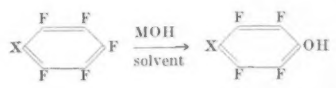

where M is any alkali metal and X is a fluorine atom or some other substituent group. The product is often the *para* isomer, but mixtures of isomers may occur.

[1] Based on research supported by the Bureau of Naval Weapons, Department of the Navy.

[2] Figures in brackets indicate the literature references at the end of this paper

In our earlier work [18], pentafluorophenol was prepared by refluxing hexafluorobenzene with potassium hydroxide in pyridine, which was found to be an effective solvent for this reaction. In similar reactions with hexachlorobenzene, it has been suggested [14] that pyridine has a specific, catalytic effect. With ethanolic pyridine as solvent, the reaction gave pentafluorophenol and tetrafluorodihydroxybenzene together with small proportions of pentafluorophenetole and diethoxytetrafluorobenzene. Since the phenol reacts further only with difficulty due presumably to the repulsion of the negative ion by the phenoxy ion, it is likely that the disubstituted products result via reaction of the base with the phenetole and that many substituted ethoxy groups are then split by the basic medium to give the hydroxy derivatives. With *tert*-butyl alcohol as diluent, other workers have prepared pentafluorophenol from hexafluorobenzene [19].

In the present work, it was found that simple, aqueous systems are adequate for these nucleophilic reactions. Thus, we have prepared pentafluorophenol in high yield (85%) by using aqueous potassium hydroxide at 175 °C in a closed pressure-vessel. For the phenol preparation, our experience suggests water to be the preferred diluent, followed by *tert*-butyl alcohol. Tetrafluoro-*p*-cresol was prepared, using *tert*-butyl alcohol as diluent. With pyridine as solvent, black tars are undesired by-products; using pyridine, the compounds 2,3,5,6-tetrafluorophenol, 2-bromo-3,4,5,6-tetrafluorophenol, 4-bromo-2,3,5,6-tetrafluorophenol, and 2,3,5,6-tetrafluoro-4-iodophenol have been prepared.

2.2. Reactions With Alkoxides

Another reaction of polyfluoroaromatics investigated was that with such alcoholates as sodium methoxide.

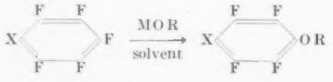

The reaction is usually carried out at reflux temperatures, to give good yields of ethers of the general type shown. With sodium methoxide in methanol, pentafluoroanisole was produced [4, 20], together with some of the tetrafluoro-*p*-dimethoxybenzene. With pyridine—methanol as the solvent [18], rapid reaction occurred to produce high yields (70%) of pentafluoroanisole. The tetrafluoro-*p*-dimethoxybenzene has also been produced by other methods [21, 22], e.g., from the reaction of diazomethane with 2,3,5,6-tetrafluorohydroquinone. Synthesis by this route established that the second methoxyl group is in the *para* position to the first.

The pentafluoroanisole may be demethylated, with difficulty, by refluxing with 47-percent hydriodic acid [3], to give a 20-percent yield of pentafluorophenol. Demethylation is also relatively poor with hydrobromic acid [20]. However, when the pentafluoroanisole is heated with anhydrous aluminum chloride and the mixture is poured onto ice, a 58 percent yield of pentafluorophenol [20] is obtained.

Pentafluorophenol is extremely resistant to further substitution by nucleophilic reagents, probably because these reactions would require the attack of a negative species on the negative phenoxide ion. Ammonium 2,3,4,5,6-pentafluorophenoxide was the only product obtained from treatment of (a) pentafluorophenol, (b) sodium pentafluorophenoxide, or (c) ammonium pentafluorophenoxide with sodamide in liquid ammonia. Thus, the tetrafluorodihydroxybenzene [18] produced in the reaction with ethanolic potassium hydroxide in pyridine probably arises form the attack of a nucleophilic species on the phenetole. In another study [19], only the phenetole was produced in 48 percent yield, and 45 percent of the hexafluorobenzene was recovered after reaction with ethanolic potassium hydroxide for 30 min at 120 °C. In accord with this result is the observation made in this work that the treatment of pentafluoroanisole with aqueous ammonia results in the isolation of ammonium pentafluorophenoxide. With hydrazine hydrate in ethanol, hydrazinium pentafluorophenoxide is obtained [20]. However, benzyl pentafluorophenyl ether is not readily split by nitrogen bases, and a fair yield (13%) of benzyloxytetrafluoroaniline was obtained by treating it with aqueous ammonia.

In this work, bromo- and iodo-pentafluorobenzene were converted to the corresponding anisoles in which a fluorine atom is replaced by a methoxyl group. Reaction of sodium benzyloxide (in excess benzyl alcohol or in *tert*-butyl alcohol) with hexafluorobenzene gave benzyl pentafluorophenyl ether. A higher yield of purer material was obtained when the latter solvent was used, since benzyl alcohol is difficult to remove from the product.

Anhydrous sodium phenoxide was found to react rapidly with hexafluorobenzene at room temperature in *N*,*N*-dimethylformamide, giving 2,3,4,5,6-pentafluorophenyl phenyl ether. This compound was also prepared by treating potassium pentafluorophenoxide with bromobenzene, using activated copper as a catalyst. This reaction failed to give the perfluorophenyl ether when bromopentafluorobenzene was used instead of bromobenzene; the starting materials were recovered.

Perfluorophenyl ether was, however, prepared, although in relatively low yield, by reacting potassium pentafluorophenoxide with hexafluorobenzene in *N*,*N*-dimethylformamide. This reaction was more sluggish than that involved in the preparation of the pentafluorophenyl phenyl ether and required refluxing. This difference may be partially explained by the poorer nucleophilic nature of the potassium pentafluorophenoxide as compared to the sodium phenoxide.

By the reaction of sodium ethoxide in ethanol with pentafluoro-*N*,*N*-dimethylaniline, 4-ethoxy-2,3,5,6-tetrafluoro-*N*,*N*-dimethylaniline was synthesized. No pyridine was used in this reaction, since phenol formation is likely to occur under these conditions.

2.3. Reactions With Amines

Hexafluorobenzene has been shown to undergo reaction with sodamide at −70 °C in liquid ammonia,

to give 2,3,4,5,6-pentafluoroaniline [23]. In ether, reaction with sodamide did not produce pentafluoroaniline; a solid which slowly sublimed at 85 °C was obtained [24]. The preferred reaction for replacing fluorine atoms with amino groups is treatment with aqueous amines [14].

In this investigation, the reaction of aqueous amines with polyfluoroaromatic compounds has been extensively explored.

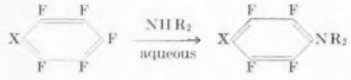

Our result differed in certain respects from those obtained when aqueous ethanolic amine solutions were used [25]. The reactions were carried out at 160 to 230 °C in a steel pressure-vessel. Control of temperature and time of the reaction is critical since, at low temperature, the reaction does not occur and, at higher temperatures, unidentified tars are produced.

In this investigation, bromo- and iodo-tetrafluoroanilines, pentafluoroaniline, and various polyfluoromethylanilines were prepared by the aqueous amine process. Although (benzyloxy)tetrafluoroaniline was formed by the reaction of benzyl pentafluorophenyl ether with aqueous ammonia, only ammonium pentafluorophenoxide was produced from 2,3,4,5,6-pentafluoroanisole. It was found, however, that, in the reaction of pentafluoroanisole with sodamide in liquid ammonia, normal replacement of a fluorine atom occurred (instead of cleavage of the methoxy group) to give 2,3,5,6-tetrafluoroanisidine. Since the fluoroanisidine formed is amphoteric, such products as the di- and tri-anisylamines were also formed.

a. Diazotization of Pentafluoroaniline

The versatility of the "diazo reactions," i.e., the Sandmeyer reactions, is well known in aromatic chemistry as they provide a means of preparing a variety of compounds not obtainable by other methods. It was of interest, therefore, to determine the usefulness of the Sandmeyer reaction for preparing pentafluoroiodobenzene and bromopentafluorobenzene.

Pentafluoroaniline is weakly basic, reacts slowly with nitrous acid, and dissolves only in concentrated strong acids [23]. On dilution with water, however, the free base is regenerated; this demonstrates that the salt of the amine hydrolyzes readily, which is an important factor in the diazotization process in aqueous solutions. Diazotization of pentafluoroaniline in anhydrous hydrogen fluoride and concentrated sulfuric acid has been studied by us. It can be oxidized to give a variety of products; pentafluoronitrobenzene [26], pentafluoronitrosobenzene [27], and decafluoroazoxybenzene are described herein.

The diazotization of pentafluoroaniline to yield decafluorodiazoaminobenzene, $C_6F_5—N=N—\overset{H}{N}—C_6F_5$, has been reported previously [23], but no experimental details were given. We have found that this compound is obtained when concentrated hydrobromic acid (48%) is used as the reaction medium; its formation may be attributable to the slow diazotization of the amine (rather than to a too low concentration of acid, which is sometimes the cause for this coupling reaction [28]). The reaction also appears to be temperature-dependent, because the rate of formation of the diazoaminobenzene is much faster at 10 °C than at −10 °C. Allowing the latter reaction mixture to warm to 5 °C causes the compound to be precipitated.

Decafluorodiazoaminobenzene can be decomposed in warm hydrobromic acid solution in the presence of cuprous bromide. The products obtained are bromopentafluorobenzene (5.4%) and a mixture of dibromotetrafluorobenzenes (11.7%), presumably the *o*- and *p*-isomers. The isolation of the latter compounds suggests that the diazo group exerts a considerable influence on the *ortho* and *para* fluorine atoms, making possible the replacement with bromide anion. This replacement reaction apparently occurs prior to the decomposition of the diazo group, because bromopentafluorobenzene is stable to concentrated mineral acids [12, 29]. Similar replacement reactions have been observed [23] when the diazotizations were performed under neutral or alkaline conditions.

In such nonaqueous solvents as concentrated sulfuric acid, the diazotization of pentafluoroaniline is extremely slow, even at 25 °C. The addition of glacial acetic acid tends to hasten the reaction slightly. The deep-red color appears only after 24 hrs. Deamination with hypophosphorous acid yields a product believed to be a mixture of pentafluorobenzene and tetrafluorobenzene. These compounds are difficult to separate, even by vapor-phase chromatography. Dilution of the diazo solution with water reprecipitates the yellow diazoaminobenzene, as mentioned previously.

The use of anhydrous liquid hydrogen fluoride as the solvent and reaction medium resulted in a decided improvement in the yield of product. Liquid hydrogen fluoride has found moderate use in diazonium reactions, even though fluorobenzene can be prepared in 86 percent yield from aniline in this medium [30]. We have found that the diazotization of pentafluoroaniline is fairly rapid, even at −25 °C. Pentafluoroidobenzene and bromopentafluorobenzene can be prepared in 50 percent and 35 percent yield, respectively, by normal Sandmeyer reagents (potassium iodide—or potassium bromide—cuprous bromide mixture). No other replacement products were observed during these reactions.

Another synthesis involving diazotization was the attempted preparation of the fluorinated diazo ether $C_6F_5—N=N—O—C_6F_5$. Thermal decomposition of this material could possibly lead to the hitherto unknown perfluorophenyl ether. The product isloted from the reaction of lithium pentafluorophenoxide and the diazotized amine could be extracted into methylene chloride. However, after partial removal of the solvent, the material detonated violently. The instability of some substituted aroyl diazo ethers is well known [28], and our results

indicate that this fluorodiazo ether may also be unstable.

The Sandmeyer nitrile synthesis failed to give any identified products with diazotized pentafluoroaniline. It has been previously observed [12, 29] that cyanide ion has an adverse effect on aromatic fluorine compounds, causing multiple replacement with subsequent decomposition, followed by carbonization. These results indicate that the diazonium reaction may have only limited usefulness in aromatic fluorocarbon chemistry.

b. Oxidation of Pentafluoroaniline

The oxidation of aromatic amines to nitro derivatives has been accomplished previously by using peroxy acids [31, 32, 33]. This procedure can also be applied to pentafluoroaniline [26, 27], and both pentafluoronitrobenzene [26] and pentafluoronitrosobenzene [27] have been synthesized. For oxidation of pentafluoroaniline, we used the conditions described by Holmes [34]. However, instead of the expected pentafluoronitrosobenzene, only decafluoroazoxybenzene was isolated as the final product, regardless of whether the reaction was allowed to proceed at room temperature or if heat was applied: when heat (60 to 75 °C) was used, the reaction proceeded mush faster. Presumably, from the color changes observed during the course of the reaction, it should be feasible to isolate the pentafluoronitrosobenzene by quenching the reaction at the green-color stage. Pentafluoronitrosobenzene has been shown [27] to exist as a monomer. However, one attempt to terminate the reaction at this stage led only to tarry products.

The formation of the decafluoroazoxybenzene as the main product seems to indicate the relative ease of the oxidation of decafluoroazobenzene (orange stage) with excess hydrogen peroxide. This reaction also occurs in the hydrocarbon series. The fact that no pentaflouronitrobenzene was obtained indicates that oxidation is not the sole reaction. In view of the rapid oxidation occurring when 90 percent peroxide was used [26], it would appear that, at the nitroso stage in our work, coupling with unused pentafluoroaniline predominates over further oxidation of the nitroso derivative. These reactions are illustrated as follows:

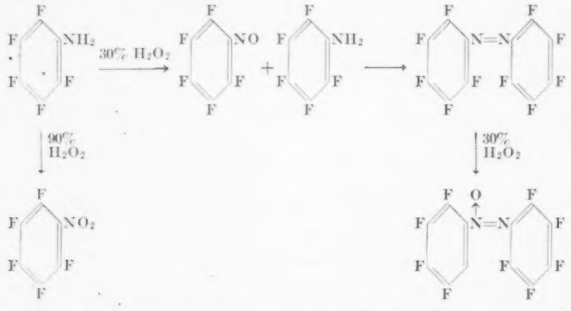

The decafluoroazobenzene can be readily prepared from the azoxy compound by reduction with zinc and ammonium chloride in methanol. Traces of pentafluoroaniline and an additional compound (which may be the decafluorohydroazobenzene) were also obtained.

2.4. Reactions With Organolithium Compounds

In some earlier work from this laboratory, it was found that the Grignard reagent, methylmagnesium bromide, reacts with hexafluorobenzene to produce 2,3,4,5,6-pentafluorotoluene. Under the conditions described [18], the yield was low (3%). Alkyl-, alkenyl-, and aryl-lithium reacted readily to give the corresponding substituted pentafluorobenzenes.

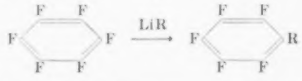

Methyl- and butyl-lithium reacted readily [35], as well as phenyl-, vinyl-, and isopropenyl-lithium [36].

The reactions are rapid, and some di- [35, 36, 37], as well as tri- [26, 35], substituted products were obtained. The preferred method of reaction is usually the addition of a solution of the lithium reagent to a solution of the aromatic fluorocarbon. Even so, disubstitution readily occurs. In the methyllithium reaction, 2,3,5,6-tetrafluoroxylene was identified [37], indicating that the second displacement of fluorine is *para* to the first. The yields of the pentafluorotoluene and 2,3,4,5,6-pentafluorobiphenyl reach 70 percent or higher. Butyllithium has so far given lower yields, but this reagent has been studied relatively little. The alkenyllithium reactions gave yields of the order of 30 to 50 percent, but this is the result of the further reaction of the products to give polymeric solids [38]. The lithium reagents themselves are good catalysts for the anionic polymerization of olefins.

2,3,4,5,6-Pentafluorotoluene can be halogenated to the corresponding benzyl chloride and bromide [37]. With chlorinating reagents, ring addition of halogen interferes with the production of the benzotrichloride [39]. The benzyl halides are versatile reagents for further synthesis of fluoroaryl compounds [37, 39].

In the course of our investigations of the reactions of hexafluorobenzene with organolithium compounds, it was decided to study the reaction of the simplest nucleophile, the hydride ion, with hexafluorobenzene. It was found that hexafluorobenzene does indeed undergo nucleophilic attack by the hydride ion to give pentafluorobenzene as the major product (together with traces of tetrafluorobenzene). The extent of conversion seems to depend on the proportion of lithium aluminum hydride used.

The reaction apparently occurs only when lithium aluminum hydride is the source of the hydride ions. When lithium hydride was employed, no formation of pentafluorobenzene or other products was observed. However, if the lithium hydride was used together with a small quantity of lithium aluminum hydride as a hydrogen carrier [40], a 25-percent conversion to pentafluorobenzene was observed. Again, a very small proportion of disubstitution product was formed; this product was presumably 1,2,4,5-tetrafluorobenzene, since this compound has

been reported to be formed [40] when pentafluorobenzene is treated with lithium aluminum hydride. In the latter case, in addition to the tetrafluorobenzene, a high-boiling liquid is obtained in about 5-percent yield; the residue distils in the range of 80 to 20 °C at 5 mm. (Direct replacement of fluorine atoms by hydrogen atoms on the aromatic nucleus can also be accomplished by the use of hydrogen over platinum-on-carbon at 300 °C [17].)

2.5. Mechanism of Reaction

In this work, the reactivity of hexafluorobenzene toward a great variety of nucleophilic reagents has been explored. No specific investigations of the mechanistic features of the reactions involved were carried out, and the details of the various mechanisms must be left for future studies. No single mechanism is likely to be adequate for all of the reactions reported. In fact, the variety of conditions and reagents examined render it extremely likely that a variety of mechanisms is involved in the reactions reported.

The mechanisms of the nucleophilic reactions of aromatic systems have been reviewed [42, 43, 44]. The effects of solvents on these reactions has, apparently, not yet been investigated in great detail. However, review [45] of the effects of solvation on the properties of anions in dipolar, aprotic solvents discusses many aspects of nucleophilic mechanisms and the role of the solvent in them. In our work a variety of solvents, protic and aprotic, were utilized.

Although no specific kinetic work was carried out, the large amount and variety of results obtained allow certain mechanistic concepts to be developed. It seems evident, for instance, that a benzyne intermediate is not involved in our reported reactions of hexafluorobenzene in which a monosubstituted pentafluorobenzene is produced (even when it is treated with sodamide in liquid ammonia). This reaction of hexafluorobenzene is relatively efficient and is encumbered chiefly by the reactivity of the aniline product, which can react (via the anilide ion) to afford such products as perfluorodiphenylamine [25]. Tetrafluorobenzyne has, however, been reported [46] as a decomposition product of lithium pentafluorophenyl prepared from lithium amalgam and bromopentafluorobenzene. It is apparently stable but quite reactive. It would seem that benzyne formation in alkali-metal amide reactions in liquid ammonia is a secondary aspect of these nucleophilic reactions, although it explains various isomerizations observed in systems containing aromatic hydrogen atoms.

The reactions of hexafluorobenzene with alkali-metal hydroxides and alkoxides, sodamide, and organolithium compounds presumably involve attack on the hexafluorobenzene by negative ions, and it seems evident that, as a rule, unimolecular ionization of the hexafluorobenzene does not occur. The preparation of pentafluorophenol by treating potassium hydroxide in *tert*-butyl alcohol with hexafluorobenzene, and the preparation of benzyloxypentafluorobenzene using sodium benzylate in *tert*-butyl alcohol, indicate this; otherwise, it would be expected that *tert*-butyl pentafluorophenyl ether would have been produced. The use of alcoholic and aqueous amine solutions to produce various anilines in which moieties from the solvents are not part of the final products also indicates absence of any appreciable ionization. Furthermore, no reaction occurs between hexafluorobenzene and pure water up to 300 °C, the highest temperature studied. At the higher temperature, addition of a drop of pyridine led to the rapid formation of tarry material, which gave a phenolic odor on acidification; the quantities of tar or char were approximately proportional to the pyridine added. The effect of aqueous potassium cyanide on hexafluorobenzene was also studied in the temperature range of 150 to 250 °C. Only at 250 °C did a reaction occur. However, no identified products were obtained, but only intractable chars. The reaction was violent and was essentially a contained explosion. Extensive damage to the pressure vessel occurred in one instance, although without violent fragmentation of the vessel. A similar study of the effect of aqueous sodium carbonate showed no reaction up to 250 °C, at which temperature, there were formed extensive tars which again gave a phenolic odor on acidification.

Specific complexes probably play an important role in the reported reactions of hexafluorobenzene. It has been observed that a 1:1 molar mixture of benzene, mp 5.4 °C, and hexafluorobenzene, mp 5.0 °C, forms a solid melting at 23.7 °C [47], which demonstrates the formation of a molecular complex between the two species. Freezing-point data indicate complex-formation between hexafluorobenzene and fluorobenzene also, but not between pentafluorobenzene and benzene [47]. These complexes are presumably similar to the charge-transfer complexes known to form between picric acid and certain aromatic compounds. Benzene and 1,3,5-trinitrobenzene, for instance, form a complex [48] which is certainly of a similar character. With more electron-releasing substituents on a benzene nucleus, a more stable complex should form, as with hexafluorobenzene. In the case of mesitylene and hexafluorobenzene, a complex melting at 24 °C has been observed; one melting at 56 °C is formed between hexafluorobenzene and 2-methylnaphthalene [47]. These observations point to a specific complex-formation as an explanation of the role of pyridine in enhancing the reactivity of hexafluorobenzene in the reactions reported here. In aqueous systems, pyridine may be effecting simple ionization of the hexafluorobenzene.

In the reactions of hexafluorobenzene with ammonia or primary and secondary amines, the mechanism is probably one in which the un-ionized amine directly attacks the fluoroaromatic molecule:

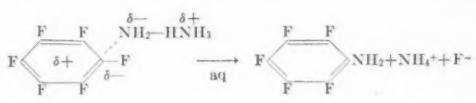

Whether the second ammonia molecule is nearby or

not appears to be unimportant; a transitory hydronium ion would be equally effective.

The action of neutral water species, although obviously much less effective than nitrogen compounds, is likely to be involved to some extent in the formation, for instance, of pentafluorophenol by the reaction of aqueous alkali hydroxides with hexafluorobenzene.

By analogy with the formation of such complexes as that [42] formed by the addition of a methoxide ion to 2,4,6-trinitrophenetole, it is likely that hexafluorobenzene in its reactions with the amide, hydroxy, alkoxy, and alkyl anions forms a relatively stable, transition state.

A somewhat startling and puzzling facet of the reactions of fluorobenzene derivatives is the splitting of the alkoxypentafluorobenzenes by aqueous ammonia or hydrazine [20] and, presumably, by alcoholic potassium hydroxide [18]. In the hydrazine reaction, the hydrazine salt of pentafluorophenol is obtained. This reaction has been postulated to occur via a splitting of the methyl—oxygen link [20], presumably, as shown in the following series of reactions.

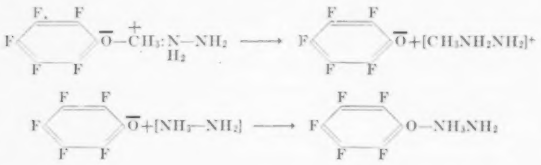

This splitting has only been observed in the presence of water, and is not necessarily related to the basicity of the medium; it does not occur in the liquid ammonia—sodamide reaction, where a fluorine atom is replaced without splitting of the ether link. However, sodamide in liquid ammonia does split anisole. Thus, it is possible that the split occurs at the pentafluorophenyl—oxygen link, and that water is the key reagent. For the reaction to occur at the phenyl—oxygen link, one can logically postulate either an attack by the hydroxide ion, which implies that the ring carbon atom at this site is highly positive, or some direct reaction at this carbon atom with a neutral water molecule. The former implies easier ionization of the phenyl—oxygen link, and not necessarily an enhancement of the positive character of the ring carbon atom linked to the oxygen atom. It is conceivable that the methyl—oxygen link is quite covalent. Since water was present in all of the reactions in which cleavage of the ether moiety was observed, it seems feasible that simple hydrolysis may have occurred. However, distilled water failed to react with pentafluoroanisole under conditions identical with those under which aqueous amine bases produced cleavage. Thus, the role played by the water molecules may simply be as a co-catalyst with the base, to aid polarization of the ether linkage, in much the manner suggested previously for pyridine. Determination of the bond actually ruptured would require experiments with H_2O^{18}.

3. Identification of Isomers

The orientation of the isomers of most of the difunctional derivatives of hexafluorobenzene of the general formula, C_6F_4XY, where X and Y may be similar or dissimilar groups (but not a fluorine atom), has been determined by nuclear magnetic-resonance spectroscopy. Direct syntheses of these derivatives for comparison and identification purposes by alternative routes has been difficult, although this has been accomplished in several cases [22, 25]. Infrared and ultraviolet spectroscopy have so far not found extensive use in identifying structural isomers of aromatic fluorocarbons. In a series of articles, Baker [49, 50] has described the vibrational spectra of *o*-halophenols in the near-infrared region; these compounds show a doubling of the hydroxyl stretching frequencies at low concentrations. This doubling of the hydroxyl band is absent for *para*-substituted halophenols and presumably for *meta*-substituted halophenols, although slight shifts of hydroxyl frequency do occur. Therefore, this method appeared to be a useful supplement to nuclear magnetic-resonance in distinguishing between the isomeric phenols obtained from the reaction of various pentafluorohalobenzenes with alkali hydroxides. The procedure appears to be specific for *o*-halophenols, in particular when the halogen atoms differ, because of the two types of hydrogen bonding that can occur. For example, the structures applied in our case to the 2-bromo-3,4,5,6-tetrafluorophenol are:

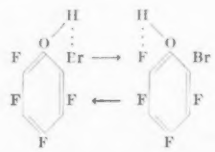

In figure 1–A, this compound exhibits the split hydroxyl band indicative of different halogen atoms, surrounding the hydroxyl group at the *ortho* positions. In this case, the $\Delta\nu$ OH for fluorine is at 2.80 μ, and the $\Delta\nu$ OH for bromine at 2.84 μ is in agreement with values shown by Baker [50]. This doublet is absent from, and only a lone hydroxy band appears in, the spectrum of 4-bromo-2,3,5,6-tetrafluorophenol at 2.80 μ. However, since the 3-bromo-2,4,5,6-tetrafluorophenol is unknown at present, it is impossible to ascertain whether or not the (large) bromine atom at this position would cause some steric effect on the *ortho* fluorine atom so as to change the electron environment whereby a doublet may be obtained instead of the single band. However, as expected, various tetrafluorophenols having substituents in the *para* position show the single hydroxyl band at 2.80 to 2.81 μ, similar to those shown in figure 1–B. Some of these phenols are: 2,3,5,6-tetrafluorophenol, 2,3,4,5,6-pentafluorophenol, 2,3,5,6-tetrafluoro-p-cresol, and 2,3,5,6-tetrafluoro-4-iodophenol. By reverse reasoning, therefore, the absence of the split hydroxyl band in the near-infrared region in these simple

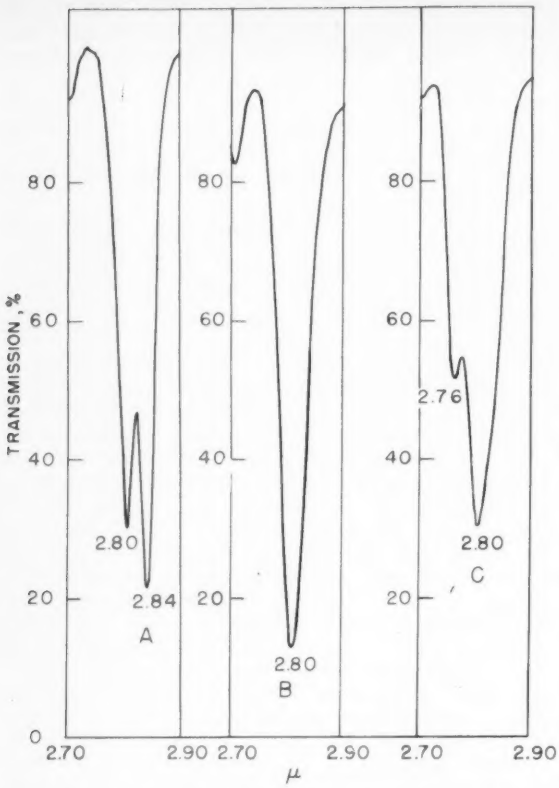

FIGURE 1. *The* OH *spectra of halophenols in carbon tetrachloride.*

A. 2-Bromo-3,4,5,6-tetrafluorophenol;
B. 2-Chloro-trifluoro-α,α,α-trifluoro-*p*-cresol;
C. 2-Chloro-trifluoro-α,α,α-trifluoro-*o*-cresol.

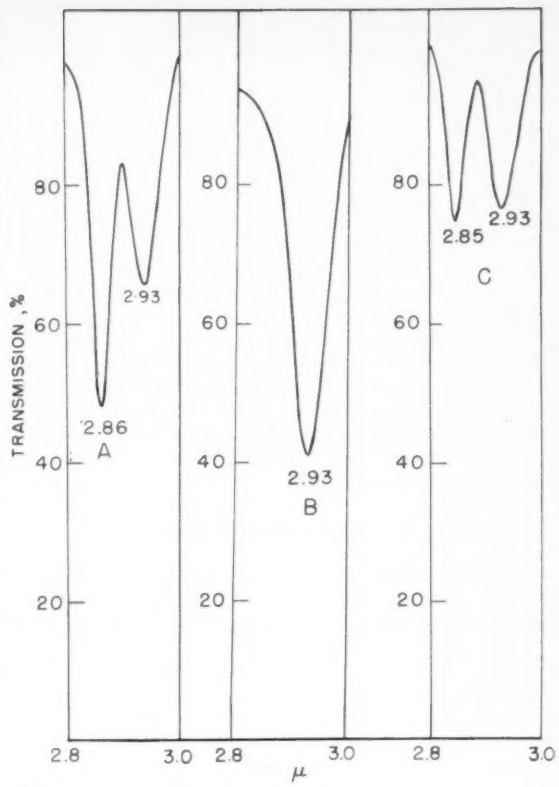

FIGURE 2. *The* NH_2 *and* NH *spectra of haloanilines in carbon tetrachloride.*

A. 2,3,4,5,6-Pentafluoroaniline;
B. 2,3,5,6-Tetrafluoro-1,4-bis(*N*-methylamino)benzene;
C. 2-Chloro-trifluoro-α,α,α-trifluoro-*p*-toluidine.

halophenols is indicative that groups other than fluorine atoms are not *ortho* to each other. These compounds were further confirmed by nuclear magnetic-resonance spectroscopy to be *para* isomers.

An attempt to extend this method of distinguishing isomeric phenols to a more complex molecule has met with partial success. For example, in figures 1–B and 1–C are shown the spectra of two phenolic products obtained from the reaction of 2-chloro-3,4,5,6-tetrafluoro-α,α,α-trifluorotoluene with potassium hydroxide in pyridine. Since, in figure 1–B, only the single hydroxyl band appears, it is obvious that the hydroxyl group is located in either the 4 or the 5 position. From other considerations, the trifluoromethyl group would be expected to exert a greater directive effect than the chlorine atom. In this case, then, the hydroxyl group is probably located *para* to the trifluoromethyl group. However, in figure 1–C, the hydroxyl group would appear to be *ortho* to the trifluoromethyl group, since the $\Delta\nu$ OH for chlorine would be expected to be at a higher wavelength (at 2.82 μ). The band at 2.76 μ may in this instance again arise from the change in frequency of the hydroxyl group because of the two types of hydrogen bonding possible, for example, a five-membered bridge (I) versus a six-membered bridge (II), as shown below:

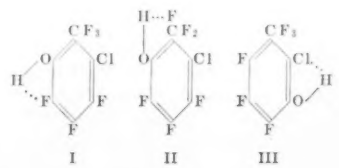

It could be argued that this band may be attributable to a free (*trans*) hydroxyl group, such as occurs with other *ortho*-monohalogenated (Cl, Br, I) phenols, but this doubling has not been observed in *o*-fluorophenol [49]. Similarly, the vapor infrared spectrum of pentafluorophenol has a strong band at 2.75 μ attributed to a free hydroxyl group [19], but, in a nonpolar solvent such as carbon tetrachloride, the band is shifted to a higher wavelength (at 2.80 μ). Therefore, the band observed in figure 1–C at 2.76 μ is probably associated with the *o*-trifluoromethyl group, and not with a free hydroxyl group or an *o*-chlorine atom. On this basis, then, tentative identification of 3-chloro-4,5,6-trifluoro-2-(α,α,α-trifluoromethyl) phenol has been made, and the com-

pound has been assigned the structures shown in I and II.

Attempts to apply this "*ortho* effect" to other derivatives of hexafluorobenzene, particularly to the aniline compounds, has been fruitless. For example, in the near-infrared region, 2,3,4,5,6-pentafluoroaniline shows two distinct peaks, at 2.86 μ and 2.93 μ (fig. 2–A). This is also true of 3-chloro-2,5,6-trifluoro-4-(α,α,α-trifluoromethyl)aniline, figure 2–C. In these aniline derivatives, the bands appear to be associated with the number of hydrogen atoms on the nitrogen atom. Replacing one of the hydrogen atoms by a methyl group merely eliminates one of the bands. This is also evident in figure 2–B, even though the compound contains two methylamino groups. Further evidence is obtained from the fact that 2,3,4,5,6-pentafluoro-*N*,*N*-dimethylaniline does not have an absorption band in this region. However; this near-infrared region does offer the possibility of distinguishing between primary, secondary, and tertiary fluoroanilines.

4. Directional Effects

A considerable number of disubstituted (nonfluorine groups) derivatives of tetrafluorobenzene have been prepared and their structures confirmed by unequivocal means. The directional effects determining the site of the second substitution in the electrophilic reaction of benzene has been the subject of much investigation. These effects are directly related to the charge distribution in the monosubstituted benzene and can be estimated from dipole-moment data [51]. Dipole moments of some fluorobenzenes have been reported [52]. The compounds studied do not, however, include any pentafluorobenzenes. The present work affords an insight into the character of the directional effects in polyfluorobenzenes. In table 1 are summarized these effects as observed from the reactions of various bases with a variety of monosubstituted pentafluorobenzenes. For example, the reaction of pentafluorobenzene, where R=H, with potassium hydroxide yields the 2,3,5,6-tetrafluorophenol. On further examination of table 1, it is apparent that, from the three possible isomers, the *para* product was obtained in most cases. This was true even though a great variety of conditions was used. It seems, therefore, that the isomer finally obtained depends on a number of involved parameters rather than on any single condition. From table 1, it is also evident that, in those cases where very reactive nucleophiles (such as the amide ion, lithium reagents, or alkoxides) were used, the *para* product was always isolated. These bases react to form salts with such functional groups as amines or hydroxyl groups, and no displacement of fluorine occurs.

With less reactive nucleophiles, such as aqueous hydroxides, ammonia, or alkylamines, isomers other than the *para* were *also* isolated. However, in these reactions, the isomer obtained probably depends to a large degree on the group (R) *already* present in the molecule, as well as on the nucleophile used. For example, the nitro group in pentafluoronitrobenzene exerts a powerful influence on the *ortho* positions, and, on reaction with ammonia, gives almost theoretical yields of *o*- and *p*-nitroamines in 7:3 ratio. Conversely, the amino group in pentafluoroaniline exhibits a strong influence in nucleophilic reactions at the *meta* position; as a result, the *m*-diamine is, with ammonia, the primary reaction-product. But the reaction of methylamine with pentafluoro-*N*-methylaniline yields only the *para* isomer, whereas the reaction of pentafluoro-*N*,*N*-dimethylaniline with dimethylamine yields the *para*, *meta*, and *ortho* isomers in a 10:4:1 ratio. Although the reactions of these amines appear to be "anomalous," a point could be made of the fact that the methyl- and dimethylamines are stronger nucleophiles than ammonia. In this case, then, the *para* structure would be the expected predominant isomer, which, indeed, it was. Similarly, it has been observed that the reaction of pentafluoro-*N*,*N*-dimethylaniline with ethoxide ion results in only the *para* product. It is likely that not only the attacking nucleophile but also the resonance effects (due to nonfluorine groups) determine the isomer(s) that are obtained. The ease of fluorine displacement is probably increased by the ability of the solvent molecules to localize the electron density around this fluorine atom. Consideration must also be given to the possibility that resonance effects in the ground state may be altered in the transition state by the relative reactivity of the attacking nucleophile, thereby making possible the attack at a position other than the preferred site. For example, consider the following two structures

TABLE 1. *Orientational effects of* C_6F_5R *with nucleophiles* [a]

Base \ R	H	Br	I	CH_3	OCH_3	$O\Phi$	$OCH_2\Phi$	Φ	NO_2	NH_2	$NHCH_3$	$N(CH_3)_2$
CH_3ONa	*p*	*p*	*p*		*p*							
C_2H_5ONa						*p*						*p*
C_6H_5ONa												
KOH	*p*	*p*>*o*	*p*	*p*								
NaSH	*p*											
CH_3Li				*p*								
C_6H_5Li		E						*p*				
C_6H_5Li												
$NaNH_2$					*p*					S		
NH_3	*p*	*p*	*p*		C		*p*		*o*>*p*	*m*>*p*		
CH_3NH_2											*p*	
$(CH_3)_2NH$												*p*>*m*>*o*
NH_2NH_2	*p*>*o*>*m*											
$LiAlH_4$	*p*>*o*>*m*											

[a] *o*=*ortho*; *m*=*meta*; *p*=*para*; S=salt formation; C=cleavage of ether moiety; E=exchange (−78 °C).

from simple charge [2] effects:

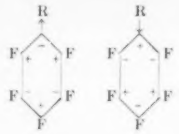

(1) (2)

In (1), the incoming anion, $-R_1$, would be expected to attack at the electron-deficient *ortho* and *para* positions, giving rise to either *ortho* or *para* products. In (1), if $R = NO_2$, the ground state could be visualized as shown, and the transition state as either (3) or (4).

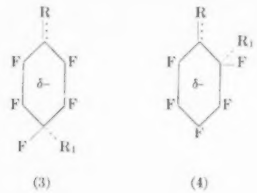

(3) (4)

The *o*- and *p*-nitroamines obtained indicate occurrence of this mode of reaction for pentafluoronitrobenzene, and it is doubtful whether use of a stronger nucleophile would alter the outcome. In (2), if $R = NH_2$ (an electron-donating group), the *meta* position relative to R appears to be the preferred site, and *meta* products would be expected. With a base such as ammonia, this is indeed the case. From consideration of the possible resonance structures (5) to (7a), it would appear that (7) is the predominant reacting species with a weak base, since the *meta* positions

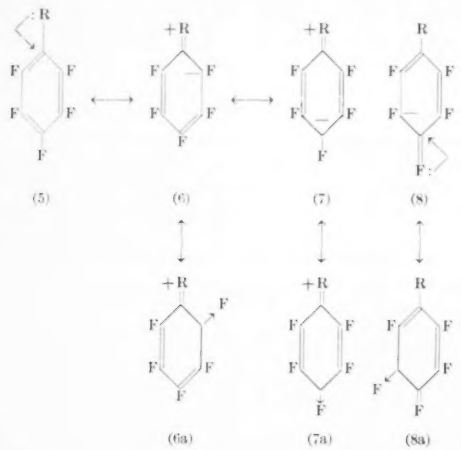

(5) (6) (7) (8)

(6a) (7a) (8a)

appear least negative. An alternative explanation could be offered in that a resonance structure, as in (8a), could be the reacting species. The induced charge would "prefer" to reside closer to the fluorine atom than to the carbon atom, and this effect would favor separation of a fluoride ion. Reaction would then be expected to occur at this site, giving rise to *meta* products. Effects similar to these have been used to explain the decrease in acidity of *p*-fluorophenol [53]. On the other hand, following similar reasoning, the resonance form (7a) would be expected to afford *para* products. This structure (7a) again appears to be the reacting species in the reaction of pentafluoro-*N*-methylaniline with methylamine, because only the *para* isomer was isolated. All three isomers were obtained with dimethylamine and pentafluoro-*N*,*N*-dimethylaniline. This indicates much less selectivity in structures (6a), (7a), and (8a), although the para isomer was obtained in greater proportions (somewhat surprisingly, since methylamine and dimethylamine have about equal basicity). In several other reactions also, all three isomers have been detected. Refluxing of pentafluorobenzene with lithium aluminum hydride in ether produces *o*:*m*:*p* isomers of tetrafluorobenzene in 7:1:92 ratio, the orientational prefixes referring to the relative positions of the *hydrogen* atoms [54]. On treating pentafluorobenzene with ethanolic hydrazine, an *o*:*m*:*p* distribution of 6:1:93 is obtained [52]. Sodium hydrogen sulfide reacts with pentafluorobenzene in a glycol—pyridine mixture to yield only 2,3,5,6-tetrafluorothiophenol [55].

The reactions of pentafluoroanisole with bases yield additional information regarding directional effects of the anilines, since the amino and methoxyl groups have nearly equivalent influence on electrophilic substitution. However, the reaction of pentafluoroanisole with aqueous ammonia causes cleavage of the ether moiety. Resonance structures, such as (9), probably aid in the cleavage reaction.

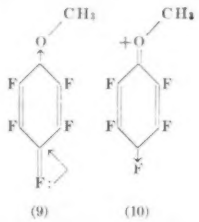

(9) (10)

Other factors (such as solvent, and the ability of various groups to coordinate with the oxygen atom) also play an important role. The reaction with aqueous bases, therefore, simply becomes a competition between cleavage and replacement. With strong nucleophiles, such as amide ion or methoxide ion, only substitution occurs, presumably through a resonance form (10). In fact, such structures as (6a), (7a), and (10) appear to explain the majority of the products observed in nucleophilic reactions of aromatic fluorocarbons. For, if such forms as (8a), (6), and (7) were major contributing resonance forms, it should be possible to isolate *meta* products from most of the reactions encountered, which has not been the case. The effects, in general, do not show any specific differences qualitatively incompatible with the usual interpretations of directional effects in electrophilic reactions of monosubstituted benzenes. The predominance of *para* substitution

suggests that the most important effect is simply an inductive one, since few of the monosubstituents can compete in electron withdrawability with fluorine. A much greater knowledge of the mechanisms of these reactions is needed before the directional effects can be satisfactorily classified.

5. Experimental Procedure

5.1. Reaction With Hydroxides

a. 2,3,4,5,6-Pentafluorophenol

In a 188-ml bomb were placed 40 g (0.207 mole) of hexafluorobenzene, 26.5 g (0.39 mole) of 85 percent potassium hydroxide, and 75 ml of distilled water. The bomb was sealed and heated at 175 °C for 5 hr with agitation. It was then cooled and opened, and the contents were filtered. The white salt of potassium pentafluorophenoxide hydrate was acidified with dilute hydrochloric acid, and the pentafluorophenol was separated from the aqueous phase. The aqueous solution was extracted several times with 50-ml portions of dichloromethane. The organic layers were combined, dried (sodium sulfate), evaporated, and distilled. After removal of the solvent, there was obtained 33.1 g (83.5%) of pentafluorophenol, bp 144 to 145 °C.

b. 2,3,5,6-Tetrafluorophenol

In a 500-ml, three-necked flask were placed 67 g (0.4 mole) of pentafluorobenzene, 21.6 g (0.4 mole) of potassium hydroxide, 150 ml of pyridine, and 2 ml of water. The contents were heated to reflux with vigorous stirring, and reflux was continued for 1 hr after the hydroxide had dissolved. Then, 21.6 g (0.4 mole) of potassium hydroxide was added through the condenser, and heating and stirring were continued for 24 hr. The pyridine was removed by distillation under reduced pressure, and the residue was recrystallized twice from water, yielding 70 g of potassium tetrafluorophenoxide dihydrate. The salt was acidified with dilute hydrochloric acid, the phenol was separated and dissolved in dichloromethane, and the solution was dried (sodium sulfate), evaporated, and distilled under reduced pressure, bp 47 °C/20 mm. Yield: 21 g (32% based on pentafluorobenzene). The structure of the compound was verified by nuclear magnetic-resonance spectra due to fluorine atoms.

Analysis: Calculated for $C_6H_2F_4O$: C, 43.3; H, 1.2. Found: C, 43.5; H, 1.5.

c. 2,3,5,6-Tetrafluoro-*p*-cresol

In a 500-ml, three-necked flask, a mixture of 36 g (0.2 mole) of pentafluorotoluene, 28 g (0.5 mole) of potassium hydroxide, and 300 ml of *tert*-butyl alcohol was refluxed, with stirring, for 2 hr. The flask was cooled and 100 ml of water was added, after which 100 ml of the alcohol was distilled off. This process was repeated until all of the alcohol had been removed, the temperature of the takeoff rising from 73 to 100 °C. The distillation was continued until 6 g of pentafluorotoluene had been recovered. The residue was made acid with dilute hydrochloric acid, cooled, extracted with three 100-ml portions of ether, and the extracts were dried (sodium sulfate) overnight. After evaporation of the ether, the black, oily residue was sublimed twice, yielding 12 g (32%) of white crystals; mp 52 °C. Fluorine and proton absorption in the nuclear magnetic-resonance spectra confirmed the structure.

Analysis: Calculated for $C_7F_4H_4O$: C, 46.6; H, 2.2. Found: C, 46.3; H, 2.4.

d. 2,3,5,6-Tetrafluoro-4-iodophenol

To 20 g (0.068 mole) of pentafluoroiodobenzene in 100 ml of pyridine were added 2 g (0.136 mole) of potassium hydroxide and 1 ml of water, and the mixture was refluxed for 4 hr. At the end of this period, an additional 2 g of potassium hydroxide was added and the mixture was refluxed for an additional 8 hr. After being cooled, 300 ml of 10% aqueous hydrochloric acid was added, and the crude, yellow tetrafluoroiodophenol (10.1 g) was removed by filtration. Extraction of the aqueous layers with two 100-ml portions of dichloromethane gave an additional 2 g of the phenol. Net yield (based on pentafluoroiodobenzene, 1.5 g of which was recovered): 66 percent.

The tetrafluoroiodophenol was recrystallized from ether—petroleum ether as white plates, mp 79 to 81 °C. Nuclear magnetic resonance showed this to be the *para* isomer; no other isomer was isolated. The near-infrared absorption spectrum showed only one hydroxyl peak, at 2.81 μ.

The benzoate was prepared in the usual way. Recrystallization from ether—petroleum ether, followed by vacuum sublimation (60 °C/1 mm), gave white microcrystals, mp 59 to 60.2 °C.

Analysis: Calculated for $C_{13}H_5F_4IO_2$: C, 39.41; H, 1.26; F, 19.1; I, 32.04. Found: C, 40.0; H, 1.35; F, 18.8; I, 31.9.

e. Bromotetrafluorophenols

The preparation of the bromotetrafluorophenols is essentially the same as that for the tetrafluoroiodophenol, except that the following quantities were used: 66 g (0.26 mole) of bromopentafluorobenzene, 150 ml of pyridine, 1 ml of water, and 28.5 g (0.53 mole) of potassium hydroxide. After acidification of the reaction mixture, the products were extracted with three 100-ml portions of dichloromethane. The combined extracts were dried (sodium sulfate) and the solvent was evaporated. Vacuum distillation of the residual liquid gave 10.5 g (16%) of unreacted bromopentafluorobenzene and two phenolic fractions.

Fraction 1: 31 g (56.3%); bp 73 to 75 °C/2 mm; mp 19 to 21 °C; was shown by analytical, vapor-phase chromatography (Viton A column at 175 °C) to be a mixture of two components in a 3:1 ratio.

One component was 2-bromo-3,4,5,6-tetrafluorophenol, 3.5 g (6.3%), mp 41 to 43 °C. Nuclear magnetic-resonance spectra showed this compound to be the *ortho* isomer. This is also evident from

the near-infrared spectra, which showed a split hydroxyl peak at 2.81 μ and 2.84 μ, presumably due to the two types of hydrogen bonding that can occur.

The 3,5-dinitrobenzoate had mp 104 to 105 °C.

Analysis: Calculated for $C_{13}H_3BrF_4N_2O_6$: C, 35.6; H, 0.69; Br, 18.1. Found: C, 35.7; H, 0.7; Br, 18.7.

The second (and main) component of fraction 1 was 4-bromo-2,3,5,6-tetrafluorophenol, 11.5 g (20.9%). The 3,5-dinitrobenzoate had mp 131 to 133 °C.

Analysis: Calculated for $C_{13}H_3BrF_4N_2O_6$: C, 35.6; H, 0.69; Br, 18.1. Found: C, 35.4; H, 0.6; Br, 20.3.

Fraction 2: 4 g (7.2%); bp 90 to 92 °C/2 mm; mp 58 to 60 °C; was shown by nuclear magnetic resonance to be 4-bromo-2,3,5,6-tetrafluorophenol. Also, the near-infrared absorption spectrum showed only one peak in the 2.8-μ region. The 3,5-dinitrobenzoate had mp 133 to 134 °C. There was no depression of melting point on mixing the 3,5-dinitrobenzoate of this fraction with that of the second component of fraction 1.

f. 2-Chlorotrifluoro-α,α,α-trifluoro-*o*-(and-*p*-)Cresols

To 100 g (0.4 mole) of 2-chlorotetrafluoro-α,α,α-trifluorotoluene in 100 ml of pyridine were added 45.6 g (0.8 mole) of potassium hydroxide and 1 ml of water. The mixture was slowly heated to 90 °C for 2 hr with stirring, cooled, poured into 1 liter of 20 percent sulfuric acid, and allowed to settle overnight. It was filtered, and the bottom (fluorocarbon) layer was separated from the aqueous filtrate. The aqueous layer was further extracted with several 100-ml portions of ether. The combined organic layers were dried (sodium sulfate) and the solvent removed, yielding 38 g (38.6%) of a mixture of two isomeric cresols, bp 97 to 103 °C/15 mm. The components were separated by preparative vapor-phase chromatography using a Viton A column at 190 °C. The first compound eluted was 2-chlorotrifluoro-α,α,α-trifluoro-*o*-cresol: 0.5 g; bp 92 to 93 °C/15 mm; n_D^{24} 1.4510; infrared absorption showed a split hydroxyl band, at 2.76 μ and 2.81 μ. The second compound was 2-chlorotrifluoro-α,α,α-trifluoro-*p*-cresol: 15 g; bp 102 to 103 °C/15 mm; n_D^{24} 1.4510; infrared absorption showed only one (strong) hydroxyl band, at 2.81 μ.

5.2. Reactions With Alkoxides

a. 4-Bromo-2,3,5,6-tetrafluoroanisole

A solution of 11.5 g (0.5 g-atom) of sodium in 150 ml of anhydrous methanol was added dropwise to a stirred solution of 123.5 g (0.5 mole) of bromopentafluorobenzene in 70 ml of dry pyridine at reflux temperature. The addition required 1.5 hr; refluxing was continued for an additional 15 hr. The mixture was cooled and poured into 1 liter of 10 percent aqueous hydrochloric acid. The usual isolation, as described above, gave 89 g (68.8%) of bromotetrafluoroanisole, bp 76 to 79 °C/5 mm. Analytical vapor-phase chromatography (Viton A column at 175 °C) showed slight contamination of the product with another compound. Separation was accomplished by preparative scale vapor-phase chromatography, using 10-g samples (Viton A column at 175 °C). The fore-cut, 8 g, still gave two peaks. The (main) second fraction, 66 g, showed only one peak in analytical vapor-phase chromatography; bp 79 to 81 °C/5 mm; n_D^{25} 1.4812. Nuclear magnetic resonance showed this to be the *para* isomer.

Analysis: Calculated for $C_7H_3BrF_4O$: C, 32.4; H, 1.2; Br, 30.9. Found: C, 32.7; H, 1.3; Br, 31.9.

A higher-boiling fraction (2 g), 72 to 76 °C/2 mm, had three components; these were not investigated further.

b. 2,3,5,6-Tetrafluoro-4-iodoanisole

To a stirred solution of 10 g (0.034 mole) of pentafluoroiodobenzene and 50 ml of dry pyridine, heated to reflux temperature, was added a solution of 0.8 g (0.034 g-atom) of sodium in 15 ml of anhydrous methanol. After being refluxed for 3 hr, the cooled solution was poured into 100 ml of 6 *N* aqueous hydrochloric acid. The orange (fluorocarbon) layer was separated, and the aqueous layer extracted twice with 50-ml portions of ether. The combined organic layers were dried (sodium sulfate), evaporated, and distilled. After removal of the unreacted pentafluoroiodobenzene (1.5 g), there was obtained 5.5 g (63% based on reacted pentafluoroiodobenzene) of 2,3,5,6-tetrafluoro-4-iodoanisole; bp 113 to 115 °C/20 mm; n_D^{22} 1.5229; the structure was confirmed by nuclear magnetic resonance. Analytical, vapor-phase chromatography (at 190 °C) showed a 3-percent contamination with starting material. The sample was redistilled before elementary analysis.

Analysis: Calculated for $C_7H_3F_4IO$: C, 27.48; H, 0.98; F, 24.83; I, 41.48. Found: C, 27.8; H, 1.0; F, 24.4; I, 41.0.

c. Octafluoro-4,4′-dimethoxybiphenyl

A mixture of 1 g of 2,3,5,6-tetrafluoro-4-iodoanisole and 1 g of activated copper powder was gently refluxed for 12 min, cooled, and extracted first with 10 ml of acetone and then with 10 ml of benzene. The combined extracts were filtered and the solvents evaporated. The yellow solid obtained was decolorized with charcoal, and recrystallized from petroleum ether. There was obtained 0.2 g (17%) of octafluoro-4,4′-dimethoxybiphenyl as white plates; mp 90 to 91.2 °C.

Analysis: Calculated for $C_{14}H_6F_8O_2$: C, 46.94; H, 1.69; F, 42.44. Found: C, 47.5; H, 1.88; F, 42.8.

d. Benzyl Pentafluorophenyl Ether

Method A. In a 500-ml flask equipped with stirrer and reflux condenser, 9 g (0.4 g-atom) of sodium was treated with 250 ml of benzyl alcohol, and the solution cooled overnight. Then, 75 g (0.41 mole) of hexafluorobenzene was added, stirring was resumed, and the mixture slowly heated to the reflux temperature of hexafluorobenzene. Heating and stirring were continued for 24 hr, and then the mixture was cooled overnight with stirring. The

691-886—63——7

precipitate was filtered off with suction, the filtrate was concentrated, ethanol was added, and the resulting solution was refrigerated. The resulting precipitate was recrystallized until a constant melting point (44 °C) was obtained; yield, 30 g (28%) of white crystals.

Method B. In a 500-ml flask, 4.6 g (0.2 mole) of sodium was added to a solution of 22 g of benzyl alcohol in 250 ml of *tert*-butyl alcohol. The solution was cooled overnight and 40 g of hexafluorobenzene (0.22 mole) was added. The solution was stirred and refluxed for 40 hr, after which the alcohols were distilled off. The product was recrystallized twice from ethanol; yield, 33 g (60%); mp 44 °C.

Analysis: Calculated for $C_{13}F_8H_7O$: C, 56.9; H, 2.6. Found: C, 56.8; H, 2.6.

e. 2,3,4,5,6-Pentafluorophenyl Ether and 2,3,5,6-Tetrafluoro-1,4-diphenoxybenzene

Method A. To 8 g (0.043 mole) of hexafluorobenzene in 30 ml of *N,N*-dimethylformamide was added 5.28 g (0.04 mole) of potassium phenoxide in one portion at room temperature. After the initial reaction had ceased, the mixture was heated at 120 °C for 0.5 hr, cooled, and diluted with 100 ml of water. The bottom (fluorocarbon) layer eventually solidified, and the white solid was separated by filtration. After drying, and fractional sublimation at 70 °C/1 mm, there was obtained 3.5 g (31.3%) of 2,3,4,5,6-pentafluorophenyl phenyl ether, mp 28 to 29 °C. This compound was identical with that described under Method B.

There was also obtained 1 g (7%) of 2,3,5,6-tetrafluoro-1,4-diphenoxybenzene as white crystals, mp 147 to 149 °C.

Analysis: Calculated for $C_{18}H_{10}F_4O_2$: C, 64.6; H, 2.99; F, 22.7. Found: C, 64.75; H, 2.98; F, 23.1.

Method B. In a 43-ml bomb were placed 11 g (0.05 mole) of potassium pentafluorophenoxide, 15 g (0.10 mole) of bromobenzene, and 1 g of copper which had been activated by Vogel's method [56]. The bomb was heated to 210 °C with rocking, maintained at this temperature for 6 hr, and rocked overnight as it cooled to room temperature. The mixture was filtered and the filtrate distilled through a short column. After the excess bromobenzene had been removed, 2 g (15.5%, based on the potassium salt of 2,3,4,5,6-pentafluorophenol) of 2,3,4,5,6-pentafluorophenyl phenyl ether was obtained, which boiled at 240 °C and solidified slightly below room temperature.

Analysis: Calculated for $C_{12}H_5F_5O$: C, 55.4; H, 1.9. Found: C, 55.7; H, 2.1.

f. Perfluorophenyl Ethers

To 30 ml of *N,N*-dimethylformamide was added 6 g (0.027 mole) of potassium pentafluorophenoxide and 12.8 g (0.069 mole) of hexafluorobenzene; heat was not evolved. After being refluxed for 14 hr, the black solution was poured into 100 ml of water, and the mixture was extracted with several 50-ml portions of ether. The organic layer was separated, dried (sodium sulfate), and evaporated. After the removal of 4.5 g of unreacted hexafluorobenzene, the residual solid was sublimed at 50 °C/50 mm to give 1.5 g (16%) of perfluorophenyl ether; white crystals, mp 67 to 69 °C. Confirmation of the structure was obtained from mass-spectrometer analysis, which showed the parent peak at 350 mass units.

Analysis: Calculated for $C_{12}F_{10}O$: C, 41.15; F, 54.3. Found: C, 41.53; F, 53.0; H, 0.0.

A second product was obtained from the sublimation; mp 145 to 148 °C. Although its structure has not been confirmed, it may be *p*-bis(pentafluorophenoxy)2,3,5,6-tetrafluorobenzene.

g. 4-Ethoxy-2,3,5,6-tetrafluoro-*N,N*-dimethylamine

In a 100-ml flask, 0.6 g of sodium was dissolved in 50 ml of absolute ethanol and the solution was refluxed for 1 hr. To this solution was added 5.3 g (0.025 mole) of 2,3,4,5,6-pentafluoro-*N,N*-dimethylaniline, and the mixture was refluxed for 2 hr and poured into an excess of water. The organic layer was separated, washed with water, dried, and distilled. Yield: 5.1 g (85%) of a clear, colorless liquid boiling at 34 °C/1 mm.

Analysis: Calculated for $C_{10}H_{11}F_4NO$: C, 50.6; H, 4.7; N, 5.9; F, 32.1. Found: C, 50.8; H, 5.0; N, 5.9.

5.3. Reactions With Amines

a. 2,3,4,5,6-Pentafluoroaniline

The reactions using ammonia or amines were carried out in a stainless-steel, silver-lined bomb. A mixture of 280 g (1.5 mole) of hexafluorobenzene and 400 ml of 28-percent aqueous ammonia was sealed in an 800-ml bomb, which was placed in a heater-rocker mechanism previously heated to 235 °C. The bomb was rocked for 2 hr at 235 °C, removed, and rapidly cooled to room temperature in running water. The contents were poured into a large beaker, and the aqueous layer was separated and extracted three times with ether. The ether extracts were dried (sodium sulfate), and evaporated. The substituted aniline obtained in this way was added to the oily layer from the bomb, and the mixture was evacuated in a vacuum desiccator for 8 hr, the volatile materials, mostly hexafluorobenzene and ammonia, being collected in a dry ice—acetone trap. The residual mass of brown crystals was partially sublimed at atmospheric pressure onto a cold-finger condenser, to yield 236 g (86%) of white crystals of pentafluoroaniline; mp 34 °C.

The remainder of residue was heated to about 75 °C at less than 1 mm pressure. White crystals lacking a definite melting point sublimed onto the cold finger. Yield: 28 g (10%). Elementary analysis indicated it to be tetrafluorophenylenediamine, and nuclear magnetic resonance indicated it to be the *meta* isomer contaminated with a small proportion of the *para* isomer.

Analysis: Calculated for $C_6H_4F_4N_2$: C, 40.0; H, 2.2; N, 15.5. Found: C, 40.2; H, 2.4; N, 15.2.

b. 2,3,4,5,6-Pentafluoro-*N*-methylaniline

In a 200-ml bomb, 56 g of hexafluorobenzene and 110 ml of 30-percent aqueous methylamine were heated at 220 °C for 3 hr with continuous rocking. The products were dissolved in ether and the ether was evaported. The pentafluoro-*N*-methylaniline was distilled at atmospheric pressure, and redistilled under reduced pressure. Yield; 59 percent; bp 170 to 172 °C at 760 mm.

Analysis: Calculated for $C_7H_4F_5N$: C, 42.6; H, 2.1; N, 7.1. Found: C, 42.7; H, 2.2; N, 7.0.

The residue was crystallized from absolute alcohol, yielding 2,3,5,6-tetrafluoro-*N*,*N'*-dimethylphenylenediamine, which was purified by sublimation and recrystallization. Yield: 25 percent; mp 94 °C.

Analysis: Calculated for $C_8H_8F_4N_2$: C, 46.2; H, 3.8; N, 13.5. Found: C, 46.1; H, 3.9; N, 13.6.

c. 2,3,4,5,6-Pentafluoro-*N*,*N*-dimethylaniline

A mixture of 110 ml of 25-percent aqueous dimethylamine and 50 g of hexafluorobenzene was heated at 235 °C for 2 hr. The reaction products were purified as described for pentafluoroaniline. A colorless liquid which distilled at 88 °C/1 mm was pentafluoro-*N*,*N*-dimethylaniline (65% of the oily layer). Four additional fractions were collected.

Analysis: Calculated for $C_8H_6F_5N$: C, 45.6; H, 2.6; N, 6.6. Found: C, 45.7; H, 2.8; N, 6.5.

Fraction 2, bp 88 to 126 °C/1 mm, was identified by vapor-phase chromatography to be a mixture of dimethylaniline with three other compounds. *Fraction 3*, bp 126 to 134 °C/1 mm, contained the three isomers of bis(dimethylamino)tetrafluorobenzene, with the *meta* isomer predominant. *Fraction 4*, bp 134 to 140 °C/1 mm, contained equal amounts of *m*- and *p*-isomer. *Fraction 5*, bp 140 to 148 °C/1 mm, was almost pure *p*-isomer. Analysis for C, H, and N indicated the same elementary composition for all fractions.

Analysis: Calculated for $C_{10}H_{12}F_4N_2$: C, 50.9; H, 5.1; N, 11.8. Found: C, 50.9; H, 5.1; N, 11.7.

Nuclear magnetic resonance analysis showed that the predominant isomer in Fraction 3 had three different fluorine-bond peaks, one twice as large as the other two, indicating the *meta* isomer; the high-boiling isomer (Fraction 5) showed only one fluorine bond and was, therefore, the *para* compound. The *meta* and *para* isomers were obtained relatively pure by vapor-phase chromatography; the *ortho* isomer was present in such small proportion as to warrant no further purification.

d. *p*-Bromotetrafluoroaniline

Thirty grams of bromopentafluorobenzene and 70 ml of 28-percent ammonium hydroxide were placed in a 110-ml bomb, heated to 200 °C, and shaken at this temperature for 2 hr. The product was purified as previously described for pentafluoroaniline. The yield of crystalline product, mp 61 °C, was 22 g (77%). Nuclear magnetic resonance indicated that the compound was the *para* isomer.

Analysis: Calculated for $C_6H_2BrF_4N$: C, 29.5; H, 0.8; N, 5.7; Br, 32.7. Found: C, 29.4; H, 0.8; N, 5.8; Br, 32.8.

e. Tetrafluoro-*p*-iodoaniline

Sixteen grams of pentafluoroiodobenzene and 30 ml of 8-percent aqueous ammonium hydroxide were heated to 165 °C in a 43-ml bomb and shaken at this temperature for 2 hr. The product was purified as described previously, except that, after sublimation, the compound was recrystallized from petroleum ether, yielding 7.6 g (46.7%) of slightly yellow crystals; mp 77 °C. Nuclear magnetic-resonance spectra indicated it to be the *para* isomer.

Analysis: Calculated for $C_6H_2F_4IN$: C, 24.7; H, 0.7; N, 4.8; I, 43.6. Found: C, 24.7; H, 0.8; N, 4.6; I, 42.9.

f. *p*-(Benzyloxy)tetrafluoroaniline

Twenty grams of benzyl pentafluorophenyl ether and a large excess of 28-percent aqueous ammonium hydroxide were heated in a 110-ml bomb to 160 °C and shaken at this temperature for 2 hr. A small amount of white crystals was observed clinging to the inside of the bomb. This material was removed and recrystallized three times from ethanol. Yield: 3 g (13%) of slightly yellow needles, mp 97 °C; it was shown by nuclear magnetic resonance to be the *para* isomer.

Analysis: Calculated for $C_{13}H_9F_4NO$: C, 53.1; H, 3.3; N, 5.1. Found: C, 53.0; H, 3.4; N, 4.9.

g. 2-Chlorotrifluoro-α,α,α-trifluoro-*p*-toluidine

A mixture of 50 g of 2-chlorotetrafluoro-α, α, α-trifluoro-toluene and 120 ml of 28-percent ammonium hydroxide was heated to 210 °C in a 200-ml bomb and shaken at this temperature for 2 hr; the crude substituted toluidine was purified by sublimation, giving 22 g (43%) of white crystals which readily decomposed at room temperature in the presence of air (accounting for discrepancies in the analysis).

Analysis: Calculated for $C_7H_2ClF_6N$: C, 33.7; H, 0.8; N, 5.6; Cl, 14.2. Found: C, 32.6; H, 1.1; N, 6.2; Cl, 14.9.

h. 2,3,5,6-Tetrafluoro-*p*-anisidine

To 100 ml of anhydrous liquid ammonia and 0.1 g of ferric nitrate at −70 °C was added, in small pieces, 2.99 g (0.13 g-atom) of sodium. When the blue color had permanently disappeared, 25 g (0.13 mole) of pentafluoroanisole was added slowly during 45 min. The mixture was stirred for 5 hr at −70 °C, and the ammonia was allowed to evaporate overnight at room temperature. After the addition of 100 ml of water, the fluorocarbon layer was separated, and the aqueous layer was extracted with three 50-ml portions of dichloromethane. The unreacted pentafluoroanisole, 7 g (28%), was removed by distillation; bp 137 to 138 °C. By vacuum sublimation (80 °C/1 mm) of the residue, tetrafluoro-*p*-anisidine, 2.8 g (14% based on reacted penta-

fluoroanisole), was obtained as white needles, mp 75 to 76.5 °C; the structure was identified by nuclear magnetic resonance.

Analysis: Calculated for $C_7H_3F_4NO$: C, 45.05; H, 2.56; N, 7.19. Found: C, 43.10; H, 2.7; N, 7.1.

After removal of the above compound, the residue liquefied, and 1.2 g (6.7%) of solid 4,4′-dimethoxyoctafluorodiphenylamine was obtained by distillation, bp 80 to 82 °C/1 mm. Sublimation at 80 °C/1 mm, and recrystallization from petroleum ether gave white needles, mp 78 to 79 °C. The melting point of a mixture of the fluoroanisidine and the diphenylamine compound was depressed. Nuclear magnetic resonance showed that a substituted anisyl group was linked to the nitrogen atom at the *para* position.

Analysis: Calculated for $C_{14}H_7F_8NO_2$: C, 45.0; H, 1.88; N, 3.75. Found: C, 45.4; H, 2.0; N, 3.5.

The residue gave 4,4′,4″-trimethoxydodecafluorotriphenylamine as a yellow oil; 2.2 g; bp 157 to 159 °C/1 mm; n_D^{23} 1.5005.

Analysis: Calculated for $C_{21}H_9F_{12}NO_3$: C, 46.4; H, 1.66; N, 2.57. Found C, 46.7; H, 2.1; N, 2.50.

5.4. Diazotization of Pentafluoroaniline

a. Pentafluoroiodobenzene

In a 250-ml, 3-necked, Monel flask (fitted with a metal inlet tube, Monel reflux condenser, and Teflon-covered, magnetic stirring-bar) was placed 20 g (0.108 mole) of pentafluoroaniline. Approximately 75 ml of anhydrous hydrogen fluoride was condensed into the flask at −20 °C and 7.27 g (0.105 mole) of sodium nitrite was added during 30 min. The flask was allowed to warm to −10 °C, stirring was continued for an additional 1 hr, 17.6 g (0.106 mole) of granular potassium iodide was added during 30 min, and the mixture was allowed to warm to 25 °C in 1 hr. The residual hydrogen fluoride was removed by warming the flask at 50 °C and the mixture was poured into 100 ml of water in a Monel beaker. The organic layer was separated, washed with three 50-ml portions of saturated sodium bicarbonate solution and water, and dried (sodium sulfate). On distillation, 16.5 g (50%) of pentafluoroiodobenzene, bp 77 to 79 °C/35 mm, was obtained. Analytical, vapor-phase chromatography (Viton A column at 150 °C) showed only one product, with a retention time identical with that of pentafluoroiodobenzene.

Bromopentafluorobenzene (35% yield) was prepared by the same procedure, except that 12 g of potassium bromide and 15 g of cuprous bromide was used in place of the potassium iodide.

5.5. Oxidation of Pentafluoroaniline

a. Decafluoroazoxybenzene

In a 250-ml flask were placed 10 g (0.055 mole) of pentafluoroaniline, 100 ml of glacial acetic acid, and 25 ml (0.22 mole) of 30-percent hydrogen peroxide. At 25 °C, the solution turned blue, green, dark brown, yellow, red, and finally orange within 24 hr. During an additional 24 hr, an orange liquid separated on the bottom. The reaction was stopped by dilution with 300 ml of water. The orange liquid was separated and, when chilled in ice, solidified. Yield: 4.5 g (22%). On sublimation at 80 °C/1 mm, followed by recrystallization (decolorization with charcoal) from petroleum ether, white plates of decafluoroazoxybenzene, mp 53 to 54 °C, formed. On standing, the material acquired a green tint. Confirmation of the structure was obtained from mass-spectrometer analysis, which showed the parent mass peak at 378. The ultraviolet absorption spectrum showed two maxima, one at 230 mμ and the other at 296 mμ.

b. Decafluoroazobenzene

A mixture of 5 g (0.013 mole) of decafluoroazoxybenzene, 15 g of zinc powder, 5 g of ammonium chloride, 10 ml of water, and 75 ml of 95-percent ethanol was stirred under reflux for 30 min. The mixture was filtered hot, and the zinc was extracted with two 50-ml portions of hot alcohol. The alcoholic filtrates were poured onto 100 g of ice, and the tan precipitate was filtered off and dried. Sublimation at 60 °C/1 mm gave 2 g (41.5%) of orange decafluoroazobenzene, mp 57 to 59 °C. Confirmation of the structure was obtained from mass-spectrometer analysis, which showed the parent mass peak at 362. The ultraviolet absorption spectrum showed one peak at 230 mμ, but this had two slight inflections, one at 280 mμ and the other 326 mμ. Solutions of decafluoroazoxybenzene are yellow and show one absorption peak at 370 mμ in the visible range, whereas the solutions of decafluoroazobenzene are orange and absorb at 465 mμ.

5.6. Reactions With Organolithium Compounds

a. 2,3,4,5,6-Pentafluorotoluene

Methyllithium was prepared in a 500-ml, three-necked flask equipped with a dropping funnel, magnetic stirrer, and a fitting for introducing a continuous flow of argon. Clean lithium, 4.5 g (0.61 mole) cut into small pieces, and 200 ml of sodium-dried ether were placed in the flask. A solution of 43 g of iodomethane in 50 ml of absolute ether was added dropwise to the mixture while vigorous stirring and a constant atmosphere of argon were maintained. After the reaction of the iodomethane with the lithium had begun (as evidenced by a clouding of the ether), the mixture was cooled to −10 °C with dry ice-acetone. The temperature was maintained between −10 °C and −20 °C during the entire preparation of the methyllithium.

The ether solution of methyllithium was transferred to a dropping funnel while under an argon atmosphere, and was added dropwise to a solution of 60 g of hexafluorobenzene in 250 ml of dry pentane initially at room temperature, slight refluxing from the heat of reaction being maintained. Continuous stirring under an argon atmosphere was maintained throughout the addition and for an additional 17 hr; during the final 2 hr, the solution was refluxed gently. After being cooled to room temperature, the suspension was filtered and the filtrate was washed with water and dried (sodium sulfate). The liquid was

distilled through a packed column. Yield: 34 g (70%), bp 115 °C.

Analysis: Calculated for $C_7H_3F_5$: C, 46.2; H, 1.6. Found: C, 46.4; H, 1.8.

b. Butyl-2,3,4,5,6-pentafluorobenzene

In a 250-ml, three-necked flask (fitted with a dropping funnel, stirrer, and reflux condenser, and containing a helium atmosphere) were placed 1.86 g (0.268 g-atom) of ⅛-in. lithium wire and 30 ml of anhydrous ether. To this mixture was added 5 ml of a solution of 18.3 g (0.134 mole) of 1-bromobutane in 25 ml of anhydrous ether at 25 °C. Gentle refluxing initiated the reaction, and the remainder of the solution of 1-bromobutane was added dropwise at −10 °C. After the addition was completed, the reaction mixture was stirred for an additional 1 hr at this temperature and finally allowed to warm to room temperature. The mixture was filtered, under helium, directly into a dropping funnel, and was slowly added to a solution of 25.3 g (0.134 mole) of hexafluorobenzene in 25 ml of anhydrous ether at −10 °C. The mixture was allowed to warm slowly to room temperature, refluxed for 90 min, and cooled in ice, and 100 ml of ice water added. It was then filtered and the ethereal layer was separated, dried (sodium sulfate), evaporated, and distilled. After removal of 10.5 g (30%) of unreacted hexafluorobenzene, there was obtained 7 g (33.2% based on reacted hexafluorobenzene) of butyl-2,3,4,5,6-pentafluorobenzene; bp 86 to 87 °C/25 mm; n_D^{20} 1.4229.

Analysis: Calculated for $C_{10}H_9F_5$: C, 53.31; H, 4.02. Found: C, 54.0; H, 4.2. There was also obtained 2.5 g (11%) of a compound, bp 230 °C/1 mm, n_D^{20} 1.4683, which, from its chemical analysis, appeared to be impure tributyldifluorobenzene. This product was not investigated further.

Analysis: Calculated for $C_{18}H_{28}F_2$: C, 76.9; H, 10.2. Found: C, 76.5; H, 11.9.

c. 2,3,4,5,6-Pentafluorobiphenyl

In a 1-liter, three-necked flask (equipped with a stirrer having a polytetrafluoroethylene blade, a Friedrichs condenser carrying a drying tube, and a pressure-equalizing dropping-funnel fitted with a nitrogen inlet) was placed 32.7 g (0.18 mole) of hexafluorobenzene in 150 ml of anhydrous ether. A solution of 0.18 mole of phenyllithium in 250 ml of ether was added dropwise under a nitrogen atmosphere, with constant stirring. After the first 25 ml had been added, heat was applied to initiate a vigorous exothermic reaction marked by the formation of a heavy, white precipitate. The remainder of the phenyllithium was added carefully so that the refluxing was vigorous but not violent. The mixture was stirred for 24 hr at room temperature and then treated with about 200 ml of 10 percent aqueous hydrochloric acid to destroy excess phenyllithium and to dissolve the precipitated lithium fluoride.

The aqueous layer was separated and extracted with several portions of ether. The ether solutions were combined, washed with small portions (10 ml) of saturated sodium bicarbonate solution until the washing remained basic and with saturated sodium chloride solution until neutral, and dried (sodium sulfate). Most of the ether was removed by evaporation at atmospheric pressure through a 16-in. Vigreux column; on cooling the concentrated solution, a white precipitate formed. This was removed by filtration and was shown by nuclear magnetic resonance to be 2,3,5,6-tetrafluoro-*p*-terphenyl, mp 220 °C. Yield: 8.5 g (17%).

Analysis: Calculated for $C_{18}H_{10}F_4$: C, 71.5; H, 3.3; F, 25.1. Found: C, 68.3; H, 3.2; F, 24.7.

The filtrate was evaporated under Vigreux column to remove the residual ether. Sublimation of the residue gave white crystals which appeared to be impure 2,3,4,5,6-pentafluorobiphenyl. Yield: 33 g (70%); mp 69 °C.

Analysis: Calculated for $C_{12}H_5F_5$: C, 59.0 H, 2.1; F, 38.9. Found: C, 59.5; H, 2.4; F, 37.5.

d. 2,3,4,5,6-Pentafluoro-α-methylstyrene

In a 1-liter, three-necked vessel (equipped similarly to the flask used in the addition of phenyllithium) was placed a solution of 18.6 g (0.1 mole) of hexafluorobenzene in 100 ml of anhydrous ether. A solution of isopropenyllithium in 250 ml of ether (prepared from 12.1 g of purified 2-bromopropene by the method of Braude and Evans [57]) was transferred under helium to the dropping funnel and added dropwise to the hexafluorobenzene solution. After 25 ml of reagent had been added, heat was applied to initiate refluxing; the solution became cloudy at once. On completing the addition of the isopropenyllithium, the mixture was refluxed for 1 hr and then kept overnight at room temperature. After addition of about 50 ml of 5-percent sulfuric acid, the solid was removed by filtration through a sintered-glass funnel. The ether layer of the filtrate was separated from the aqueous layer, washed with small portions of water until neutral, and dried (sodium sulfate) overnight. Fractional distillation through a 16-in. Vigreux column gave, after removal of the ether, 9 g of hexafluorobenzene and 5 g of 2,3,4,5,6-pentafluoro-α-methylstyrene; bp 72 to 74 °C/52 mm. Yield: 24 percent (50% based on unrecovered hexafluorobenzene).

Analysis: Calculated for $C_9H_5F_5$: C, 51.9; H, 2.4; F, 45.9. Found: C, 51.8; H, 2.6; F, 44.6.

About 0.1 g of a higher-boiling liquid was isolated. Vapor-phase, chromatographic analysis (Viton A column at 125° C) of this fraction revealed the presence of two main components. The first component had the same retention time as 2,3,4,5,6-pentafluoro-α-methylstyrene. The second component (about 50% of the fraction) had a considerably longer retention time and may possibly have been a disubstituted derivative of hexafluorobenzene. No further attempt was made to identify the higher-boiling product.

A considerable amount of a crystalline product, not readily soluble and apparently polymeric in nature, was found in the filtered solid. Hence, it appears that anionic polymerization of the olefinic products occurs quite readily under the conditions of the reaction.

e. 2,3,4,5,6-Pentafluorostyrene

Using essentially the same type of apparatus and technique as previously described, a solution of vinyllithium (prepared from 0.1 mole of phenyllithium and 0.025 mole of tetravinyltin according to the method of Seyferth and Weiner [58]) in about 150 ml of ether was added dropwise to 18.6 g (0.1 mole) of hexafluorobenzene in 50 ml of anhydrous ether. The reaction at room temperature was accompanied by precipitation of a white solid and vigorous refluxing of the solution. The flask was cooled to 0 °C about halfway through the addition, to moderate the vigorous refluxing. On completion of the addition, the mixture was kept at room temperature overnight and then refluxed for 30 min. After being cooled, the mixture was filtered, and the filtrate was flash vacuum-distilled into a trap at −78 °C. Some polymeric solid was left in the flask. The distillate was fractionated through a 12-in. column packed with glass helices. After removal of the ether, about 4 g of hexafluorobenzene was recovered. The higher-boiling residue was distilled under vacuum. A considerable quantity of solid was left in the distilling flask; it may have been polymeric vinyl derivative(s) of hexafluorobenzene. The colorless, liquid distillate, bp 34 °C/25 mm, was shown to be identical with 2,3,4,5,6-pentafluorostyrene obtained by dehydration of 2,3,4,5,6-pentafluoro-α-methylbenzyl alcohol (prepared by the reaction of pentafluorophenyl Grignard reagent with acetaldehyde [12]). Vapor-phase, chromatographic analysis showed the monomer to be of high purity. Yield: 20 percent (based on unrecovered hexafluorobenzene).

5.7. Reaction of Hexafluorobenzene With Lithium Aluminum Hydride and Lithium Hydride

In a 300-ml, three-necked flask equipped as described previously was placed 21 g (0.11 mole) of hexafluorobenzene in 50 ml of anhydrous ether. A slurry of 3 g (0.08 mole) of lithium aluminum hydride in 200 ml of anhydrous ether was filtered into a dropping funnel, and the filtrate was added dropwise, under a slow stream of nitrogen, to the stirred, refluxing solution of hexafluorobenzene. After all of the lithium aluminum hydride solution had been added, the mixture (containing a white precipitate) was refluxed for 8 hr. Aliquots of the mixture were periodically analyzed by vapor-phase chromatography, in order to determine the conversion of hexafluorobenzene to pentafluorobenzene as a function of time. After 1 hr, an aliquot of the ethereal solution contained two components (in addition to the ether). The component having the shorter retention time was the starting material. The other component, after isolation by preparative, vapor-phase chromatography, was shown by mass-spectrometric analysis to have a parent mass of 168, corresponding to pentafluorobenzene. The conversion of hexafluorobenzene to pentafluorobenzene was estimated to be about 30 percent. After 6 hr, the conversion was about 50 percent, and, after 8 hr, 60 percent. Further refluxing did not increase the percent conversion appreciably.

The reaction mixture was cooled to −78 °C and the excess hydrides were destroyed by adding wet ether, water, and 20-percent aqueous hydrochloric acid until the mixture was acid. The ether layer was separated, combined with the ether extracts of the water layer, and dried (sodium sulfate). The ether was removed by evaporation through a 24-in. column packed with glass-helices. The higher-boiling residue was fractionated, to give 17 g of a mixture of hexafluorobenzene and pentafluorobenzene, bp 78 to 84 °C. Some of the hexafluorobenzene (about 3 g) was apparently lost during the reaction or distillation, or both. The products were separated by preparative, vapor-phase chromatography, using a column 8 ft by ⅝ in. packed with acid-washed firebrick coated with 20 percent (by weight) of silicone oil (SE 30). The final recovery of unreacted hexafluorobenzene was 8 g; the yield of pentafluorobenzene was 7.5 g (61%, based on unrecovered hexafluorobenzene). Less than 0.5 g of disubstitution product (presumably 1,2,4,5-tetrafluorobenzene) was also isolated. About 1 g of a higher-boiling, unidentified product remained in the pot.

Several other experiments were tried, using equimolar proportions of hexafluorobenzene and lithium hydride in ether. Very little, if any, pentafluorobenzene was formed, even after long periods of reflux. The same materials were sealed in a dry, evacuated bomb, which was then heated at various temperatures (80 to 200 °C) for various times (up to 24 hr). Again, no pentafluorobenzene or other product was detected by vapor-phase, chromatographic analysis [24 by 0.25-in. column, with a packing of 30 percent (by weight) of silicone oil (Dow Corning 550) on 40–60-mesh, acid-washed firebrick] of the ether solution. However, the use of lithium aluminum hydride in 10-percent molar proportion together with equimolar proportions of lithium hydride and hexafluorobenzene in ether resulted in a 25-percent conversion to pentafluorobenzene after 48 hr of reflux.

The authors express their appreciation and thanks to R. A. Paulson for elementary analysis, James Brown for mass-spectrometric analysis, Max Tryon for infrared spectra, and Harold Finegold for nuclear magnetic-resonance spectra.

6. References

[1] Y. Desirant, Bull. Acad. Roy. Belg. Classe. Sci [5] **41,** 759 (1955).
[2] Y. Desirant, Bull. Soc. Chim. Belg. **67,** 676 (1958).
[3] M. Hellman, E. Peters, W. J. Pummer, and L. A. Wall, J. Am. Chem. Soc. **79,** 5654 (1957).
[4] J. A. Godsell, M. Stacey, and J. C. Tatlow, Nature **178,** 199 (1956).
[5] G. C. Finger, F. H. Reed, D. M. Burness, D. M Fort, and R. B. Blough, J. Am. Chem. Soc. **73,** 145 (1951).
[6] V. H. Dibeler, R. M. Reese, and F. L. Mohler, J. Chem. Phys. **26,** 304 (1957).
[7] L. A. Wall, R. E. Donadio, and W. J. Pummer, J. Am. Chem. Soc. **82,** 4846 (1960).
[8] R. E. Florin, L. A. Wall, and D. W. Brown, J. Research NBS **64A** (Phys. and Chem.) No. 4,269 (1960).
[9] M. Hellmann and A. J. Bilbo, J. Am. Chem. Soc. **75,** 4590 (1953).

[10] M. Hellmann, A. J. Bilbo, and W. J. Pummer, J. Am. Chem. Soc. **77,** 3650 (1955).
[11] W. J. Pummer, R. E. Florin, and L. A. Wall, J. Research NBS **62,** 113 (1959) RP 2939.
[12] E. Nield, R. Stephens, and J. C. Tatlow, J. Chem. Soc. 166 (1959).
[13] M. Szwarc (private communication).
[14] A. L. Rocklin, J. Org. Chem. **21,** 1478 (1956).
[15] M. Liveris and J. Miller, Chem. Ind. 954 (1957).
[16] J. F. Bunnett, Quart. Rev. **12,** 4 (1958).
[17] R. E. Florin, W. J. Pummer, and L. A. Wall, J. Research NBS **62,** 119 (1959) RP 2940.
[18] W. J. Pummer and L. A. Wall, Science **127,** 643 (1958).
[19] J. M. Birchall and R. N. Haszeldine, J. Chem. Soc. 13 (1959).
[20] E. J. Forbes, R. D. Richardson, M. Stacey, and J. C. Tatlow, J. Chem. Soc. **2019** (1959).
[21] E. Nield and J. C. Tatlow, Tetrahedron **8,** 38 (1960).
[22] K. Wallenfels and W. Draber, Chem. Ber. **90,** 2819 (1957).
[23] E. J. Forbes, R. D. Richardson, and J. C. Tatlow, Chem. Ind. **630** (1958).
[24] J. E. Fearn and L. A. Wall (unpublished results).
[25] G. M. Brooke, J. Burdon, M. Stacey, and J. C. Tatlow, J. Chem. Soc. **1768** (1960).
[26] G. M. Brooke, J. Burdon, and J. C. Tatlow, J. Chem. Soc. **802** (1961).
[27] G. M. Brooke, J. Burdon, and J. C. Tatlow, Chem. Ind. **832** (1961).
[28] K. H. Saunders, The aromatic diazo compounds, pp. 141, 158 (Edward Arnold and Co., London, 1949).
[29] W. J. Pummer and L. A. Wall, J. Research NBS **63A,** (Phys. and Chem.) No. 2, 167 (1959).
[30] K. Wiechert, Newer methods of preparative organic chemistry p. 336 (Interscience Publishers Inc., New York, 1947).
[31] J. H. Boyer and S. E. Ellzey, Jr., J. Org. Chem. **24,** 2038 (1959).
[32] W. D. Emmons, J. Am. Chem. Soc. **79,** 5528 (1957).
[33] W. J. Mijs, S. E. Hoekstra, R. M. Ulmann, and E. Haringa, Rec. Trav. Chim. **77,** 746 (1958).
[34] R. R. Holmes and R. P. Boyer, J. Am. Chem. Soc. **82,** 3454 (1960).
[35] W. J. Pummer and L. A. Wall, Abstracts Papers Am. Chem. Soc. **136,** 24M (1959).
[36] J. M. Antonucci and L. A. Wall, Abstracts Papers Am. Chem. Soc. **140,** 25M (1961).
[37] A. K. Barbour, M. W. Buxton, P. L. Coe, R. Stephens, and J. C. Tatlow, J. Chem. Soc. **808** (1961).
[38] M. A. Doran and R. Waack, Chem. Ind. **1165** (1961).
[39] J. M. Birchall and R. N. Haszeldine, J. Chem. Soc. **3719** (1961).
[40] J. E. Johnson, R. H. Blizzard, and H. W. Carhart, J. Am. Chem. Soc. **70,** 3664 (1948).
[41] J. C. Tatlow (private communication).
[42] J. F. Bunnett, Quart. Rev. **12,** 1 (1958).
[43] J. F. Bunnett, Kekule symposium, p. 144 (Butterworths, London, 1959).
[44] R. Huisgen, Kekule symposium, p. 158 (Butterworths, London, 1959).
[45] A. J. Parker, Quart. Rev. **16,** 163 (1962).
[46] P. L. Coe, R. Stephens, and J. C. Tatlow, J. Chem. Soc. **3227** (1962).
[47] C. R. Patrick and G. S. Prosser, Nature **187,** 1021 (1960).
[48] D. M. G. Lawrey and H. McConnell, J. Am. Chem. Soc. **74,** 6175 (1952).
[49] A. W. Baker, J. Am. Chem. Soc. **80,** 3598 (1958).
[50] A. W. Baker and W. W. Kaeding, J. Am. Chem. Soc. **81,** 5904 (1959).
[51] T. Ri and H. Eyring, J. Chem. Phys. **8,** 433 (1940).
[52] C. C. Meredith and G. Wright, Can. J. Chem. **38,** 1177 (1960).
[53] C. K. Ingold, Structure and mechanism in organic chemistry, p. 741 (Cornell Univ. Press, Ithaca, New York, 1953).
[54] G. M. Brooke, J. Burdon, and J. C. Tatlow, J. Chem. Soc. 3253 (1962).
[55] P. Robson, M. Stacey, R. S. Stephens, and J. C. Tatlow, J. Chem. Soc. 4754 (1960).
[56] A. I. Vogel, Practical organic chemistry, p. 188 (Longmans, Green and Co., Inc., New York, 1954).
[57] E. A. Braude and E. A. Evans, J. Chem. Soc. **333** (1956).
[58] D. Seyferth and M. A. Weiner, Chem. Ind. **402** (1959).

(Paper 67A5–237)

JOURNAL OF RESEARCH of the National Bureau of Standards—A. Physics and Chemistry
Vol. 67A, No.5, September-October 1963

Publications of the National Bureau of Standards*

Selected Abstracts

Standard X-ray diffraction powder patterns, H. E. Swanson, M. C. Morris, R. P. Stinchfield, and E. H. Evans, *NBS Mono. 25, Section 2 (May 3, 1963), 35 cents.*
Standard X-ray diffraction powder patterns are presented for the following thirty-seven substances: Al $(PO_3)_3$, SbF_3*, $Ba_3(AsO_4)_2$*, $Ba(ClO_4)_2 \cdot 3H_2O$, $Cd(CN)_2$*, $CdWO_4$, Cs_2OsBr_6*, Cs_2OsCl_6*, α-$CrPO_4$, $Co[Hg(CNS)_4]$*, β-$CoSO_4$, $Dy_3Ga_2(GaO_4)_3$*, $ErMnO_3$*, $Eu_3Ga_2(GaO_4)_2$*, $Gd_3Ga_2(GaO_4)_3$*, Li_3AsO_4*, $Li_3P_3O_9 \cdot 3H_2O$*, $Li_2WO_4 \cdot \frac{1}{2}H_2O$*, $Lu_3Ga_2(GaO_4)_3$*, $LuMnO_3$*, $MnWO_4$ (huebnerite), HgF_2*, $NiSO_4$, $NiWO_4$*, K_2ReCl_6, K_2RuCl_5NO*, $RbClO_4$*, $RbIO_4$*, Ag_2SeO_4*, NaCNO*, $Na_2WO_4 \cdot 2H_2O$, β-$Na_4P_4O_{12} \cdot 4H_2O$, $Sr_3(AsO_4)_2$*, Tl_3AsO_4*, $TlClO_4$*, $YAsO_4$, $ZnWO_4$*. Eleven are to replace patterns already given in the X-ray Powder Data File issued by the American Society for Testing and Materials, and twenty-six patterns indicated by asterisks are for substances not previously included. The X-ray Powder Data File is a compilation of diffraction patterns from many sources and is used for the identification of unknown crystalline materials by matching spacing and intensity measurements. The patterns were made with a Geiger counter X-ray diffractometer using samples of high purity. When possible, the *d*-values were assigned Miller indices determined by comparison with calculated interplanar spacings and from space group extinctions. The densities and lattice constants were calculated, and the refractive indices were measured whenever possible.

Mechanical behavior of crystalline solids (*Proceedings of an American Ceramic Society Symposium, New York City, April 1962), NBS Mono. 59 (Mar. 25, 1963), $1.75.*
This Monograph represents the Proceedings of a Symposium on *The Mechanical Behavior of Crystalline Solids,* held under the auspices of the Ceramic Educational Council of the American Ceramic Society, with the cooperation of the National Bureau of Standards, and under the sponsorship of the Edward Orton Junior Ceramic Foundation, and the Office of Naval Research. The Symposium took place at the 64th Annual Meeting of the American Ceramic Society, in New York, on April 28 and 29, 1962.

Testing of metal volumetric standards, J. C. Hughes and B. C. Keysar, *NBS Mono. 62 (Apr. 1, 1963), 15 cents.*
The National Bureau of Standards has for many years calibrated and certified metal measures which are used as standards by weights and measures officials and others in the calibration of instruments for measuring the volumes of fluids. No complete specifications or tolerances for these standards have ever been published, however, nor have standardized procedures for the calibration and use of the liquid measures been available.
The information contained in this Monograph should assist in the purchase of quality instruments and the proper use of the standards in calibrating other measures for liquids and gases.

Radiobiological dosimetry, *Recommendations of the International Commission on radiological units and measurements, NBS Handb. 88 (April 30, 1963), Supersedes parts of Handb. 78. Handbooks 84 through 89 will completely replace H78, 25 cents.*
This publication deals primarily with radiobiological dosimetry, and considers methods of improving the accuracy and intercomparability of absorbed dose measurements in radiobiology. It is in effect a handbook for the experimental radiobiologists. It emphasizes the great importance of planning the experimental work in a way which makes the dosimetry easier and more accurate and it illustrates how this can be done.
The publication was prepared by a committee of the International Commission on Radiological Units and Measurements.

Transistorized building blocks for data instrumentation, R. L. Hill, *NBS Tech. Note 168 (Apr. 1, 1963), 55 cents.*
The National Bureau of Standards has developed a number of modular transistorized digital circuits that have been used in automatizing many data recording and preliminary processing tasks encountered in its scientific operations. These versatile building blocks can be connected together systematically to form digital circuits that accept raw data from experimental equipment and transpose these data into a form suitable for input to a high-speed electronic computer.
Each assembly of packages can be tailored to fit the special requirements of the project and can be used at the site of the experiment. The output from the system can be: 1) fed directly to a computer, 2) recorded on a medium (paper tape, magnetic tape, etc.) suitable for computer input at a later date, or 3) used to drive display equipment that keeps the scientist informed of the progress of his experiment.
As a result of experience in the application of these units, some of the original packages have been modified and additional types developed. In addition to describing the modified and new package types, this report also includes a description of a new series of packages consisting of identical circuitry, but utilizing a different type of mating connector and a smaller circuit-board.

Practical methods for calibration of potentiometers, D. Ramaley, *NBS Tech. Note 172 (Mar. 25, 1963), 30 cents.*
Potentiometer circuitry, particularly as related to calibration, is discussed with the primary consideration given to the required circuit measurements. The more feasible means of calibrating potentiometers are described in considerable detail. Emphasis is placed upon the use of the Universal Ratio Set as the basic implement for accomplishing the major portion of potentiometer calibrations.

Tables to facilitate the determination of the ferrimagnetic resonance linewidth of non-metallic magnetic materials, C.C. Preston and W. E. Case, *NBS Tech. Note 173 (Apr. 15, 1963), 25 cents.*
A common test procedure for measuring ferrimagnetic resonance linewidth, ΔH, and gyromagnetic ratio, γ, of microwave ferrites is based upon a perturbation analysis of the complex frequency shift obtained when a small sample is placed in a resonant cavity and an applied d-c magnetic field. However, this method necessitates the plotting of a ferrimagnetic resonance loss curve. To find ΔH it is possible to derive an equation using lumped circuit theory which reduces the number of needed measurements to four attenuator readings.
This paper provides a table which gives values of attenuation according to the following formula which facilitates the determination of linewidth:

$$A = 20 \log 2 - 20 \log \left(10 \frac{A_0 - A_r}{20} + 1\right) \text{ for } A_0 - A_r$$
$$= 0.41\ (0.01)\ 32.40.$$

Calibration of volt-ampere converters, E. S. Williams, *NBS Tech. Note 188 (Apr. 25, 1963), 20 cents.*
These notes have been prepared to describe the National Bureau of Standards calibration services for volt-ampere converters (or transfer volt-ammeters), to suggest procedures for d-c standardization in the user's laboratory, and to de-

scribe a voltage comparator which can be used to make such calibrations quickly and easily.

Degradation of polymers, L. A. Wall and J. H. Flynn, *Rubber Chem. Technol.* **XXV,** *No. 5, 1157–1221 (December 1962).*
Recent literature pertaining to both the theoretical aspects and experimental results of the degradation of polymers by heat and radiation is reviewed and critically evaluated.
Theories of random and chain thermal degradation of vinyl polymers and copolymers are reviewed. The degradation of polymethacrylates, polyacrylates, poly-α-methylstyrene, polyolefins, polystyrene, other vinyl polymers, cellulose, polyesters, polyamides, dienes, natural rubber, and copolymers are discussed in the light of these theories. The thermodynamics and energetics of the degradation of these polymers is also reviewed.
Chain scission, crosslinking, and gel formation and the kinetic mechanisms of these processes which take place during degradation of polymers by ionizing radiation and ultraviolet light are included. Degradative, rather than synthetic, effects are emphasized in the discussion.

Chemical and magnetic enhancement of perturbed lines in the violet spectrum of CN, H. E. Radford and H. P. Broida, *J. Chem. Phys.* **38,** *No. 3, 644–657 (Feb. 1, 1963).*
A chemical kinetic theory based on the quantum mechanical properties of perturbed molecular states is developed to explain the rotational intensity anomalies observed in the CN band spectrum emitted by an active nitrogen flame. Relative intensities of perturbed lines are calculated in terms of parameters which specify the rates of chemical formation, collisional relaxation, and radiative decay of CN molecules in the excited electronic states where the perturbed lines originate. Numerical values of these parameters are found which, inserted in the intensity expressions, predict correctly the observed pressure-dependent enhancement of each perturbed line. From this analysis the approximate value 6×10^{-7} sec is found for the radiative lifetime of the $A^2\Pi_i$, $v'=10$ state of CN. It is also found that nearly every gas kinetic collison changes the rotational state of an excited CN molecule, but that only about 1 collision in 100 can cause the exchange of vibrational energy for electronic energy represented by the transition $A^2\Pi_i$, $v'=10\rightarrow B^2\Sigma^+$, $v'=0$. The theory also predicts, in agreement with recent observations, an additional selective enhancement of certain perturbed lines by a strong magnetic field.

Profiles of Stark-broadened Balmer lines in a hydrogen plasma, W. L. Wiese, D. R. Paquette, and J. E. Solarski, *Phys. Rev.* **129,** *No. 3, 1225–1232 (Feb. 1, 1963).*
A stationary hydrogen plasma was generated in a high current stabilized arc and its temperature was determined spectroscopically from the diagnostics of the line and continuum radiation. Extensive measurements of the profiles of the Balmer lines H_β and H_γ where made and show that recent improvements in the theory of Stark broadening described the observed line shapes well. Electron densities determined from line width measurements are slightly higher than those derived from temperature measurements. In the covered range of electron densities from 10^{16}–10^{17} cm^{-3} and temperatures around 10^4 °K the difference amounts to 25% for H_γ and 12% for H_β, for which a refined Stark broadening theory is available. In addition, the intensity distribution in the distant linewings of Hα and Hβ was measured and compared with asymptotic formulae. Satisfactory agreement is obtained.

Magnetic susceptibilities and dilution effect in low-spin d^4 complexes: Osmium (IV), R. B. Johannesen and G. A. Candela, *Inorg. Chem.* **2,** *67–72 (1963).*
Magnetic susceptibility measurements were made on a series of hexachloro- and hexabromoosmates, M^2OsX_6, and on potassium hexachlororuthenate, K_2RuCl_6. The paramagnetism of the Os (IV) complexes is independent of temperature and increases as the osmium ions are separated. It is shown that the effect of dilution is described by the equation

$$\chi=\frac{\chi_\infty}{1+\lambda d^{-n}\chi_\infty}$$

where χ_∞ is the susceptibility at infinite dilution, d is the average distance between the osmium ions, λ is a constant, and n is approximately 2.
An intermediate coupling scheme is necessary to explain the experimental results for the $5d^4$ configuration. In this scheme the only parameters are the spin-orbit coupling constant and the orbital reduction factor. The values of 2300 ± 300 cm^{-1} for the spin-orbit coupling constant and 3500 ± 200 cm^{-1} for the Coulomb interaction coefficient were calculated.

New absolute null method for the measurement of magnetic susceptibilities in weak low-frequency fields, C. T. Zahn, *Rev. Sci. Instr.* **34,** *No. 3, 285–291 (Mar. 1963).*
Use is made of the magnetic equivalence of a uniformly polarized volume of paramagnetic material and a solenoid carrying electric current, to design a permanent variable standard of magnetic susceptibility. Such a standard is incorporated into a magnetic susceptibility bridge in a simple manner, surrounding the specimen; and the bridge is thereby transformed into an absolute null instrument of high accuracy and sensitivity, and of great ease and low cost of construction and operation. By this method numerous particular advantages of other methods are combined; and some of their notable limitations are overcome. A preliminary application was made showing that the bridge performs as expected. Important features in the design of this bridge are discussed. A detailed consideration of sources of error suggests that it may eventually be possible by this method to obtain greater absolute accuracy than by other known methods.

A method for measuring the instability of resistance strain gages at elevated temperatures, R. L. Bloss and J. T. Trumbo, *ISA Trans.* **2,** *No. 2, 112–116 (Apr. 1963).*
The usefulness of resistance strain gages at elevated temperatures is frequently limited by the instability of gage resistance with time. Methods and equipment that have been developed to measure this effect are described.

Intercomparison of national roentgen and gamma ray exposure-dose standards, H. O. Wyckoff, A. Allisy, G. H. Aston, G. P. Barnard, W. Hubner, T. Loftus, and G. Taupin, *Acta Radiol.* **1,** *No. 1, 57–78 (Feb. 1963).*
Indirect intercomparisons of calibrations of ionization chambers for exposure dose measurements in roentgens have been completed between the national standards of France, Germany, U.K., and U.S.A., with an estimated maximum uncertainty of about 0.5 percent. This is somewhat larger than that assigned to direct comparisons (Aston and Attix, 1957). Several revisions in the calibration procedure are indicated which may reduce the uncertainty in the indirect intercomparisons.
The present calibrations agree with those obtained earlier between three of the laboratories to within the expected uncertainty, 0.5 percent; also the calibrations at PTB agree with those at NBS to within 0.6 percent. However the results from NPL and PTB disagree by slightly more than one percent for nearly the same quality of the harder radiations. A detailed redetermination of some of the correction factors may be needed to remove this discrepancy.

Wavelengths, energy levels, and pressure shifts in mercury 198, V. Kaufman, *J. Opt. Soc. Am.* **52,** *No. 8, 866–870 (Aug. 1962).*
The vacuum wavelengths of 27 lines of Hg^{198} and 6 lines of Kr^{86} have been measured relative to the international standard of length, the Kr^{86} line at 6057.80211 Å, by photographic Fabry-Perot interferometry. These measurements were made with Hg^{198} electrodeless lamps containing argon at pressures of ¼, 3, and 10 mm Hg and a Kr^{86} hot-cathode lamp operated according to the conditions prescribed by the International Conference on Weights and Measures in 1960. Energy-level values have been derived from the wavelengths of each of the Hg^{198} sources, and on the basis of these values, the energy level and wavelength shifts per unit pressure of argon have been calculated. The suitability of the Hg^{198} electrodeless lamp as a source of wavelength standards for interferometric measurement of length and wavelength is discussed.

Audio-frequency compliances of prestressed quartz, fused silica, and aluminum, M. Greenspan and C. Tschiegg, *Proc. Fourth Intern. Congr. on Acoustics, Part I, Paper P12 (Copenhagen, Denmark, Aug. 21–28, 1962).*
An attempt was made to find the excess compliances associated with dispersions found by Fitzgerald. Compliances were obtained from resonant frequencies of fixed-free composite reeds. Prestress was either piezoelectrically or thermally induced. No excess compliances were observed.

X-ray microscopy of polymers by point projection, S. B. Newman, *Mod. Plastics* **40,** *No. 7, 165–179 (Mar. 1963).*
A two-lens electromagnetic microfocus X-ray tube has been used for studying the microstructure of a number of polymeric materials. Long wavelength radiation from aluminum targets was used in most of the work, though copper targets were used in a few experiments. Results obtained from foams, laminates, fibers, and fabrics are presented. The potential of available instrumentation for application to this general material area is considered.

Microwave spectrum and structure of difluoramine, D. R. Lide, Jr., *J. Chem. Phys.* **38,** *No. 2, 456–460 (Jan. 15, 1963).*
The microwave spectra of NF_2H and NF_2D have been analyzed. Rotational constants are 53017.12, 10895.43, 9307.22 Mc for NF_2H and 44884.92, 10749.38, 9126.26 Mc for NF_2D. The structure obtained from these constants is: $r_{NF}=1.400\pm0.002$ A, $r_{NH}=1.026\pm0.002$ A, $\angle FNF=102.9°\pm0.2°$, and $\angle HNF=99.8°\pm0.2°$. Quadrupole coupling constants have been measured for both isotopic species and the complete field-gradient tenser has been determined. The dipole moment has a magnitude of 1.93 ± 0.02 D and makes an angle of 19° with the NH bond. An upper limit of 0.2 Mc may be set on the inversion splitting in the ground state.

Design of low voltage electron guns, J. A. Simpson and C. E. Kuyatt, *Rev. Sci. Instr.* **34,** *No. 3, 265–268 (Mar. 1963).*
It is shown that by use of a multistage technique in which electrons are drawn from a cathode by a high potential and decelerated to the required final energy, guns can be designed capable of forming beams in which the current is limited only by space charge in the beam itself. The design principles and procedures are given and illustrated by two examples of electron guns giving highly collimated beams and operating at energies of 30 and 500 eV. The measured currents obtained are somewhat greater than the space charge limited beam maximum because of ion neutralization.

Determination of source self-absorption in the standardization of electron-capturing radionuclides, S. B. Garfinkel and J. M. R. Hutchinson, *Intern. J. Appl. Radiation and Isotopes* **13,** *629–639 (1962).*
A method is described for measuring source self-absorption in the standardization of radionuclides which decay by electron capture directly to the ground state. Auger electrons are used as a tracer in order to determine the X-ray absorption. Data are presented which indicate that X-ray absorption in a certain type of electroplated source is less than 0.2%. A method for determination of ejected photoelectrons from absorbing foils in 4π X-ray counting is described.

Mean first-passage times and the dissociation of diatomic molecules, K. E. Shuler and G. H. Weiss, *J. Chem. Phys.* **38,** *No. 2, 505–509 (Jan. 15, 1963).*
The collisional activation of diatomic molecules to dissociation can be considered as a random walk with an absorbing barrier in the energy space of the molecules. In such a model, the rate of activation to dissociation is related to the mean first passage time of the molecules across the absorbing barrier. We have computed here the mean first passage time for an ensemble of oscillators in an initial Boltzmann distribution with transitions limited to nearest neighbor states ($|\Delta v|=1$) and for an ensemble of oscillators initially in the ground state ($v=0$) which undergo transitions between non-nearest neighbor states ($|\Delta v|\geq1$). It is shown that the magnitude of the mean first passage time is very sensitive to the height (in energy space) of the absorbing barrier and to the "jump distance", $|\Delta v|>1$, for non-nearest neighbor transitions. The implications of these results on the mechanism of the activation and dissociation of diatoms are discussed briefly.

Infrared absorption spectra of carbon suboxide and malonotitrile in solid argon matrices, L. L. Ames, D. White, and D. E. Mann, *J. Chem. Phys.* **38,** *No. 4, 910–917 (Feb. 15, 1963).*
The infrared spectra of carbon suboxide and malononitrile isolated in solid argon matrices at low temperatures have been measured in the spectral region 440–4400 cm^{-1}. A detailed comparison with prior spectroscopic data is made. It is shown that the matrix spectra of C_3O_2 support the linear symmetric model. A comparison of the matrix spectra and vibrational assignments of the three isoelectronic molecules C_3O_2, $CH_2(CH)_2$, and B_2O_3 is shown to favor a large apex angle in B_2O_3.

Interaction matrix element in a shell model, U. Fano, F. Prats, and Z. Goldsmith, *Phys. Rev.* **129,** *No. 9, 2643–2652 (Mar. 16, 1963).*
The matrix elements of two-particle interactions between states of many-particle configurations are expressed as products of one-particle reduced matrix elements and of a single recoupling coefficient. Applications are given to the Coulomb interaction of $l^n l'$ configurations and to all three-electron configurations.

Electron impact ionization of atomic hydrogen, S. Geltman, M. R. H. Rudge, and M. J. Seaton, *Proc. Phys. Soc.* **81,** *Pt. 2, No. 520, 375–378 (1963).*
The cross section for ionization of atomic hydrogen is calculated by several methods, including the Born-Oppenheimer and Born-Exchange Approximation, and the resulting curves compared with experiment.

Effective diffusion constant in a polyelectrolyte solution J. L. Jackson and S. R. Coriell, *J. Chem. Phys.* **38,** *No. 4, 959–968 (Feb. 15, 1962).*
A general theory of the effective diffusion constant of ions in a periodic electric field is presented. The predictions of the theory are compared with the results of experiments on the diffusion of labeled sodium in a sodium hydroxide—polyacrylic acid solution.

Electron attachment coefficients of some hydrocarbon flame inhibitors, T. G. Lee, *J. Phys. Chem.* **67,** *360–366 (1963).*
The electron attachment coefficients of a number of halogenated hydrocarbons, particularly flame inhibitors, were determined as a function of the average agitation energy of electrons between 0.1 and 1.2 ev at atmospheric pressure and room temperature. A sensitive electron swarm technique was used for the measurement. The gas under study was introduced, at low concentrations, by means of a nitrogen carrier into an ionization chamber.
The electron attachment coefficients for the compounds examined range from 1×10^{-5} to 10 for CF_4 and CF_2Br_2, respectively. All inhibitors studied were found to have a higher electron attachment coefficient than O_2. It was found, with some exceptions, that gases reported as effective hydrocarbon flame inhibitors exhibited high electron attachment coefficients.

The measurement of moisture boundary layers and leaf transpiration with a microwave refractometer, D. M. Gates, M. J. Vetter, and M. C. Thompson, Jr., *Nature* **197,** *1070–1072 (Mar. 16, 1963).*
A microwave refractometer has been used as a hygrometer to measure the moisture gradient found near a free water surface and near the surface of a leaf. Interesting transpiration effects were observed for begonia and bean leaves when the leaves were stimulated with light. The instrument samples the air through a small orifice and thereby produces very little disturbance to the moisture boundary layer under investigation.

The history of Pt 27, E. Wichers, *Book, Temperature, Its Measurement and Control in Science and Industry,* **3,** *Pt. 1, 259–262 (Reinhold Publ. Corp, New York, N.Y., 1962).*
This is a brief account of work done at the National Bureau of Standards in the period 1919–22 on the preparation of platinum of high purity and the conditions required to melt

the purified metal with minimum contamination by the crucible material. Contamination with calcium was correlated wit . a positive thermal emf toward purer specimens. Negative thermal emf was also found to correlate with an increasing temperature coefficient of electrical resistivity. Trial melts were identified by numbers referring to notebook descriptions of the experimental methods used. The melt numbered 27 turned out to be thermoelectrically negative to all other specimens prepared up to that time, as well as to all specimens from commercial sources. It thus came into use as a standard for further comparisons in the NBS laboratory and later into similar use in the platinum industry.

Some causes of resonant frequency shifts in atomic beam machines. I. Shifts due to other frequencies of excitation, J. H. Shirley, *J. Appl. Phys.* **34,** *783–788 (Apr. 1963).*
The quantum theory of an atomic beam machine is set up in matrix form. A new method is then used to derive the Bloch-Siegert shift in resonance. The results are extended to the case of Ramsey type excitation. Finally the Bloch-Siegert shift is computed for the present atomic beam frequency standards and found to be well below the accuracy of measurement.

Some causes of resonant frequency shifts in atomic beam machines. II. The effect of slow frequency modulation on the Ramsey line shape, J. H. Shirley. *J. Appl. Phys.* **34,** *789–791 (Apr. 1963).*
The effect of slow frequency modulation of the exciting radiation on the Ramsey line shape observed in an atomic beam experiment is formulated theoretically. It is shown that the presence of second harmonic in the modulation can introduce measurable frequency shifts, whether observed directly or with a servo-system.

The specific heat at constant volume of parahydrogen at temperatures from 15 to 90° K and pressures to 340 atm, B. A. Younglove and D. E. Diller, *Cryogenics* **2,** *No. 6, 1–5 (Dec. 1962).*
The specific heats at constant volume of parahydrogen have been measured at temperatures from 15 to 90°K and at densities from 0.7 to 2.6 times the critical density. This paper describes the experimental method, the analysis and reduction of the data, and presents the results in the form of tables and graphs.

Electron spin resonance of gamma-irradiated cellulose, R. E. Florin and L. A. Wall, *J. Polymer Sci.* **1,** *Pt. A, 1163–1173 (1963).*
Irradiation of purified cellulose with cobalt-60 gamma rays, in vacuo, produced moderate yields of radicals detectable by electron spin resonance. The ESR spectrum is asymmetric, with five partially resolved peaks occupying a total region about 50 gauss wide, for spectroscopic splitting factor near g=2. The peaks show differing saturation behavior with increasing microwave power. Differences of crystallinity have no obvious effect on the yield or nature of the radical ESR spectrum. The presence of about 8% water during irradiation decreases the yield greatly and modifies the hyperfine structure. For dry cellulose the initial G-value for radicals is near 2.8 radicals per 100 e.v. absorbed, but the concentration levels off at doses a little over 6×10^{20} ev/g. Despite the early falling-off in yield, the radicals in stored irradiated specimens do not decay appreciably in several days. Even upon opening to the air the decay is quite slow. Thermal decay is imperfectly second-order, fairly rapid above 120° C, and indicates several radicals of differing lifetime.

The speed of light, A. G. McNish, *IRE. Trans. Instr.* **I–11,** *Nos. 3 & 4, 138–148 (Dec. 1962).*
Numerous measurements of the speed of light published during the last 30 years lead to widely divergent results as compared with the assigned experimental uncertainties. Because of wide diversity in the methods employed in the measurements, all of the data may not be combined effectively in a grand average. Sufficient data had been obtained by the geodimeter method to group them and derive a statistical estimate of the uncertainty in the speed of light by this method. This result, and conclusions reached from careful examination of several experiments, leads to the conclusion that the value 299,792.5 km per sec which has been internationally adopted for use in radio propagation and geodetic work is very close to the best value and not likely to be in error by as much as one part in one million.

Optimum estimators of the parameters of negative exponential distributions from one or two order statistics, M. M. Siddiqui, *Ann. Math. Stat.* **34,** *117–121 (Mar. 1963).*
Optimum estimators for the parameters of negative exponential populations from one or two order statistics are obtained analytically, thus providing solutions for all sample sizes to the problems solved by Harter (Ann. Math. Stat. **32,** pp. 1078–1090) numerically for samples of sizes up to 100.

Crystallographic changes with the substitution of aluminum for iron in dicalcium ferrite, D. K. Smith, *Acta Cryst.* **15,** *1146–1152 (Jan. 1962).*
Single-crystal X-ray precession patterns of several compositions in the solid solution series

$$Ca_8\ (Fe_1{}^{-}{}_pAl_p)_8O_{20}\ (0\leq p\leq 0{\cdot}69)$$

show that the series is not completely isostructural. Systematic extinctions of X-ray reflections indicte that the space group for compositons with the ratio $p\equiv Al/(Al+Fe)$ less than 0·30 is *Pnma*, whereas the space group for p greater than 0·33 is *Imma*. The cell constants vary continuously throughout the symmetry change.

The crystal structure determined by Bertaut, Blum & Sagnières (1957, 1959) for the iron end-member has the 8 Fe in two 4-fold sites, one site octahedrally coordinated with oxygen and one tetrahedrally coordinated with oxygen. The layers of octahedra correspond to the space group *Imma*, but the layers of tetrahedra reduce the symmetry to *Pnma*. The substitution of Al for Fe in this structure causes the tetrahedral layer to adjust gradually to the *Imma* symmetry. Steric considerations and relative intensities of $0k0$ reflections for various compositions suggest that the Al atoms substitute preferentially for tetrahedrally-coordinated Fe atoms until about half the tetrahedral cations are Al. Then additional Al distributes itself nearly equally between the tetrahedral and octahedral sites until it saturates the tetrahedral sites at approximately p=0·69, the composition limit for crystallization of this phase from $CaO-Fe_2O_3-Al_2O_3$ melts.

Other NBS Publications

J. Research NBS 67B (Math. and Math. Phys.), No. 3 (July–Sept. 1963), 75 cents.
Remarks on hypo-elasticity. C. Truesdell.
Error bounds in the pointwise approximation of solutions of elastic plate problems. J. H. Bramble and L. E. Payne.
Effect of error in measurement of elastic constants on the solutions of problems in classical elasticity. J. H. Bramble and L. E. Payne.
Eigenfunctions of the f^3 configuration. J. C. Eisenstein.
Zeros of first derivatives of Bessel functions of the first kind, $J_n'(x)$, $21\leq n\leq 51$, $0\leq x\leq 100$. G. W. Morgenthaler and H. Reismann.

J. Research NBS 67C (Eng. and Instr.), No. 3 (July–Sept. 1963), 75 cents.
Apparatus for the detection of piezoelectric coupling. L. Frenkel.
Large aperture interferometers with small beam dividers. J. B. Saunders.
A far-infrared vacuum grating spectrometer. L. R. Blaine.
Relation of emittance to other optical properties. J. C. Richmond.
Minimization of the arrestment error in one-pan two-knife balance systems. H. A. Bowman and H. E. Almer.
Determination of residual thiosulfate in processed film. C. I. Pope.
Drag compensation and measurement with manned satellites: feasibility study. R. M. Langer and J. P. Vinti.
Surface flame propagation on cellulosic materials exposed to thermal radiation. D. Gross and J. J. Loftus.
Parallel reversible permeability measurement techniques from 50 kc/s to 3 Gc/s. C. A. Hoer and R. D. Harrington.

J. Research NBS 67D (Radio Prop.), No. 5 (Sept.–Oct. 1963) 70 cents.

Ionespheric VHF scattering near the magnetic equator during the International Geophysical Year. R. Cohen and K. L. Bowles.

Radio pulse propagation by a reflection process at the lower ionosphere. J. R. Johler.

Field of a horizontal magnetic dipole in the presence of a magnetoplasma halfspace. G. Tyras, A. Ishimaru, and H. M. Swarm.

Reflection of VLF radio waves from an inhomogeneous ionosphere. Part II. Perturbed exponential model. J. R. Wait and L. C. Walters.

Collisional detachment and the formation of an ionospheric *C* region. E. T. Pierce.

Magnetic torques and Coriolis effects on a magnetically suspended rotating sphere. J. C. Keith.

Radiation field characteristics of lightning discharges in the band 1 kc/s to 100 kc/s. W. L. Taylor.

Low-frequency radio propagation into a moderately rough sea. D. F. Winter.

VLF superdirective loop arrays. E. W. Seeley.

Curves of ground proximity loss for dipole antennas (a digest). L. E. Vogler and J. L. Noble.

Observations and results from the "hiss recorder," an instrument to continuously observe the VLF emissions. J. M. Watts, J. A. Koch, and R. M. Gallet.

Influence of a sector ground screen on the field of a vertical antenna, J. R. Wait and L. C. Walters, NBS Mono. 60 (Apr. 15, 1963), 25 cents.

Quarterly radio noise data, June, July, August 1962, W. Q. Crichlow, R. T. Disney, and M. A. Jenkins, NBS Tech. Note 18–15 (Mar. 1, 1963), 45 cents.

Mean electron density variations of the quiet ionosphere, November 1959, J. W. Wright, L. R. Wescott, and D. J. Brown, NBS Tech. Note 40–9 (April 22, 1963), 35 cents.

Mean electron density variations of the quiet ionosphere, December 1959, J. W. Wright, L. R. Wescott, and D. J. Brown, NBS Tech. Note 40–10 (March 24, 1963), 35 cents.

The error rates in multiple FSK systems and the signal-to-noise characteristics of FM and PCM–FS systems, H. Akima, NBS Tech. Note 167 (Mar. 25, 1963), 40 cents.

Bibliography on atmospheric aspects of radio astronomy, including selected references to related fields, W. Nupen, NBS Tech. Note 171 (May 1, 1963), $2.00.

Curves of ground proximity loss for dipole antennas, L. E. Vogler and J. L. Noble, NBS Tech. Note 175 (May 20, 1963), 30 cents.

An interpolation procedure for calculating atmospheric band absorptions from laboratory data, L. Droppleman, L. R. Megill, and R. F. Calfee, NBS Tech. Note 178 (June 3, 1963), 20 cents.

Relative power transmission characteristics of the ear and skull from hearing threshold data, E. L. Smith, Proc. Fourth Intern. Congr. on Acoustics, Part I, Paper H48 (Copenhagen, Denmark, Aug. 21–28, 1962).

Polymer research at the U.S. National Bureau of Standards, Part I, G. M. Kline, SPE J. **19,** No. 3, 278–283 (Mar. 1963).

Polymer research at the U.S. National Bureau of Standards, Part 2, G. M. Kline, SPE J. **19,** No. 4, 403–408 (Apr. 1963).

Radiation and the world we live in, L. S. Taylor, Radiology **80,** No. 3, 358–368 (Mar. 1963).

Natural and synthetic rubbers, E. J. Parks and F. J. Linnig, Anal. Chem. **35,** No. 5, 160R–178R (Apr. 1963).

Low-temperature thermometry, K. D. Timmerhaus, Book, Applied Cryogenic Engineering, Ed. R. W. Vance, Chapt. 4, 60–103 (John Wiley & Sons, Inc., New York, N.Y., 1962).

On the isomerization of isobutyl radicals, J. R. McNesby and W. M. Jackson. J. Chem. Phys. **38,** No. 3, 692–693 (Feb. 1, 1963).

The electrophoretic mobility of asphaltenes in nitromethane, J. R. Wright and R. R. Minesinger, J. Colloid Sci. **18,** 223–236 (Mar. 1963).

A suggestion for improving forecasts of geomagnetic storms, Y. Hakura and J. V. Lincoln, J. Geophys. Res. **68,** No. 5, 1563–1564 (Mar. 1, 1963).

Observation of a 6300 A arc in France, America, and Australia, F. E. Roach, D. Barbier, and R. A. Duncan, Ann. Geophys. **18,** 390–391 (Oct.–Dec. 1962).

Maximum efficiency of a two-arm waveguide junction, R. W. Beatty, IEEE Trans. Microwave Theory and Tech. **MTT–11,** 94 (Jan. 1963).

Applications of a semiconductor-surface-state charge-storage device, L. J. Swartzendruber, Solid-State Elec. **6,** 59–61 (Pergamon Press, Inc., New York, N.Y., 1963).

Electric fields in the ionosphere and the excitation of the red lines of atomic oxygen, L. R. Megill, M. H. Rees, and L. K. Droppleman, Planetary Space Sci. **11,** 45–56 (Jan. 1963).

Ten-kilocycle pound-type klystron stabilizer, H. E. Radford, Rev. Sci. Instr. **34,** No. 3, 304–305 (Mar. 1963).

International geophysical calendar for 1963, A. H. Shapley and J. V. Lincoln, J. Geophys. Res. **68,** No. 4, 1157–1159 (Feb. 15, 1963).

Kihara parameters and second virial coefficients for cryogenic fluids and their mixtures, J. M. Prausnitz and A. L. Myers, A. I. Ch. E. Journal **9,** No. 1, 5–11 (Jan. 1963).

Standards and the microwave profession, J. M. Richardson, IRE Trans. Microwave Theory and Tech. **MTT–10,** No. 6, 413–415 (Nov. 1962).

Transparent rigid mount for vacuum stopcock, M. M. Anderson, Rev. Sci. Instr. **34,** No. 2, 178 (Feb. 1963).

Delay time of polar-cap blackout and its relation to decay time of geomagnetic disturbance, C. S. Warwick, J. Geophys. Res. **68,** No. 5, 1561–1562 (Mar. 1, 1963).

Electrolytic conductance of ammonium dihydrogen phosphate solutions in the saturation region, J. L. Torgesen and A. T. Horton, J. Phys. Chem. **67,** 376–381 (1963).

Thermometry, low temperature, R. P. Hudson, Encyclopaedic Dictionary of Physics **7,** 323–325 (1962).

Standards for the 70s, W. A. Wildhack, Ind. Res. **5,** No. 3, 15–20 (Mar. 1963).

Effect of outdoor exposure on some properties of chrome-retanned leather, T. J. Carter, J. Am. Leather Chemists Assoc. **LVIII,** No. 3, 155–160 (Mar. 1963).

Nuclear orientation, E. Ambler, Book, Methods of Experimental Physics **5,** Sect. 2.4.2.3, 162–214 (Academic Press Inc., New York, N.Y., 1963).

APPA–TAPPI reference material program II. Effectiveness of a reference material in reducing the between-laboratory variability of TAPPI standard T 414 m–49 for internal tearing resistance of paper, T. W. Lashof, Tappi **46,** No. 3, 145–150 (Mar. 1963).

Some characteristics of a simple cryopump, L. O. Mullen and R. B. Jacobs, 1962 Trans. Ninth Natl. Vacuum Symp., Am. Vacuum Soc., pp. 220–226 (1963).

The ionosphere over Antarctica, W. R. Piggott and A. H. Shapley, Antarctic Research, Geophysical Mono. 7, pp. 111–126 (1962).

The personal side of a research project, A. T. McPherson, J. Wash. Acad. Sci. **53,** No. 3, 63–66 (Mar. 1963).

Indication limit, E. L. R. Corliss, Proc. Fourth Intern. Congr. Acoustics, Pt. I, Paper N22 (Copenhagen, Denmark, Aug. 21–28, 1962).

Nuclear resonance and the hyperfine field in dilute alloys of nickel in iron, R. L. Streever, L. H. Bennett, R. C. La Force, and G. F. Day, J. Appl. Phys. **34,** No. 4, Pt. 2, 1050–1051 (Apr. 1963).

The history of Pt 27, E. Wichers Book, Temperature, Its Measurement and Control in Science and Industry **3,** Pt. 1, 259–262 (Reinhold Publ. Corp., New York, N.Y., 1962).

Some causes of resonant frequency shifts in atomic beam machines. I. Shifts due to other frequencies of excitation, J. H. Shirley, J. Appl. Phys. **34,** 783–788 (Apr. 1963).

Some causes of resonant frequency shifts in atomic beam machines. II. The effect of slow frequency modulation on the Ramsey line shape, J. H. Shirley, J. Appl. Phys. **34,** 789–791 (Apr. 1963).

On the dependence of absorption coefficients upon the area of the absorbent material, E. D. Daniel, J. Acoust. Soc. Am. **35,** No. 4, 571–573 (Apr. 1963).

The role of the International Union of Pure and Applied Chemistry, E. Wichers, J. Chem. Doc. **3,** No. 7, 7–11 (1963).

New scale of nuclidic masses and atomic weights, E. Wichers, Nature **194,** No. 4829, 621–624 (May 19, 1962).

Note on a subgroup of the modular group, M. Newman and J. R. Smart, Proc. Am. Math. Soc. **14,** No. 1, 102–104 (Feb. 1963).

Calibration of photogrammetric lenses and cameras at the National Bureau of Standards, F. E. Washer, Photogrammetric Eng. **XXIX,** No. 1, 113–119 (Jan. 1963).

The orthobaric densities of parahydrogen, derived heats of vaporization and critical constants, H. M. Roder, D. E. Diller, L. A. Weber, and R. D. Goodwin, Cryogenics **3,** 16–22 (Mar. 1963).

Melting pressure equation for the hydrogens, R. D. Goodwin, Cryogenics **2,** No. 6, 1–3 (Dec. 1962).

Isotopic fractionation of uranium in sandstone, J. N. Rosholt, W. R. Shields, and E. L. Garner, Science **139,** 224–226 (Jan. 18, 1963).

The total electron content of the ionosphere at middle latitudes near the peak of the solar cycle, R. S. Lawrence, D. J. Posakony, O. K. Garriott, and S. C. Hall, J. Geophys. Res. **68,** 1889–1898 (Apr. 1, 1963).

Present status of our knowledge of atomic transition probabilities, W. L. Wiese, Proc. Tenth Colloquium Spectroscopic Intern., pp. 37–56 (Univ. of Maryland, College Park, Md., 1962).

Rubber and rubber products, W. P. Tyler and M. Tryon, Book, Industrial and Natural Products and Noninstrumental Methods, 6th Ed., Standard Methods of Chemical Analysis **IIB,** Chapt. 43, 2146–2226 (D. Van Nostrand Co., Inc., New York, N.Y., 1963).

The formation and oxidation of high-area carbon films, V. R. Deitz and E. F. McFarlane, Proc. Fifth Carbon Conference II, 219–232 (Pergamon Press, Inc., London, England, 1963).

Pure substance and mesaurement, E. Wichers, Mater. Res. Stds. **1,** No. 4, 314–315 (Apr. 1961).

The specific heat at constant volume of parahydrogen at temperatures from 15 to 90 °K and pressures to 340 atm, B. A. Younglove and D. E. Diller, Cryogenics **2,** No. 6, 1–5 (Dec. 1962).

Radiation detectors, L. Costrell, Science **139,** No. 3558, 899 (Mar. 8, 1963).

Intercomparisons of laboratory test results, J. Mandel, ISA Proc. **17,** 44.3.62–1 to 44.3.62–5 (1962).

Electron spin resonance of gamma-irradiated cellulose, R. E. Florin and L. A. Wall, J. Polymer Sci. **1,** Pt. A, 1163–1173 (1963).

The speed of light, A. G. McNish, IRE Trans. Instr. **I–11,** Nos. 3 & 4, 138–148 (Dec. 1962).

Fundamentals of measurement, A. G. McNish, Electro-Technol. **53,** 113–128 (May 1963).

Optimum estimators of the parameters of negative exponential distributions from one or two order statistics, M. M. Siddiqui, Ann. Math. Stat. **34,** 117–121 (Mar. 1963).

Building a simple transistor tester, G. F. Montgomery, Electronics **36,** No. 16, 56 (Apr. 19, 1963).

Electron microscopy studies of the surfaces of magnetic recording media, F. Nesh and D. B. Ballard, IEEE Trans. Audio **AU–11,** No. 1, 15–18 (Jan. 2, 1963).

Two-stream plasma instability as a source of irregularities in the ionosphere, D. T. Farley, Jr., Phys. Rev. Letters **10,** 279–282 (Apr. 1, 1963).

A magnetic amplifier for use with diode logic, E. W. Hogue, Proc. IEEE 1963 Intern. Conf. Nonlinear Magnetics No. T–149, 8.6–1 to 8.6–6 (Apr. 1963).

Kinetics of the acid-catalyzed hydrolysis of acetal in water-acetone solvents at 15, 25, and 35°, R. K. Wolford, J. Phys. Chem. **67,** 632–636 (1963).

Performance characteristics of split-type residential air-to-air heat pumps, J. C. Davis and P. R. Achenbach, Suppl. Bull. Inst. Intern. Refrigeration, pp. 1–7 (1961–1962).

Crystallographic changes with the substitution of aluminum for iron in dicalcium ferrite, D. K. Smith, Acta Cryst. **15,** 1146–1152 (Jan. 1963).

Methods for the analysis of rubber and related products, M. Tryon and E. Horowitz, Handb. Analytical Chemistry, Sect. 13, pp. 233–256 (McGraw-Hill Book Co., Inc., New York, N.Y., 1963).

Pressure-density-temperature relations of freezing liquid parahydrogen to 350 atmospheres, R. D. Goodwin, Cryogenics **3,** 12–15 (Mar. 1963).

Nuclear magnetic resonance in metal powders at low temperatures, R. J. Snodgrass and L. H. Bennett, J. Appl. Spectry. **17,** No. 2, 53–54 (1963).

Millimeter wavelength resonant structures, R. W. Zimmerer, M. V. Anderson, G. L. Strine, and Y. Beers, IEEE Trans. Microwave Theory Tech. **MTT–11,** 142–149 (Mar. 1963).

Lunar point-to-point communication, L. E. Vogler, Book, Technology of Lunar Exploration, Progress in Astronautics and Aeronautics **9,** 533–559 (Academic Press Inc., New York, N.Y., 1963).

Comment on "Parametric behavior of an ideal two-frequency varactor," G. F. Montgomery, Proc. IEEE **51,** No. 3, 491 (Mar. 1963).

Distribution of latitude of red ares, E. Marovich and F. E. Roach, J. Geophys. Res. **68,** No. 7, 1885–1888 (Apr. 1, 1963).

U.S. participation in international standardization, A. T. McPherson, ASTM Mater. Res. Stds. **3,** No. 4, 310–311 (April 1963).

Experimental investigation of Fabry-Perot interferometer, R. W. Zimmerer, Proc. IEEE **51,** 475–576 (Mar. 1963).

The following papers were published in the Proc. Intern. Conf. Ionosphere, London, 1962 (The Institute of Physics and The Physical Society, London, England):

A model of the atmosphere and the ionosphere in the *E* and *F*1 regions, R. B. Norton, T. E. VanZandt, and J. S. Denison, pp. 26–34.

Doppler studies of the ionospheric effects of solar flares, K. Davies, pp. 76–83.

Ionospheric variations during geomagnetic storms, S. Matsushita, pp. 120–127.

The Location of the irregularities responsible for ionospheric scintillation of a radio source, H. J. A. Chivers, pp. 258–266.

Equatorial spread-*F* motions, W. Calvert, K. Davies, E. Stiltner, and J. T. Brown, pp. 316–322.

Evidence for field-aligned ionization irregularities between 400 and 1000 km above the earth's surface, W. Calvert, T. E. VanZandt, R. W. Knecht, and G. B. Goe, pp. 324–329.

Experimental observations and theoretical calculations leading to a model for the lower ionosphere, R. H. Doherty, pp. 428–434.

Radio wave reflections at a continuously stratified plasma with electron collision frequency proportional to energy and arbitrary magnetic induction, J. R. Johler, pp. 436–445.

Very low frequency propagation in the earth-ionosphere waveguide of non-uniform width, J. R. Wait, pp. 446–451.

**Publications for which a price is indicated are available by purchase from the Superintendent of Documents, U.S. Government Printing Office, Washington D.C., 20402 (foreign postage, one-fourth additional). Reprints from outside journals and the NBS Journal of Research may often be obtained directly from the authors.*

UNIVERSITY MICROFILMS
313 NORTH FIRST STREET
ANN ARBOR, MICHIGAN
SJR-A-OCT

Uni
GOVERNMEN
DIVISION OF PUBLIC DOCUMENTS
WASHINGTON, D.C. 20402

OFFICIAL BUSINESS

PENALTY FOR PRIVATE USE TO AVOID PAYMENT OF POSTAGE, $300 (GPO)

JOURNAL OF RESEARCH of the National Bureau of Standards Vol. 67A, No. 5 September–October 1963
A. Physics and Chemistry

Contents

Page

Reduction of space groups to subgroups by homogeneous strain. H. S. Peiser, J. B. Wachtman, Jr., and R. W. Dickson. 395

High-temperature thermodynamic functions for zirconium and unsaturated zirconium hydrides. Thomas B. Douglas. 403

Heat of oxidation of aqueous sulfur dioxide with gaseous chlorine. Walter H. Johnson and John R. Ambrose. 427

Thickness of adsorbed polystyrene layers by ellipsometry. Robert R. Stromberg, Elio Passaglia, and Daniel J. Tutas. 431

Melting temperature and change of lamellar thickness with time for bulk polyethylene. James J. Weeks. 441

Precise coulometric titrations of potassium dichromate. George Marinenko and John K. Taylor. 453

Resolution limits of analyzers and oscillatory systems. Edith L. R. Corliss. 461

Synthesis, purification, and physical properties of seven twelve-carbon hydrocarbons. Thomas W. Mears, Connie L. Stanley, Edward L. Compere, Jr., and Frank L. Howard. 475

Reactions of polyfluorobenzenes with nucleophilic reagents. Leo A. Wall, Walter J. Pummer, James E. Fearn, and Joseph M. Antonucci. 481

Publications of the National Bureau of Standards. 499

Library of Congress Catalog Card Number: 62-37059

For sale by the Superintendent of Documents, U.S. Government Printing Office, Washington, D.C., 20402. Price 70 cents (single copy)
Subscription price: $4.00 a year; 75 cents additional for foreign mailing.
UNITED STATES GOVERNMENT PRINTING OFFICE, WASHINGTON : 1963

6